Rijkswaterstaat
Ministerie van Infrastructuur en Milieu

Rijkswaterstaat Technisch Document (RTD)

Validation of the Guidelines for Nonlinear Finite Element Analysis of Concrete Structures

Part: Slabs

Doc.nr.: RTD 1016-3C:2017
Versie: 1.0
Status: Final
Datum: 15 June 2017

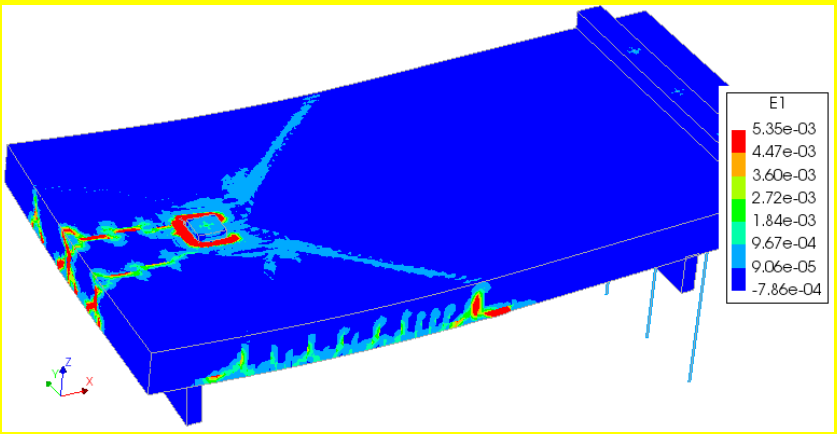

Water. Wegen. Werken. Rijkswaterstaat

Preface

At an international workshop on shear force capacities of concrete structural element, held in Rotterdam, the Netherlands in 2007, predictions of the ultimate limit state of three different girder experiments were presented. This workshop was initiated by the Dutch Ministry of Infrastructure and organized by TNO (Vervuurt & Leeghwater, 2008). The ultimate capacities, predicted by six teams using different nonlinear software packages, showed a large scatter. Also the predicted crack patterns showed a large scatter.

With this in mind, research on the development of a "guideline for nonlinear analysis of concrete girders" was started. The *fib* Model Code 1990 was the background document when Peter Feenstra started with the development of the guideline. Also, Joop den Uijl was involved in validating the guidelines. From 2010 the draft version of the *fib* Model Code 2010 was used as background document. Today, both the MC2010 and the Eurocode2 allow the use of nonlinear analysis to verify the design capacity of concrete objects.

The validation of the guidelines is done by simulating old and new experiments. To verify human and software factors, several people were involved in this project and two commercially available software packages were used. Finally the first version of the guideline was published in May 2012. It is used by the Dutch Ministry of Infrastructure and the Environment when commissioning engineering work for re-examinations of existing concrete structures in the Netherlands to reveal extra remaining structural capacity.

To verify whether the guideline is also valid for a larger group of international end-users and for other software packages, a prediction contest of T-shaped prestressed girders was set up in 2014. The tests were performed by Sebastiaan Ensink in the Stevin Laboratory of the Delft University of Technology. The participants of the contest gathered in a workshop in Parma. The outcome of this contest showed that the guidelines are indeed helpful for reducing model and human factors when predicting the behaviour of concrete structures by means of nonlinear finite element analysis.

As a result of additional validation studies and making use of the experiences of the workshop in Parma a new version of the guidelines has been published in 2016. The present document gives an overview of validations studies for this version of the guideline. Maciej Kraczla has contributed to this document.

This document is one from a series of documents. At the time of writing, the following documents have been drafted:

RTD 1016-1:	Guidelines for Nonlinear Finite Element Analysis of Concrete Structures
RTD 1016-2:	Validation of the Guidelines for Nonlinear Finite Element Analysis of Concrete Structures - Part: Overview of results
RTD 1016-3A:	Validation of the Guidelines for Nonlinear Finite Element Analysis of Concrete Structures - Part: Reinforced beams
RTD 1016-3B:	Validation of the Guidelines for Nonlinear Finite Element Analysis of Concrete Structures - Part: Prestressed beams
RTD 1016-3C:	Validation of the Guidelines for Nonlinear Finite Element Analysis of Concrete Structures - Part: Slabs

Beatrice Belletti, Cecilia Damoni, Max A.N. Hendriks, Ane de Boer
March 2017

Contents

1 Introduction

In the period 2008-2015 the Dutch Ministry of Infrastructure and the Environment has financed a project lading to a set of guidelines for the nonlinear finite element analysis of concrete structures (RWS, 2016). Apart from the guidelines document itself, the project resulted in the present publication: a document that describes the validation of the guidelines.

This introductory chapter starts with describing the background of the project. It continues with presenting the objectives and the outline of the present validation report.

1.1 Background

Modern codes of practice for civil engineering projects offer so-called levels-of-approximations (Muttoni & Ruiz, 2012). Depending on the stage of the project, e.g. preliminary design, executive design or a reassessment study, a modern code distinguishes several levels of design expressions and design methods. The *fib* Model Code for concrete structures 2010 (fib, 2013) is a good example. The idea is: the higher the level-of-approximation, the more sophisticated the analysis, the more realistic the estimation of the safety, the more possibilities of finding "hidden" structural capacities, the higher is the likelihood of avoiding over-conservative designs and reassessments, the more probable is that unnecessary costs can be avoided. The highest level-of-approximation, sometimes denoted as level IV, is a design or reassessment method based on nonlinear finite element analysis.

Whereas the lower levels-of-approximations are usually well-described using clear-cut expressions, applicability statements and examples, the situation is remarkably different when it comes to using nonlinear finite element analysis for design or reassessment studies. The *fib* Model Code has made an important step by providing safety formats to be used in connection with nonlinear finite element analysis. These safety formats define safety factors for the material properties and the global structural resistance. However the development of specifications on *how to perform* the analyses has not kept pace with the development of safety formats. It is beyond doubt that the results of nonlinear finite element analysis can be substantially influenced by model and human factors.

1.2 Scope and objectives

The development of guidelines for the nonlinear finite element analysis of concrete structures (RWS, 2016) has the primary goal to advice the analysts and consequently to reduce the model and human factors. The development of the guidelines went hand in hand with the performance of numerical benchmark studies. The guidelines were tuned and, in the end, validated by comparing the results of numerical analyses with experimental results. It is believed that by this process a coherent set of advices was obtained. This document gives an overview of the main case studies that have been used during the development of the guidelines.

The case studies include numerical examples with reinforced concrete beams, prestressed beams and slabs. The main objective is comparing the results of the numerical analyses with the experimental results for these cases and, in this way, validating the set of advices.

Next to the main objective, the case studies reported in this document are used to demonstrate sensitivities of modelling choices, to compare the applications of different safety formats and to show examples of documenting finite element analysis results.

1.3 Outline

After this introductory chapter, Chapter 2 summarizes the used methods. Each subsequent chapter addresses a single case study of a reinforced concrete beam. These chapters use a similar structure of sections, describing respectively: the experimental setup and results, the finite element model adopting the advices of the guidelines, analytical verifications, the nonlinear finite element results using mean or "measured" material properties and the application of safety formats. Additional sections are e.g. used to show sensitivity studies.

2 Methods used for modelling reinforced concrete members

This chapter summarizes the methods that are used in the subsequent chapters.

2.1 Analytical code provisions

The analytical methods used in this report are based on EC2 and MC2010.

2.2 Nonlinear finite element modelling approach

There is a great variety of modelling options for the modelling the nonlinear behaviour of concrete structures. The guidelines for the nonlinear finite element analysis of concrete structures (RWS, 2016) comprise specific modelling choices. It is important to consider these modelling choices as a coherent set of advices. For the details about these advises the reader is referred to the guidelines document itself. This section includes a summary of the main advices.

Units. The preferred units are the base units of the International System of Units (SI). Possibly, the length unit might be replaced by millimetres.

Constitutive models for concrete. Smeared cracking models are considered. A total strain-based rotating crack model is recommended for solid elements. Adequate tensile softening and compressive hardening-softening relations should be considered, based on the specification of tensile and compressive fracture energies and the definition of equivalent lengths to define "crack-band" widths. Tension-compression interaction needs to be addressed in structures subjected to 3D multi-axial stress states. The reduction of the compressive strength due to lateral cracking is ignored while a diminishing Poisson effect upon cracking is taken into account.

Constitutive models for reinforcement. Elasto-plastic material models with hardening should be used.

Constitutive models for concrete-reinforcement interaction. At the macro-level, simplified models can be used, taking into account tension stiffening effects. Limited attention is devoted to modelling slip and dowel action.

Finite elements for concrete. Elements with quadratic interpolation of the displacement filed should be used. Typically, at least 6 elements over the height of a structural element should be used.

Finite elements for reinforcement. Embedded reinforcement elements are preferred; both embedded bars and grids can be used.

Prestressing. Prestressing should be applied taking into account prestress losses.

Existing cracks. Existing cracks in the structure should be taken into account whenever detailed information about location and crack widths is available.

Loads. The design codes and national guidelines in force should be applied.

Boundary conditions. Unless the objective if the analysis is to study the detailed behaviour of the loading and support points, the support and loading platens should be modelled such that local stress concentrations are reduced.

Loading. The loading sequence will contain an initial phase where dead weight, permanent loads and, if appropriate, prestressing is applied to the structure. Following the initial phase, the variable loads are increased until a clear failure model is present or a significant load reduction has been achieved.
Note that in the current report, for all cases, we are referring to experimental tests. For this reason, when safety formats are applied to obtain the design resistance, we are considering a load combination of action with a partial safety factor related to self-weight of 1.0.

Equilibrium iterations. Equilibrium between internal and external forces should be achieved iteratively using a Newton-Raphson method with arc-length procedure. Preferably an energy-norm together with a force-norm should be used.

2.3 Nonlinear finite element limit state verifications

Serviceability limit states. As requested by current codes (EC2, MC 2010) serviceability limit states verifications must be performed as post-analysis checks. For the crack opening calculation, the average strain values are obtained from the analysis, whereas crack spacings are obtained from codes.

Ultimate limit states. Three alternative methods to obtain the design resistance from the non-linear finite element analysis: the Global Resistance Factor method (GRF), the Partial Factor method (PF) and the Estimate of Coefficient of Variation or resistance method (ECOV).

3 Case RS1: Cope and Rao (1983)

The experimental program of Cope and Rao (Cope and Rao 1983) is an examination of the behaviour of skewed slabs designed for standard highway loading. The complete experimental programme consisted of four one-fifth scale slabs. Two of the models were reinforced with rebars perpendicular and parallel to the supported edges and two had orthogonal reinforcement with respect to the free edges.
Slab 1A is selected as a case study as this slab had the highest stiffness and resulted in a punching shear failure mechanism in the obtuse corner due to the concentration of reaction force.

3.1 Experimental setup and results

Geometry

The geometry of slab 1A is shown in Figure 3-1(a). The slab had a right span and right width of 1880mm, thickness of 100mm and a skew angle of 45 degrees. The given dimensions refer to the scaled model in scale 1:5.
For the reinforcement, 8 mm Torbar bars were used. The reinforcement was placed parallel and orthogonal to the lines of the supports.
In order to comply with design office practice, maximum spacing of 150 mm and 300 mm for the main and secondary directions respectively were applied in the bottom reinforcement. Nominal stirrups fabricated from 3 mm round bars were provided at a spacing of about 70 mm along the line of support and at about 40 mm centres along the free edge for 1 m from the obtuse corners. Top and bottom reinforcement layout is presented in Figure 3-1(b) and (c).

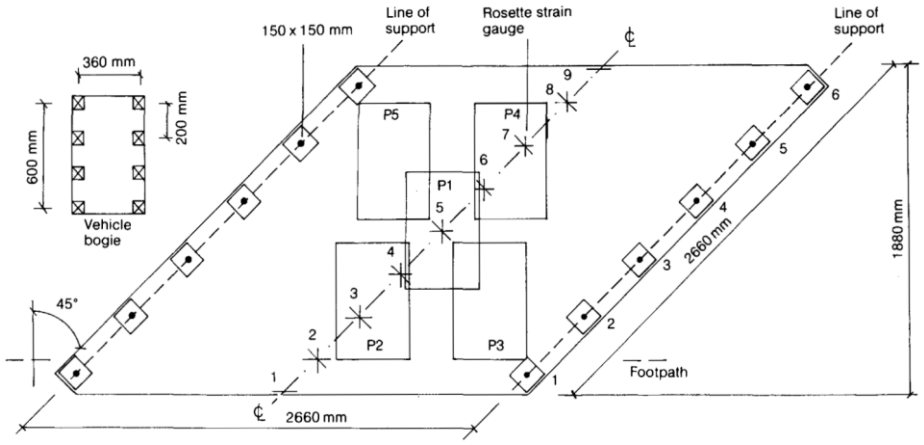

(a)

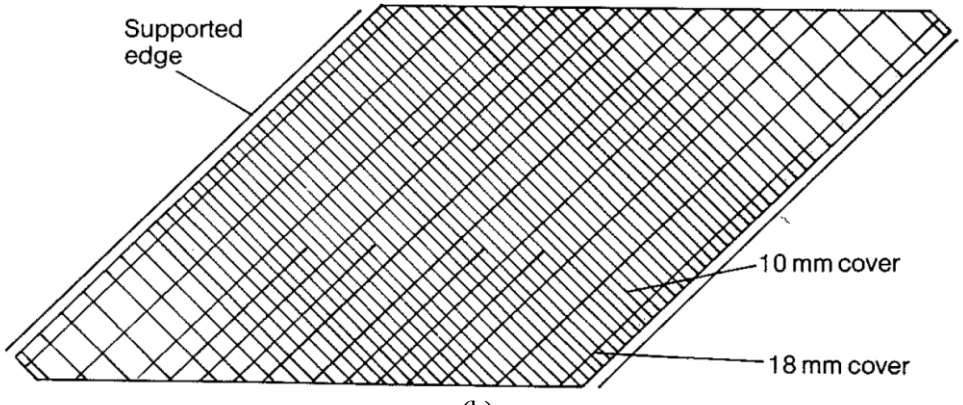

(b)

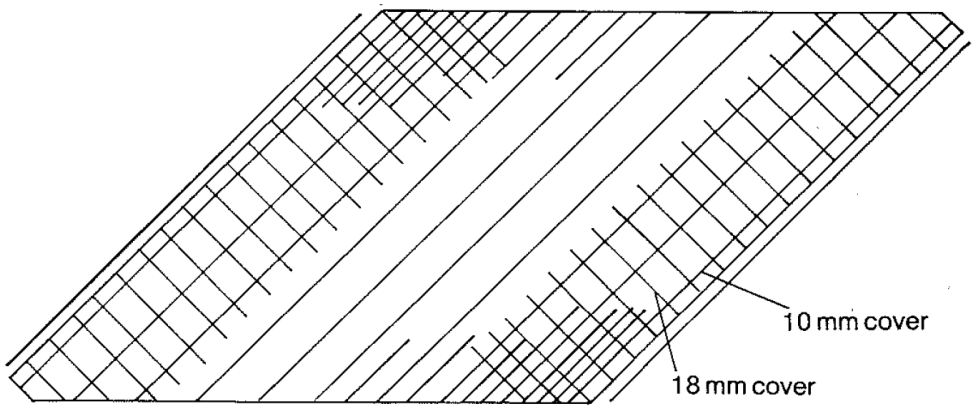

(c)

Figure 3-1: Case RS1: Geometry (a); reinforcement of the slab: bottom reinforcement layout (b), top reinforcement layout (c) (Cope and Rao1983)

Material Properties

Concrete and reinforcement properties from the reference are given in Table 3-1.

Table 3-1: Case RS1. Concrete and reinforcement properties

Concrete properties			
$f_{cm,cub}$ (N/mm^2)	$f_{ctm,sp}$ (N/mm^2)	d_{max} (mm)	E_c (N/mm^2)
42.10	3.07	7	31300
Reinforcement properties			
Bar	Φ (mm)	A_s (mm^2)	E_s (N/mm^2)	f_{tm} (N/mm^2)
Torbar	8.0	50	219200	620

Loading and Boundary Conditions

The slab was subjected to uniformly distributed loading and loading by a HB bogie. The position of the HB bogies, denoted as P1, P2, P3, P4 and P5 is illustrated in Figure 3-1(a). In the reference, the selection of loading to two levels was justified by an attempt to simulate serviceability load intensity – 40kN and long terms effect along with additional cracking with load 60kN. At each position, the intensity of load on the bogie was raised to 40kN, five times. The loading cycle was then repeated for the intensity increased to 60kN (Cope and Rao 1984). Lastly, the slab was loaded to failure at the bogie stationed at P2. The entire sequence of loading therefore is:

1. Global load: dead weight
2. Uniformly distributed loading: additional load of 52 kN (9.64kN/m^2)
3. Bogie located at position P1: loading raised to 40 kN followed by unloading, repeated five times
4. Bogie located at position P2: loading raised to 40 kN followed by unloading, repeated five times
5. Bogie located at position P3: loading raised to 40 kN followed by unloading, repeated five times
6. Bogie located at position P4: loading raised to 40 kN followed by unloading, repeated five times
7. Bogie located at position P5: loading raised to 40 kN followed by unloading, repeated five times
8. Bogie located at position P1: loading raised to 60 kN followed by unloading, repeated five times

9. Bogie located at position P2: loading raised to 60 kN followed by unloading, repeated five times
10. Bogie located at position P3: loading raised to 60 kN followed by unloading, repeated five times
11. Bogie located at position P4: loading raised to 60 kN followed by unloading, repeated five times
12. Bogie located at position P5: loading raised to 60 kN followed by unloading, repeated five times
13. Uniformly distributed loading: increase of the additional load to 64 kN (11.86 kN/m^2)
14. Bogie located at position P2: loading to failure

The skew slab was supported in six points on each side as shown in Figure 3-1(a). The supports were 150×150×30 mm steel bearing pads lined with hard rubber. The in-plane restraints were minimized by means of a thrust bearing assembly incorporated between each load cell and a steel pad. The average support assembly stiffness was about 250 kN/mm.

Experimental Results

Initial cracks were observed on the soffit at the centre of slab RS1 at a load of 20 kN when the vehicle bogie was first positioned at P1. They propagated towards both free edges along lines roughly parallel to the supports and at a spacing of about 65 mm. The directions of additional cracks in the edge zones, which formed when the loading was applied at positions P2 and P4, where approximately orthogonal to the free edges. Under 60 kN load cycling the extent of the soffit cracking spread towards the obtuse corners, and the short lengths of cracks, initiated during the 40 kN load cycling, grew parallel to the initially established cracks to produce a more uniform spread of cracking. After the application of a load of 100 kN in position P2, a shear crack opened suddenly right through the depth of the free edge near the line of supports in the obtuse corner. Despite this crack, in further loading, the midspan deflection continued to increase at about the same rate. Soffits cracks began to spread towards the loaded acute corner and from about 120 kN, offshoots of cracks began to produce an intersecting crack pattern When the load reached 180kN, a sudden punching shear failure in the obtuse corner occurred. The crack pattern at failure is shown in Figure 3-2. It is important to note that the position P2 of the load is at the top of the figure. It can be also deduced based on the concentration of sagging failure cracks in the process of forming near the top free edge.

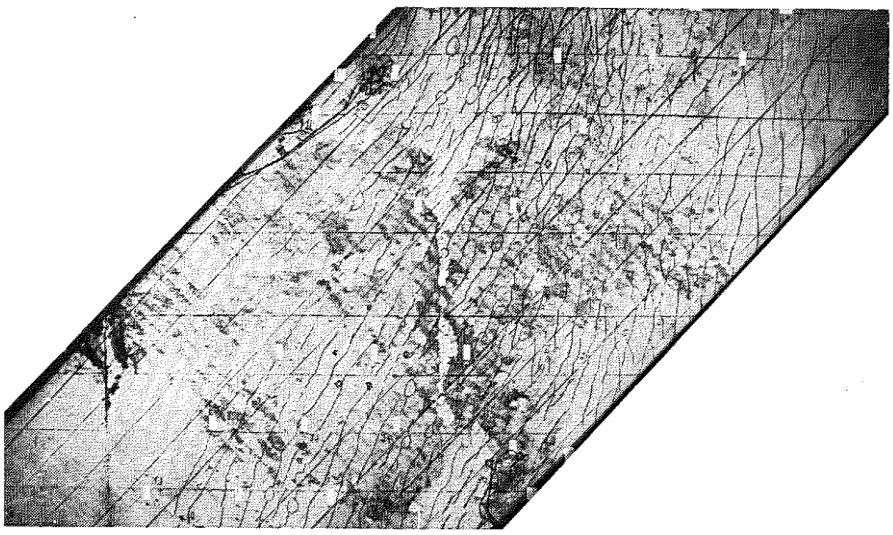

(a)

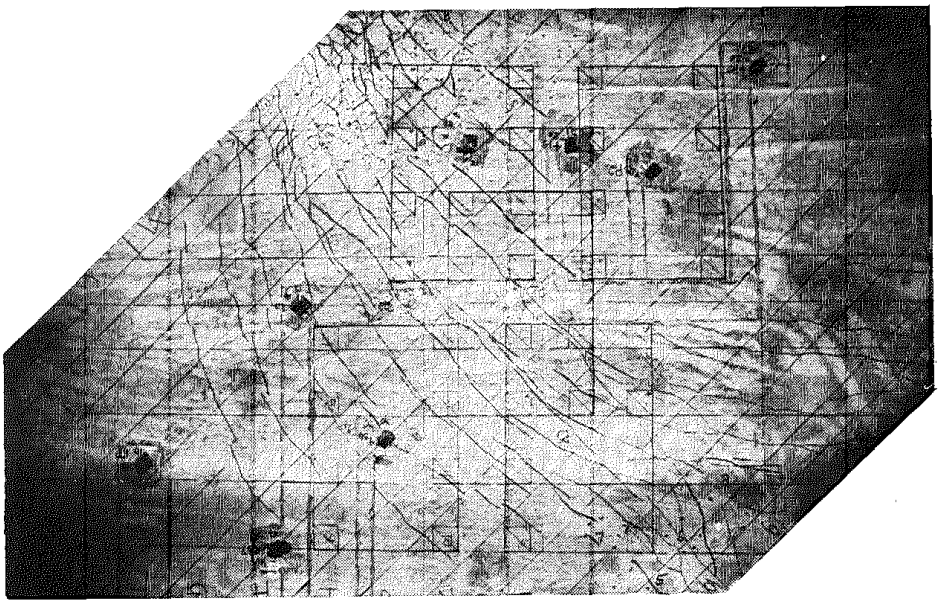

(b)

Figure 3-2: Case RS1: Crack pattern at: (a) soffit of the slab at failure, (b) top of the slab at failure (Cope and Rao1983)

3.2 Analytical analysis

Punching strength: Eurocode 2 formulation

The control perimeter *u*, outlined in red in Figure 3-3, is determined to calculate the punching strength.

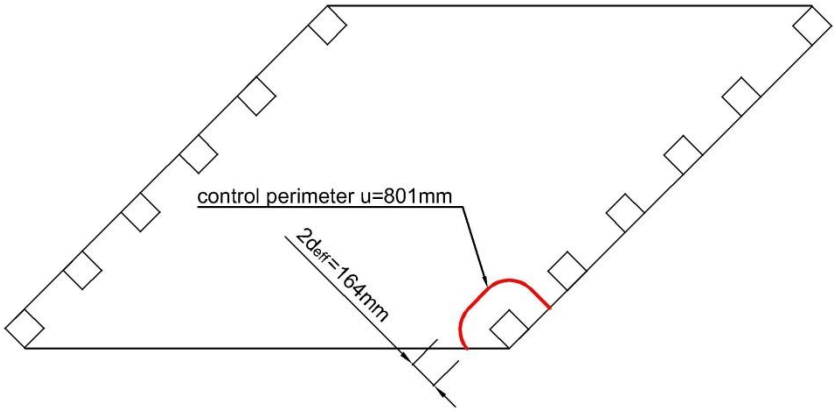

Figure 3-3: Case RS1. Control perimeter according to Eurocode 2 formulation

$$V_{Rdc} = v_{Rdc} \times u \times d_{eff}$$

$$d_l = h - c - \phi/2 = 100mm - 10mm - 4mm = 86mm$$

$$d_t = h - c - \phi - \phi/2 = 100mm - 10mm - 8mm - 4mm = 78mm$$

$$d_{eff} = \frac{d_l + d_t}{2} = \frac{86mm + 78mm}{2} = 82\,mm$$

$$k = 1 + \sqrt{\frac{200}{d_{eff}}} = 1 + \sqrt{\frac{200}{8}} = 2.562 > 2 \quad \text{thus} \quad k = 2$$

$$\rho_l = \frac{\pi\phi^2}{4 s_l d_l} = \frac{\pi \times (8mm)^2}{4 \times 50mm \times 86mm} = 0.012$$

$$\rho_t = \frac{\pi\phi^2}{4 s_t d_t} = \frac{\pi \times (8mm)^2}{4 \times 200mm \times 78mm} = 0.00322$$

$$\rho = \sqrt{\rho_l \times \rho_t} = \sqrt{0.012 \times 0.00322} = 0.00614$$

$$v_{Rdc} = C_{Rd,c} k (100 \times \rho \times f_{ck})^{1/3} = 0.12 \times 2 \times (100 \times 0.00614 \times 34.1MPa)^{1/3} = 0.661MPa$$

$$V_{Rdc} = v_{Rdc} u d_{eff} = 0.661MPa \times 801mm \times 82mm = 43.44kN$$

Including the self-weight of the punching cone restricted to *d* from the loading plate (mid-point of the crack) the resistance is:

$$V_{Rdc} = 43.44kN - 0.16kN = 43.28kN$$

Apart from the above calculations, the analytical solution from the reference document is given (Cope and Rao 1983). This solution was an attempt to predict the full load histories of the tested slab using the non-linear methods. The slab according to the results failed at about 150kN. The indications were intense damage to concrete and steel and non-satisfaction of the convergence norms, with large values of out-of-balance loads. For more detailed information, reference to the source document is made.

In Table 3-2 the design values of slab resistance against punching shear and the analytical solution given in the reference are summarized. It can be concluded that from the results of available analytical calculations the failure of RS1 slab is due to punching shear failure. This appears to be in agreement with the experimental results.

Table 3-2: Case RS1. Design values of slab resistance

Mode	**Punching**	**Shear**
	EC2 (kN)	*Reference document*
P_{Rd} **(kN)**	43.28	150

3.3 Finite element model

Units

Units are N, mm.

Material models and parameters

The concrete model is based on a total strain rotating crack model with:

- exponential softening in tension and parabolic behavior in compression,
- variable Poisson's ratio of concrete,
- reduction of compressive strength of concrete due to lateral cracking with a lower limit of 0.6.
- increase in compressive strength due to lateral confinement according to the model proposed by Selby and Vecchio (Selby and Vecchio 1993).

The mechanical properties of concrete are summarized in Table 3-3. On input, the G_F value has been decreased with a factor $\sqrt{2}$ in order to compensate for an underestimation of the crack bandwidth for cracks with an inclination angle of 45 degrees. The uniaxial stress-strain curve is shown in Figure 3-4 (a)

The model for the reinforcing bars and stirrups is based on hardening plasticity. Geometrical and mechanical properties of reinforcement are given in Table 3-3. The stress-strain curve of Φ8 Torbar and stirrups is plotted in Figure 3-4(b).

Table 3-3: Case RS1. Constitutive model parameters for concrete

	$f_{cm,cub}$ (N/mm^2)	f_{ctm} (N/mm^2)	E_c (N/mm^2)	ν	G_F (Nmm/mm^2)
Mean measured value	34.93**	2.76***	31300	variable	0.141*

*Not specified in reference; estimated according to Model Code 2010 (fib, 2013)
**Estimated from the measured cubic compressive strength as: $f_{cm} = 0.83 \cdot f_{cm,cub}$
***Estimated from the mean splitting tensile strength of concrete as $f_{ctm} = 0.9 \cdot f_{ctm,sp}$

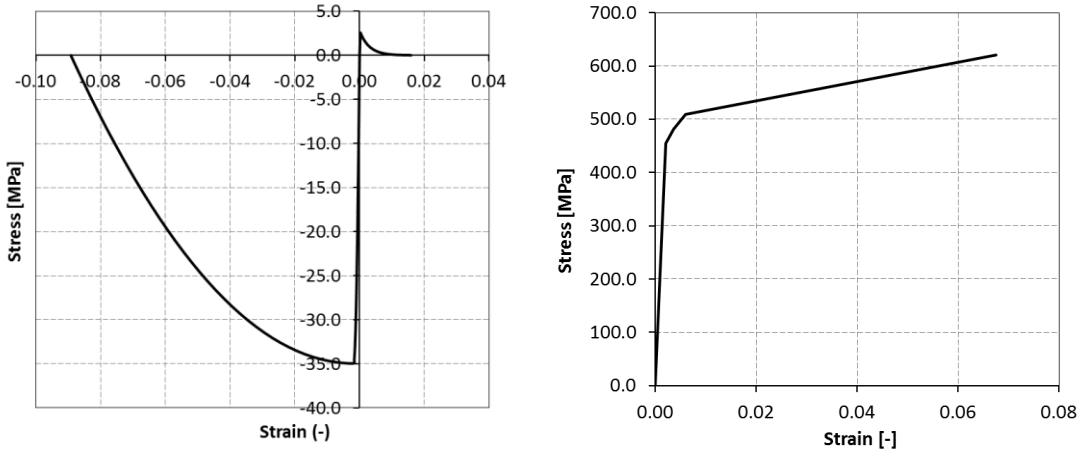

(a) (b)

Figure 3-4: Case RS1. Case RS1. Stress-strain curve for: (a) concrete, (b) Φ8 Torbar reinforcement and Φ3 stirrups

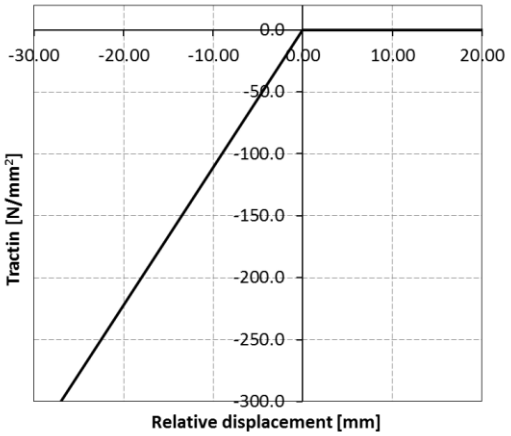

Figure 3-5: Case RS1. Traction-relative displacement of interface elements

The contact between supports and the slab was modelled using a boundary interface. The average support assembly stiffness from the reference is 250 kN/mm. A bilinear relation is assumed in the normal direction with a stiffness value in compression according to experimental data and the stiffness in tension almost equal to zero, Figure 3-5. Shear stiffness was assumed very small equal to 1.1 N/mm^3.

Element types and finite element mesh

For meshing the concrete slab 20-node solid elements (CHX60) are used. The specified element size of 17×17×17 mm is determined with respect to the minimum number of elements over the slab thickness which for a 3D model of a slab is *h/6*. The reinforcement bars were modelled with embedded truss elements with two Gauss integration points along the axis of the element. Perfect bond was assumed. The properties of bearing pads lined with hard rubber were assigned through 16-node (CQ48I) interfaces elements.
The mesh of the slab is depicted in Figure 3-6(a)

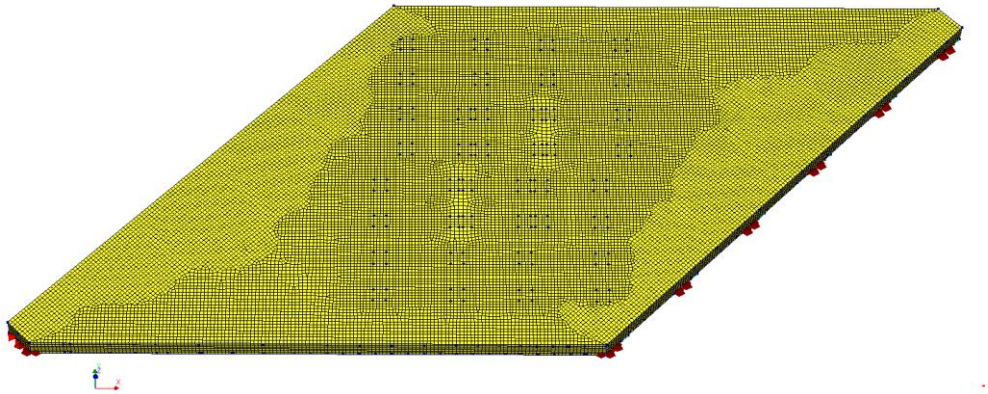

Figure 3-6: Case RS1. Mesh

Layouts of the reinforcement are illustrated in Figure 3-7 to Figure 3-9. Stirrups fabricated from 3mm round wires spaced at about 70 mm apart along supports' lines were aligned with the rebar the closest to the edge. At the free edges, two additional diagonal rebars were added.

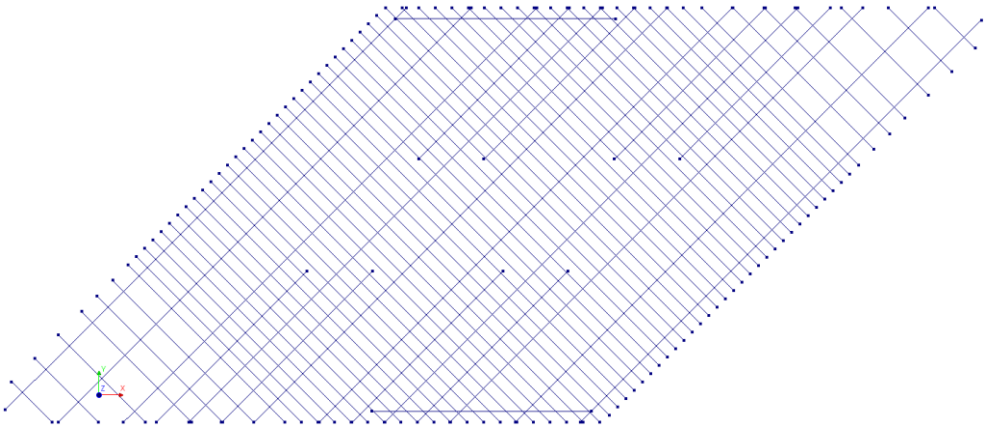

Figure 3-7: Case RS1. Bottom reinforcement

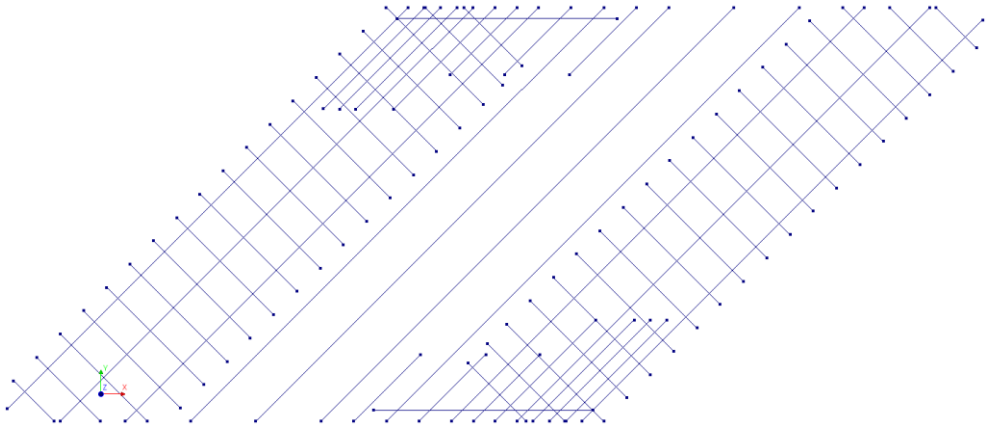

Figure 3-8: Case RS1. Top reinforcement

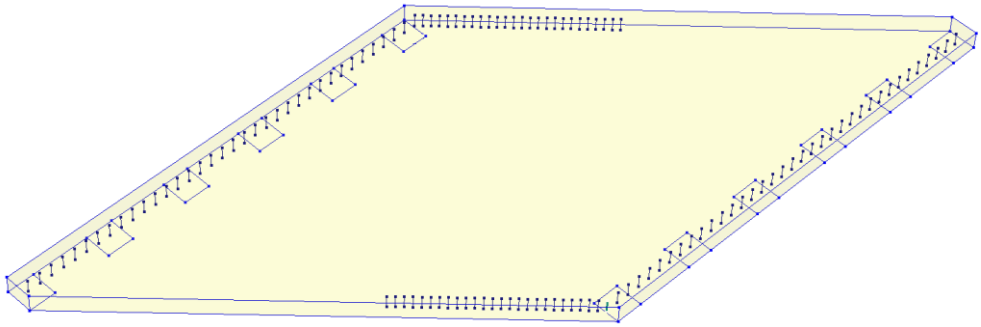

Figure 3-9: Case RS1. Stirrups

Boundary conditions and loading

The supports and loading were applied to imprinted areas at the true locations as given in the reference. As described earlier, interfaces were modelled as a boundary interface. It is schematically shown in Figure 3-10. Constrains in *x*, *y* and *z* directions were attached to the surfaces located at the position of bearing pads on each side.

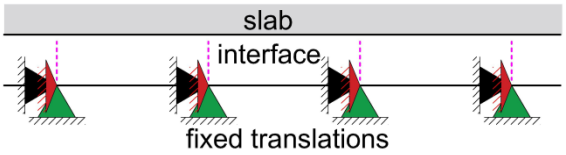

Figure 3-10: Case RS1. Interface and supports

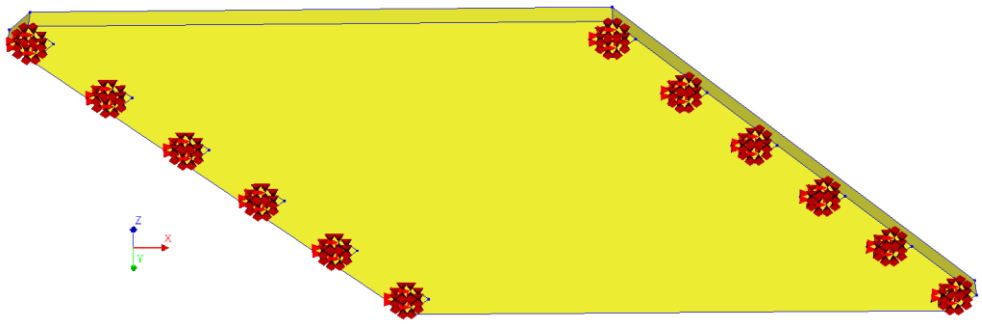

Figure 3-11: Case RS1. Boundary conditions

Please note that simplifications related to the experimental loading sequences have been made. Instead of five repetitions of loading at each station P1-P5 at two load levels, only one cycle of loading and unloading at stations P1 to P5 at each load level was taken into account in the analysis. Refer also to Table 3-4. It is motivated by the extensive time required to perform the NLFEA.

The slab was subjected to uniformly distributed loading modelled as a face pressure and loading by an HB bogie. The HB bogie load is modelled by a configuration of 8 wheel loads applied to a surface of 60×60 mm^2 for each wheel. The distributed load of 52kN along with positioning of the wheel loads for the first sequence of loading to the load level 40kN is illustrated below.

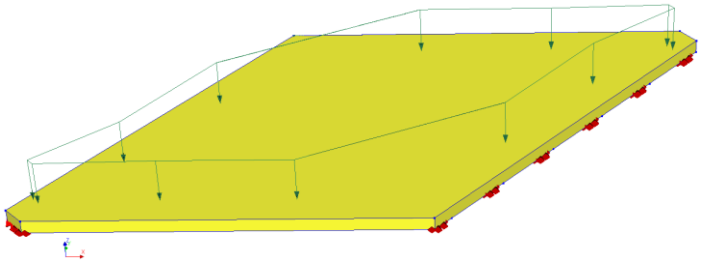

1. Application of the global load – self weight and uniformly distributed load of 52kN (9.64kN/m^2)

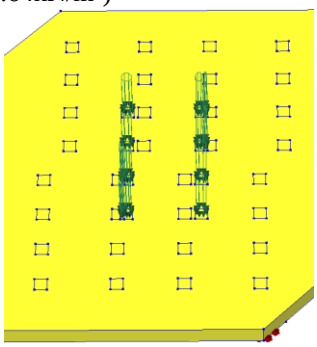

2. Boogie load at position P1

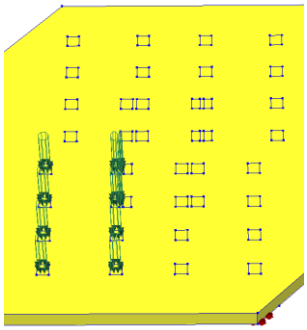

3. Boogie load at position P2

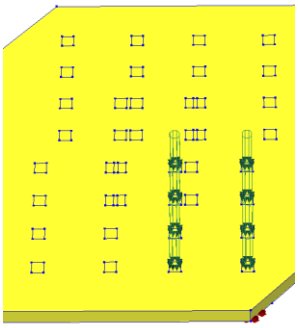

4. Boogie load at position P3

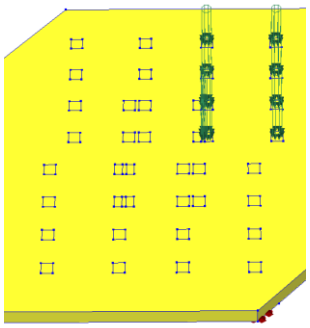

5. Boogie load at position P4

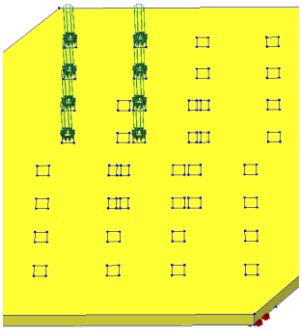

6. Boogie load at position P5

7. The loading sequence at the stations P1-P5 was repeated for the second load level of 60 kN
8. Before test to failure, the uniformly distributed load was increased to 64kN
9. Test to failure at boogie stationed at P2

Load increments and convergence criteria

Global load – self-weight and uniformly distributed load 52kN
Self-weight was applied in one load step. Uniformly distributed load was applied with a load factor set to 0.25(4). Regular Newton-Raphson method with a maximum of 25 iterations was adopted.

Loading sequence at positions P1-P5 to load level 40 kN
At each position P1 to P5, loading and unloading was applied with a load factor: 0.25(4), -0.25(4). Regular Newton-Raphson method with a maximum of 50 iterations was used. The analysis continued even if the convergence criteria were not satisfied. Convergence tolerances equal to 1×10^{-3} and 1×10^{-2} were selected for energy and force norms, respectively.

Loading sequence at positions P1-P5 to load level 60 kN
After loading to the load level 40 kN, the same sequence was applied to the load level 60kN. Loading was executed in the load steps: 0.25(4) while unloading -0.25(4). Regular Newton-Raphson method with a maximum of 50 iterations was used. The analysis continued even if the convergence criteria were not satisfied. Convergence tolerances equal to 1×10^{-3} and 1×10^{-2} were selected for energy and force norms, respectively.

Uniformly distributed load 64kN
Before loading to failure, the uniformly distributed load of 52kN was increased to 64kN. The additional load was applied in 4 steps thus: 0.25(4). Regular Newton-Raphson method with a maximum of 50 iterations was used.

Loading to failure at station P2
Loading to failure was carried out with a load magnitude of 10.08kN distributed among 8 wheels ($0.35kN/mm^2 \times 60mm \times 60mm \times 8 = 10.08kN$). At each step load was applied with load factor of 0.5. Regular Newton-Raphson method with a maximum number of iterations increased to 80 was used. The analysis continued even if the convergence criteria were not satisfied. Convergence tolerances equal to 1×10^{-3} and 1×10^{-2} were selected for energy and force norms, respectively.

Table 3-4: Case RS1: Summary of loading sequences

Load increments	Iterative procedure	Max. number of iterations	Convergence criteria & tolerance
Self-weight and uniformly distributed load 52kN			
1+0.25(4)	Regular Newton-Rapson	25	Force 1.0E-03, energy 1.0E-02
Loading sequence at positions P1-P5 to load level 40 kN			
0.25(4) and unloading -0.25(4)	Regular Newton-Rapson	50	Force 1.0E-03, energy 1.0E-02
Loading sequence at positions P1-P5 to load level 60 kN			
0.25(4) and unloading -0.25(4)	Regular Newton-Rapson	50	Force 1.0E-03, energy 1.0E-02
Uniformly distributed load 64kN			

0.25(4)	Regular Newton-Rapson	50	Force 1.0E-03, energy 1.0E-02
Loading to failure at station P2			
0.5(40)	Regular Newton-Rapson	80	Force 1.0E-03, energy 1.0E-02

3.4 Nonlinear finite element analysis

Load deflection

Figure 3-12 presents the response of the slab to the load positioned at the station P2 and increased to failure. The response obtained from NLFEA was compared with the results given in the reference. The actual load-displacement curve was not included in the source document; therefore the blue curve from the figure was derived from the midspan deflection profile for four load increments. This profile is given in Figure 3-13. Because the profile includes only loading till 140kN and from the description of the response to loading results that the slab failed at the load of 180kN, the missing part was extrapolated based on the trend from the previous results.

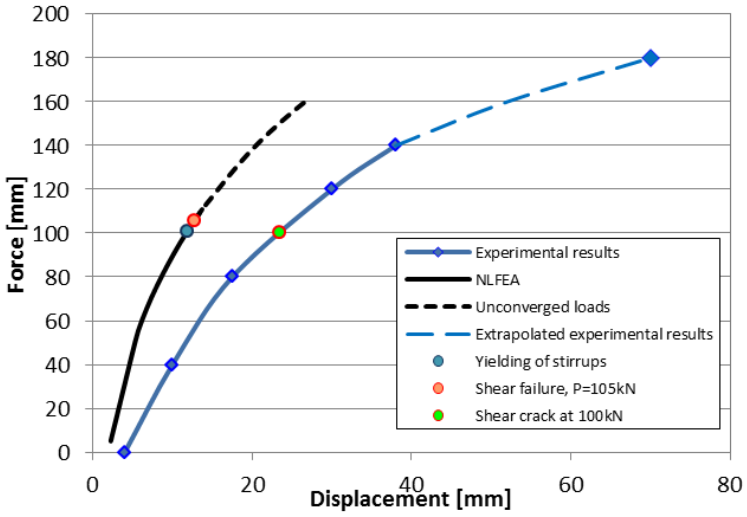

Figure 3-12: Case RS1. Load-deflection curve for position P2

The NLFEA stopped with the load 105 kN due to shear crack near the obtuse corner. From the deflection profile in Figure 3-13, it is clear that response of the slab is much stiffer that the real behavior. This phenomenon could be advocated by the fact that in the NLFEA as compared to the experiment, a total of eight (four for load level 40kN and four for load 60kN) loading cycles at each station was omitted prior to loading to failure resulting in less extensive “pre-cracking".

Convergence behavior

Convergence behavior of all loading sequences is presented in Figure 3-14 and Figure 3-15. It can be noticed that for the majority of steps convergence was reached based on the energy criterion whereas the force norm was satisfied only for few load steps at the beginning of the analysis. Prior to the loading to failure, all loads steps converged within the specified maximum number of iterations. The peak load defined as the load increment which fully complies the convergence criteria is marked with a red marker. This load steps corresponds to the onset of shear crack near the obtuse corner. It can be see, that it is followed by 3 load steps (steps 108,109,110) for which the relative energy variation is very close to the specified tolerance. It is therefore expected that for a higher number of iteration chosen, the 3 consecutive would have converged. It can also

be justified by the behavior of the slab which displayed shear crack widening and yielding of 3mm stirrups near the obtuse corner. After that, the relative energy variation is much further from the equilibrium probably due to development of diagonal cracking across the width and depth of the slab, see Figure 3-17.

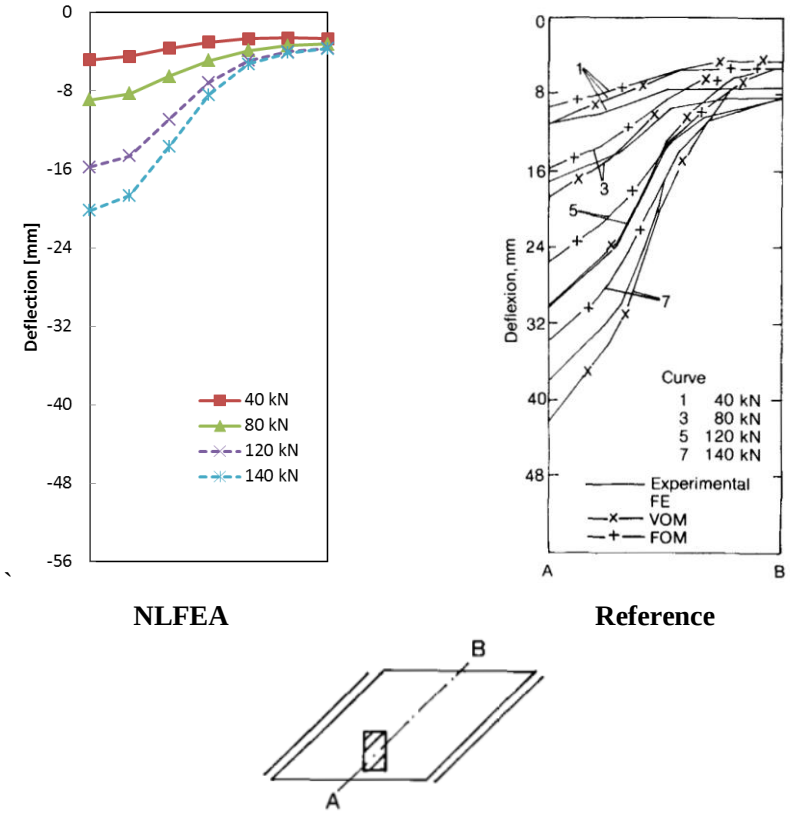

Figure 3-13: Case RS1. Midspan deflection profile

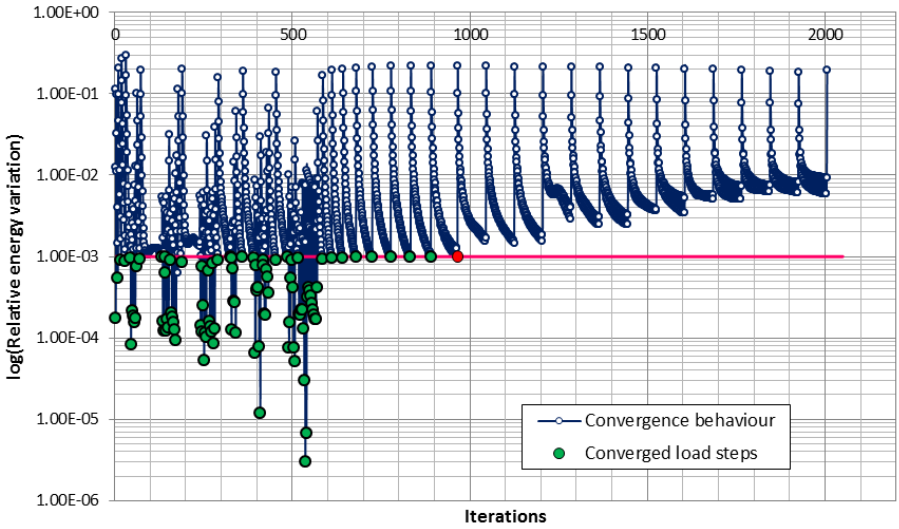

Figure 3-14: Case RS1. Evolution of the energy norm (red marker indicate peak load, pink line indicate convergence tolerance)

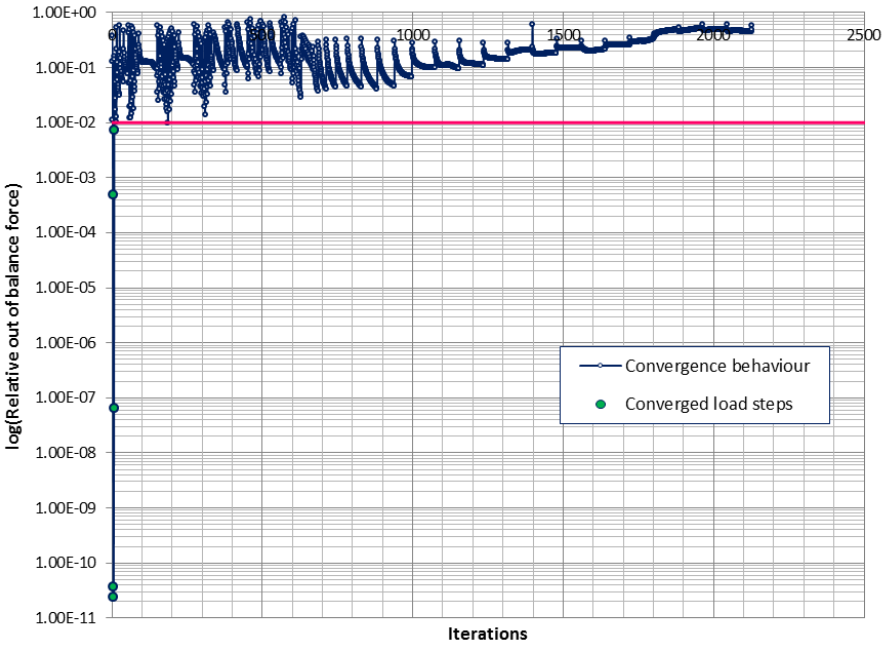

Figure 3-15: Case RS1. Evolution of the force norm (pink line indicates convergence tolerance)

Strains

The description of the experiment explains that, even though at a load 100 kN local shear failure through the depth of the free edge near the obtuse corner seemed to imminent, further loading was still possible, till the slab failed abruptly due to punching shear. The NLFEA stopped with the load 105.84 kN due to shear failure near the obtuse corner.

In Figure 3-16 and Figure 3-17 positive principal strain contour at step 108 (load factor 9.5) and step 111 (load factor 11.0) are shown.

Emphasis is laid on three values of principal strain. The first principal strain value 8.827e-5 indicates occurrence of cracking. The second principal strain value equal to 0.00295, corresponds to the ultimate strain value (indication of a stress free crack) calculated as $\varepsilon_{t,u} = \frac{G_F}{h \cdot f_{ctm}} = \frac{0.138}{17 \times 2.76} = 0.00295$, while the third principal strain value, equal to 0.01356, is the strain value corresponding to 1% of f_{ctm}. It can be seen that prior to failure extensive cracking occurred with a number of open critical shear cracks as well as sagging and hogging bending cracks. Comparing steps 108 and 111, besides further opening of existing cracks, the diagonal crack on the top surface propagates towards the opposite corner. This crack is open right through the depth of slab.

In Figure 3-18 contour plot with negative principal strains at step 108 is presented. Strain values beyond the limit strain of the elastic range of -3.72e-4 dominate across the whole slab. Neither compression softening nor crushing of concrete was observed prior to the failure. Lastly, in Figure 3-19 yielding of stirrups at the failure is presented.

Concluding on the crack pattern, which can be determined from the contour of positive principal strain, a satisfactory resemblance can be observed even though Figure 3-2 shows crack pattern at failure at the load 180 kN. Apart from the shear crack noticed in the experiment, band of sagging open cracks orthogonal to the free edge propagating from the load position towards the opposite obtuse corner can be seen. Also on the top surface, hogging cracks are clearly visible. In relation to flexural behavior of the slab, the reference comments that if the shear failure had been prevent, a “yield-line”

flexural mechanism might have formed with a sagging yield-line running from the vehicle to the opposite obtuse corner and with a hogging yield-line between the obtuse corners. This statement could only be confirmed in case of more flexible behavior accompanied with more yielding of reinforcement.

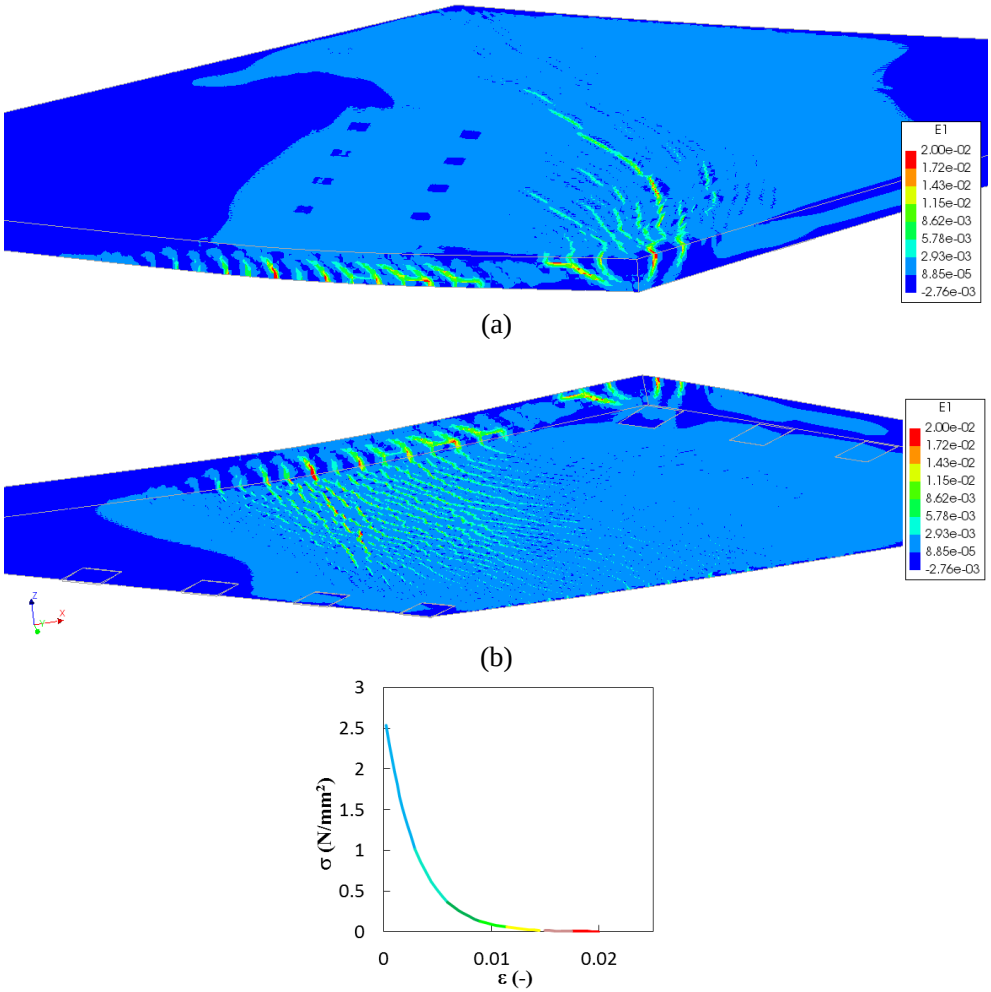

Figure 3-16: Case RS1. Positive principal strain values at step 108 (peak load): (a) top surface, (b) soffit of the slab

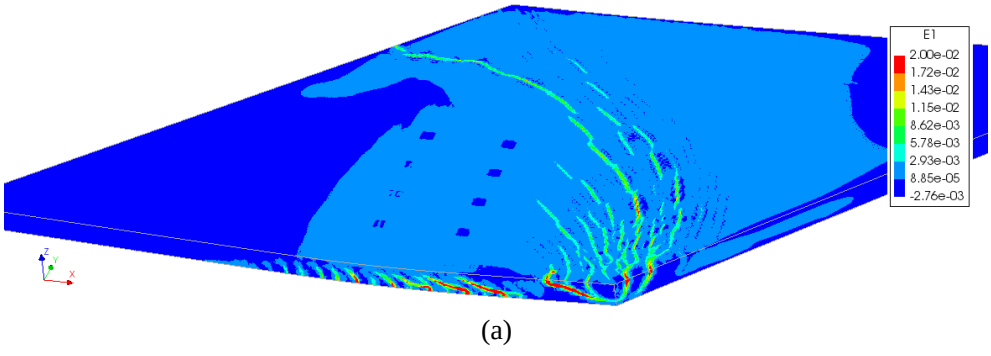

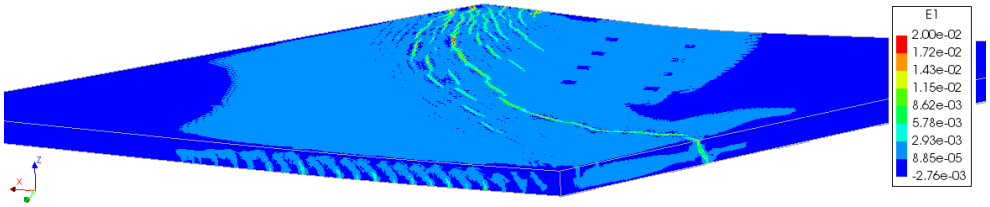

(b)

Figure 3-17: Case RS1. Positive principal strain values at step 111 on: (a) top surface, (b) top surface seen from the opposite obtuse corner

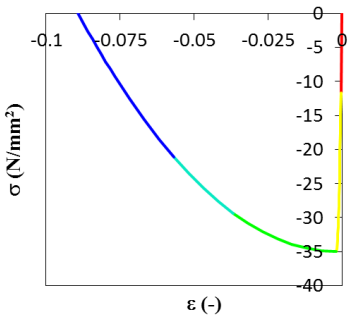

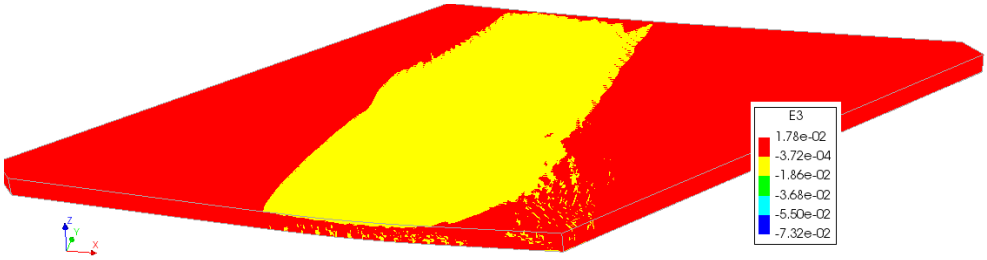

Figure 3-18: Case RS1. Minimum principal strain values at step 108

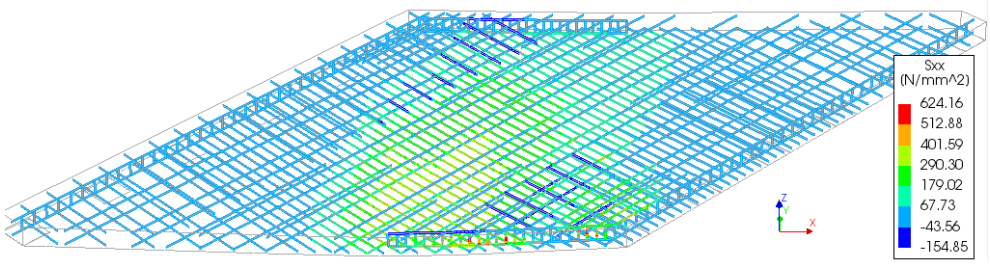

(a)

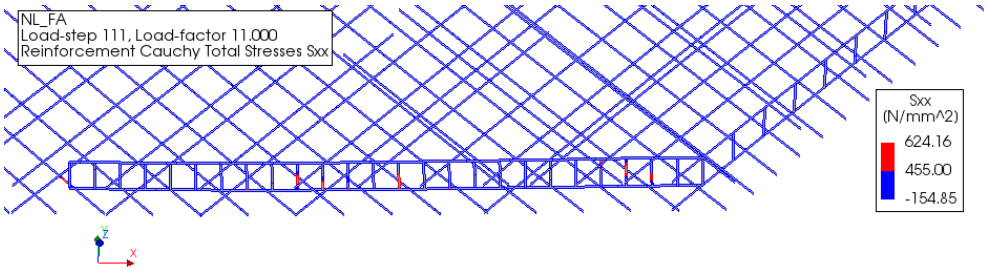

(b)

Figure 3-19: Case RS1. Local stresses: (a) in reinforcement of the slab, (b) yielding of 3mm stirrups in the loaded obtuse corner

3.5 Application of safety format

The analysis with mean material properties stops prematurely as a result of a shear failure at a significantly lower load than the ultimate load from the experiment. Application of safety format would result in even lower design resistance. Consequently, design resistance assessment of models with material properties for safety format methods was not evaluated.

3.6 Concluding remarks

Slab RS1 is a skew 45° inclined slab with a right span and right width of 1880 mm and a depth of 100 mm (the given dimensions refer to the scaled model in scale 1:5). The experimental setup consisted of loading sequences at two load levels in five loading positions of the bogie. The two load levels were meant to simulate serviceability load intensity (level of 40kN) and long term effect and additional cracking for the load level 60kN. The beam then was loaded till failure.
The numerical analyses of the slab considered a three dimensional model. The slab was modelled with 20-node brick elements for the concrete and embedded truss elements for the reinforcement. Perfect bond was assumed. The concrete model was based on a total strain rotating crack model with exponential tension softening in tension and parabolic behavior in compression, variable Poisson's ratio of concrete and no reduction of compressive strength of concrete due to lateral cracking. The model for the reinforcement bars was based on hardening plasticity.
The NLFEA analysis with mean measured values applied resulted in the shear failure at the load of 105 kN whereas the ultimate resistance from experiment was 180 kN with the slab failing in punching shear. The prediction of the shear failure seems to be in agreement with the experiment as prior to the punching shear failure, a local shear failure at the load level 100 kN seemed to be imminent, yet further loading was possible. In addition to that, a comparison of responses shows that the response of the numerical model is less flexible than the tested slab. The crack pattern of the slab appears to be consistent with the reference's description.
Alternative safety verification through application of safety formats was not performed.

In conclusion, due to an extensive computation time, only a model with mean measured material properties and the interface properties as given in the reference was analysed. The model satisfactorily predicts the occurrence of shear crack (step 108, load factor 9.5 = 96 kN) however it results in too low ultimate resistance (step 110, load factor 10.5 = 105.8kN) as the slab in the experiment failed due to punching shear at the load 180kN. Further analysis of the slab with input parameters leading to a more flexible behaviour is highly recommended.

4 Case RS2: Rodrigues (2007)

The experimental research of Rodrigues and Muttoni (Rodrigues 2007) was performed at the Structural Concrete Laboratory (IS-BETON) of the Ecole Polytechnique Fédéral de Lausanne to study the actual behavior of a bridge cantilever without shear reinforcement. From the study, slab DR1-a was selected as a benchmark and denoted RS2.

4.1 Experimental setup and results

Geometry

The cantilever is a full scale model of a part of a reinforced concrete bridge box girder. Figure 4-1 illustrates the dimensions and the reinforcement layout of slab RS2. The cantilever has a span of 2.78 m and a total length of 10.0 m. The thickness of the cantilever varies from 0.19 m at the free edge to 0.38m at the fixed end. Transversal reinforcement of the top layer at the fixed end consists of ∅16/75 mm bars (reinforcement ratio ρ = 78%). Only one half of the top reinforcement spans across the whole cantilever. The other half was cut-off at 1380 mm from the clamped edge. No vertical reinforcement was provided between the free edge and the fixed end. The bottom reinforcement in both directions and the top longitudinal reinforcement consist of ∅12 spaced 150 mm. The bottom reinforcement bars in the transverse direction were bent up at the free edge and anchored in the top layer. Edge reinforcement consisting of 12 mm bar at 150 mm spacing was added along the side edge. The concrete cover is 30 mm.

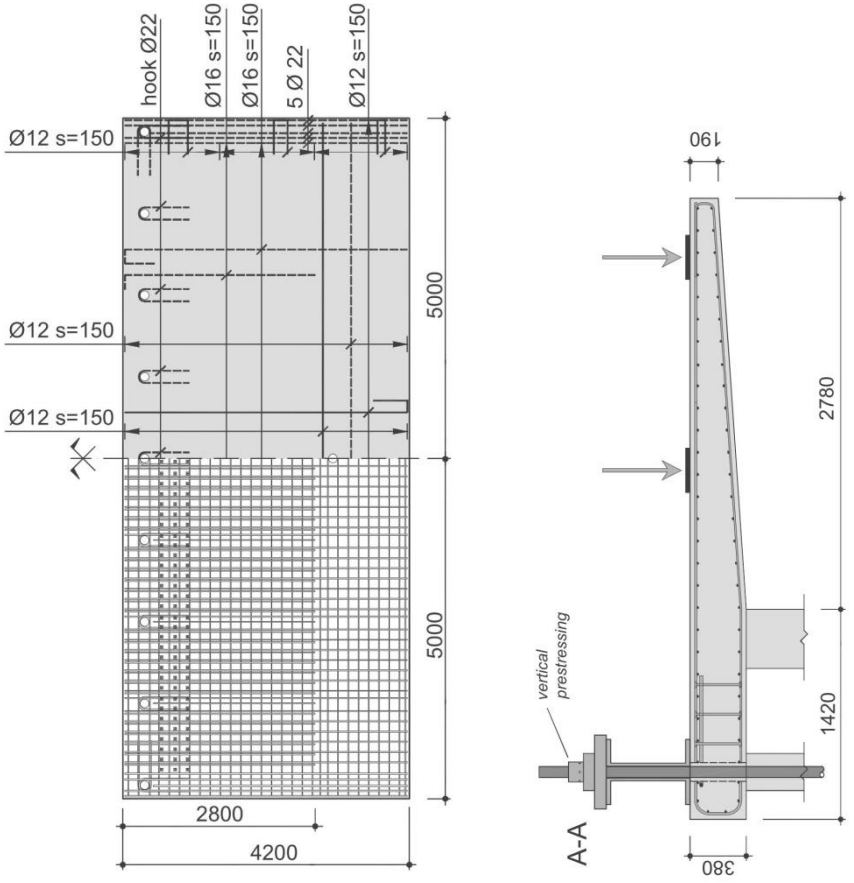

Figure 4-1: Case RS2. Geometry and reinforcement layout (Rodrigues 2007)

Material Properties

Concrete and reinforcement properties are given in Table 4-1.

Table 4-1: Case RS2. Concrete and reinforcement properties

Concrete properties					
f_{cm} (N/mm^2)		$f_{ct,sp}$ (N/mm^2)	E_c (N/mm^2)	d_{max} (mm)	
39.11		2.94	36030	16	
Reinforcement properties					
Bar	Φ (mm)	A_s (mm^2)	E_s (N/mm^2)	f_{ym} (N/mm^2)	f_{tm} (N/mm^2)
Φ16	16.0	201	210000	499	600
Φ12	12.0	113	210000	541	629
Φ22	22.0	380	210000	534	644

The stress-strain curves of reinforcement bars are shown in Figure 4-2.

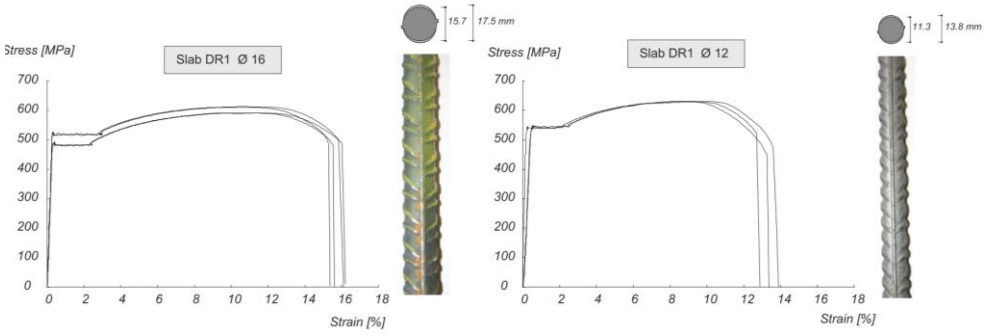

Figure 4-2: Case RS2. Stress-strain relations for reinforcing bars (Rodrigues 2007)

Loading and Boundary Conditions

Slab RS2 was tested under loading pattern of four concentrated loads as shown in the middle of Figure 4-3. The load set-up is scaled ¾ with respect to the load configuration according to EC1. The cantilever was subjected to one hundred load cycles at a load level of about 410 kN and was afterwards taken to failure, Figure 4-5. The concentrated loads were applied through steel plates with dimensions 300 x 300 x 30 mm. To ensure that the slab was properly clamped, a vertical prestressing force of 7MN was applied to the nine bars at the fixed end support, Figure 4-4. The details of the test set-up are presented in Figure 4-4.

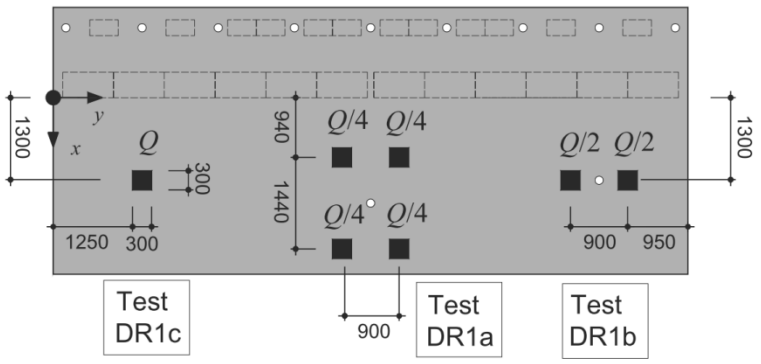

Figure 4-3: Case RS2. Loading positions (Rodrigues 2007)

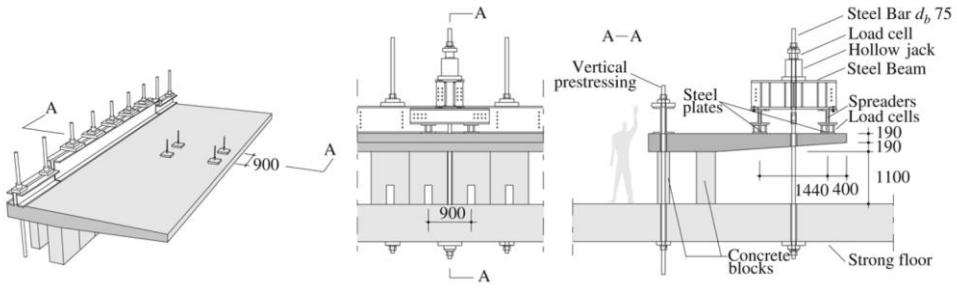

Figure 4-4: Case RS2. Details of test set-up (Rodrigues 2007)

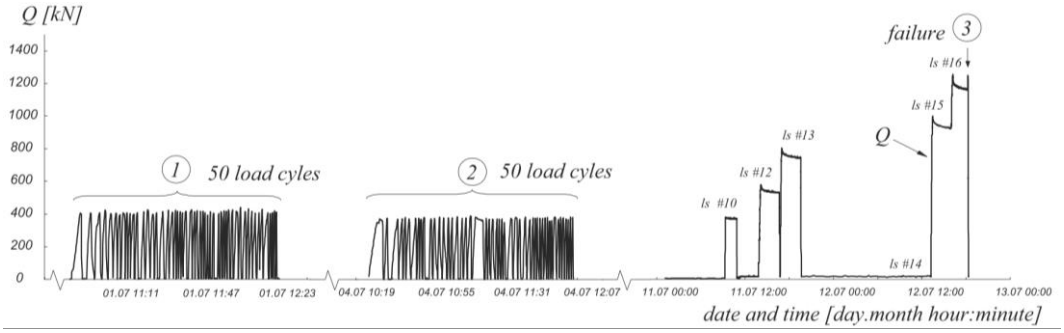

Figure 4-5: Case RS2: Loading history (Rodrigues 2007)

Experimental Results

The continuous measurements of the applied load through load cells and deflection at key locations with LVDTs were taken. The load-displacement curve shown in Figure 4-6 relates the total load *Q* (constituting individual 4 components) and the displacement at the free edge of the cantilever, w1 measured throughout the loading intervals. The whole loading history – intervals 1 to 3 corresponding to point indicated in Figure 4-6, is presented in preceding figure.

The readings of LVDTs placed behind the clamped edge suggested that prestressed bars successfully prevented rotation of the part of the beam. The measured maximum deflection equal to 0.17 at failure load was only 0.3% of the measured deflection at the tip of the cantilever.

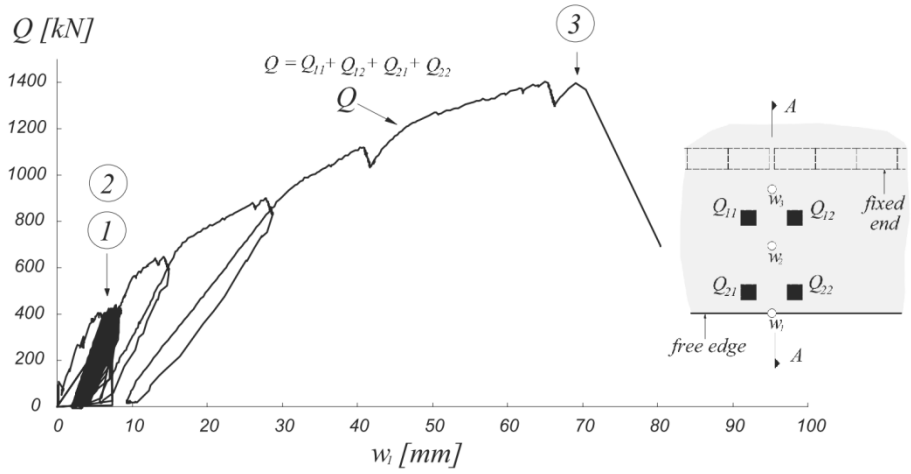

Figure 4-6: Case RS2. Load-deflection curve (Rodrigues 2007)

The remaining continuously measured values concerned:

- Strains on the concrete surface using omega-shaped extensometers placed in the zones with the largest flexural strains were expected.
- Rotation of the slab with inclinometers
- Variation of the thickness of the slab

The principal tensile strains on the top and bottom surfaces calculated from the demountable deformeter measurements of the measuring grid accompanied with the crack pattern are depicted in Figure 4-7 and Figure 4-8 respectively. The principal compressive strains are portrayed in Figure 4-9.

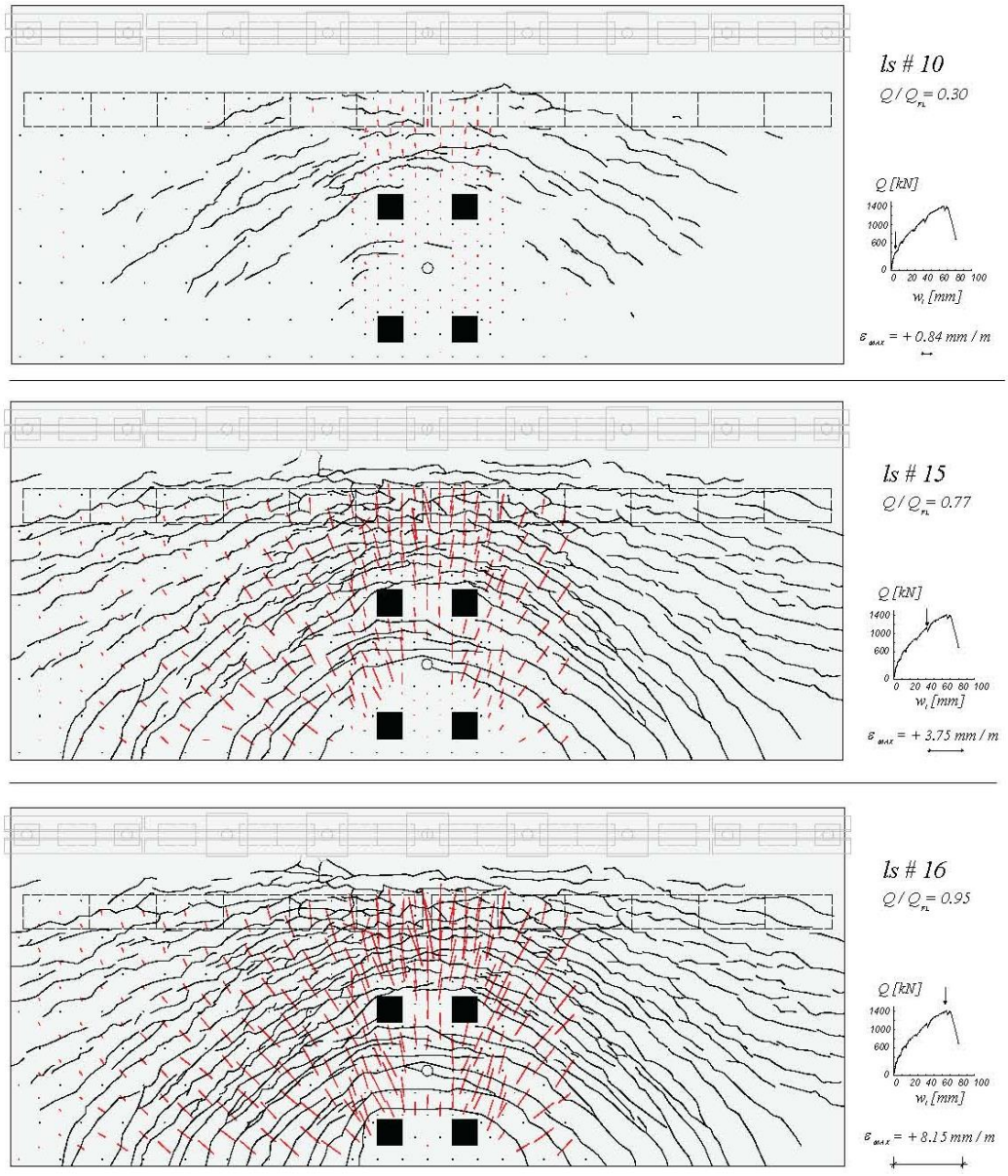

Figure 4-7: Case RS2: Crack pattern and tensile principal strains on the top surface for loading stages #10, #15 and #16 (Rodrigues 2007)

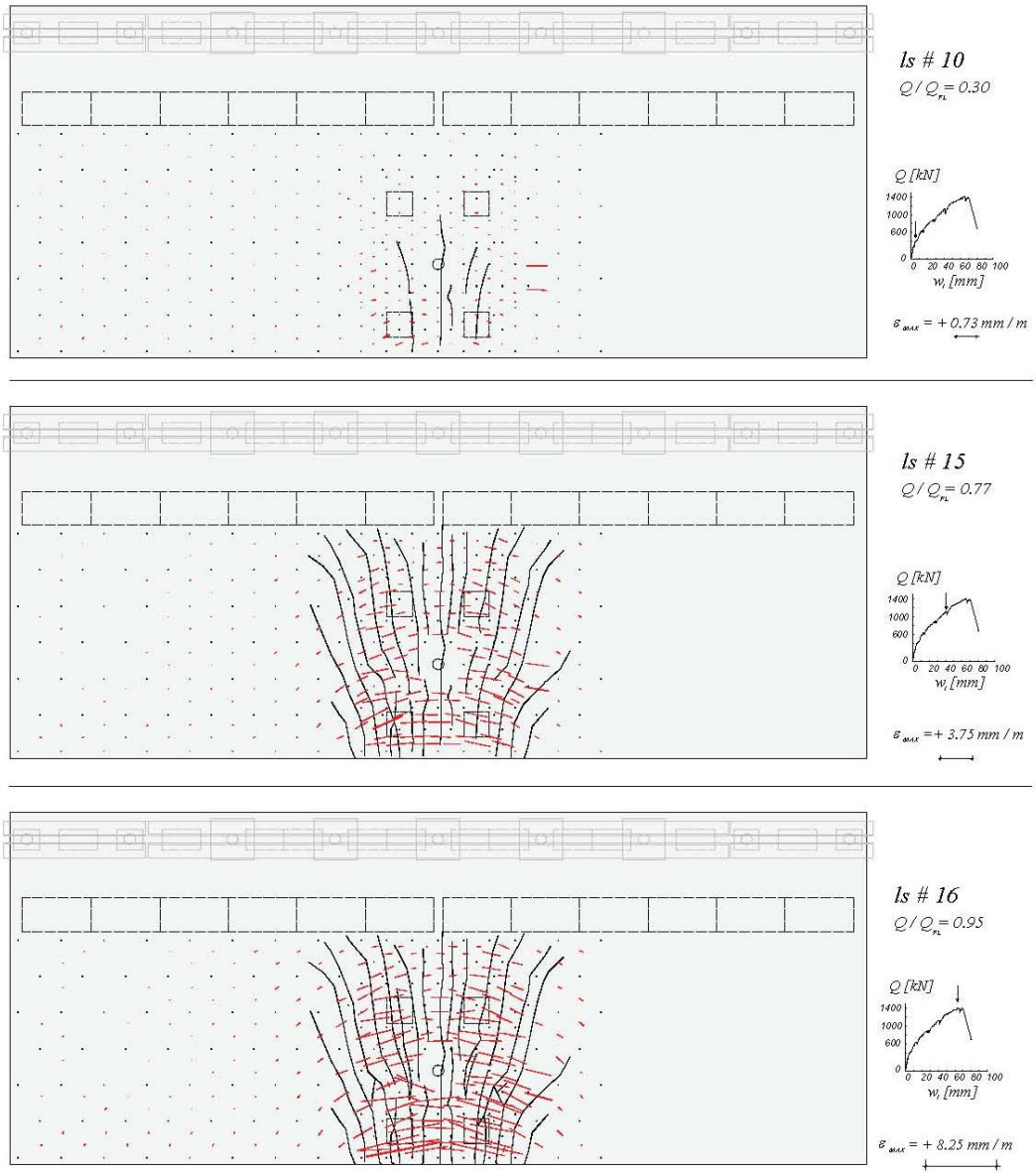

Figure 4-8: Case RS2: Crack pattern and tensile principal strains on the bottom surface for loading stages #10, #15 and #16 (Rodrigues 2007)

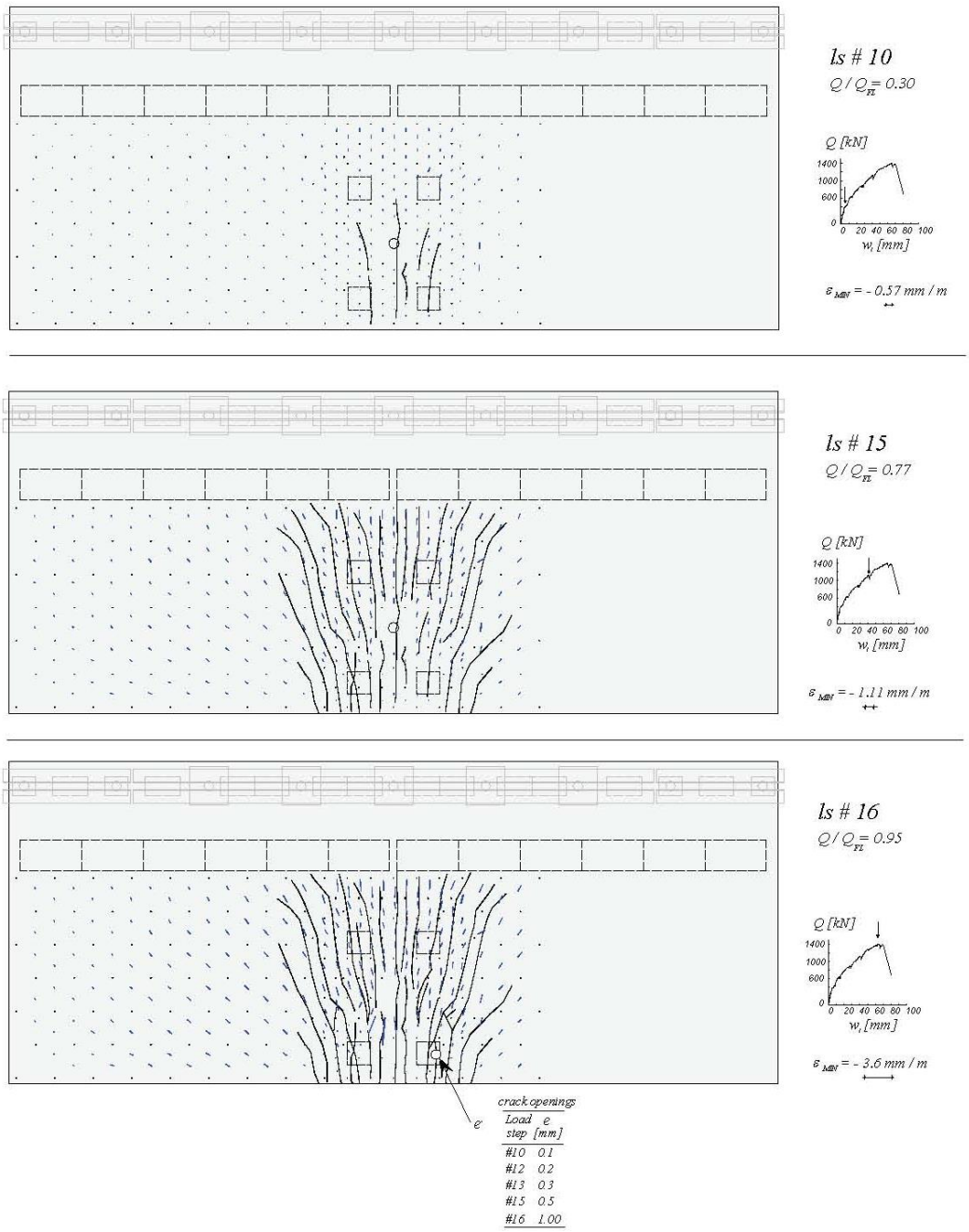

Figure 4-9: Case RS2: Crack pattern and compressive principal strains on the bottom surface for loading stages #10, #15 and #16 (Rodrigues 2007)

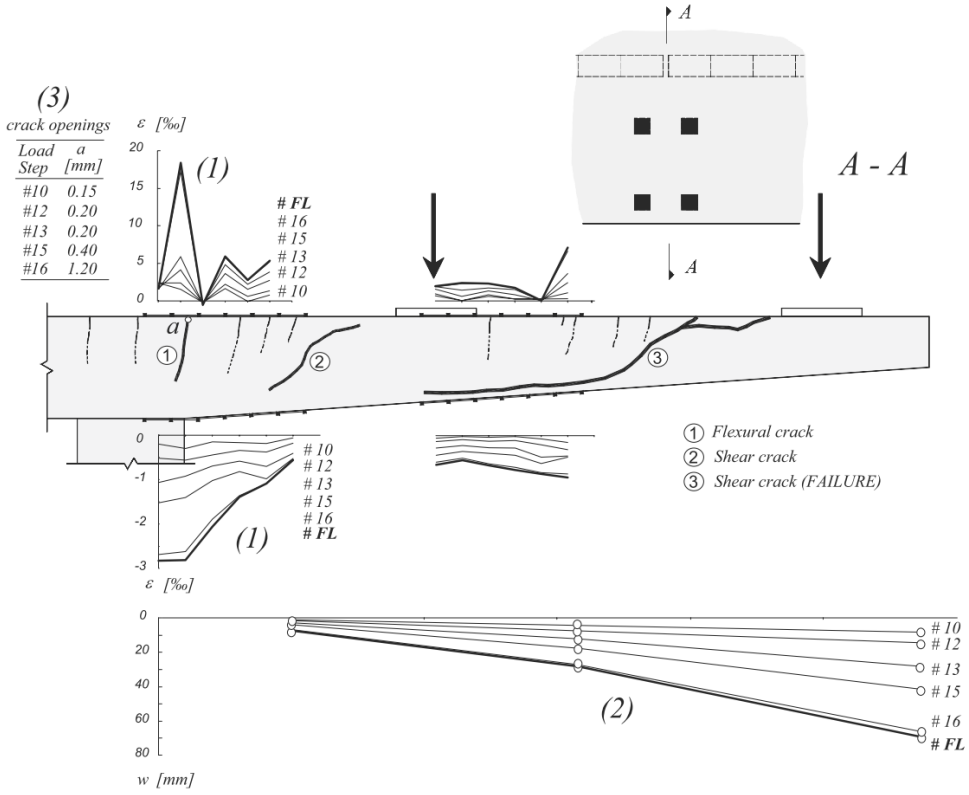

Figure 4-10: Case RS2: (1) Strain measured on the top and the bottom surface, (2) deflections and (3) crack openings (Rodrigues 2007)

For test DR1-a, a large shear crack was observed in the region between the fixed end and the applied loads, see the crack 2 in Figure 4-10. Since no failure occurred in this region, this suggests that a process of development of the shear crack was under way in this region and that redistributions of the shear flow may have occurred.

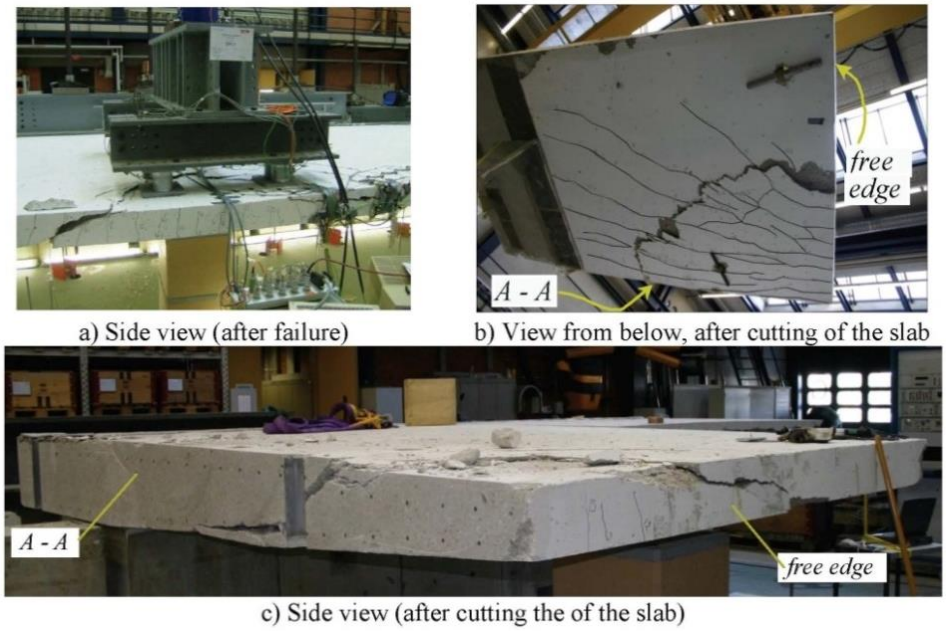

Figure 4-11: Case RS2: Photos after failure (Rodrigues 2007).

4.2 Analytical analysis

The design shear resistance of RS2 slab is calculated according to Model Code 2010 formulation (fib, 2013) and Eurocode 2 formulation while the design punching strength is evaluated according to Eurocode 2 formulation (CEN, 2005). Furthermore the bending resistance of RS2 is evaluated by applying the yield line method.
For simplicity the slab has been considered as a cantilever fixed at the inner supporting block, Figure 4-12.

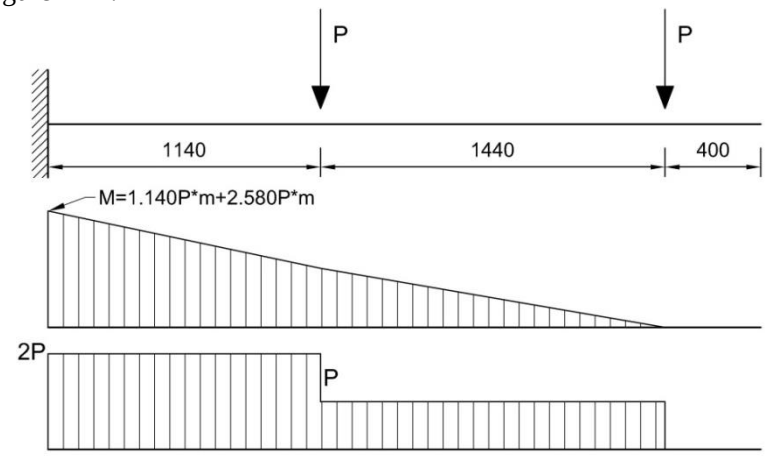

Figure 4-12: Case RS2. Internal forces (dimensions in [mm]).

One-way shear resistance: Model Code 2010
For the evaluation of the design shear resistance two failure mechanisms have been considered: the first in the zone between the inner loads and the fixed end and the second between the loads near the free edge and the inner loads. Since the first mechanism resulted to be the most critical, hand calculations are reported for this configuration, Figure 4-13.

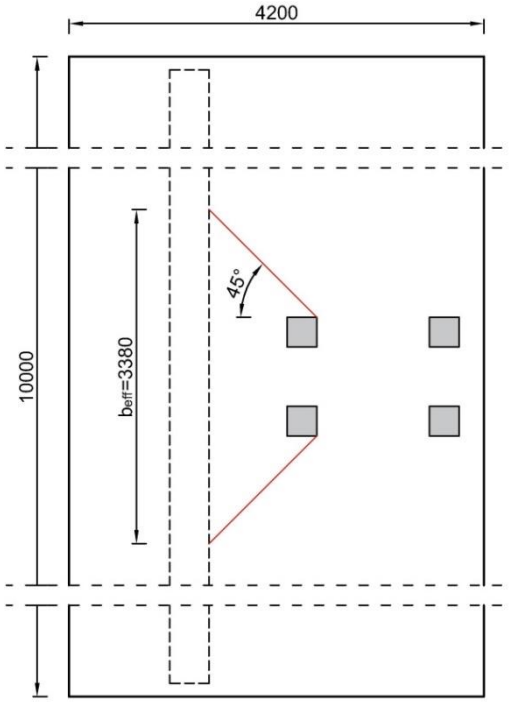

Figure 4-13: Case RS2. Assumed effective width b_{eff} (dimension in [mm])

$b_{eff} = 3380\,mm$

The design shear resistance of a slab is calculated as the design shear resistance of a member without shear reinforcement given and it can therefore be calculated with Level I and Level II of approximation (section 7.3, Model Code 2010):

$$V_{Rd,c} = \cos\alpha\, k_v \frac{\sqrt{f_{ck}}}{\gamma_c} z b_w$$

α - inclination of the sectional taper

At a distance d from the edge of the support the height of the slab is 357 mm; hence the effective depth d_l used in calculation is equal to:

$d_l = 357mm - 30mm - 16/2mm = 319\,mm$

$z = 0.9d = 0.9 \times 319mm = 287.1mm$

The formulation of k_v varies for different Levels of Approximation and is presented in the following for each considered case.

The width b_w is replaced by the effective width b_{eff}, calculated by assuming a 45-degree load spreading from the far corners of the load (the so-called French method). The loading plates nearest to the edge of the support have been taken as reference, Figure 4-13.

Level I Approximation

$$k_v = \frac{180}{1000 + 1.25z} = \frac{180}{1000 + 1.25 \times 287.1mm} = 0.132$$

$$V_{Rd,c} = \cos\alpha k_v \frac{\sqrt{f_{ck}}}{\gamma_c} z b_{eff} = 0.998 \times 0.132 \times \frac{\sqrt{31.11}MPa}{1.5} 287.1mm \times 3380mm = 476.81kN$$

The value of self-weight in kN/m at the consider location is approx. 15.2kN/m. Taking into account that the depth of the slabs varies, it is a conservative assumption.

The reduced shear resistance therefore is:

$V_{Rd,c} = 476.81kN - 15.2\,kN/m \times 3380mm = 425.4kN$

Level II Approximation

Assumed resistance $v_{Ed} = 173.85\frac{kN}{m}$ and bending moment calculated at a distance d from the support:

$m_{Ed} = 0.5v_{Ed}(1140mm - d) + 0.5v_{Ed}(1440mm + 1140mm - d) = 267.9\,kNm/m$

Steel area:

$a_s = \frac{\phi^2\pi}{4} \Big/ 125mm = 2681\,mm^2/m$

Strain parameter:

$$\varepsilon_x = \frac{1}{2E_s a_s}\left(\frac{m_{Ed}}{z} + v_{Ed}\right) = \frac{1}{2 \times 200GPa \times 2681mm^2/m}\left(\frac{267.9\,kNm/m}{287.1mm} + 173.85\frac{kN}{m}\right) = 9.83\times10^{-4}$$

$$k_{dg} = \frac{32}{16 + d_g} = \frac{32}{16+16} = 1 \geq 0.75$$

$$k_v = \frac{0.4}{1+1500\varepsilon_x} \times \frac{1300}{1000 + k_{dg} z} = \frac{0.4}{1+1500 \times 9.83\times10^{-4}} \times \frac{1300}{1000 + 287.1mm} = 0.163$$

$$v_{Rd,c} = \cos\alpha k_v \frac{\sqrt{f_{ck}}}{1.5} z = 0.998 \times 0.163 \frac{\sqrt{31.1}MPa}{1.5} 287.1mm = 173.85\frac{kN}{m}$$

equal to the assumed value.

The value of self-weight in kN/m at the consider location is approx. 15.2kN/m.

The reduced shear resistance is: $v_{Rd,c} = 173.85\frac{kN}{m} - 15.2\frac{kN}{m} = 158.65\frac{kN}{m}$

Shear resistance of the effective width:

$$V_{Rd,c} = v_{Rd,c} b_{eff} = 158.65\frac{kN}{m} \times 3380mm = 536.26kN$$

One-way shear resistance: Eurocode 2

$$V_{Rd,c} = b_{eff} d\left[C_{Rd} k (100\rho_l f_{ck})^{1/3}\right] =$$

$$= 3380mm \times 319mm\left[0.12 \times 1.792\left(100 \times 8.404 \times 10^{-3} \times 31.1\right)^{1/3}\right] = 688.1kN$$

Where:

$$k = 1 + \sqrt{\frac{200}{d}} = 1 + \sqrt{\frac{200}{319}} = 1.792 \le 2;\ \rho_l = \frac{A_s}{d \times s} = \frac{201.1mm^2}{319mm \times 75mm} = 8.404 \times 10^{-3}$$

And is bigger than:

$$V_{Rd,c,\min} = v_{\min} \times b_{eff} \times d = 0.035 k^{\frac{3}{2}} f_{ck}^{\frac{1}{2}} \times b_{eff} \times d = 0.468MPa \times 3380mm \times 319mm = 504.85kN$$

Resistance reduced by the effect of self-weight is:

$$V_{Rd,c} = 688.1kN - 15.2kN/m \times 3.38m = 636.72kN$$

Punching strength: Eurocode 2 formulation

As done for the one-way shear resistance calculation, two control perimeters have been analyzed for the evaluation of the punching strength: control perimeter u_1, around the two inner loads and control perimeter u_2, around the two loads near the free edge.

Since control perimeter u_2 resulted in lower punching strength capacity, only calculations related to the second configuration are reported. The control perimeter u_2 is outlined in red color in Figure 4-14.

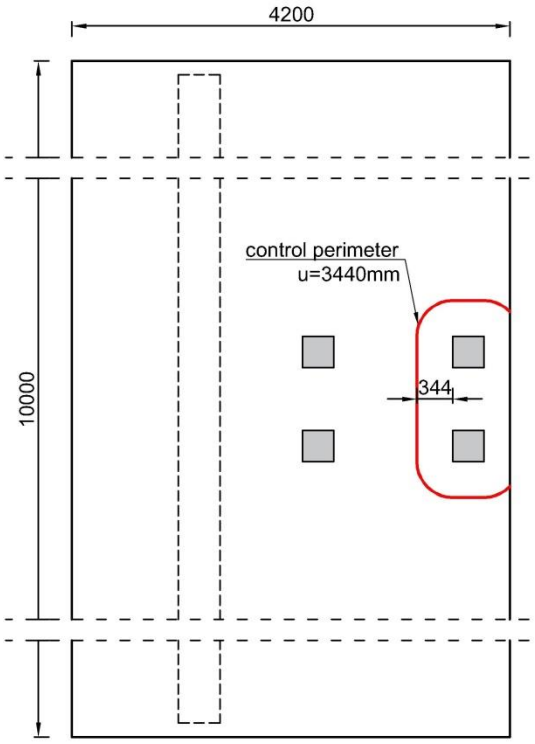

Figure 4-14: Case RS2. Control perimeter according to Eurocode 2 formulation

$$d_l = 217mm - 30mm - \frac{16mm}{2} = 179mm$$

$$d_t = 217mm - 30mm - 16mm - \frac{12mm}{2} = 165m$$

$$d_{eff} = \frac{d_l + d_t}{2} = \frac{0.179mm + 0.165mm}{2} = 172\,mm$$

$$V_{Rdc} = v_{Rdc} \times u \times d_{eff}$$

$$k = 1 + \sqrt{\frac{200}{d_{eff}}} = 1 + \sqrt{\frac{200}{172mm}} = 2.08 \text{ thus } k = 2$$

$$\rho = \sqrt{\rho_l \times \rho_t} = \sqrt{0.0084 \times 0.00457} = 0.0058$$

$$v_{Rdc} = C_{Rd,c} k (100 \times \rho \times f_{ck})^{1/3} = 0.12 \times 2 \times (100 \times 0.0058 \times 31.1)^{1/3} = 0.631MPa$$

$$V_{Rdc} = v_{Rdc} u\, d_{eff} = 0.631MPa \times 3440mm \times 172mm = 373.52MPa$$

$P_{Rd} = 747kN$ and including the self-weight of a punching cone, it is approximately:

$P_{Rd} = 741kN$

Bending resistance: yield line method

The flexural ultimate load was estimated based on the yield-line method. The yield line pattern as illustrated in Figure 4-15 (Rodrigues 2007) resulted in the ultimate load of $Q_{flex} = 1600kN$. It is important to mention that this value of failure load was never reached in the tests. For more information, reference to (Rodrigues 2007) is made.

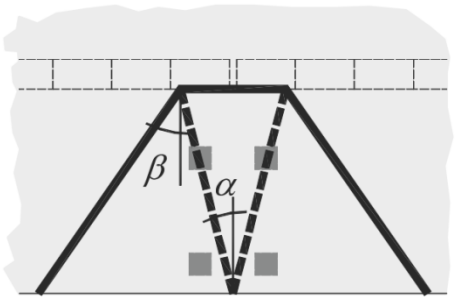

$Q_{Flex} = 1600$ kN

$\alpha = 14°$ $\beta = 35°$

Figure 4-15: Case RS2. Yield-line mechanism and yield-line failure load for considered load configuration

In Table 4-2 the design values of beam resistance expressed in terms of applied load P_{Rd} reduced by the dead load contribution, associated to one-way shear failure, punching failure and bending failure, are summarized.

Table 4-2: Case RS2. Design values of beam resistance expressed in terms of applied load P_{Rd}

	One-way shear (MC 2010)			Punching	Bending
	Level I (kN)	**Level II (kN)**	**EC2 (kN)**	**EC2 (kN)**	**Yield line (kN)**
P_{Rd} (kN)	425.4	536.3	636.7	741	1600

Slab RS2 fails due to one-way shear. Indeed, the design shear resistance associated to one-way shear failure is lower than the design punching resistance and the design bending resistance.

4.3 Finite element model

Units

Units are N, m.

Material models and parameters

The concrete model is based on a total strain rotating crack model with

- exponential softening in tension and parabolic behavior in compression,
- variable Poisson's ratio of concrete
- increase in compressive strength due to lateral confinement according to the model proposed by Selby and Vecchio (Selby and Vecchio 1993).

The mechanical properties for concrete are summarized in Table 4-3. The uniaxial stress-strain curve is shown in Figure 4-16.

Table 4-3: Case RS2. Constitutive model parameters for concrete

	f_{cm} (N/mm^2)	f_{ctm} (N/mm^2)	E_c (N/mm^2)	ν	G_F (Nmm/mm^2)
Mean measured value	39.11	2.94	36030	var	0.141*

*Not specified in reference; estimated according to Model Code 2010 (fib, 2013)

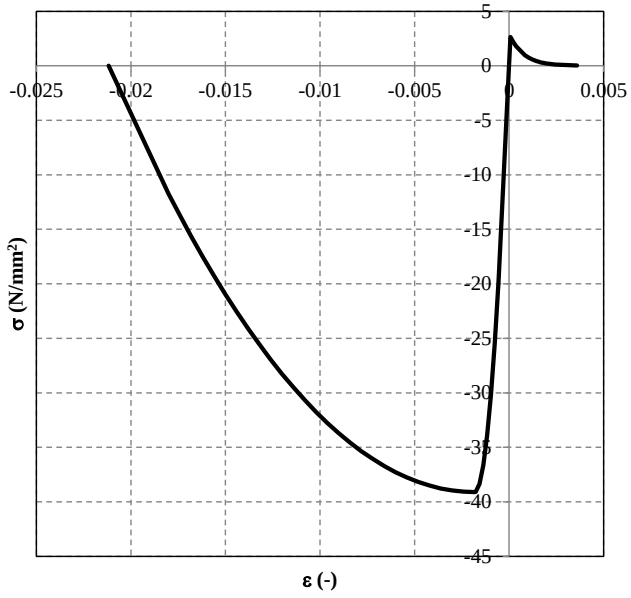

Figure 4-16: Case RS2. Stress-strain curve for concrete

The model for the reinforcement bars and stirrups is based on hardening plasticity. Geometrical and mechanical properties of reinforcing bars are summarized in Table 4-1. The stress-strain curve of the ϕ16 reinforcing bars is plotted in Figure 4-17.

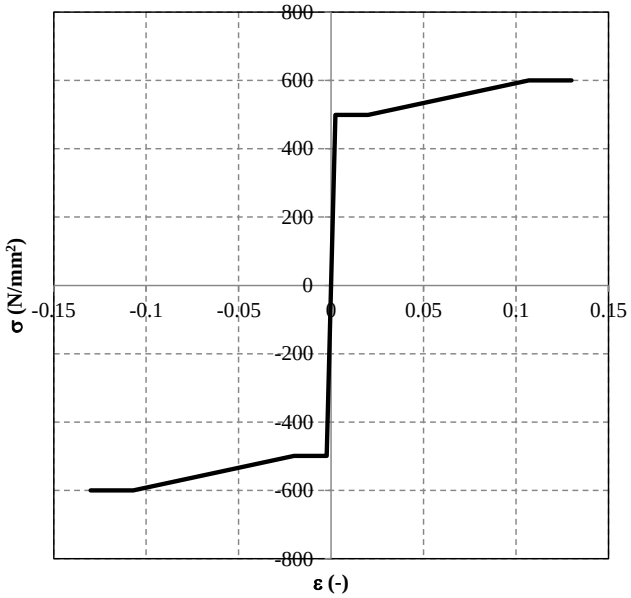

Figure 4-17: Case RS2. Stress-strain curve for ϕ16 reinforcing bars

For the steel plates a linear elastic behavior is assumed, see Table 4-4.

Table 4-4: Case RS2. Steel plates properties

E (N/mm^2)	ν
200000	0.3

Interface elements were used between the steel plates and the concrete slab and between the concrete support and the concrete slab. The thickness of interface elements equals 10 mm. Stress-strain relation in compression was derived by assuming a stiffness equivalent to the stiffness of a layer of mortar 1 mm thick having a Young's modulus equal to the Young's modulus of concrete, Table 4-5.
A bilinear behavior was assumed in the normal direction (Figure 4-18) and a linear elastic relation was assumed in the shear direction. The normal stiffness in tension and the stiffness in shear direction were assumed almost equal to zero.

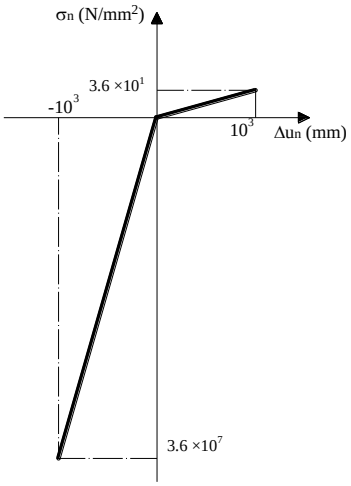

Figure 4-18: Case RS2. Traction-displacement diagram in normal direction for interfaces (not to scale)

Table 4-5: Case RS2. Interface properties

$K_{nn\ in\ tension}$ (N/mm^3)	$K_{nn\ in\ compression}$ (N/mm^3)	K_t (N/mm^3)
3.6×10^{-2}	$3.6\times10^{+4}$	3.6×10^{-2}

Element types and finite element mesh

For meshing the concrete slab, 20-node solid elements (CHX60) with a full Gauss integration scheme (3×3×3) were used. The average element size is 57×90×100 mm.
The reinforcement bars and stirrups were modelled with embedded truss elements with two Gauss integration points along the axis of the element. Perfect bond is assumed. For the steel plates and the concrete supports 20-node solid elements (CHX60) with a full Gauss integration scheme (3×3×3) are used.
The 20-node interfaces element (CQ48I) were used with the 4×4 Newton-Cotes integration points.
The adopted dimensions for the slab and for the transversal cross section of the slab are given in Figure 4-19. Due to geometrical and loading symmetry conditions, only an half of the slab was modelled.

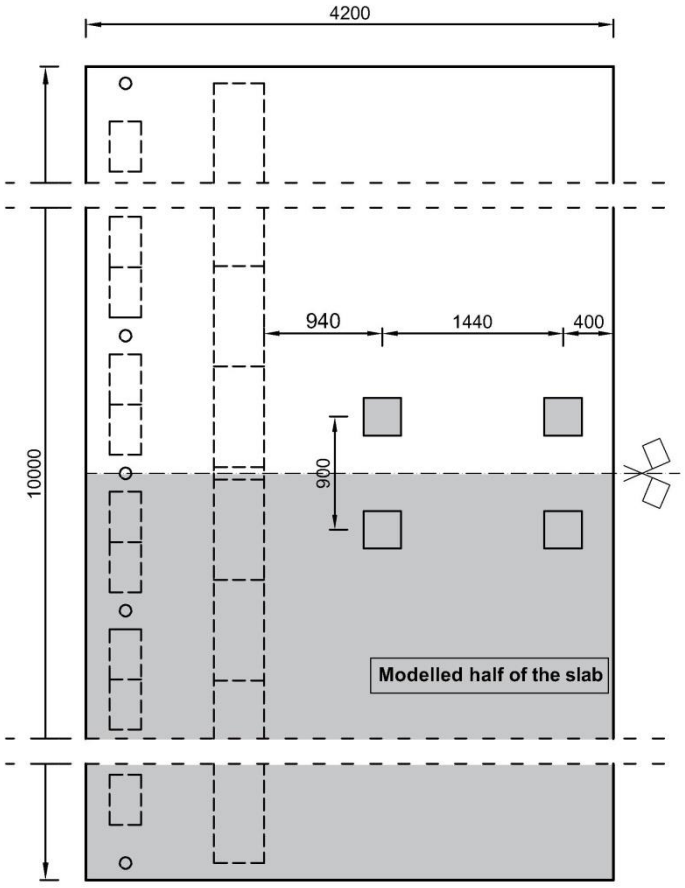

(a)

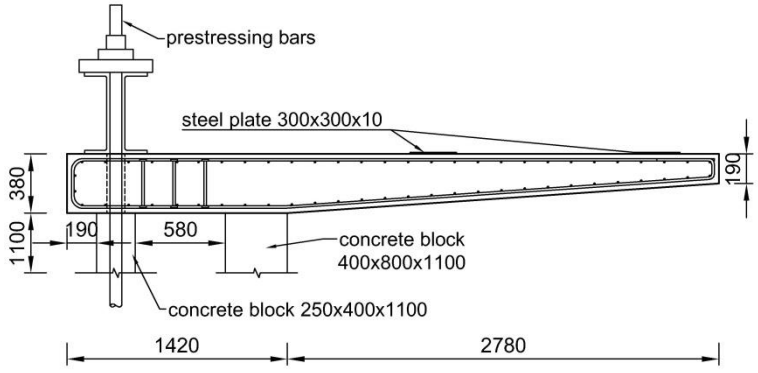

(b)

Figure 4-19: Case RS2. Dimensions adopted for the slab (in mm): (a) top view and (b) transversal section

The reinforcement layout details as modelled in the program are illustrated in Figure 4-20. For the true as given in the reference see Figure 4-1.

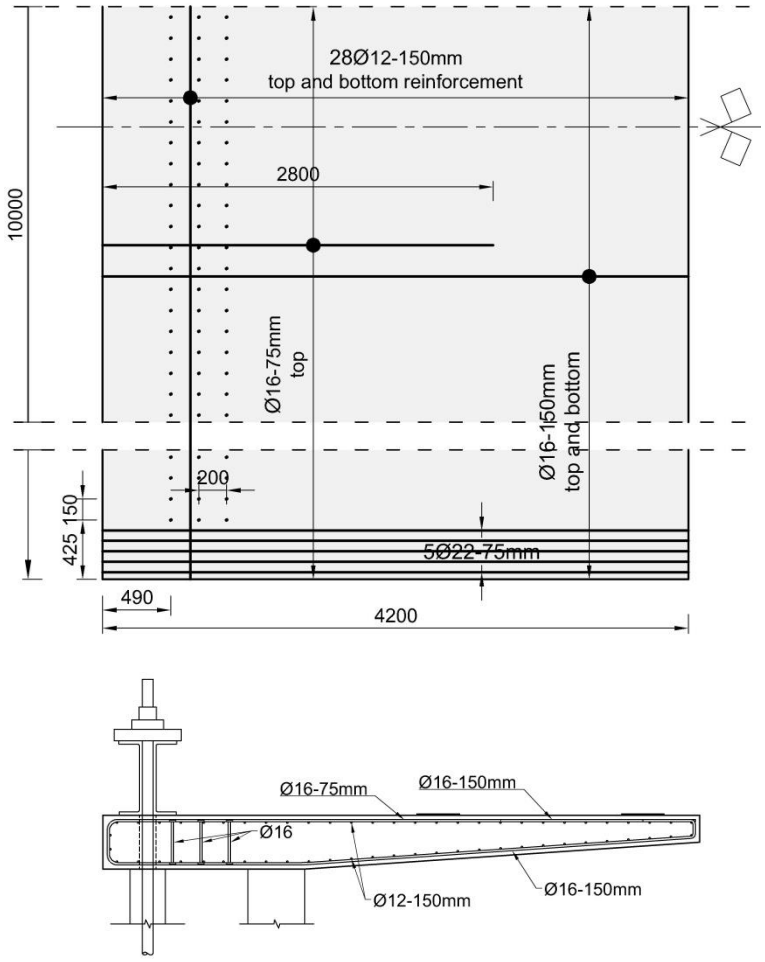

Figure 4-20: Case RS2. Top reinforcement details of the slab (in mm)

The mesh of the slab is presented in Figure 4-21(a). The different materials are indicated with different colors in Figure 4-21(b).

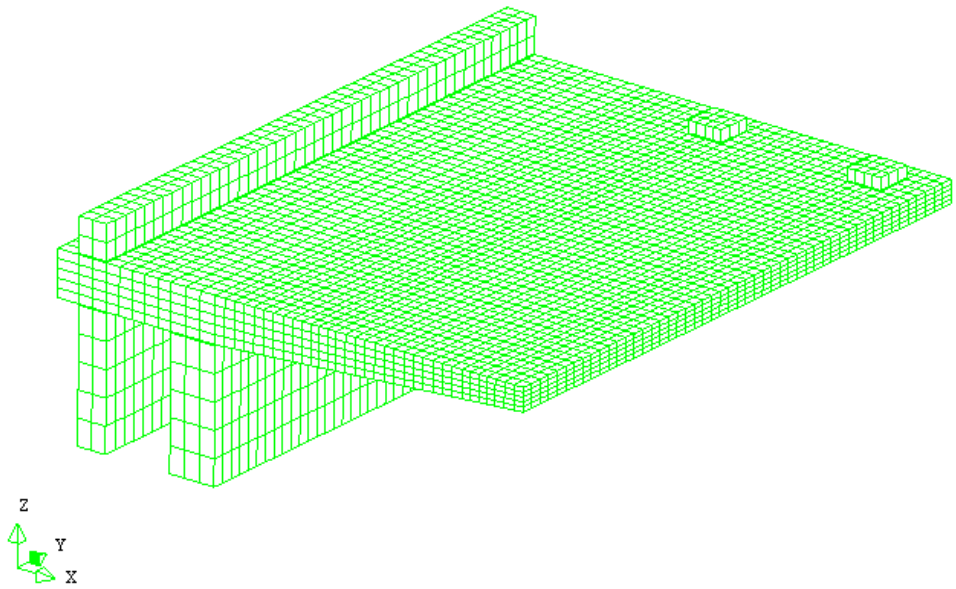

(a)

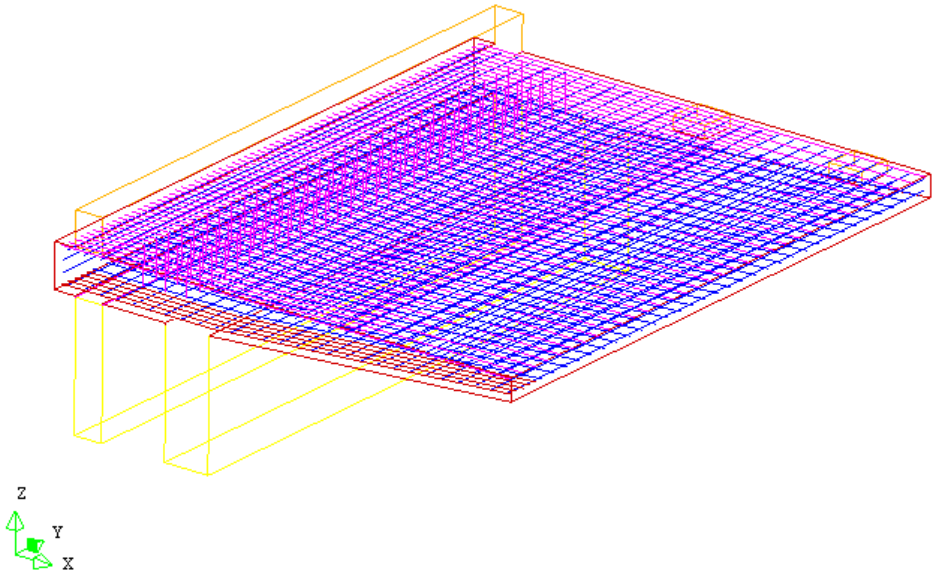

(b)

Figure 4-21: Case RS2. (a) Mesh and (b) material sets

Different groups of elements were defined to distinguish the concrete elements that can be subjected to crushing or cracking and the steel elements that can yield during the analysis. For monitoring steel yielding the groups TOPL12 (Figure 4-22), TOPT16 (Figure 4-23), BOTL12 (Figure 4-24), BOTT12 (Figure 4-25), BOTT22 (Figure 4-26) and VERT16 (Figure 4-27) referring to reinforcing bars of the slab were created.

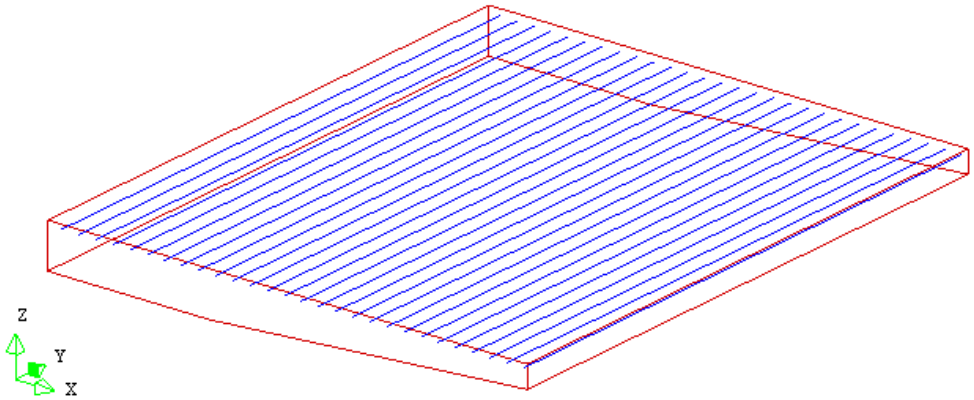

Figure 4-22: Case RS2. Group of steel elements “TOPL12”

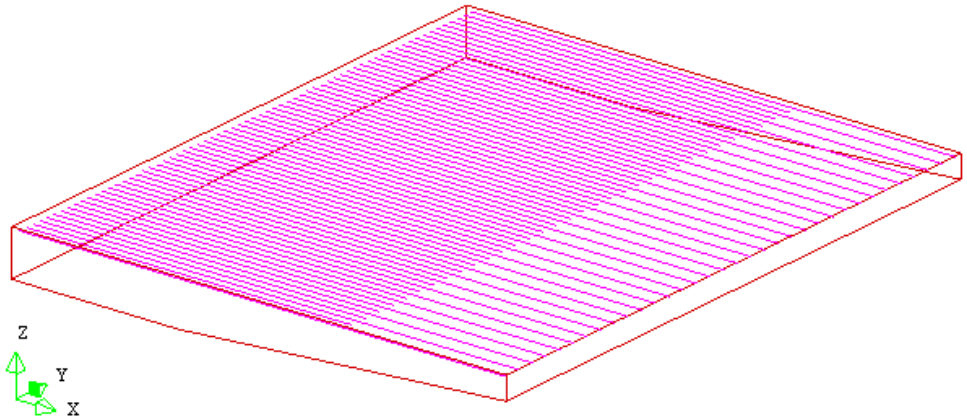

Figure 4-23: Case RS2. Group of steel elements “TOPT16”

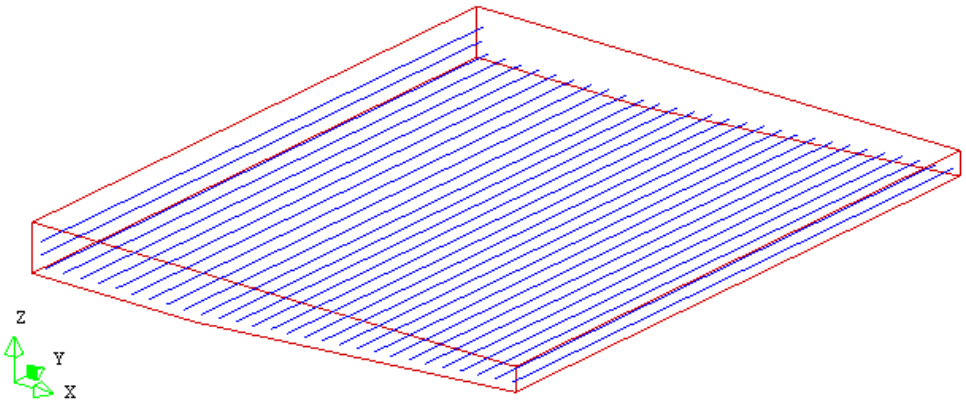

Figure 4-24: Case RS2. Group of steel elements “BOTL12”

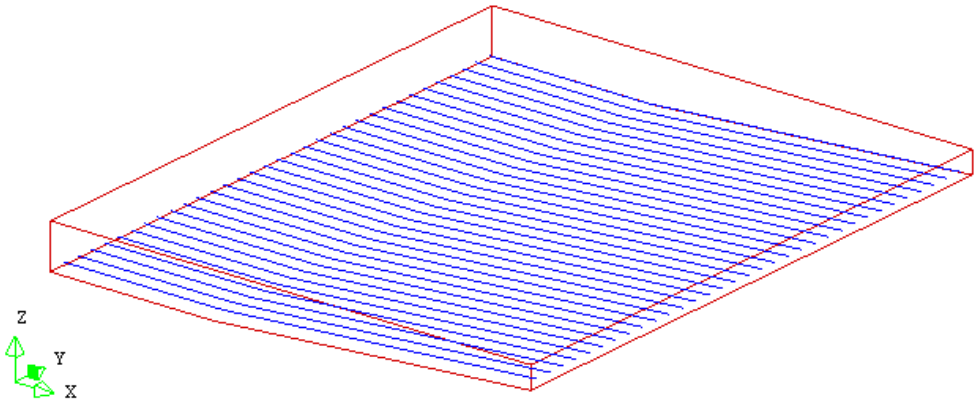

Figure 4-25: Case RS2. Group of steel elements “BOTT12”

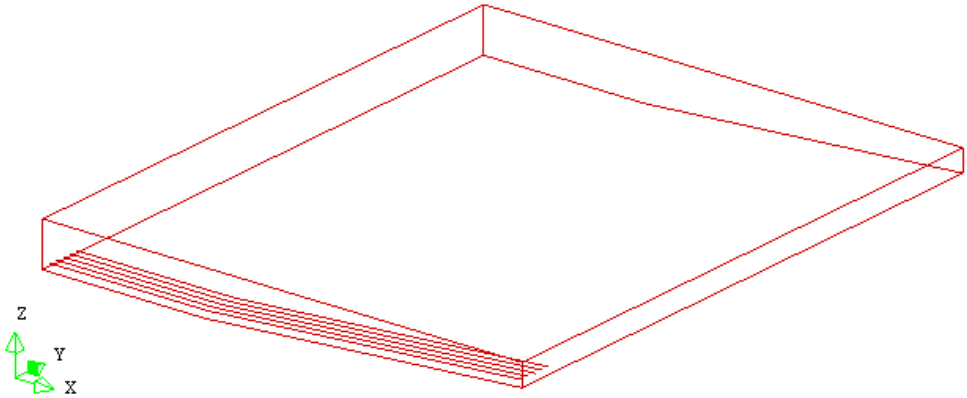

Figure 4-26: Case RS2. Group of steel elements “BOTT22”

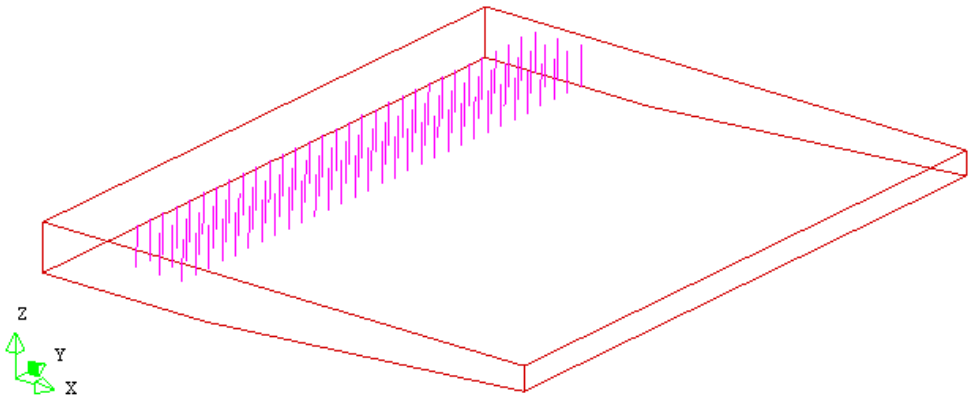

Figure 4-27: Case RS2. Group of steel elements “VERT16”

Figure 4-28 shows the group of elements named “LONG” and “TRANSVE”, used for monitoring the inelastic behavior of concrete.

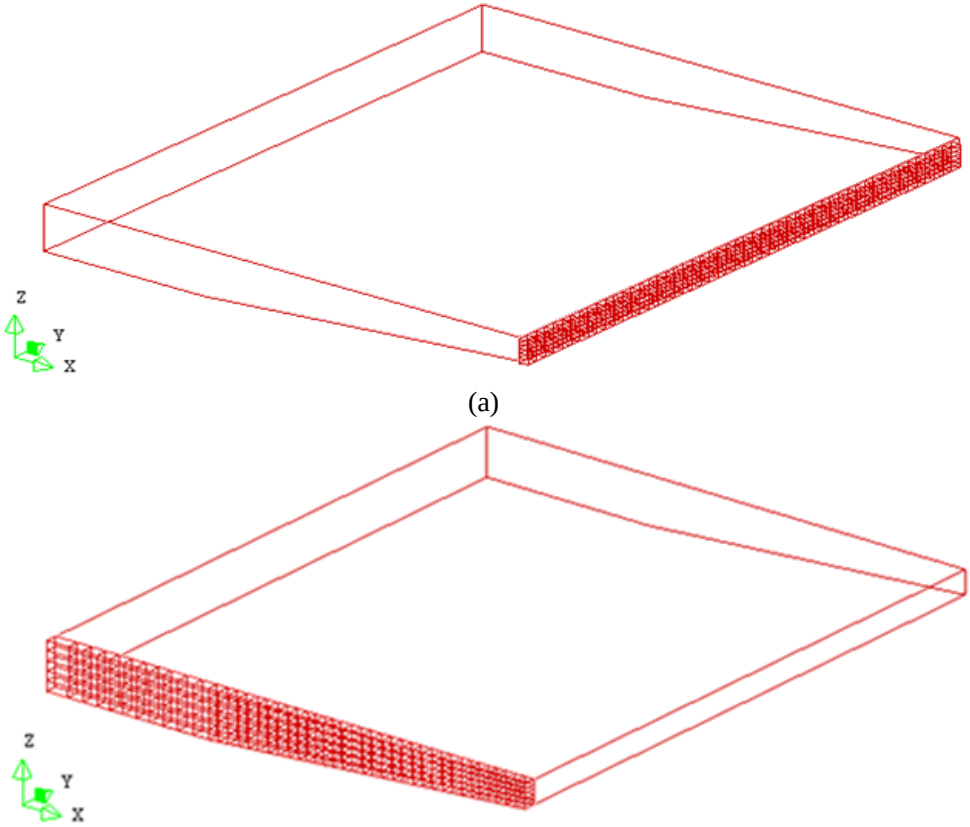

Figure 4-28: Case RS2. Definition of the element sets (a) TRANSVE and (b) LONG

Boundary conditions and loading

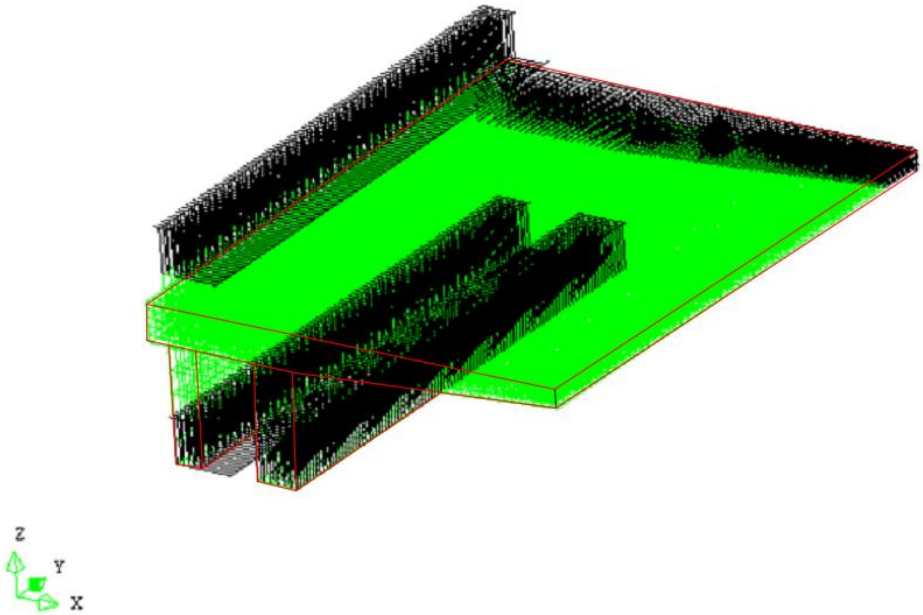

Figure 4-29: Case RS2. Boundary conditions

Due to the symmetry of geometry and loading condition only a half of the slab was analyzed. Interface elements were situated at the locations of the clamped (prestressed) end – support 1, supporting concrete block – support 2 and loading plates, Figure 4-29. Boundary conditions along the symmetry plane prevent the translations along *y* axis. Prestressed bars were not modelled; translation along *x* direction of the upper central row of steel support 1 and the lower central row of concrete support 1 are prevented. Tying along *x* direction of the lower central row and the upper central row of the concrete support 1 is applied. Translation along *z* axis of the support 1 and 2 are prevented, Figure 4-29.

Load increments and convergence criteria

Load case 1 is applied in a single step. The regular Newton-Raphson method with a maximum of 25 iterations is used. As the convergence criteria, norms of force and energy are selected. The analysis continues even if the convergence criteria are not satisfied. The convergence tolerances are equal to 1×10^{-2} for a force norm and equal to 1×10^{-3} a energy norm.

Load case 2 is applied with automatic adaptive load increments. A concentrated force is applied to the central nodes of the loading plates. The initial load factor equals 1, the upper limit of the incremental load factor is 10 and the lower limit of the incremental load factor equals 1. The maximum number of steps is 20. Arc-length control was applied based on translation along *z* axis of node 121532 ("indirect displacement control"), Figure 4-30. The analysis continues even if the convergence criteria are not satisfied. The convergence tolerances are equal to 1×10^{-3} and 1×10^{-2} for energy and force norms, respectively. A maximum of 50 iterations is used. A line search algorithm is used to improve the convergence performance.

Load case 3 is applied with automatic adaptive load increments. A concentrated force, lower than the concentrated force applied to load case 2, is applied to the central nodes of the loading plates. The initial load factor equals 1, the upper limit of the incremental load factor equals 10 and the lower limit of the incremental load factor equals 1. The maximum number of steps is 70. Arc-length control was applied based on translation along *z* axis of node 121532 ("indirect displacement control"). The analysis continues even if the convergence criteria are not satisfied. The convergence tolerances are equal to 1×10^{-3} and 1×10^{-2} for energy and force norms, respectively. A maximum of 50 iterations is used. A line search algorithm is used to improve the convergence performance. Load case 3 was added to load case 2 in order to improve the convergence path, decreasing the load step size.

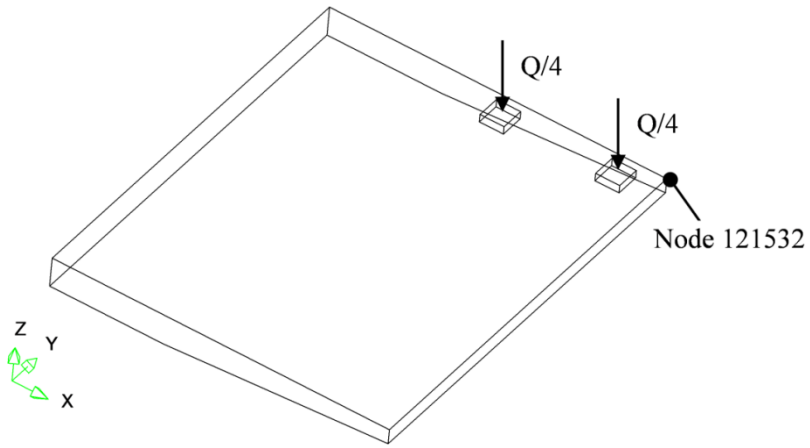

Figure 4-30: Case RS2. `Indirect Displacement control' technique applied referring to node 121532

4.4 Nonlinear finite element analysis

Load deflection

The load-deflection curve is presented in Figure 4-31 where the applied load value corresponding to the peak load is reported. Until the peak load, neither crushing of concrete nor yielding of reinforcement was observed. The plotted deflection refers to the node 121532 (deflection w1 at the free end of the slab according to the experiment).For load case 2 the peak load was defined as the highest load step for which the energy norm ratio satisfied the fixed tolerance of 1×10^{-3}. The convergence performance after reaching the peak load at step 21 was poor. After step 21, the analysis continues even though the energy and force convergence criteria were not satisfied within the maximum number of iterations equal to 50. The post peak branch of the load-deflection curve is for this reason plotted with a dot-dash line.

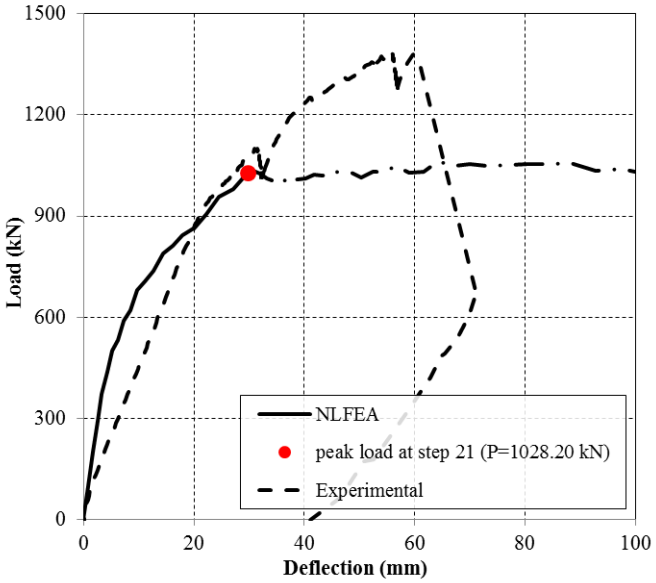

Figure 4-31: Case RS2. Load-deflection curve

In the experiments, prior to loading the cantilever to failure, the cantilever had been subjected to about two hundred load cycles from Q = 0 to Q = 400 kN. This has not been considered in NLFEA and might have influenced the response of the structure.

Convergence behavior

For most steps the convergence was reached on the basis of the energy criterion, Figure 4-32 and Figure 4-33.

For load case 2 and load case 3 the energy norm ratio satisfied the fixed tolerance of 1×10^{-3} for all the steps of the analysis till the peak was reached.

No convergence was obtained after the peak. The relatively low number of iteration permitted in each step (equal to 50) was substantiated by high computational time demand to perform the analysis.

The force norm ratio was higher than the fixed tolerance of 1×10^{-2} for the vast majority of steps.

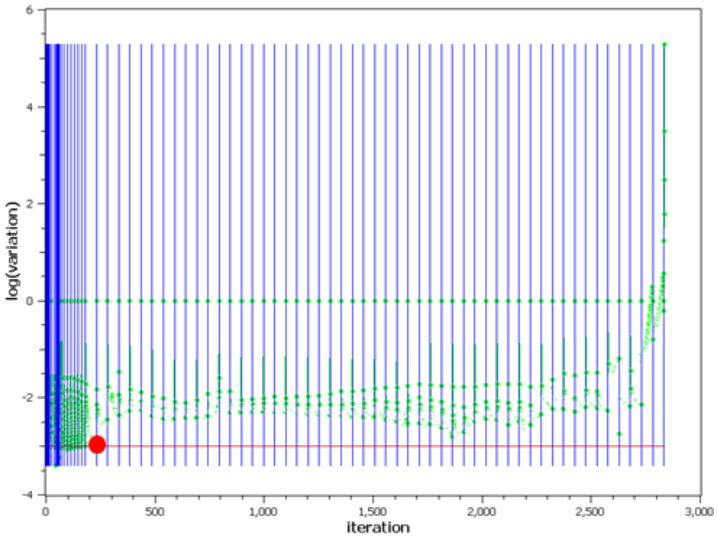

Figure 4-32: Case RS2. Evolution of the energy norm (blue lines indicate steps, red line indicates tolerance, green points indicate iterative results)

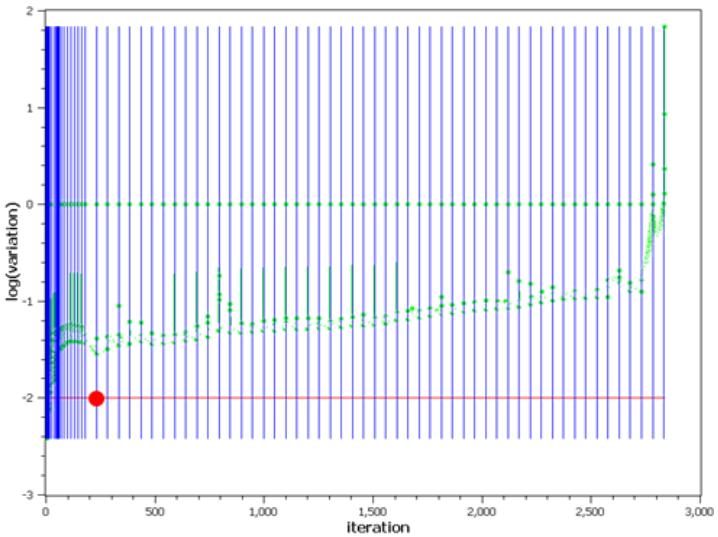

Figure 4-33: Case RS2. Evolution of the force norm (blue lines indicate steps, red line indicates tolerance, green points indicate iterative results)

Strains

Figure 4-34 till Figure 4-36 show the crack strain values at the peak load (at step 21) for the whole slab at top and bottom as well as for the groups TRANSVE and LONG.

The first crack strain value plotted, equal to 0.00076, corresponds to the ultimate crack strain value calculated as $\varepsilon_{t,u} = \frac{G_F}{h \cdot f_{ctm}} = \frac{0.141 Nmm/mm^2}{70mm \times 2.65} = 0.00076$, while the third crack strain value, equal to 0.0035, is the crack strain value corresponding to 1% of f_{ctm}. An intermediate crack strain value was added in the contour plot.

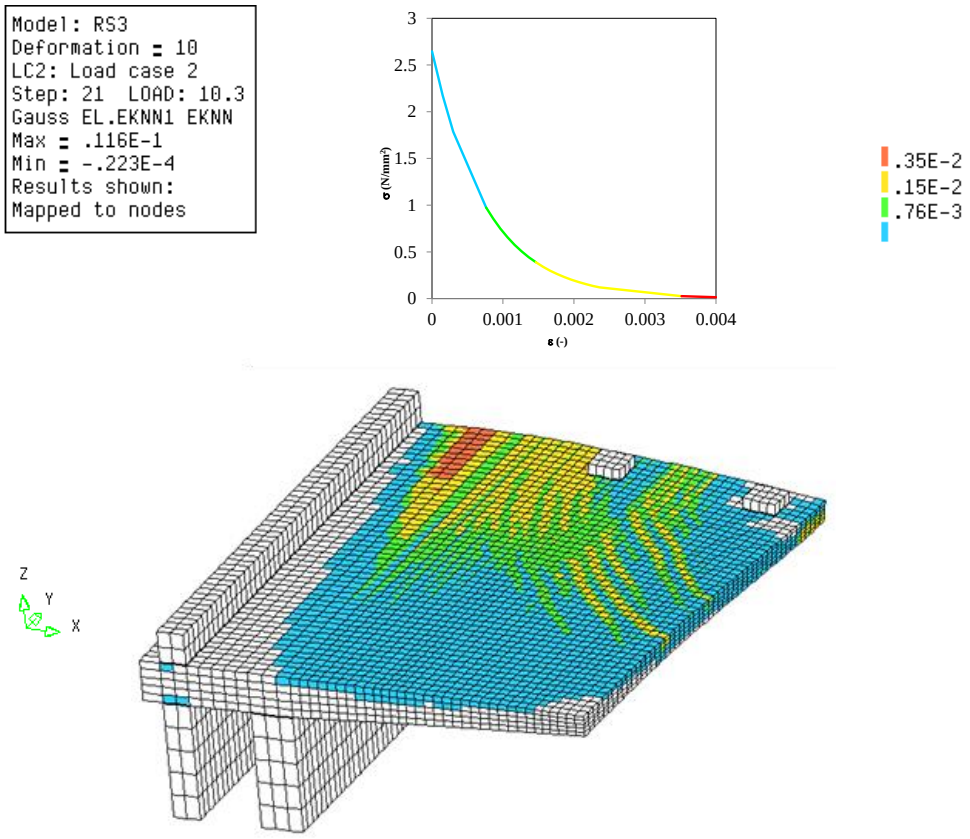

Figure 4-34: Case RS2. Crack strain values at the top of the slab at step 21 (P=1028.20 kN)

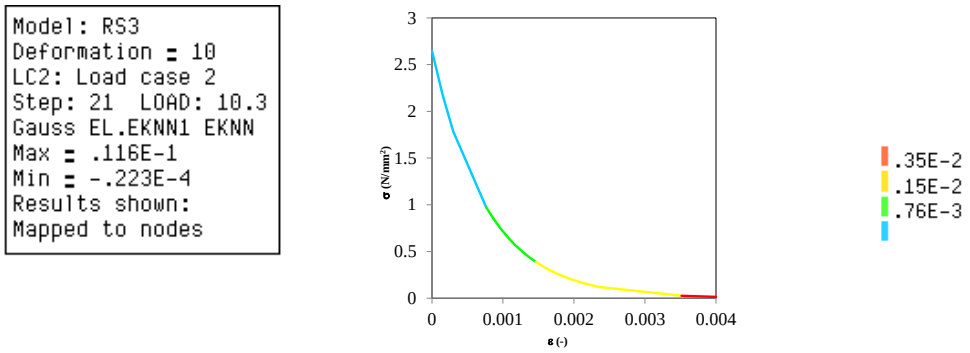

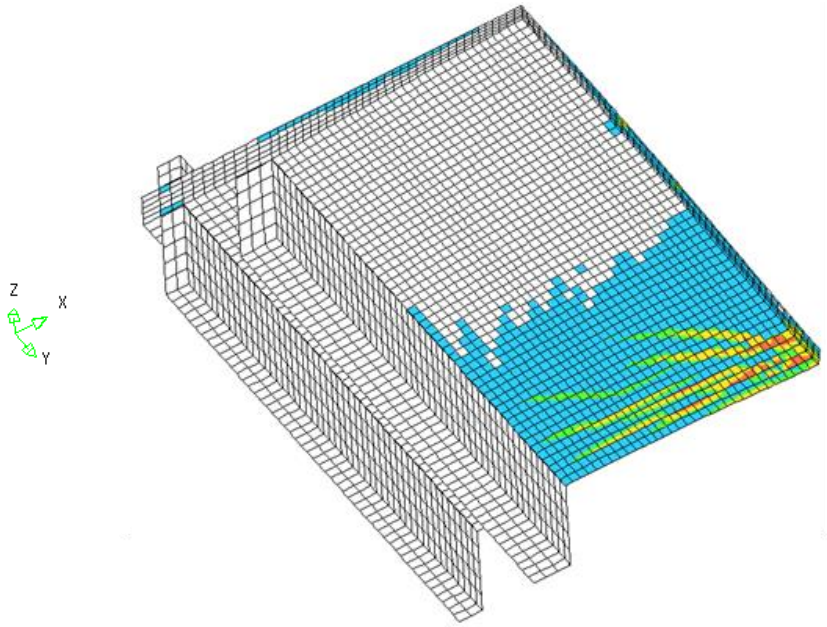

Figure 4-35: Case RS2. Crack strain values at the bottom of the slab at step 21 (P=1028.20 kN)

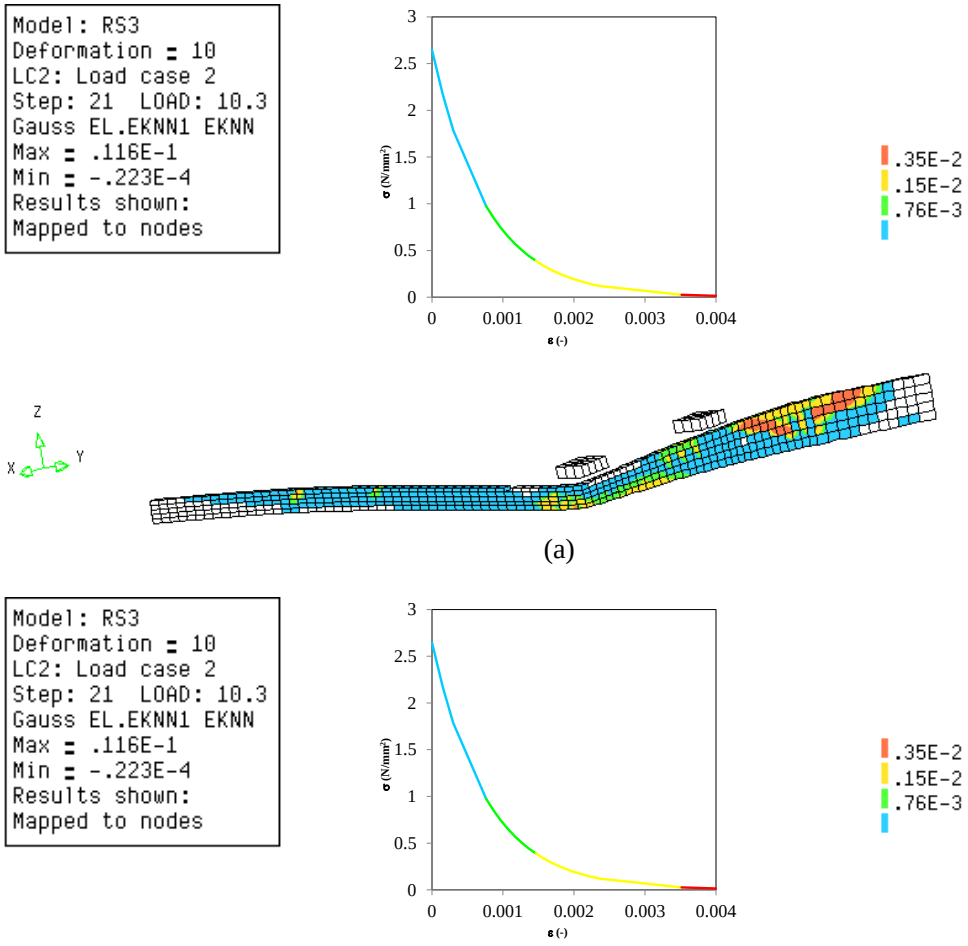

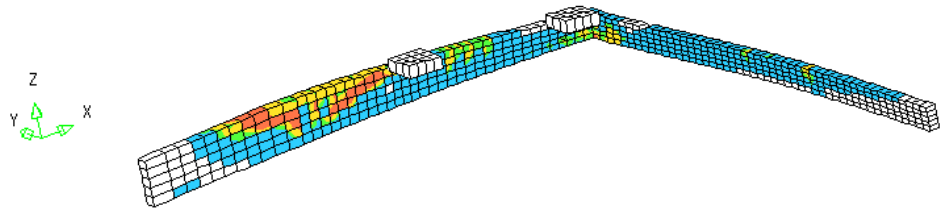

(b)

Figure 4-36: Case RS2. Crack strain values at step 21 (P=1028.20 kN) of TRANSVE and LONG groups: (a) outer side, (b) inner side

The crack pattern obtained from NLFEA well matches with the experimental crack pattern (see Figure 4-7 and Figure 4-11). The similarities featured in both NLFE analysis and experimental crack pattern are flexural cracks on the top surface as well as the shear crack between the inner loading plate and the supporting concrete block. Because the peak load resulting from the numerical analysis was reached at a relatively low load step, the shear crack between two loading plates has not developed yet.
.

Gauss point statistics

In Table 4-6 lists the number of cracking points, crushing points and yield points at step 21 (peak load) are reported.

Table 4-6: Case RS2. Number of cracking points, crushing points, and yield points

PEAK LOAD						
STEP	**21**	**ITERATIONS**		18		
GROUP NAME	**PLAST**	**PRV. PL**	**CRITIC**	**PLAST NEW**	**PRV.PL NEW**	**CRITIC NEW**
TOTAL MODEL	0	0	0	0	0	0
CRACKING LOGGING SUMMARY						
GROUP NAME	**CRACK**	**OPEN**	**CLOSED**	**ACTIVE**	**INACTI**	**ARISES**
slab_brick	151763	151761	2	116511	35252	6955
LONG	2854	2854	0	2083	771	176
TRANSVE	4856	4855	1	3909	947	353
TOTAL MODEL	151763	151761	2	116511	35252	6955

4.5 Application of Safety Formats Model Code 2010

Safety formats for non-linear finite element analyses as proposed by the Model Code 2010 (fib, 2013) include three numerical methods denoted GRF (Global Resistance Factor method), PF (Partial Factor method) and ECOV (Method of Estimation of a Coefficient of Variation of resistance). Application of safety formats requires a total of 4 non-linear analyses. Each analysis requires different material characteristics derived from the mean measured values. Table 4-7 to Table 4-10 the mechanical properties applied in the non-linear analyses are summarized.

Table 4-7: Case RS2. Constitutive model parameters for concrete

	f_c (N/mm^2)	f_{ct} (N/mm^2)	E_c (N/mm^2)	ν	G_F (Nmm/mm^2)	G_C (Nmm/mm^2)
Mean measured	39.11	2.97	36030	Var.	0.141	35.308
Characteristic	31.11	2.08	31386	Var.	0.136	33.883
Mean GRF	26.44	2.66	29731	Var.	0.132	32.906
Design	20.74	1.38	27415	Var.	0.126	31.498

Table 4-8: Case RS2. Constitutive model parameters for reinforcing bars ϕ16

	Φ (mm)	A_s (mm^2)	f_y (N/mm^2)	f_t (N/mm^2)	E_s (N/mm^2)	ε_{sy}
Mean measured	16	201	499.00	600.00	210000	0.00238
Characteristic	16	201	451.97	543.45	210000	0.00215
Mean GRF	16	201	497.16	597.79	210000	0.00237
Design	16	201	393.01	472.56	210000	0.00187

Table 4-9: Case RS2. Constitutive model parameters for reinforcing bars ϕ 12

	Φ (mm)	A_s (mm^2)	f_y (N/mm^2)	f_t (N/mm^2)	E_s (N/mm^2)	ε_{sy}
Mean measured	12	113	541.00	629.00	210000	0.00258
Characteristic	12	113	490.01	569.71	210000	0.00233
Mean GRF	12	113	539.01	626.68	210000	0.00257
Design	12	113	426.09	495.40	210000	0.00203

Table 4-10: Case RS2. Constitutive model parameters for reinforcing bars ϕ 22

	Φ (mm)	A_s (mm^2)	f_y (N/mm^2)	f_t (N/mm^2)	E_s (N/mm^2)	ε_{sy}
Mean measured	22	380	534.00	644.00	210000	0.00254
Characteristic	22	380	483.67	583.30	210000	0.00230
Mean GRF	22	380	532.03	641.63	210000	0.00253
Design	22	380	420.58	507.22	210000	0.00200

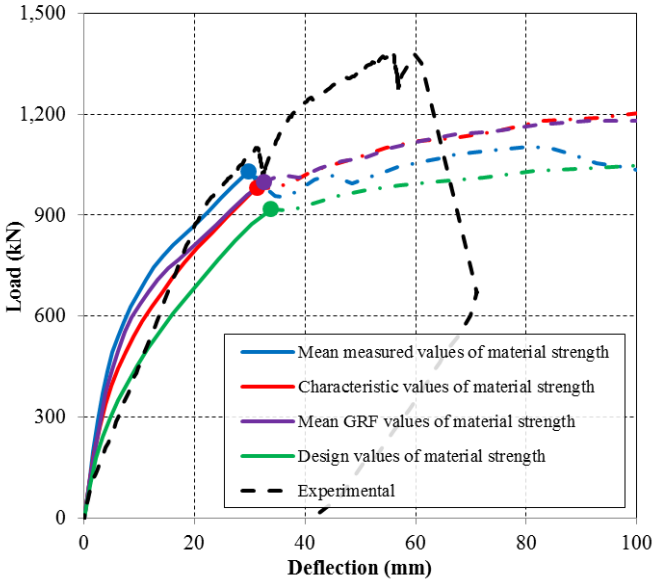

Figure 4-37: Case RS2. Load-deflection curves obtained with mean measured, characteristic, mean GRF and design mechanical properties

In Figure 4-37 the load-deflection curves obtained with mean measured, characteristic, mean GRF and design values of material strengths are shown. The peak load values are indicated in the graph with circular indicators.

The load carrying capacity of the slab RS2 was searched for by means of analytical and numerical methods. In Figure 4-38 the comparison of the found expressed in terms of percentage of the experimental ultimate value of applied load is shown. The analysis named "no safety format" refers to a NLFE analysis carried out using mean measured values of material strengths without applying any safety coefficient.
The explicit values of slab resistance resulting from the analytical and numerical analyses are given in Table 4-11. The results are presented in a form of the ultimate value of load that the slab can be subjected to.

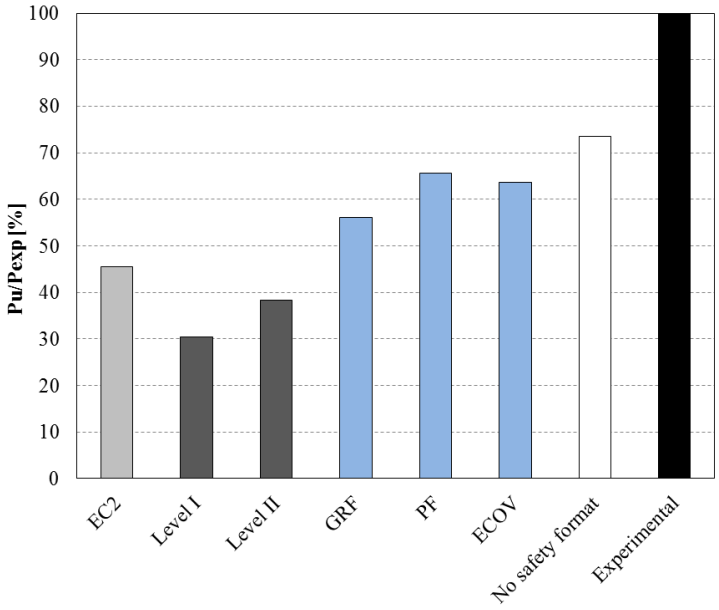

Figure 4-38: Case RS2. Analytical and numerical design values of slab resistance expressed in terms of a percentage of the experimental ultimate value of applied load, P_{Exp}=1397 kN

Table 4-11: Case RS2. Values of slab resistance, expressed in terms of applied load P_{Rd}

P_{Exp} (kN)	EC2 (kN)	Level I MC2010 (kN)	Level II MC2010 (kN)	GRF (kN)	PF (kN)	ECOV (kN)	No safety formats (kN)
1397	636.7	425.4	536.3	784.59	917.00	889.91	1028.20

4.6 Concluding remarks

Slab RS2 is a model of the bridge deck cantilever without shear reinforcement under a group of concentrated loads. The model is a ¾ scale model with a span of 2.8m, a length 10m and variable thickness ranging from 0.38 near the clamped end to 0.19 at the free edge. The slab failed in shear at the load equal to P=1397kN.
The slab was modelled with 20-node brick elements for the concrete and embedded truss elements for the reinforcement. Perfect bond is assumed. The concrete model is based on a total strain rotating crack model with exponential tension softening in

tension and parabolic behavior in compression, variable Poisson's ratio of concrete and no reduction of compressive strength of concrete due to lateral cracking. The model for the reinforcement bars is based on hardening plasticity.

The numerical model with mean measured material properties resulted in a shear failure mechanism at a load equal to P=1028.2kN (around 74% of the ultimate load from the experiment).

The design value of slab resistance was searched for with application of safety formats. The resulting values of the resistance from numerical analyses appear to be higher than the estimates from analytical methods.

5 Case RS3 (S1T1): Lantsoght et al. (2012)

An experimental program at the Stevin Laboratory, TU Delft, comprises of 10 slabs having different reinforcement ratios and different load positions.
In order to better evaluate the shear resistance of one-way slabs, a series of experiments was carried out on continuous one-way slabs subjected to concentrated loads close to the supports, in which the load position, transverse reinforcement ratio and concrete strength were basic variables. Slab S1T1 (Lantsoght, 2012; Lantsoght 2013; Lantsoght et al. 2013) has been selected and will be denoted here as RS3.

5.1 Experimental setup and results

Geometry

The dimensions of slab RS3 are 5 m × 2.5 m, the thickness is 0.3 m. In Figure 5-1 the geometry of the slab and the reinforcement layout are given. Longitudinal reinforcement at the bottom consists of 21 ϕ20/125mm whereas longitudinal reinforcement at the top is 21 ϕ20/125mm in the zone subjected to negative moments (over a distance of 3 m from the prestressed end) and 11 ϕ 10/250 in the zone subjected to positive moments (over a distance of 2.3 m from the simply supported end), see Figure 5-1. Transversal reinforcement is 21 ϕ10/250 placed both at the top and bottom sides. The concrete cover is 25 mm.

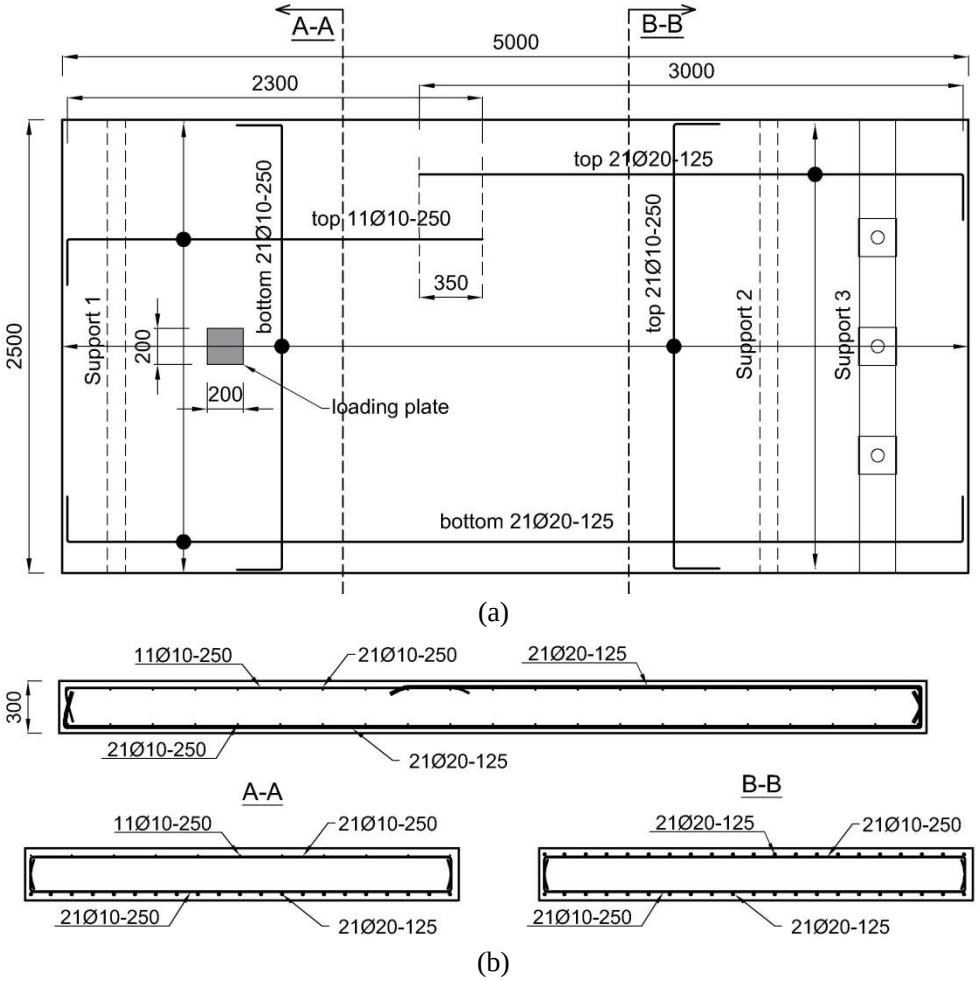

Figure 5-1: Case RS3. (a) Layout and (b) side views of reinforcement (in mm)

Material Properties

Concrete and reinforcement properties given in reference are reported in Table 5-1.

Table 5-1: Case RS3. Concrete and reinforcement properties

Concrete properties					
f_{cm} (N/mm^2)		$f_{ctm,sp}$ (N/mm^2)		d_{max} (mm)	
29.71*		3.1		16	
Reinforcement properties					
Bar	Φ (mm)	A_s (mm^2)	E_s (N/mm^2)	f_{ym} (N/mm^2)	f_{tm} (N/mm^2)
ϕ10	10.0	79	210000	537	628
ϕ20	20.0	314	210000	541	658
Φ36 Dywidag	36.0	1018	210000	1000	-

*f_{cm} is a converted value using a conversion factor of 0.83
$f_{cm,cyl} = 0.83 \times f_{cm,cub} = 0.83 \times 35.8MPa = 29.71MPa$ where 35.8MPa is given in the reference

Loading and Boundary Conditions

Continuous supports are placed along short edges of the slab. One edge of the slab is simply supported while the opposite edge is clamped by prestressed bars to eliminate rotations, Figure 5-2. The load is applied deformation controlled at a constant rate with a hydraulic jack. The load is kept constant while marking the cracks.
Steel profiles realize the continuous boundary condition. Continuous plywood and felt layers were applied to avoid concentration of stresses at supports and minimize the in-plane restraints.
3 ϕ 36 Dywidag bars, having a total length of 3 m and a used length of 2.58 m, prevent rotation. Pretension equal to 15 kN/bar was applied before the test.
The load is applied at midspan of transversal axis; the load is un-symmetric with respect to the longitudinal axis. A detail of support and loading conditions is reported in Figure 5-3 and the experimental set-up is plotted in Figure 5-4.

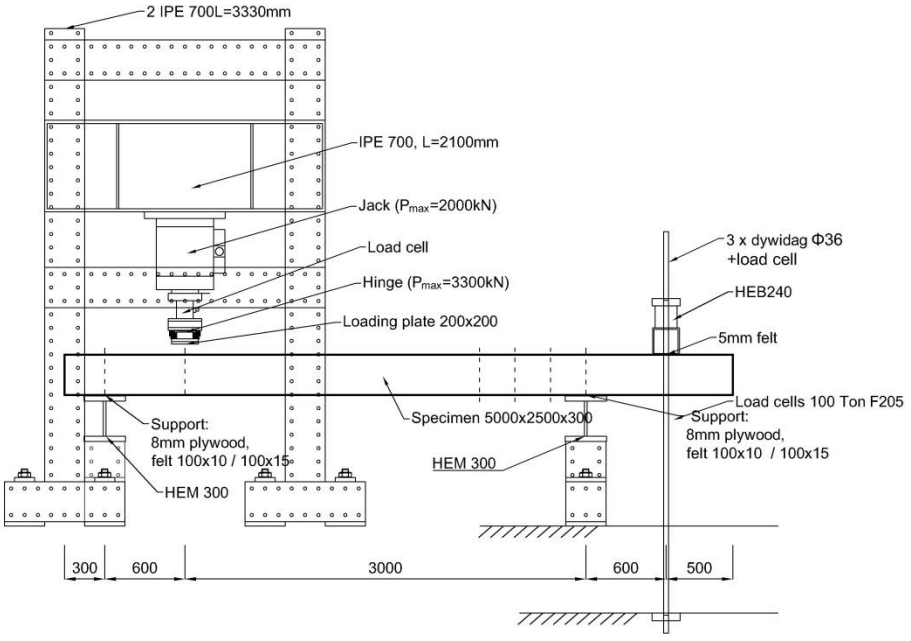

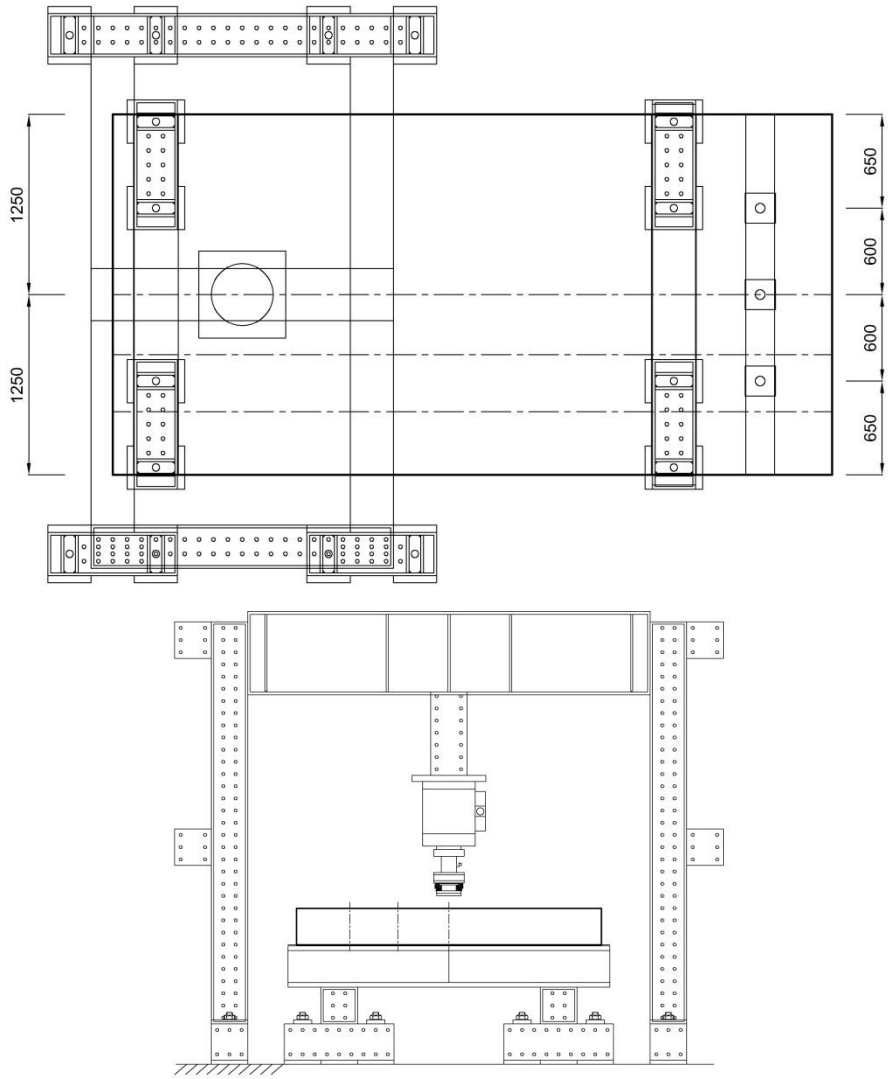

Figure 5-2: Case RS3. Experimental setup (dimension in mm)

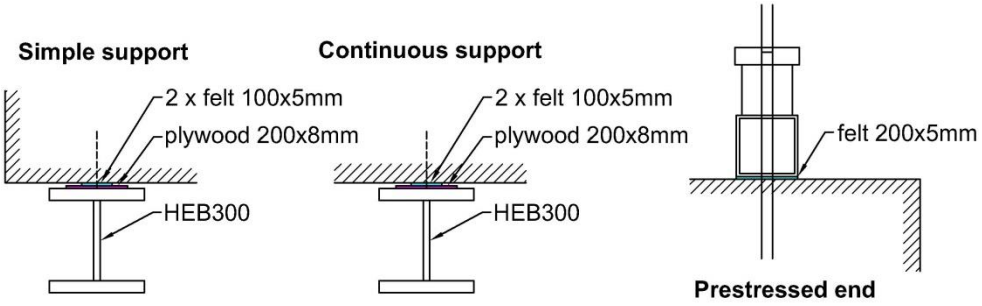

Figure 5-3: Case RS3. Details of supports

Figure 5-4: Case RS3. Experimental set-up

Experimental Results

At 700 kN a flexural crack appeared at the front face, Figure 5-5(b). Failure occurred at 954 kN. The width of the crack at the front face at failure was about 1.8 mm. On the bottom face a flexural cracking pattern could be observed. The main cracks appeared around the load and ran towards and away from the support. The load plate at failure sank into the top face of the concrete, Figure 5-5(c). The failure was detected as one-way shear failure. However the crack developed at the front face could also be due to a support subsidence. In Figure 5-5(a) the crack pattern of RS3 at bottom side is reported.

(a)

(b)

(c)

Figure 5-5: Case RS3. Experimental crack pattern (a) at bottom side, (b) on the front face, (c) on the top face

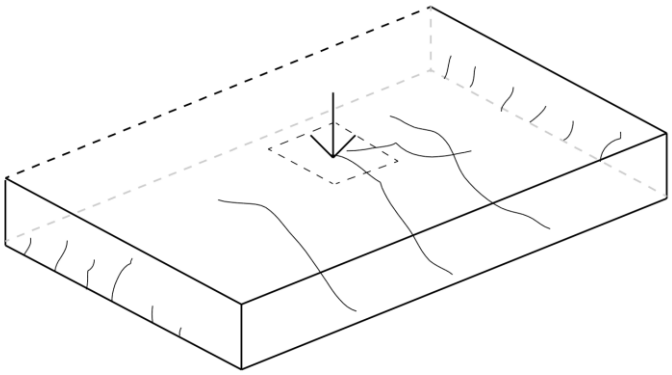

Figure 5-6: Assumed three-dimensional cracking pattern for shear failure – wide beam shear failure (Lantsoght, 2013)

In the reference document, a number of failure mechanisms was defined with assigned failure mode labels. Slab S1T1 failed as a wide beam in shear with cracks at an angle to the axis of the span direction. This failure mechanism was donated as WB (wide beam) and is schematically portrayed in Figure 5-6. Please note that this is only a general depiction of the failure mechanism of interest. Moreover, for this case, the shear crack is not visible at the side faces of the slab (Lantsoght, 2013).

5.2 Analytical analysis

The design shear resistance of RS3 slab is calculated according to Model Code 2010 formulation (fib, 2013) while the design punching strength is evaluated according to Regan's formulation (Regan et al. 1988) and according to Eurocode 2 formulation (CEN, 2005). Furthermore bending moment resistance of RS3 is evaluated by applying the yield line method on possible collapse mechanisms, identified on the basis of the supports and loading point positions.
For simplicity the slab is considered as clamped at the continuous support, Figure 5-7. The ultimate load *P* is evaluated from the maximum shear force.

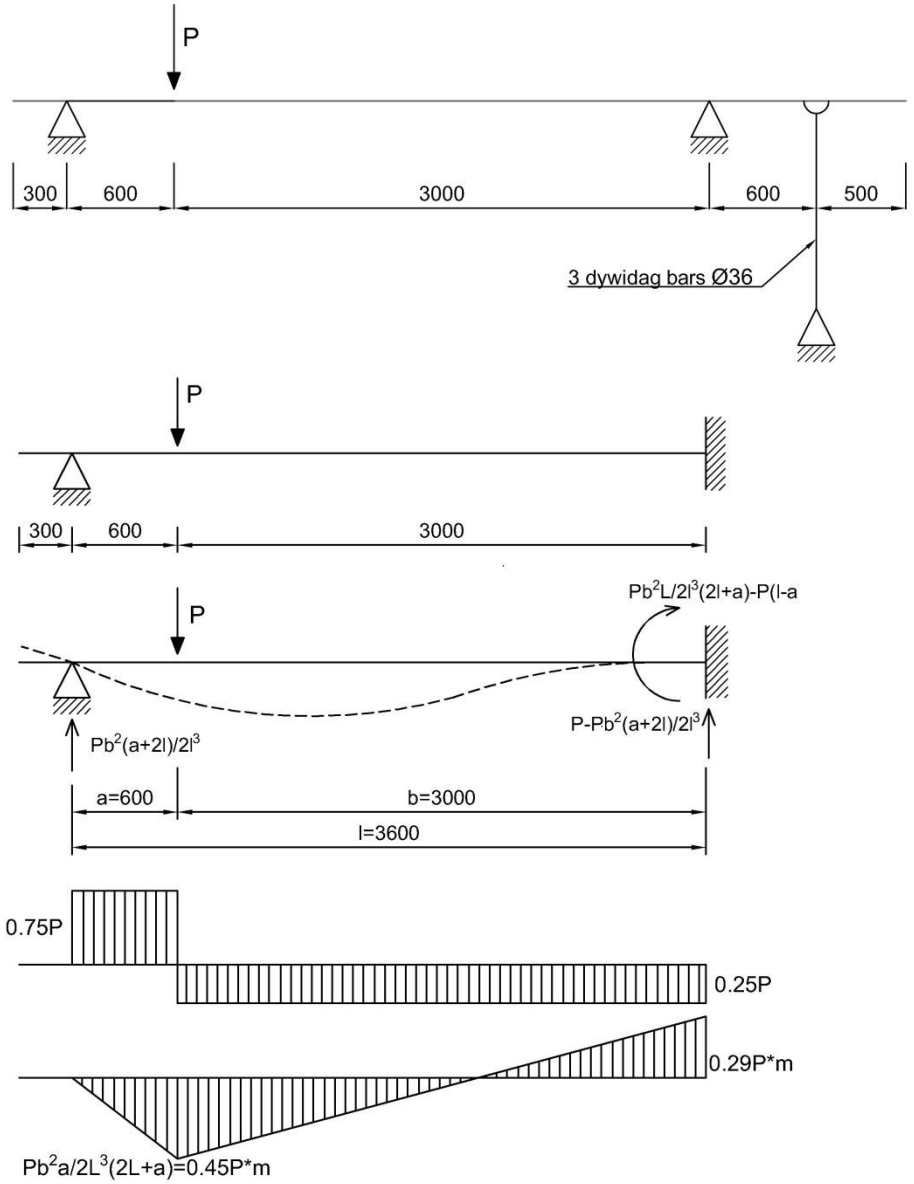

Figure 5-7: Case RS3. Internal forces (in mm)

One-way shear resistance: Model Code 2010

The design shear resistance of a slab is calculated as the design shear resistance of a member without shear reinforcement and therefore it can be calculated with Level I and Level II of approximation.

$$V_{Rd,c} = k_v \frac{\sqrt{f_{ck}}}{\gamma_c} z b_w$$

$$d_l = 300mm - 25mm - 10mm = 265mm$$

$$z = 0.9 d_l = 0.9 \times 265mm = 238.5mm$$

Value of the concrete compressive strength in the above expression is calculated as:

$$f_{ck} = 29.11MPa - 8MPa = 21.71MPa$$

The formulation of k_v varies depending on the considered Level of Approximation.

The width b_w is replaced by the effective width b_{eff}, calculated by assuming a 45-degree load spreading from the far corners of the load (the so-called French method), according to (Lantsoght et al. 2013), Figure 5-8.

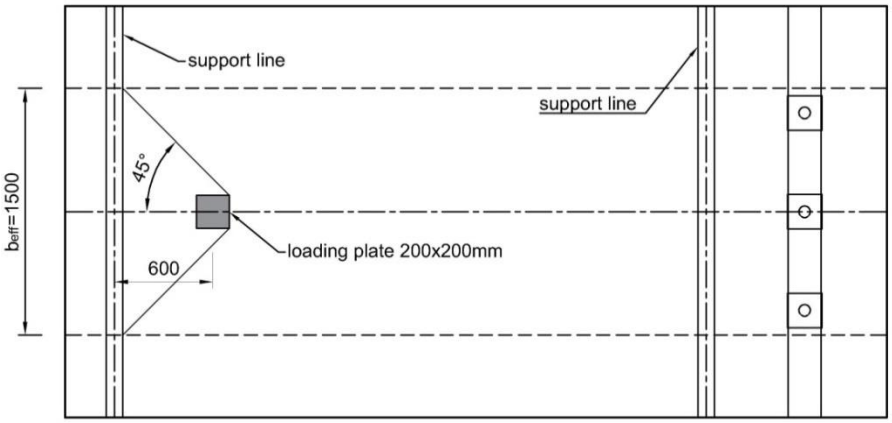

Figure 5-8: Case RS3. Assumed effective width b_{eff} (dimension in [mm])

$b_{eff} = 1500\,mm$

Because the applied load is at distance 600mm from the axis of the line support which is larger than $2d = 530mm$, the effect of the direct load transfer is not taken into account (β=0).

Level I Approximation

$$k_v = \frac{180}{1000 + 1.25z} = \frac{180}{1000 + 1.25 \times 238.5mm} = 0.139$$

$$V_{Rd,c} = k_v \frac{\sqrt{f_{ck}}}{\gamma_c} z b_{eff} = 0.139 \times \frac{\sqrt{21.71MPa}}{1.5} 238.5mm \times 1500mm = 154.10kN$$

The value of self-weight in kN/m at the consider location is approx. 7.8kN/m.
After accounting for the effect of self-weight, the shear resistance is:

$V_{Rd,c} = 154.1kN - 7.8kN/m \times 1.5m = 146.3kN$

Level II Approximation

Assumed resistance $v_{Ed} = 195.93\frac{kN}{m}$ and bending moment calculated at a distance d from the support $m_{Ed} = d \times v_{Ed} = 265mm \times 195.93kN/m = 51.92\,kNm/m$

$$a_s = \frac{\phi^2 \pi}{4} \Big/ 125mm = 2513\,mm^2/m$$

Strain parameter:

$$\varepsilon_x = \frac{1}{2E_s a_s}\left(\frac{m_{Ed}}{z} + v_{Ed}\right) = \frac{1}{2 \times 200GPa \times 2513\,mm^2/m}\left(\frac{51.92\,kN/m}{238.5mm} + 195.93\frac{kN}{m}\right) = 3.919 \times 10^{-4}$$

$$k_{dg} = \frac{32}{16 + d_g} = \frac{32}{16+16} = 1 \geq 0.75$$

$$k_v = \frac{0.4}{1+1500\varepsilon_x} \times \frac{1300}{1000 + k_{dg} z} = \frac{0.4}{1+1500 \times 3.919 \times 10^{-4}} \times \frac{1300}{1000 + 239mm} = 0.264$$

$v_{Rd,c} = k_v \frac{\sqrt{f_{ck}}}{1.5} z = 0.264 \frac{\sqrt{21.71}MPa}{1.5} 239mm = 195.92 \frac{kN}{m}$ equal to the assumed value.

The value of self-weight in kN/m at the consider location is approx. 7.8kN/m.

The reduced shear resistance is: $v_{Rd,c} = 195.92 \frac{kN}{m} - 7.8 \frac{kN}{m} = 188.12 \frac{kN}{m}$

Shear resistance of the effective width:

$$V_{Rd,c} = v_{Rd,c} b_{eff} = 188.12 \frac{kN}{m} \times 1500mm = 282.18kN$$

One-way shear resistance: Eurocode 2

$$V_{Rd,c} = b_{eff} d \left[C_{Rd} k (100 \rho_l f_{ck})^{1/3} \right] =$$

$$= 1500mm \times 265mm \left[0.12 \times 1.869 (100 \times 9.484 \times 10^{-3} \times 21.71)^{1/3} \right] = 244.33kN$$

Where:

$$k = 1 + \sqrt{\frac{200}{d}} = 1 + \sqrt{\frac{200}{265}} = 1.869 \le 2$$

$$\rho_l = \frac{A_s}{d \times s} = \frac{314.15mm^2}{265mm \times 125mm} = 9.484 \times 10^{-3}$$

and the resistance is greater than:

$$V_{Rd,c,\min} = v_{\min} \times b_{eff} \times d = 0.035 k^{\frac{3}{2}} f_{ck}^{\frac{1}{2}} \times b_{eff} \times d = 0.417MPa \times 1500mm \times 265mm = 165.615kN$$

After accounting for the effect of self-weight, the shear resistance is:

$$V_{Rd,c} = 244.330kN - 7.8kN/m \times 1.5m = 232.63kN$$

Punching strength: Regan's equation

In order to evaluate the punching strength P_R, a rectangular control perimeter u, outlined in red color in Figure 5-9 is determined.

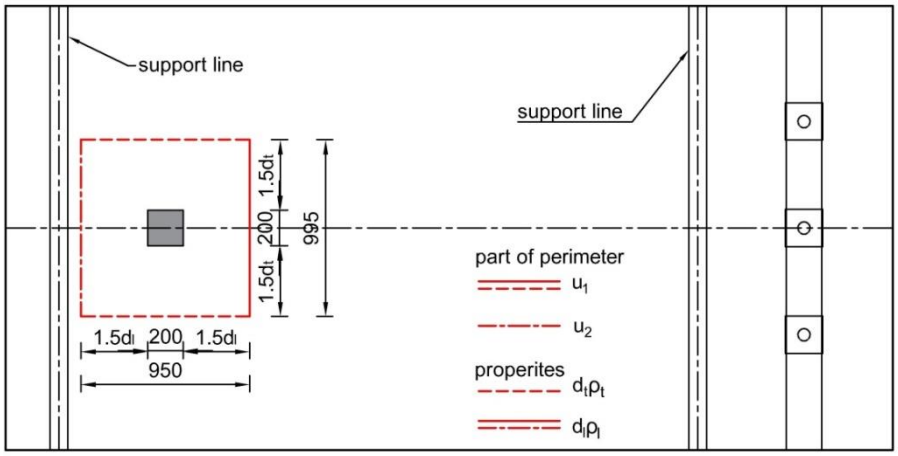

Figure 5-9: Case RS3. Control perimeter according to Regan's formulation

$$P_R = P_{R1} + P_{R2}$$

P_{R2} refers to the edge of the perimeter running parallel to the support; P_{R1} refers to the remaining part.

$$P_{R2} = \frac{2d_l}{a_v} \xi_{sl} v_{cl} u_2 d_l$$

$$\xi_{sl} = \sqrt[4]{\frac{500}{d_l}} = \sqrt[4]{\frac{500}{265}} = 1.172$$

$$\rho_l = \frac{\pi\phi_l^2}{4} \times \frac{1}{s_l \times d_l} = \frac{\pi \times (20mm)^2}{4} \times \frac{1}{125mm \times 265mm} = 9.484 \times 10^{-3}$$

$$v_{cl} = \frac{0.27}{\gamma_c} \sqrt[3]{100\rho_l f_{ck}} = \frac{0.27}{1.5} \sqrt[3]{100 \times 9.484 \times 10^{-3} \times 21.71MPa} = 0.493MPa$$

$a_v = 450mm$ is net distance between support 1 and a loading plate

$$u_2 = 1.5 \times d_t + 200 + 1.5 \times d_t = 1.5 \times 250 + 200 + 1.5 \times 250 = 950\,mm$$

And

$$d_t = h - c - \phi_1 - \phi_2/2 = 300mm - 25mm - 20mm - 5mm = 250\,mm$$

$$P_{R2} = \frac{2d_l}{a_v} \xi_{sl} v_{cl} u_2 d_l = \frac{2 \times 265mm}{450mm} \times 1.172 \times 0.493MPa \times 950mm \times 265mm = 171.45kN$$

$$P_{R1} = \xi_{sl} v_{cl} u_2 d_l + 2\xi_{st} v_{ct} u_1 d_t$$

$$\xi_{st} = \sqrt[4]{\frac{500}{d_t}} = \sqrt[4]{\frac{500}{250}} = 1.189$$

$$\rho_t = \frac{\pi\phi_t^2}{4} \times \frac{1}{s_t d_t} = \frac{\pi \times (10mm)^2}{4} \times \frac{1}{250mm \times 250mm} = 1.257 \times 10^{-3}$$

$$v_{ct} = \frac{0.27}{\gamma_m} \sqrt[3]{100\rho_t f_{ck}} = \frac{0.27}{1.5} \sqrt[3]{100 \times 0.001257 \times 21.71MPa} = 0.252MPa$$

$$u_1 = 1.5d_l + 200 + 1.5d_l = 1.5 \times 265 + 200 + 1.5 \times 265 = 995\,mm$$

$$P_{R1} = \xi_{sl} v_{cl} u_2 d_l + 2\xi_{st} v_{ct} u_1 d_t =$$
$$= 1.172 \times 0.493MPa \times 950mm \times 265mm + 2 \times 1.189 \times 0.252MPa \times 995mm \times 250mm =$$
$$= 294.38kN$$

Total punching shear resistance:

$$P_R = P_{R1} + P_{R2} = 294.38kN + 171.45kN = 465.84kN$$

Including the effect of self-weight which was assumed as the weight of a punching cone at a distance d from the edge of the column, the resistance is:

$$P_R = 464.56kN$$

Punching strength: Eurocode 2 formulation

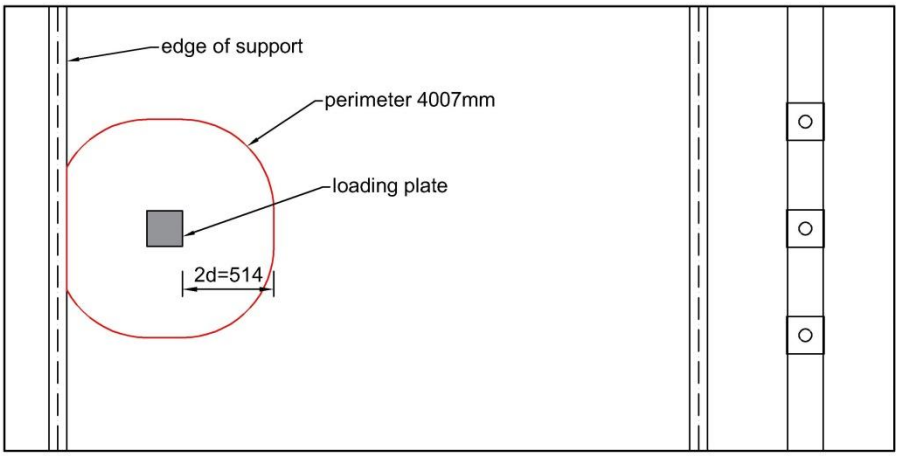

Figure 5-10: Case RS3. Control perimeter according to Eurocode 2 formulation

The reduced control perimeter *u*, outlined in red color in Figure 5-10, is determined to calculate the punching strength. This solution is a conservative approximation due to the fact that the load is located close to the edge of line support. For such a case, a portion of the applied load is transferred directly to the support increasing in this way shear resistance. In the assumed solution, the control perimeter would suggest that shear stresses are of the same value along the punching cone contour, thus it is conflicting with the statement above. The increase of the shear resistance resulting from direct load transfer can be also motivated by the final conclusion of the source document. The document claims that one-way slabs under concentrated load close to the support fail in a combination of one-way (thus where compressive strut action is permitted within a certain distance) and two-way shear.

$$V_{Rdc} = v_{Rdc} \times u \times d_{eff}$$

$$d_{eff} = \frac{d_l + d_t}{2} = \frac{265mm + 250mm}{2} = 257.5\,mm$$

$$k = 1 + \sqrt{\frac{200}{d_{eff}}} = 1 + \sqrt{\frac{200}{257.5mm}} = 1.881$$

$$\rho = \sqrt{\rho_l \times \rho_t} = \sqrt{0.00948 \times 0.00126} = 0.00345$$

$$v_{Rdc} = C_{Rd,c} k (100 \times \rho \times f_{ck})^{1/3} = 0.12 \times 1.88 \times (100 \times 0.00345 \times 21.71)^{1/3} = 0.442MPa$$

$$V_{Rdc} = v_{Rdc} u\, d_{eff} = 0.442MPa \times 4007mm \times 257.5mm = 455.88MPa$$

After taking into account the contribution of self-weight assumed as the weight of a punching cone, the resistance is:

$$V_{Rd,c} = 454.74kN$$

Punching strength: Critical Shear Crack Theory (CSCT)

The punching resistance has been calculated also by applying the critical shear crack theory (CSCT) (Muttoni 2003, Muttoni 2008). The punching resistance according to CSCT has been evaluated adopting mean measured values of material properties. The obtained results have not been compared to the punching resistance calculated according to Eurocode 2 and Regan's formulation employing design values of material properties.

According to this approach the rotation ψ of the slab is chosen as the controlling parameter for punching, since it has been found that the opening of the critical shear crack reduces the strength of the inclined concrete compression strut that carries the shear and eventually leads to the punching shear failure, Figure 5-11. The main practical advantage of this method is that the nonlinear behaviour under shear stress is no integral part of the FE analyses, which substantially simplifies the analyses.

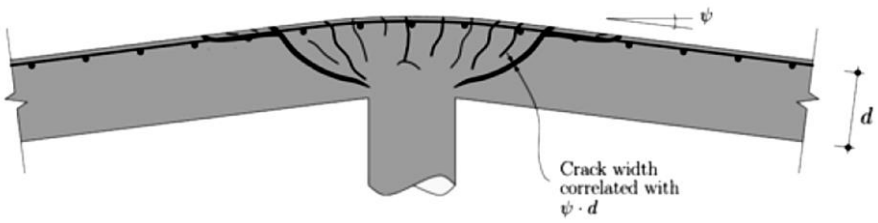

Figure 5-11: Critical shear crack theory: Relationship between the rotation ψ and the width of the critical crack and failure criterion (Muttoni 2008)

The punching shear strength V_R depends on the rotation ψ following the failure criterion (S.I. units: N, mm):

$$\frac{V_R}{b_0 d\sqrt{f_c}} = \frac{3/4}{1+15\psi d/\left(d_{g0}+d_g\right)} \tag{5-1}$$

where b_0 is the perimeter of the critical section located *d/2* from the edge of the loading plate, d is the average flexural depth equal to 257 mm, d_{g0} is the reference aggregate size equal to 16 mm and d_g is the maximum aggregate size equal to 16 mm.
The CSCT has been applied to slab S1T1 using a shell model. In this simplified FE model eight-node shell elements were used for the slab with a 3×3×9 Gauss integration scheme. The average dimensions of the elements were 300 mm × 325 mm. Reinforcements and dywidag bars were modelled as in a full 3D model.
Between the steel beams and the slab 6-node line interface elements were inserted.
Also the analysis phases and the convergence criteria were unchanged, Figure 5-12. In the model the simplification that the slab is clamped along support line 2 has been made. Both the dead load and the post-tensioning effects were neglected in this analysis. Along support line 1, the nodes which would lead to positive (tensile) reaction forces were released to move upwards, thus allowing a simplified linear analysis (LE). In the NLFE analysis this was not necessary.

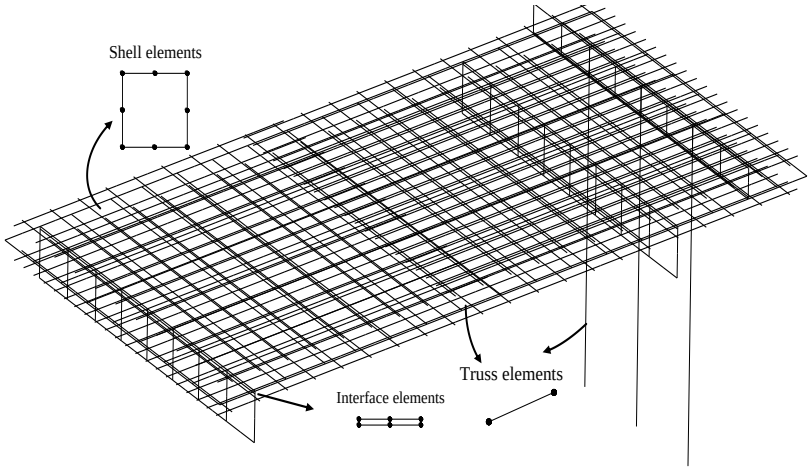

Figure 5-12: Case RS3. Mesh with plane shell elements

The application of CSCT involved three steps:

1. a linear elastic (LE) finite element analysis to determine the maximum shear force per length v_{max} and the control perimeter b_0;
2. NLFE analysis to determine the rotation ψ as a function of the applied load V;
3. the determination of failure load as the intersection point between the curve obtained from the NLFE analysis and the failure criterion (Eq.(5-1)).

In step 1, the LE analysis was carried out by applying pressure to the loading plate, 200 mm x 200 mm, with a resultant force Q=1 kN. Figure 5-13 shows the distribution of the obtained principal shear stress τ_{el} along the perimeter p, measured at a distance *d/2* from the edges of the loaded surface. The maximum principal shear stress equals to 0.00295 N/mm^2, or v_{max} = 0.00295 × 257mm = 0.758 N/mm. The control perimeter b_0 is now calculated as Q/v_{max} = 1320 mm.
Next, step 2, a NLFE analysis with load increments was carried out to determine the nonlinear relationship. In case of slabs subjected to concentrated loads, the rotation ψ is considered as the difference between the rotations of the slab at two points. The first point is located at the centre of the applied load (Point 1 in Figure 5-14), the second point, along the longitudinal symmetry axis of the slab, is chosen such that the maximum relative rotation is obtained (Point 2 in Figure 5-14). Figure 5-14 shows the rotation θ of the slab along its length for loads of 500, 750 and 1000 kN and indicates

that the position of Point 2 would depend on the load level. Relatively arbitrary Point 2 is chosen such that it maximizes the relative rotation at a load level V of 750 kN. Finally, in Figure 5-15 the failure load V_R is determined as the intersection between the results of NLFE analysis and the failure criterion. This results in **V_R = 793.0 kN**.

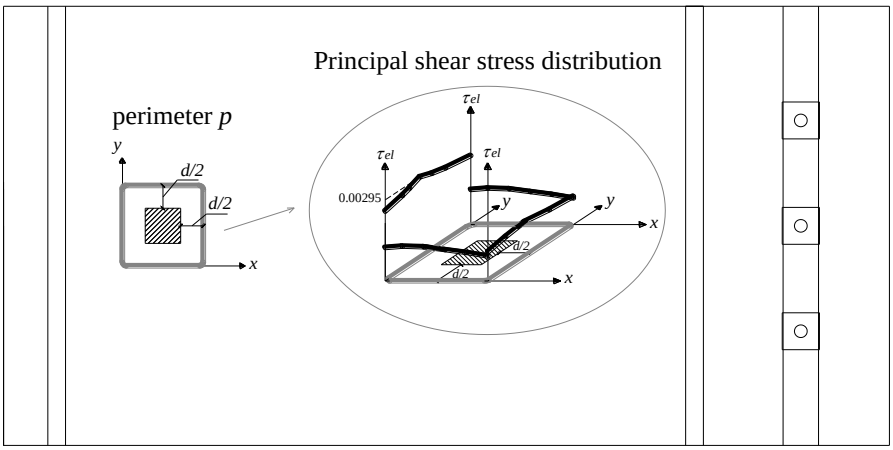

Figure 5-13: Case RS3. Principal shear stress distribution along the perimeter p

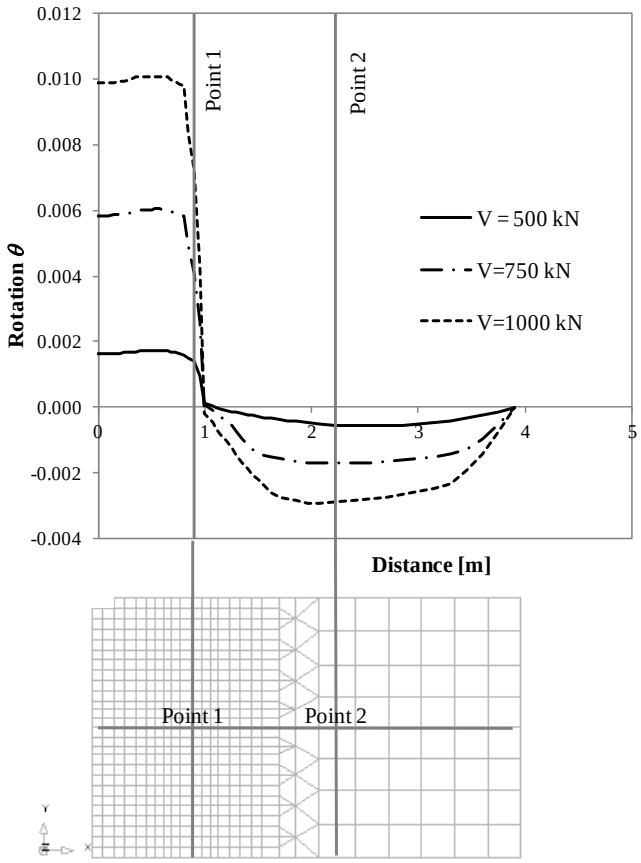

Figure 5-14: Case RS3. Rotation of the slab along its length: determination of the rotation ψ following the critical shear crack theory

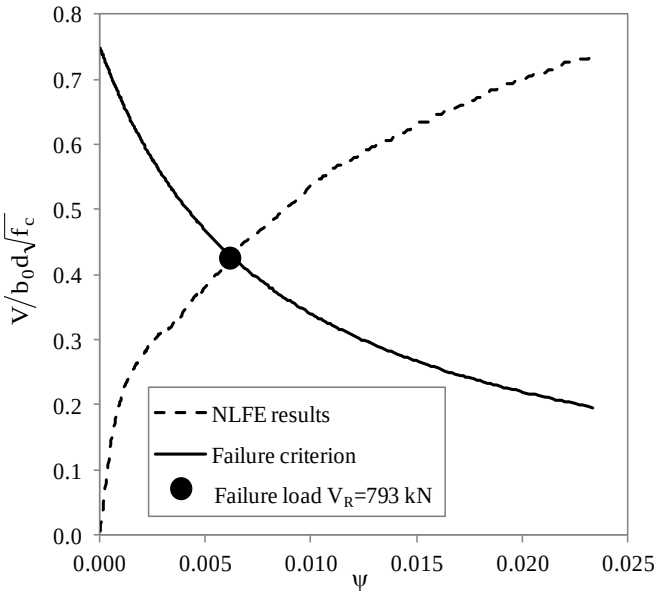

Figure 5-15: Case RS3. Determination of the failure load following the critical shear crack theory

Bending resistance: yield line method

Three collapse mechanisms, identified on the basis of the supports and loading point positions, have been analyzed to calculate the design bending resistance of RS3 slab with the yield line method, Figure 5-16.

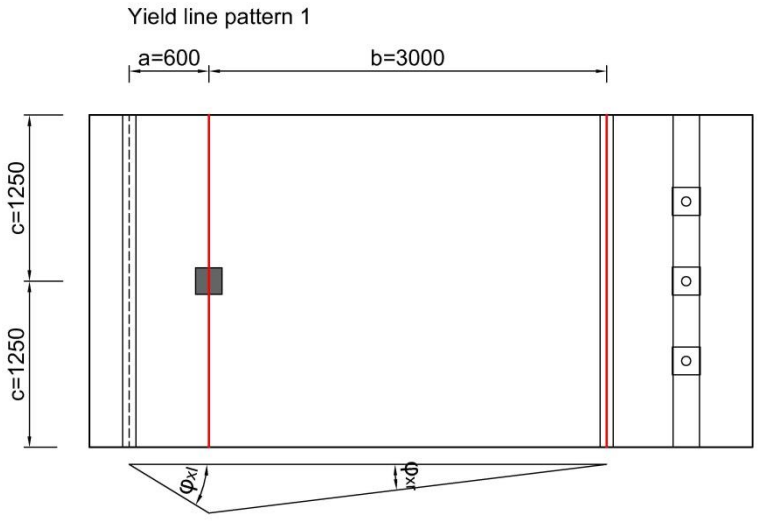

Figure 5-16: Case RS3. Yield line pattern for design bending resistance determination

Collapse mechanism 1:

$$m_x = 0.9 d_l f_{yd} A_{sl} = 0.9 \times 265mm \times 426MPa \times 2513 \frac{mm^2}{m} = 255.35 \frac{kNm}{m}$$

$$A_{sl} = \pi \frac{\phi_l^2}{4} \frac{1}{s_l} = \pi \frac{(20mm)^2}{4 \times 125mm} = 2513 \frac{mm^2}{m}$$

$$m_y = 0.9 d_t f_{yd} A_{st} = 0.9 \times 250mm \times 422.9MPa \times 314.16 \frac{mm^2}{m} = 29.89 \frac{kNm}{m}$$

$$A_{sl} = \pi \frac{\phi_l^2}{4} \frac{1}{s_l} = \pi \frac{(20mm)^2}{4 \times 250mm} = 314.16mm^2$$

$$P_{cr1} = m_x \frac{2c}{a} + 2m_x \frac{2c}{b} = 1490kN$$

In Table 5-2 the design values of beam resistance associated to one-way shear failure, punching failure and bending failure expressed in terms of the applied load P_{Rd} reduced by the effect dead weight are summarized.

Table 5-2: Case RS3. Design values of beam resistance expressed in terms of applied load P_{Rd}

	One-way shear (MC 2010)			**Punching**		**Bending**
	Level I (kN)	**Level II (kN)**	**EC2 (kN)**	**Regan (kN)**	**EC2 (kN)**	**Yield line (kN)**
P_{Rd} **(kN)**	146.3	282.18	232.63	464.56	454.71	1490

Slab RS3 fails due to one-way shear. The design shear resistance associated to one-way shear failure is lower than the design punching resistance and the design bending resistance.

5.3 Finite element model

Units

Units are N, m.

Material models and parameters

The concrete model is based on a total strain rotating crack model with:

- exponential softening in tension and parabolic behavior in compression,
- variable Poisson's ratio of concrete
- increase in compressive strength due to lateral confinement according to the model proposed by Selby and Vecchio (Selby and Vecchio 1993).

The mechanical properties are summarized in Table 5-3. The uniaxial stress - strain curve is shown in Figure 5-17. The model for the reinforcement grid is based on hardening plasticity. Geometrical and mechanical properties of reinforcement are summarized Table 5-1. The stress-strain curve of bars ϕ20 is plotted in Figure 5-18

Table 5-3: Case RS3. Constitutive model parameters for concrete

	f_{cm} **(N/mm^2)**	f_{ctm} **(N/mm^2)**	E_c **(N/mm^2)**	ν	G_F **(Nmm/mm^2)**
Mean measured value	29.71	2.79**	30910*	var	0.134*

*Not specified in reference; estimated according to Model Code 2010 (fib, 2013)
**Estimated from the mean splitting tensile strength of concrete as $f_{ctm} = 0.9 f_{ctm,sp}$ according to Eurocode 2 formulation (CEN, 2005)

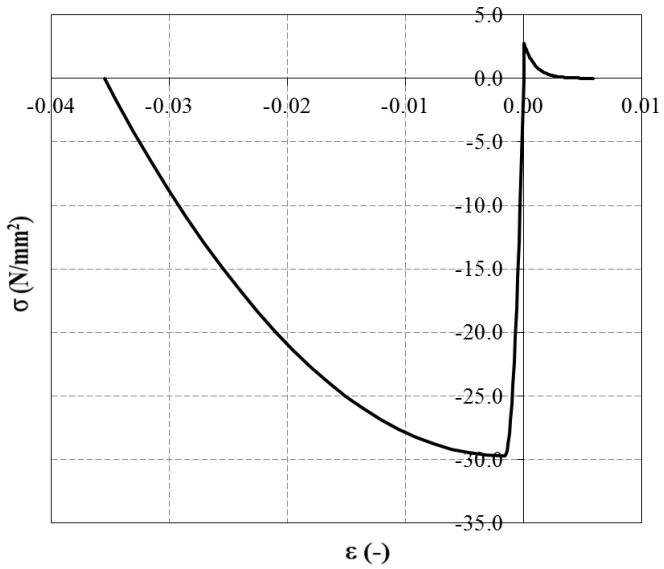

Figure 5-17: Case RS3. Stress-strain curve for concrete

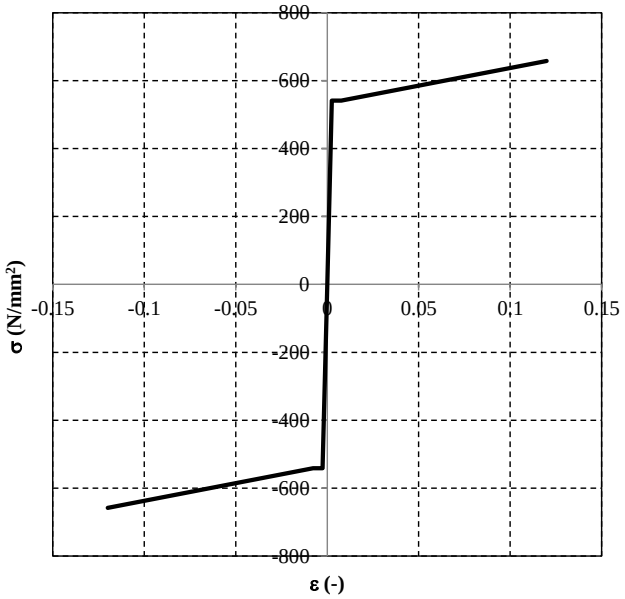

Figure 5-18: Case RS3. Stress-strain curve adopted for ϕ20

For the steel plates a linear elastic behavior is assumed, see Table 5-4.

Table 5-4: Case RS3. Steel plates properties

E (N/mm^2)	ν
210000	0.3

Interface: interface elements were placed between steel plates, steel profiles and concrete slab at the locations of supports and loading positions.
For construction of the support-concrete slab interface, 10 mm of P50 Nevima felt and 8 mm of plywood were used at the simple and continuous support. At the prestressed end, a layer of 5mm thick P50 felt was applied, (Figure 5-3). The non-linear mechanical behaviour of felt and plywood/felt in normal direction is evaluated from

experimental test, Figure 5-19. A linear elastic behaviour is assumed in shear direction and tensile direction, with stiffness value almost equal to zero. In Figure 5-20 the nonlinear mechanical behaviour of felt and plywood/felt used in the analysis is plotted. The displacement was calculated by multiplying the strain by the thickness of the felt (5 mm) and plywood/felt (18 mm) respectively.

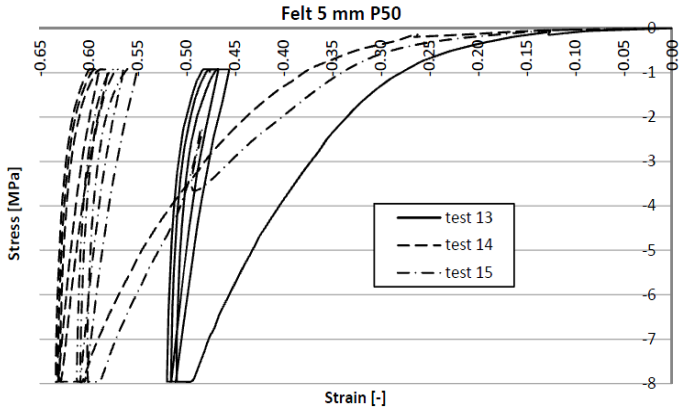

(a)

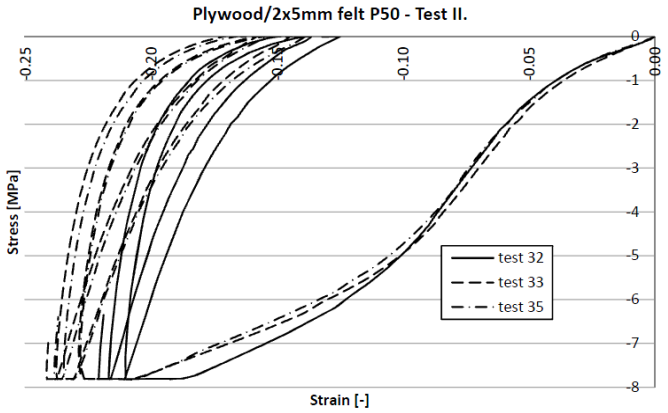

(b)

Figure 5-19: Case RS3. (a) Experimental stress-strain diagram of felt, (b) experimental stress-strain diagram of plywood/felt (Lantsoght 2012)

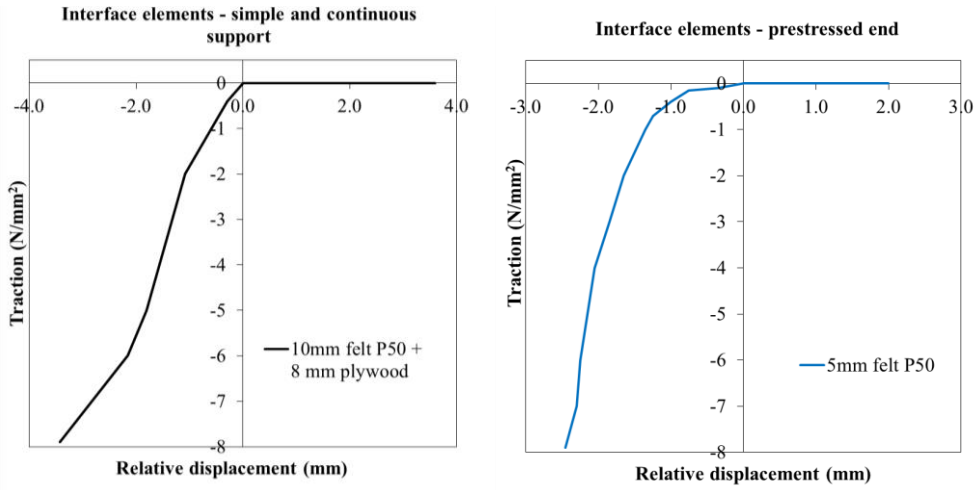

Figure 5-20: Case RS3. Traction-relative displacement diagram of plywood/felt and of felt used in NLFEA

Element types and finite element mesh

For meshing the concrete slab 20-node solid elements (CHX60) are used. The generated mesh has a regular pattern. The specified finite element size is 50×50×50 mm and is governed by the minimum number of elements over the slab thickness which for 3D slab structures is *h/6*. The reinforcement bars were modelled with embedded truss elements with two Gauss integration points along the axis of the element. Perfect bond is assumed. Dywidag bars were modelled with 2-node truss elements. It is important to note that the dywidag bars consist of only one element over the whole length. The elements in the steel plate of an increased thickness to avoid uplifting of the corners as the result of applied load were generated with 20-node solid elements (CHX60). The properties of interfaces between the loading plate, supporting steel profiles, the beam accommodating the prestressed bars and concrete slabs were assigned through 16-node (CQ48I) interface elements.

The mesh of the slab is shown in Figure 5-21(a) whereas reinforcement layout as modelled is illustrated in Figure 5-21(b). Different material properties for solid elements as well as different element geometries i.e. a cross-sectional area of reinforcement are indicated with diverse colors.

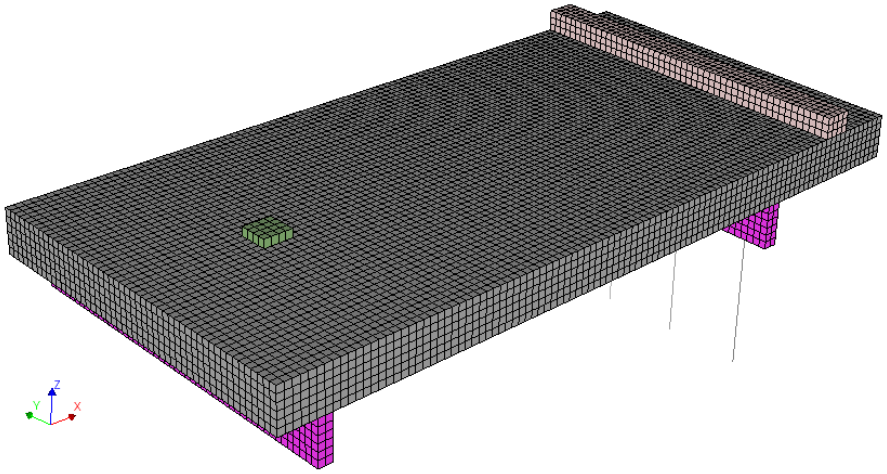

(a)

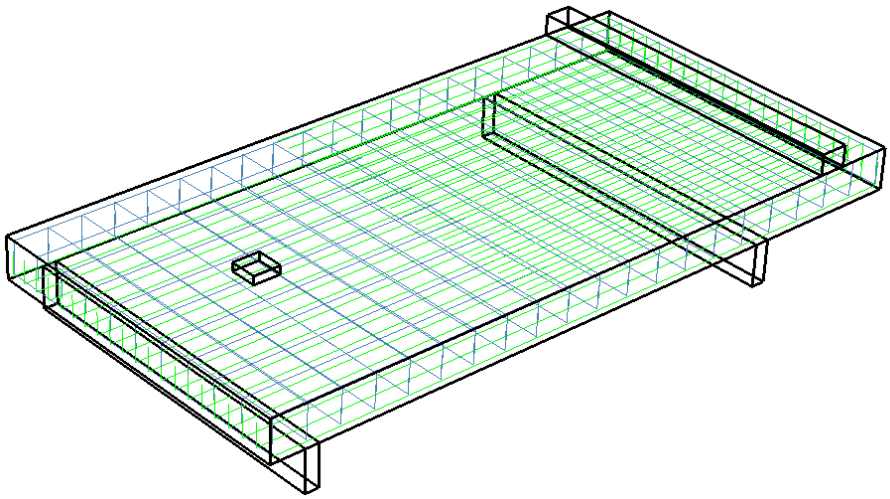

(b)

Figure 5-21: Case RS3. (a) Mesh, (b) reinforcement layout

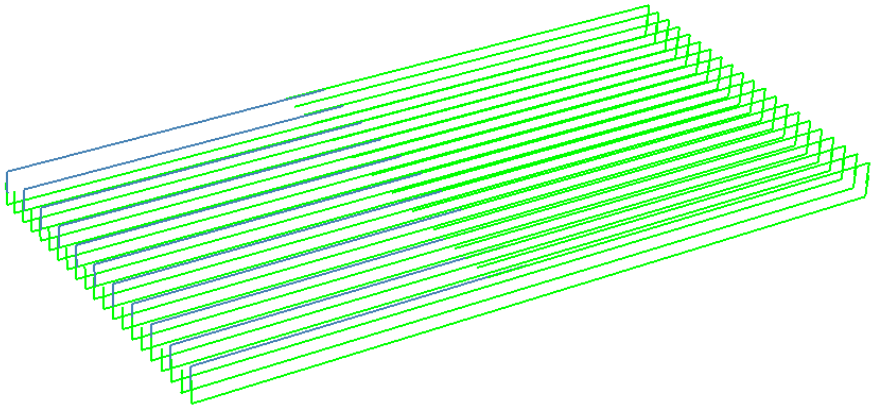

Figure 5-22: Case RS3: Groups of longitudinal reinforcement elements: "TOPF10L" (blue), "TOPF20L" (top rebars in green), "BOTF20L" (bottom rebars in green)

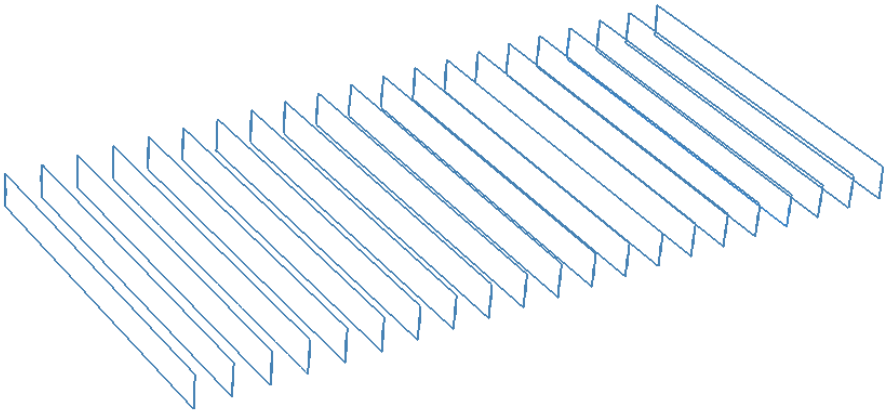

Figure 5-23: Case RS3: Groups of transverse reinforcement elements: "TOPF10T" and "BOTF10T"

Boundary conditions and loading

Boundary conditions are applied to nodes/faces of steel profiles, steel plate and dywidag bars, Figure 5-24. The following sets of constraints were applied:

- translations in the *x, y* and *z* direction were constrained through supports applied to the nodes at the bottom face of the supporting steel profiles (support 1 and support 2)
- translation along *z* direction at the middle node of the loading plate was constrained
- the dywidag bars were constrained along *z* direction at the bottom and along *y* and *x* at the top end

The analysis was carried out in displacement control by applying a displacement along *z* direction at the middle node of the loading plate.

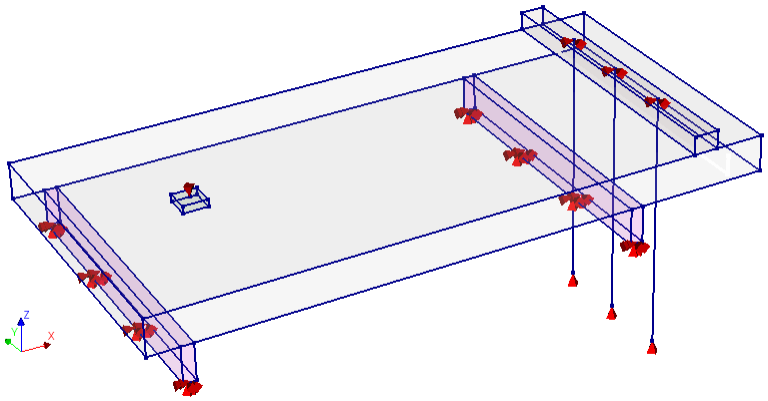

Figure 5-24: Case RS3. Boundary conditions in the model

The experimental simulation was performed by means of phased analysis with a total of 2 phases. This solution was necessitated by application of prestressing and prescribed deformation. In the first phase the global dead load *q* was applied to the slab and axial forces *F* equal to 15 kN were applied to the bottom ends of the dywidag bars, load case 1 and 2 respectively in Figure 5-25(a). In the second phase shown in Figure 5-25(b), supports were added to the bottom ends of dywidag bars to contain the prestressing forces in the elements and connect the dywiday bars to the "ground". Additionally, in the second phase, a prescribed displacement was applied to the node situated at the center of the loading steel plate as load case 3, Figure 5-26.

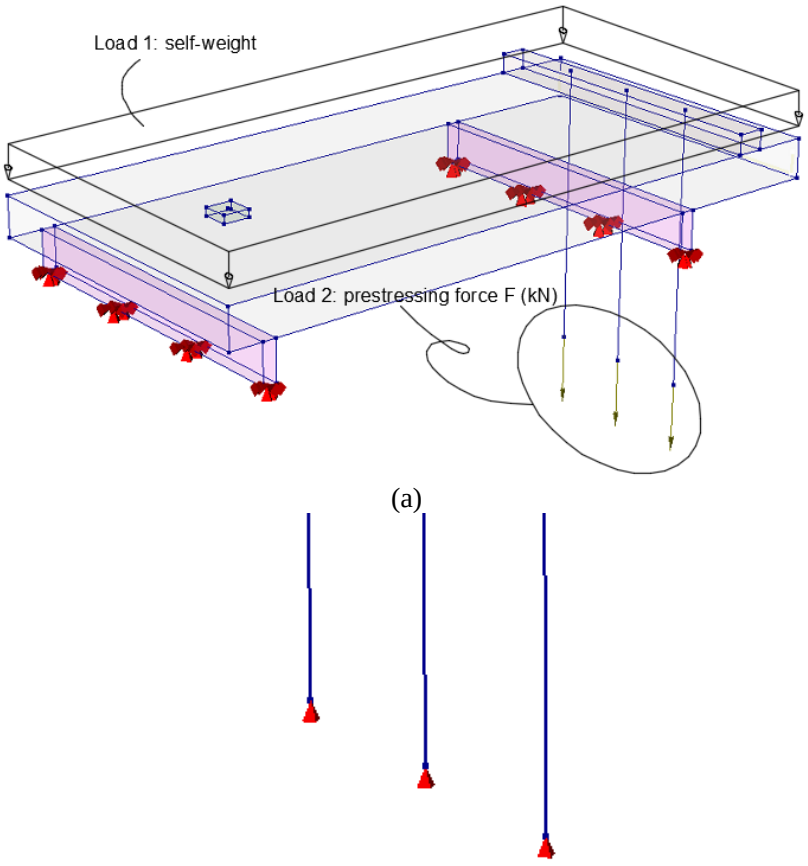

(a)

(b)

Figure 5-25: Case RS3. Loading components of phased analysis: (a) load cases 1 and 2 of analysis phase 1, (b) attached supports to dywidag bars in analysis phase 2

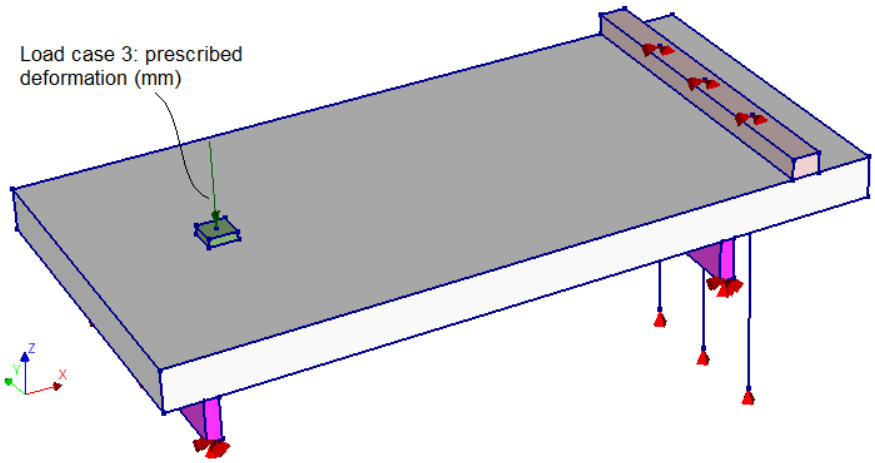

Figure 5-26: Case RS3. Load case 3 in phase 2 of the analysis

Load increments and convergence criteria

Load case 1 and Load case 2: both loads were applied simultaneously using a single load increment. Regular Newton-Raphson method with a maximum of 25 iterations was adopted. As convergence criteria, the norms of the force and energy were selected. The analysis continued even if the convergence criteria were not satisfied. Convergence tolerances equal to 1×10^{-3} and 1×10^{-2} were specified for energy and force norms, respectively.

Load case 3: the prescribed displacement along *z* axis equal to -1mm was applied in the middle of the steel plate. The user specified load step size of 0.2 of the whole prescribed deformation was applied in a total of 50 steps. To find the state of equilibrium, Regular Netwon-Raphson iterative procedure was incorporated with a maximum of 140 iterations in each load increment. The equilibrium iteration was set to continue even if the specified convergence criteria were not satisfied. Convergence tolerances are equal to 1×10^{-3} and 1×10^{-2} for energy and forces, respectively.

5.4 Nonlinear finite element analysis

Load deflection

The load-deflection curve is presented in Figure 5-27(b). Besides the general response of the structure, the curve pinpoints the load steps attributed to: onset of yielding of bottom transverse bars, beginning of yielding of top longitudinal and crushing of concrete. Crushing of concrete in the analysis was recognized as soon as the value of minimum principal strain of -3.5‰ in the first integration point was reached.

In order to preserve the consistency between the tests and the NLFEA, the same procedure of determining the mean displacement was put into effect. The value of mean deflection was established based on the readings from lasers surrounding the loading plate at the distance of 265mm from the application of the load. The positions of the lasers are designated as points A, B, C, D in Figure 5-27(a). Following suit, the mean deflection from NLFEA was obtained considering the displacements of four corresponding nodes.

The peak load is defined as the highest load which satisfies the fixed energy norm tolerance of 1×10^{-3}. Prior to the peak load all load steps converged within the specified number of iterations except for step 28 which was characterized by crushing of

concrete in the close proximity of loading plate. The relative energy variation for this step was almost equal to the given tolerance. The analysis continued as the energy tolerance was satisfied in the consecutive load step within 71 iterations. After reaching the peak load, the analysis converged in 3 consecutive load steps after which the performance was poor. This is indicated by a dotted line in the slab's response plot in Figure 5-27.

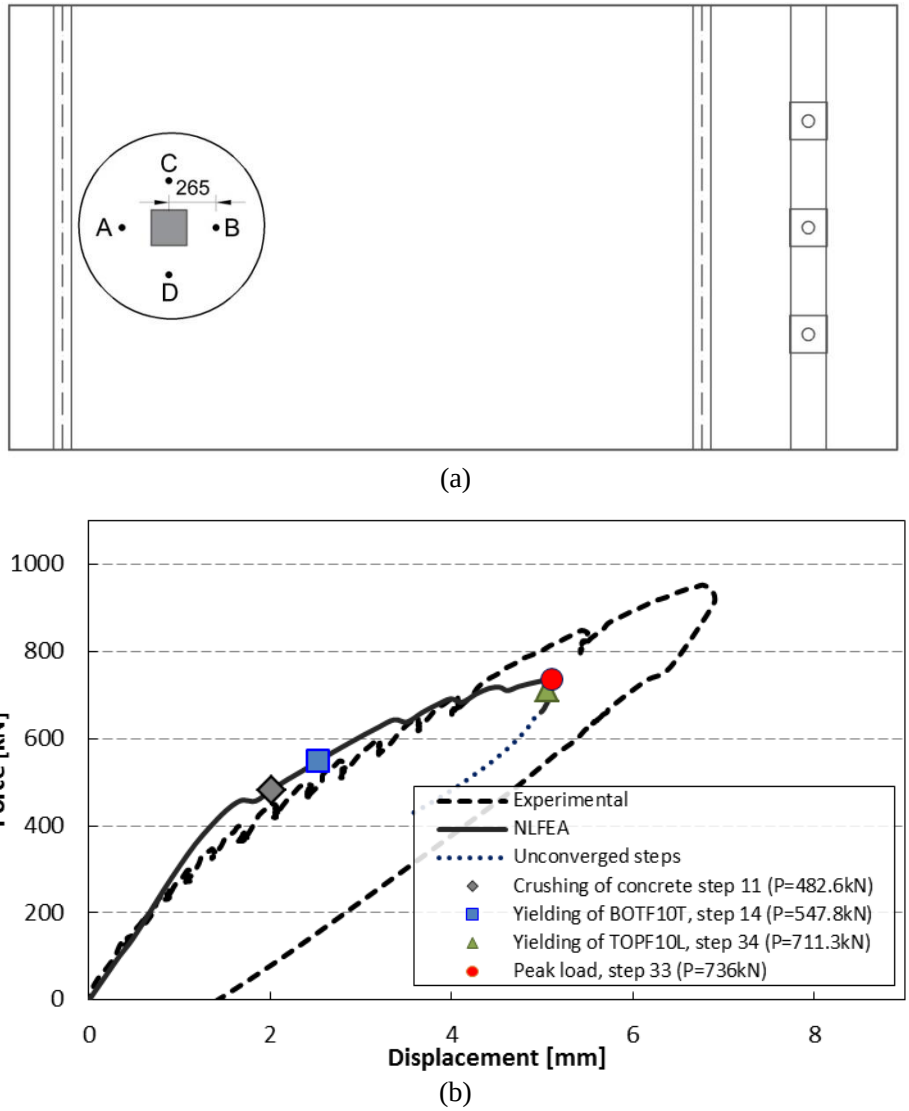

Figure 5-27: Case RS3. (a) Determination of the deflection points taken into account to calculate mean deflection, (b) Force-displacement curve

Convergence behavior

For a vast majority steps, convergence was reached only on the basis of an energy criterion, Figure 5-28-Figure 5-29. For load case 3 up to the peak load, the energy norm ratio has not satisfied the fixed tolerance of 1×10^{-3} for only one step of the analysis indicated with a yellow marker in Figure 5-28. The force norm ratios were higher than the fixed tolerance for almost all steps. In Figure 5-28 a red circle indicates the peak load position on the force-displacement graph.

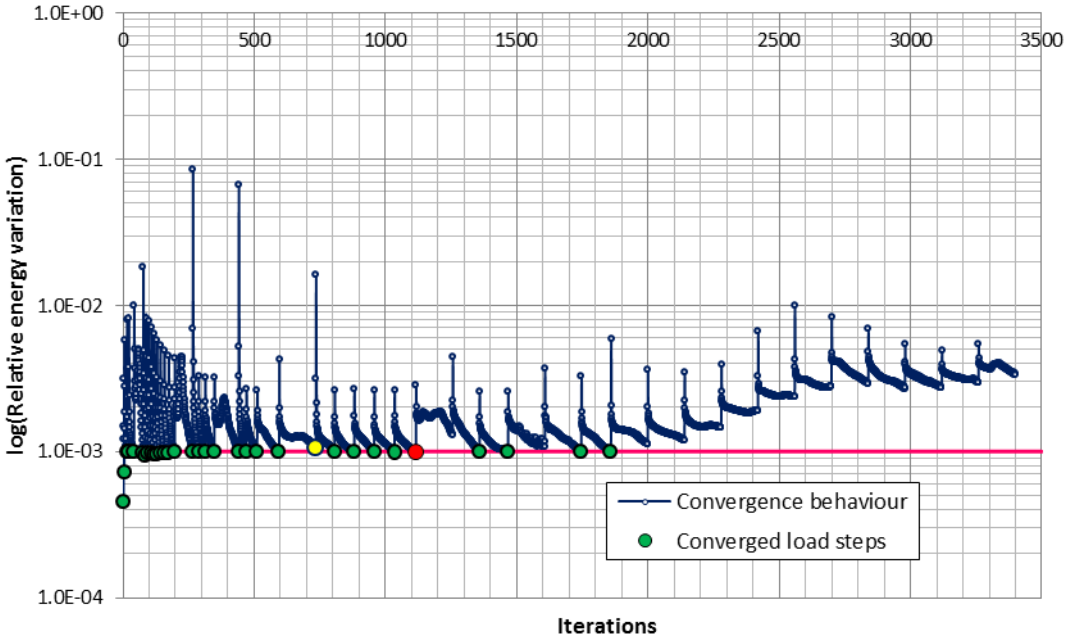

Figure 5-28: Case RS3. Evolution of the energy norm (markers indicate iterative results)

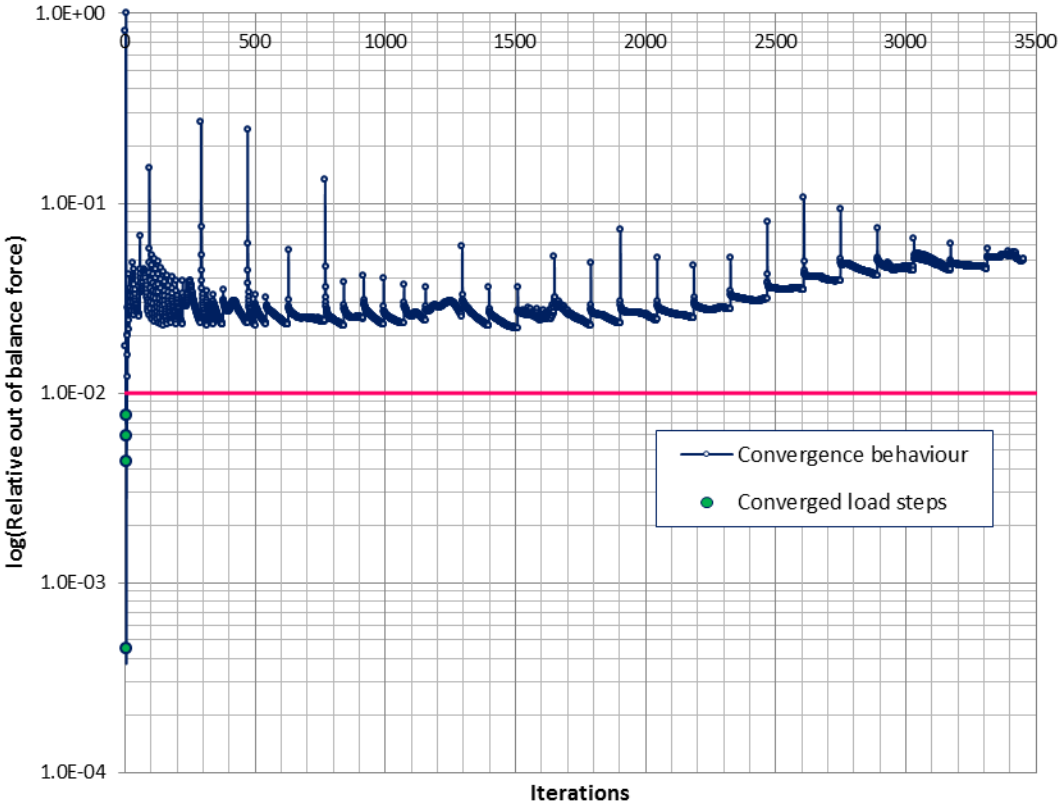

Figure 5-29: Case RS3. Evolution of the force norm

Strains in concrete

Figure 5-30 shows the positive principal strain at the peak load for the whole slab and at the section with normal in global *y* direction near the location of loading plate. The highlighted colors in the contour plots Figure 5-30(a), (b) and (c) correspond to the assigned values depicted in the concrete softening curve in Figure 5-30 (d). Special attention is drawn to three values of principal strain. The first principal strain value 9.06e-5 indicates occurrence of cracking. The second principal strain value equal to 0.000963, corresponds to the ultimate strain value calculated as $\varepsilon_{t,u} = \frac{G_F}{h \cdot f_{ctm}}$, while the third principal strain value, equal to 0.0044, is the strain value corresponding to 1% of f_{ctm}. Intermediate strain values have been added in the contour plot for clarity.

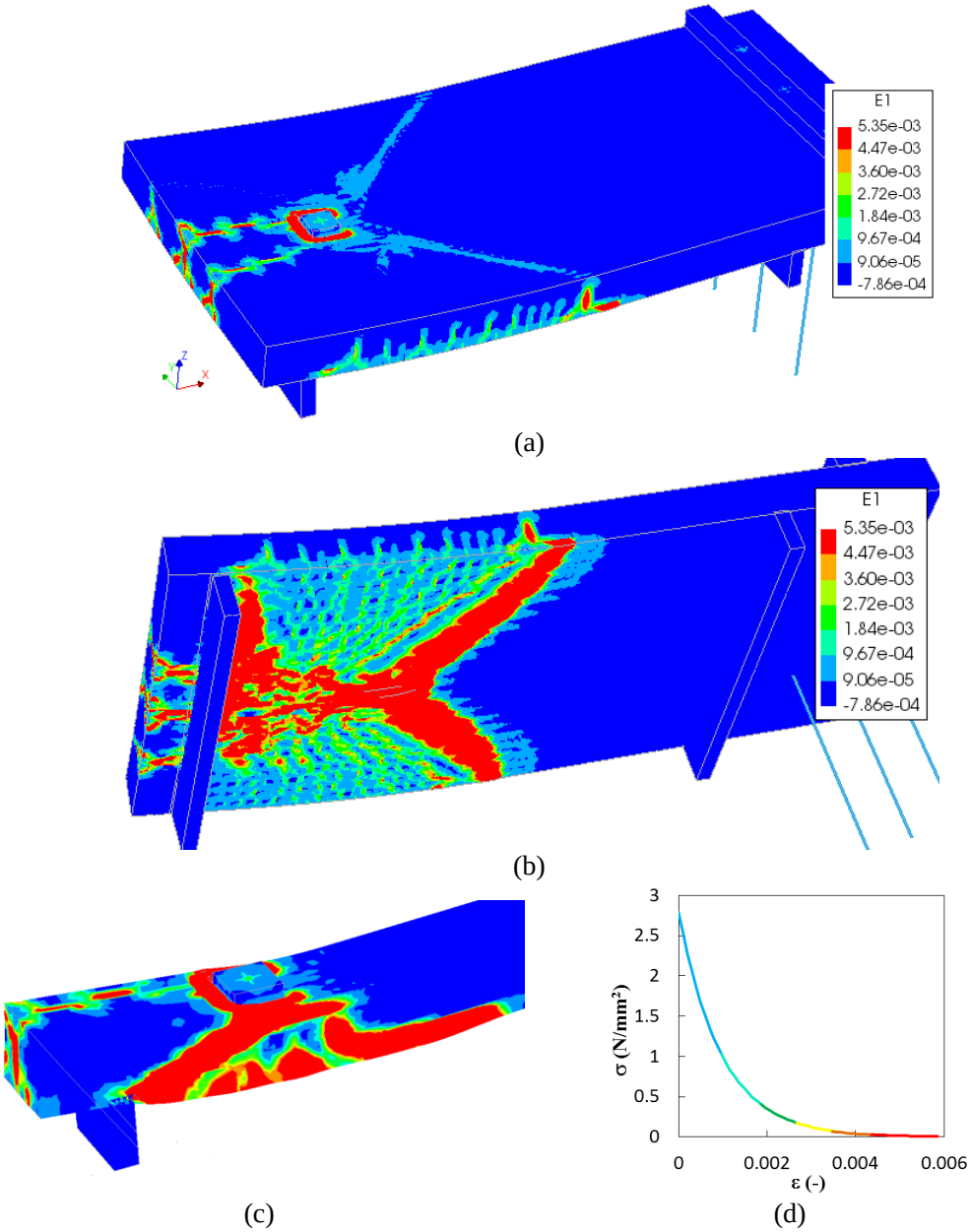

Figure 5-30: Case RS3. Crack strain at the peak load, step 33: (a) upper surface, (b) underside, (c) cross-section near the location of the loading plate (d) exponential softening

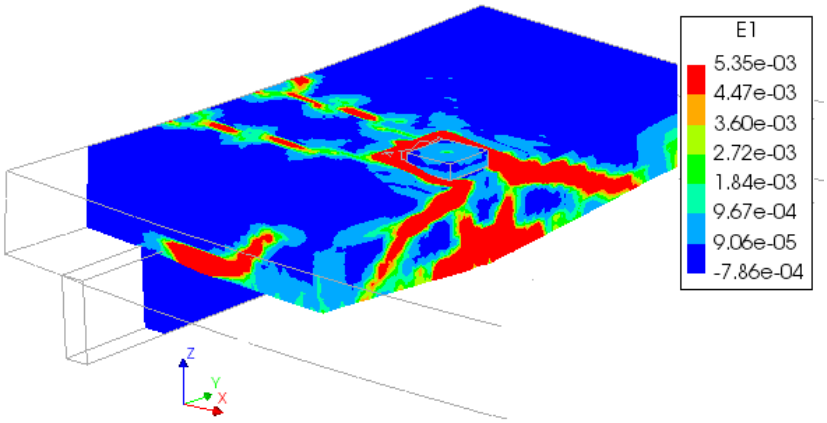

Figure 5-31: Case RS3. Positive principal strains at step 36

Figure 5-32 illustrates the minimum principal strain values at peak load for the whole slab as well as a section along the *y* axis near the loading plate. The following values of strain are of importance. The first value of minimum principal strain, equal to -3.2e-4, corresponds to the limit principal strain value in the elastic range according to expression: $\varepsilon_{c,el} = \frac{f_{cm}}{3 \cdot E_c}$. The second negative principal strain value -0.0016 is the peak strain value determined with formula: $\varepsilon_{c,p} = -\frac{5}{3}\frac{f_{ctm}}{E}$. The last minimum principal strain value, equal to -0.0355 is the crushing strain value calculated as $\varepsilon_{c,u} = \varepsilon_{c,p} - \frac{3G_c}{2hf_{cm}}$. The presented values in the legend in Figure 5-32(a) and the contour plot in Figure 5-32(b) can be related to the parabolic curve in Figure 5-32(c) where the exact compressive softening of concrete is portrayed.

From the presented contour plots, it can be observed that beside the region subjected to direct loading, compressive strains in the whole slab are lower that the peak value. Compressive stresses in concrete along two diagonals are within the nonlinear compressive stress regime with stresses between -10 MPa and -30 MPa. Complete softening of concrete appeared only along one side of the loading plate. A similar phenomenon of a steel plate penetrating into concrete was noticed in the experiments, which is reported in Figure 5-5(c).

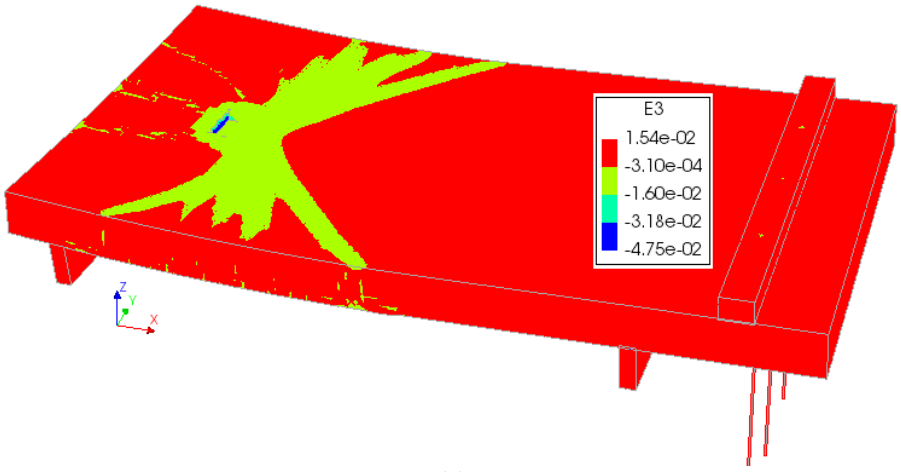

(a)

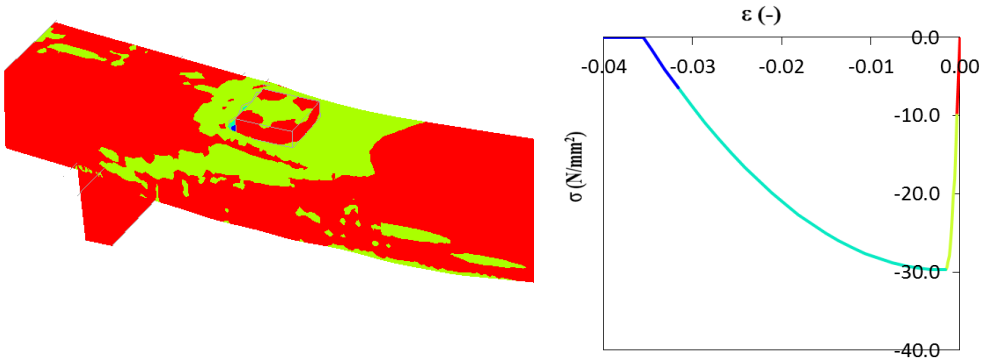

(b) (c)

Figure 5-32: Case RS3. Minimum principal strain values at peak load: (a) upper surface, (b) cross-section near the loading plate, (c) compressive softening

Strains in steel

In Table 5-5, the defined groups of reinforcement which undergo yielding are summarized. For the same value of yielding strain $536MPa/210GPa = 2.56\times10^{-3}$, the subsequent columns outline the magnitudes of the loads which led to yielding and the corresponding load steps. Figure 5-33 shows yielding strain in reinforcement one step after the peak load. It is important to note that in Figure 5-33 only bars which are subjected to yielding are selected. The remaining groups of reinforcement are not displayed.

Table 5-5: Case RS3: Summary of yielding of reinforcement

Group name	Yielding strain	Load (kN)	Step
BOTF10T	$2.56\cdot10^{-3}$	548	14
TOPF10L		711.3	34

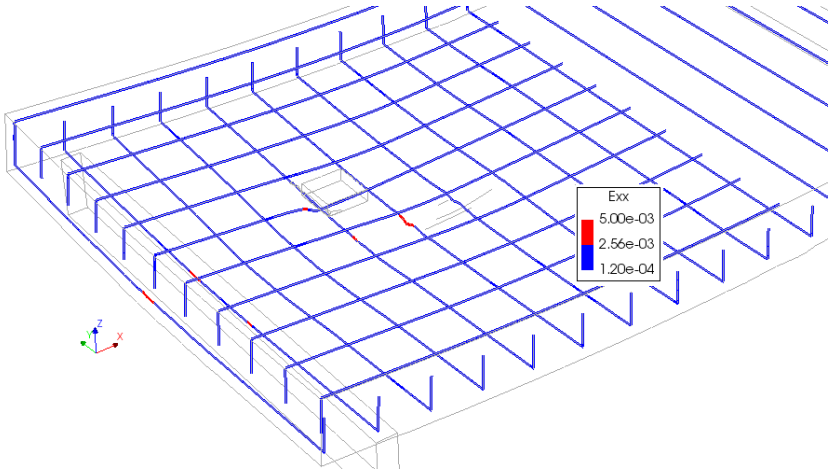

Figure 5-33: Case RS3. Yielding in tension of BOTF10T and TOPF10L at step 35

In order to conclude on the failure mechanism, the contour plots of negative and positive principal strains are scrutinized. When the positive principal strain values, which can be interpreted as a representation of a crack pattern, are compared with the experimental crack pattern depicted in Figure 5-5 and Figure 5-6, satisfactory resemblance can be observed. In both cases, on the bottom side of the slab extensive flexural cracking is noticeable. Furthermore, both numerical analysis and experimental results indicate appearance of shear cracking spreading from the loading plate towards

the support as well as crushing of concrete in direct neighborhood of the loading plate. In Figure 5-31, it can be seen that, apart from shear cracks in longitudinal direction, also crack propagating transversely takes place. Relatively small flexural crack widths and limited yielding suggest that heavily reinforced slab in longitudinal and transverse directions, properly controlled cracking and the slab does not fail in flexure. Based on extensive diagonal cracking from the positive strain contour plot and the fact that reinforcement yielded only locally prior to the peak, it is deduced that the structure fails in a combination of one-way and two-ways shear. This result is only partly in agreement with the experimental observations which were concluded by reasoning that the slab failed in so-called one-way shear with an assumed cracking pattern for wide beam shear presented in Figure 5-6. The results of the numerical analysis suggest that the mixed mode shear failure is a combination of beam shear failure, Figure 5-34(a), for which a shear crack is visible at the side face of the slab and punching shear failure, Figure 5-34(b).

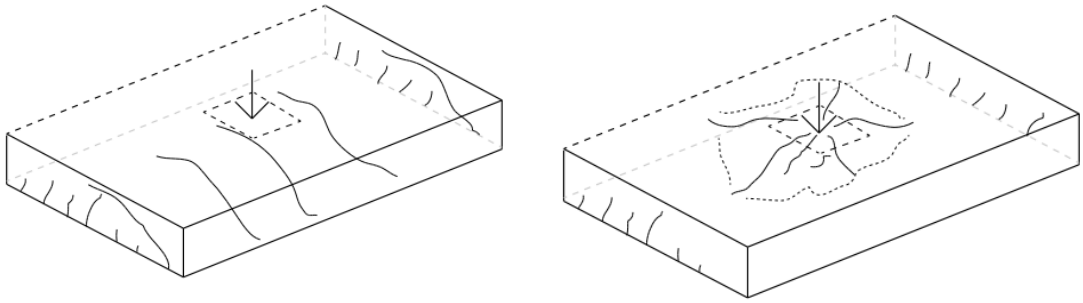

(a) (b)

Figure 5-34: Assumed three-dimensional cracking pattern for: (a) *beam shear failure*, (b) *punching shear* (Lantsoght, 2015)

5.5 Application of safety format

A safety assessment of resistance calculated by non-linear analysis is carried out with application of safety formats. The methods included, as proposed in Model Code 2010, are: GRF (Global Resistance Factor method), PF (Partial Factor method) and ECOV (Method of Estimation of a Coefficient of Variation of resistance). The safety assessment with safety formats requires a total of four nonlinear analyses. The mechanical properties of steel and concrete implemented in the analyses are given in Table 5-6 - Table 5-8.

Table 5-6: Case RS3. Constitutive model parameters for concrete

	f_c (N/mm^2)	f_{ct} (N/mm^2)	E_c (N/mm^2)	ν	G_F (Nmm/mm^2)	G_C (Nmm/mm^2)
Mean measured	29.71	2.79	30910	var	0.134	33.60
Characteristic	21.71	1.95	27841	var	0.127	31.76
Mean GRF	18.46	2.09	26373	var	0.123	30.84
Design	14.48	1.30	24321	var	0.118	29.52

Table 5-7: Case RS3. Constitutive model parameters for reinforcing bars (Φ10)

	Φ (mm)	A_s (mm^2)	f_y (N/mm^2)	f_t (N/mm^2)	E_s (N/mm^2)	ε_{sy} (-)
Mean measured	10	79	537	628	210000	0.0026
Characteristic	10	79	486.38	568.81	210000	0.0023
Mean GRF	10	79	535.02	625.69	210000	0.0025
Design	10	79	422.94	494.61	210000	0.0020

Table 5-8: Case RS3. Constitutive model parameters for reinforcing bars (Φ20)

	Φ (mm)	A_s (mm^2)	f_y (N/mm^2)	f_t (N/mm^2)	E_s (N/mm^2)	ε_{sy} (-)
Mean measured	20	314	541	658	210000	0.0026
Characteristic	20	314	490.01	595.98	210000	0.0023
Mean GRF	20	314	539.01	655.58	210000	0.0026
Design	20	314	426.09	518.24	210000	0.0020

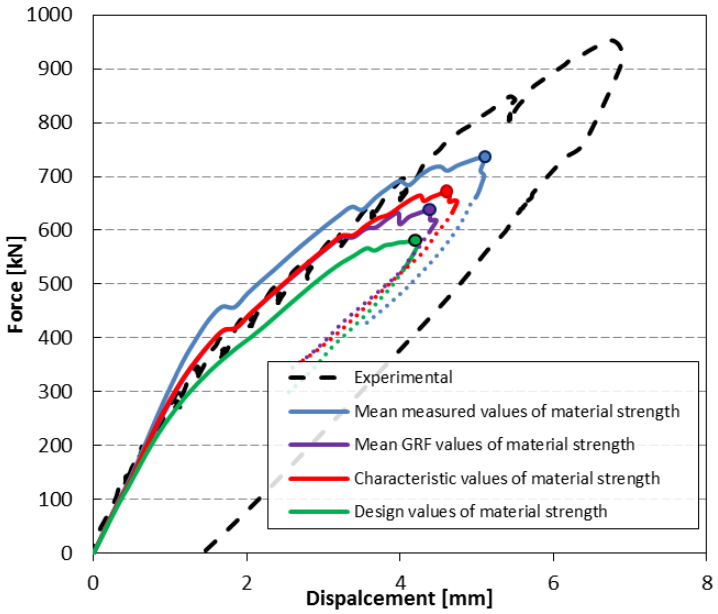

Figure 5-35: Case RS3. Load-deflection curves obtained with mean measured, characteristic, mean GRF and design mechanical properties

In Figure 5-35 the load-deflection curves obtained with mean measured, characteristic, mean GRF and design values of material strengths are shown. The peak load values are indicated in the graph with circular markers. The steps which have not converged within the specified maximum of iterations are plotted with a dotted line. The failure mechanism for all safety format methods was consistent with the result of the analysis with mean measured material properties thus the slab failed due to shear. In contrary to the crack pattern from the analysis with mean measured material properties, for the reduced material properties, the shear crack at the side face was not established. Moreover, in Figure 5-36 it can be seen that shear cracking propagates in two

directions. This means that all models failed in shear, yet the cracking pattern indicates a combination of wide beam shear and punching shear cracking pattern.

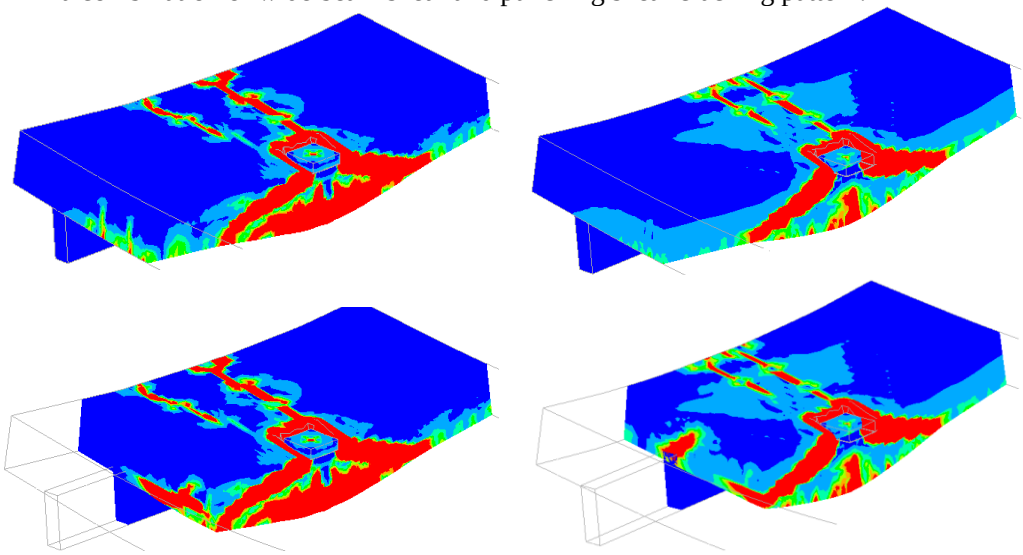

(a) (b)

Figure 5-36: Case RS3: Positive principal strain contours at step 28 for: (a) GRF method, (b) PF method

RS3 slab was analyzed with analytical and numerical procedures. Figure 5-37 the comparison of analytical and numerical design values of slab resistance P_{Rd} expressed in terms of a percentage of the experimental ultimate value of applied load.
The analysis named "no safety format" refers to a NLFE analysis carried out using mean measured values of material strengths without applying any safety coefficient.

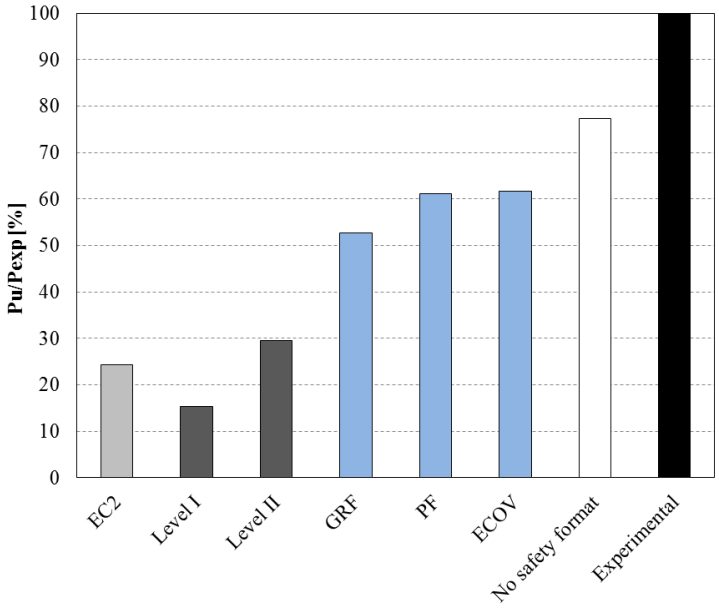

Figure 5-37: Case RS3. Analytical and numerical design values of slab resistance

The relatively high difference between the GRF, PF and ECOV design values of the resistance on the one hand and the resistance without using a safety format on the other hand confirms the critical role of the concrete properties on the loading capacity.

In Table 5-9 the design values of slab resistance, expressed in terms of applied load P_{Rd}, obtained from numerical and analytical procedures are reported.

Table 5-9: Case RS3. Values of slab resistance

P_{Exp} (kN)	EC2 (kN)	Level I MC2010 (kN)	Level II MC2010 (kN)	GRF (kN)	PF (kN)	ECOV (kN)	No safety formats (kN)
952.38	232.63	146.3	282.18	501.9	581.7	588.0	736.2

5.6 Concluding remarks

The benchmark specimen is a clamped simply supported slab subjected to a concentrated point load near the simply supported end. The slab with the total length of 5 m has width of 2.5m and thickness 0.3m.The slab is unreinforced against shear containing only longitudinal and transverse reinforcement. The exhibited failure mechanism is one-way shear at the load equal to P =952.38 kN.

In order to simulate the experiments, a numerical model of the slab was created and its behaviour analysed. The slab was modelled with 20-node brick elements for the concrete and embedded truss elements for the reinforcement. Perfect bond was assumed. The concrete model was based on a total strain rotating crack model with exponential tension softening in tension and parabolic behavior in compression, variable Poisson's ratio of concrete and no reduction of compressive strength of concrete due to lateral cracking. The model for the reinforcement bars was based on hardening plasticity.

The NLFEA on the model with mean measured material properties was concluded with a shear failure mechanism. The failure mode was characterized by crushing of concrete near the loading plate, extensive diagonal cracking and local yielding of transversal and longitudinal bars. The peak value of applied load obtained from NLFEA was equal to 736.2 kN.

Additional safety assessments were performed with application of safety formats for NLFEA. The resulting values of the slab design resistance are much higher than estimates from any analytical approach. Despite of being overly conservative, the analytical calculations predicted the same failure mechanism as numerical methods.

Based on the results it can be concluded that consistent and reliable results can be obtained with a rotating crack model including a variable Poisson's ratio decreasing from its actual value in the elastic phase up to 0 as the slab cracks. Reliable results were obtained by neglecting the reduction of the compressive strength of concrete due to lateral cracking. This assumption is also tied to the more simplified 3D material modeling with respect to the 2D modeling.

6 Case RS4 (S1T2): Lantsoght et al. (2012)

The present chapter treats a one-way slab in the test configuration S1T2(Lantsoght, 2012; Lantsoght 2013; Lantsoght et al. 2013) tested in an experimental program at Stevin Laboratory executed at Delft University of Technology. The focus of the program was to derive design recommendations for evaluation of shear resistance of slabs with loads near line support applicable for the assessment of both new and old structures. The considered variable of the test program were: load position, transverse reinforcement ration, concrete strength, size of a loading plate and type of support (simple or continuous). The selected specimen S1T2 is denoted here as case RS4.

6.1 Experimental setup and results

Geometry

The dimensions of slab RS4 are 5 m × 2.5 m, the thickness is 0.3 m. In Figure 6-1the geometrical dimensions of the slab and the reinforcement layout are given. Longitudinal reinforcement at the bottom consists of 21ϕ20/125 whereas longitudinal reinforcement at the top is 21 ϕ20/125 in the zone subjected to negative moments (over a distance of 3m from the prestressed end) and 11ϕ10/250 in the zone subjected to positive moments (over a distance of 2.3 m from the simply supported end). Transversal reinforcement comprises of 21ϕ10/250 placed both at the top and bottom sides. The concrete cover is 25 mm.

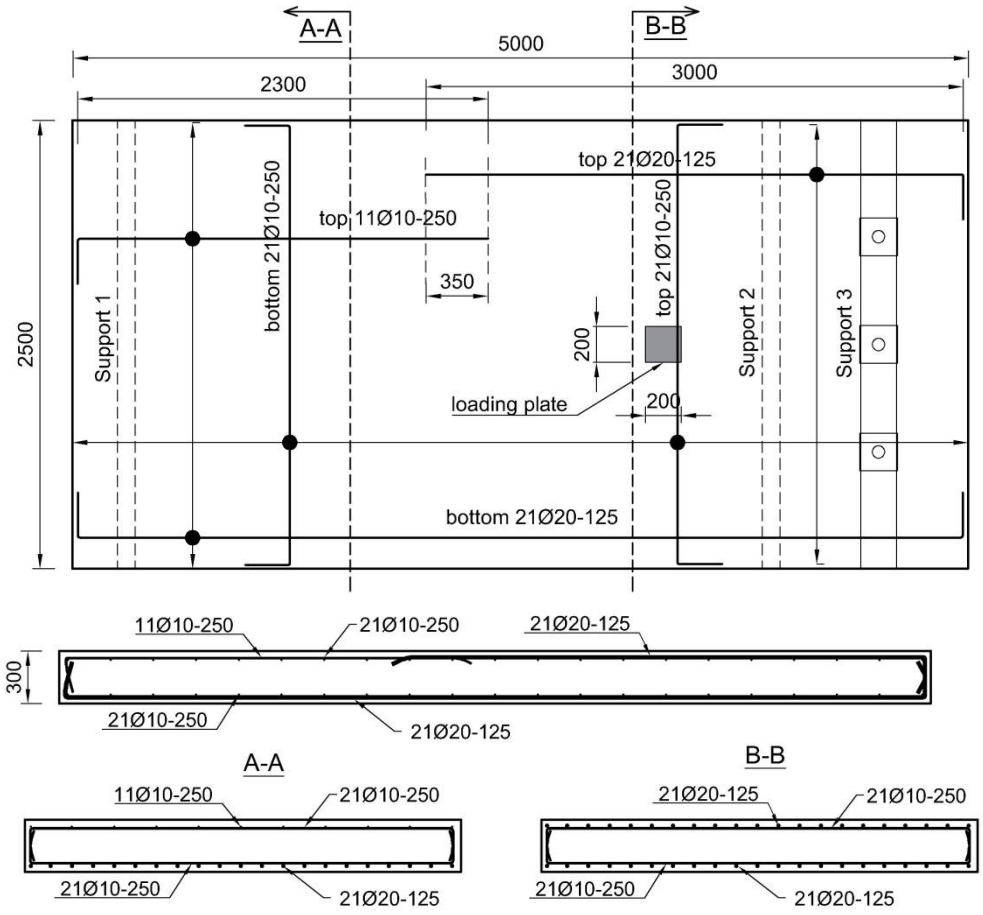

Figure 6-1: Case RS4. (a) Geometrical and (b) reinforcement details (in mm)

Material Properties

Concrete and reinforcement properties given in the reference are reported in Table 6-1.

Table 6-1: Case RS4. Reinforcement properties

Concrete properties					
f_{cm} (N/mm^2)		$f_{ctm,sp}$ (N/mm^2)		d_{max} (mm)	
29.71*		3.1		16	
Reinforcement properties					
Bar	ϕ(mm)	A_s (mm^2)	E_s (N/mm^2)	f_{ym} (N/mm^2)	f_{tm} (N/mm^2)
ϕ10	10.0	79	210000	537	628
ϕ20	20.0	314	210000	541	658
ϕ36 Dywidag	36.0	1018	210000	1000	-

*f_{cm} is a converted value using a conversion factor of 0.83
$f_{cm,cyl} = 0.83 \times f_{cm,cub} = 0.83 \times 35.8MPa = 29.71MPa$ where 35.8MPa is given in the reference

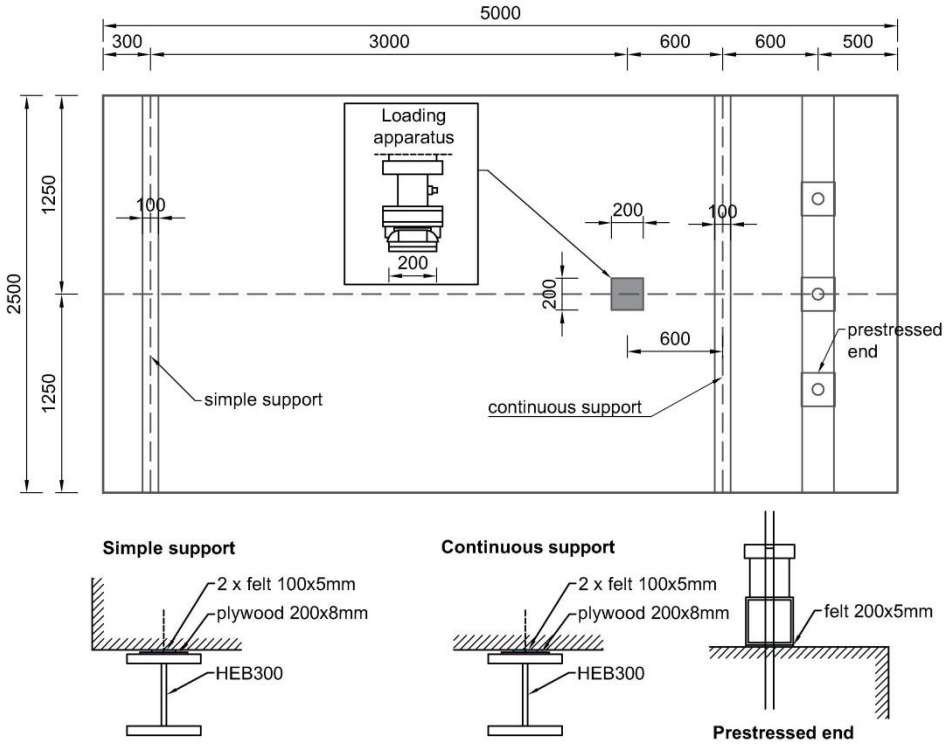

Figure 6-2: Case RS4. Dimensions of the slab, boundary conditions and details of support and of loading apparatus (dimensions in mm)

Loading and Boundary Conditions

The test setup for slab S1T1 (RS 3, see previous section) and S1T2 (RS4) does not differ apart from the location of application of the load. For the complete visualization of the experimental setup, reference to the description in the preceding case study is made. In the current case, the load applied in a displacement-controlled way through a hydraulic jack is located in vicinity of the continuous support. The slab is supported by two line support placed along the short edges. The support consist of a steel beam 300mm wide, a layer of plywood and a layer of felt 100 mm wide restraining the longitudinal translation at supports and mitigating stress concentration. The overview of boundary conditions is presented in Figure 6-2. The support 1 represents a simple

support. The other end of the beam is fixed to the laboratory floor through vertical 3Φ36 Dywidag prestressing bars. This measure restrains the rotation at Support 2 causing hogging moment over the support and therefore simulating the conditions of a continuous support. The applied prestress equal to 15kN/bar was applied before the test, initially compensating for the self-weight.

Experimental Results

The first cracks appeared at the bottom side around the position of the load at 200 kN. At the load value of 600kN, a flexural cracking pattern on the bottom face developed accompanied with first cracking on the front face. At 800 kN, the bottom face showed a fully developed flexural cracking pattern. When the load reached 900 kN for the second time the concrete was touching the plywood of the support. Failure occurred at 1023 kN. The largest observed crack, located along the middle of the width and extended over more than half of the span length, was on the bottom face with a width of 2.5 mm. At failure the loading plate sank into the top surface of the concrete. The failure was detected as wide beam **one-way shear failure,** Figure 5-6. In Figure 6-3 the crack pattern of RS4 at bottom side and on the front face at failure are depicted.

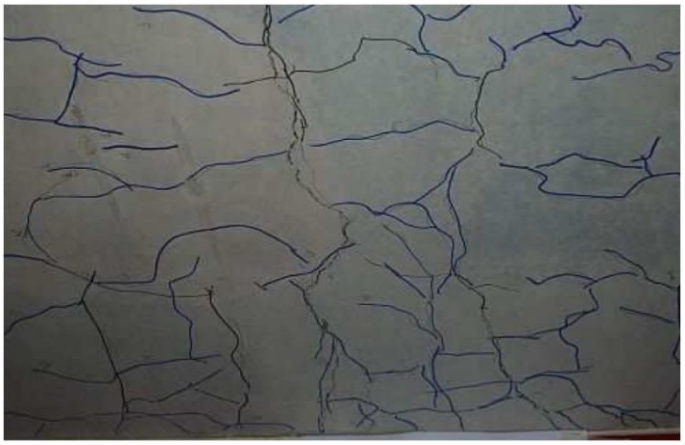

(a)

(b)

Figure 6-3: Case RS4. Experimental crack pattern: (a) at bottom side, (b) on front face

6.2 Analytical analysis

The design shear resistance of RS4 slab is calculated according to Model Code 2010 formulation (fib, 2013) while the design punching strength is evaluated according to Regan's formulation (Regan et al. 1988) and Eurocode 2 formulation (CEN, 2005).
For simplicity the slab is considered as simply supported at one end and clamped at the continuous support, Figure 6-4. The ultimate load *P* is evaluated from the maximum shear force.

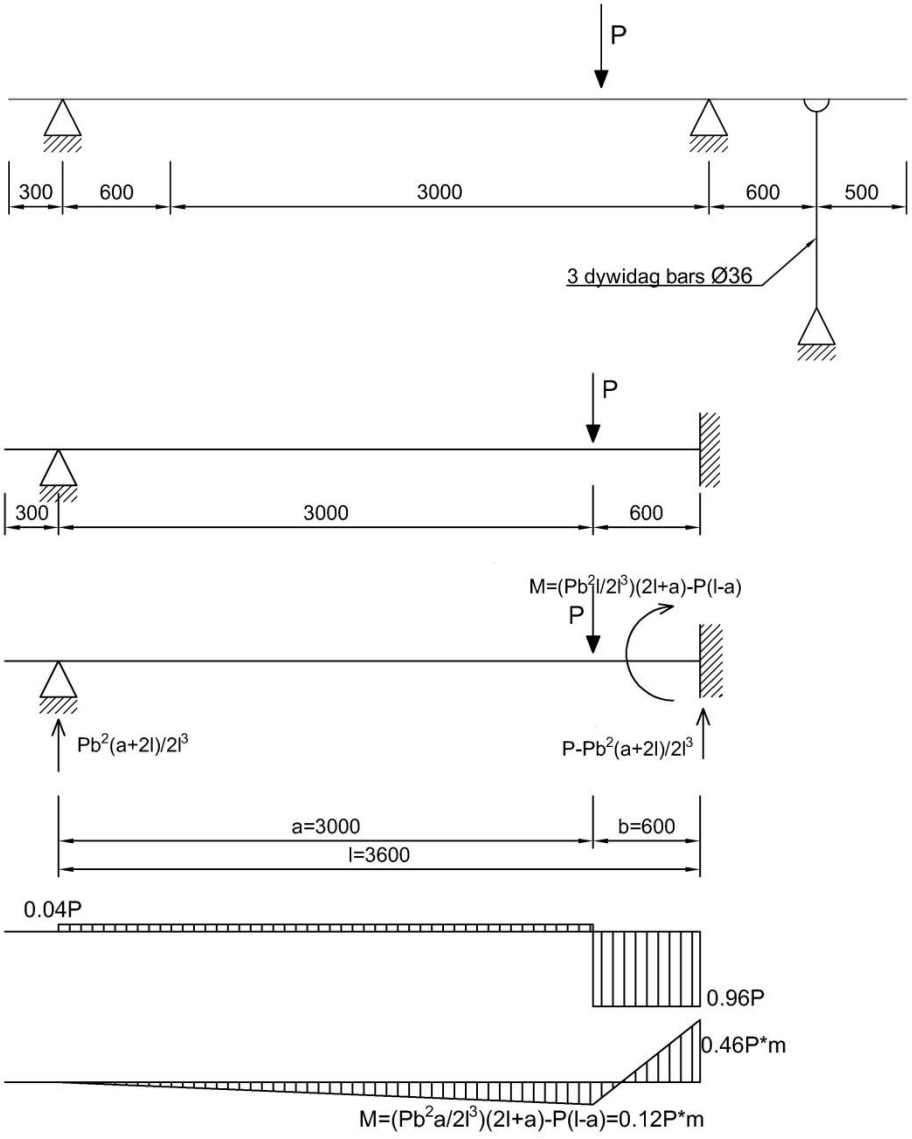

Figure 6-4: Case RS4. Internal forces (in mm)

One-way shear resistance: Model Code 2010
The design shear resistance of a slab is calculated as the design shear resistance of a member without shear reinforcement given and therefore it can be calculated with Level I and Level II of approximation:

$$V_{Rd,c} = k_v \frac{\sqrt{f_{ck}}}{\gamma_c} z b_w$$

$$d_l = 300mm - 25mm - 10mm = 265mm$$

$z = 0.9d_l = 0.9 \times 265mm = 238.5mm$

Value of the concrete compressive strength in the above expression is calculated as: $f_{ck} = 29.11MPa - 8MPa = 21.71MPa$

The formulation of k_v changes depending on the considered Level of Approximation.

The width b_w is replaced by the effective width b_{eff}, calculated by assuming a 45-degree load spreading from the far corners of the load (the so-called French method), according to (Lantsoght et al. 2013), Figure 6-5.

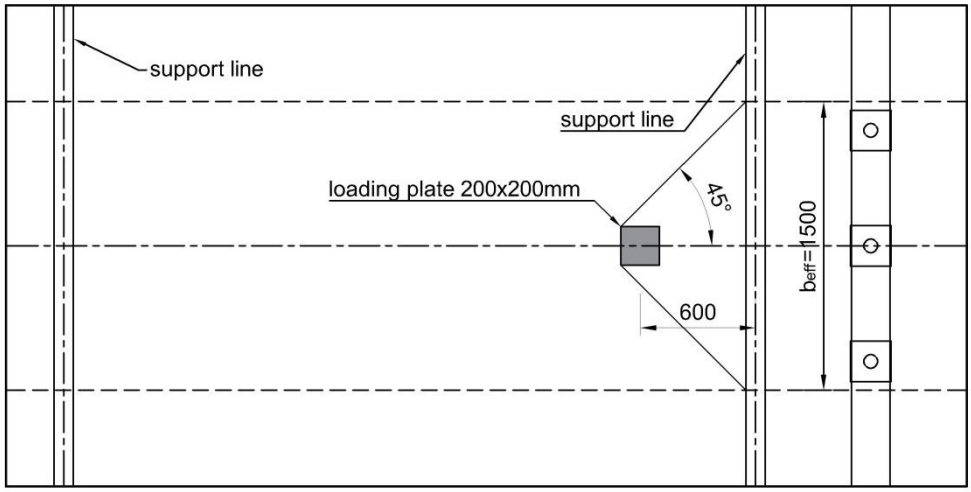

Figure 6-5: Case RS4. Assumed effective width b_{eff} (in mm)

$b_{eff} = 1500mm$

Level I Approximation

$$k_v = \frac{180}{1000 + 1.25z} = \frac{180}{1000 + 1.25 \times 238.5mm} = 0.139$$

$$V_{Rd,c} = k_v \frac{\sqrt{f_{ck}}}{\gamma_c} z b_{eff} = 0.139 \times \frac{\sqrt{21.71MPa}}{1.5} 238.5mm \times 1500mm = 154.09kN$$

Shear resistance reduced by the effect of self-weight equal at the considered location d from the support $14.2kN/m \times 15m = 21.3kN$:

$V_{Rd,c} = 154.09kN - 21.3kN = 132.79kN$ assuming concrete weight equal to 24kN/m^3.

Level II Approximation

Assumed resistance $v_{Ed} = 195.93\frac{kN}{m}$ and bending moment calculated at a distance d from the support $m_{Ed} = d \times v_{Ed} = 265mm \times 195.93kN/m = 51.92kNm/m$

$a_s = \frac{\phi^2 \pi}{4} \Big/ 125mm = 2513mm^2/m$

Strain parameter:

$$\varepsilon_x = \frac{1}{2E_s a_s}\left(\frac{m_{Ed}}{z} + v_{Ed}\right) = \frac{1}{2 \times 200GPa \times 2513mm^2/m}\left(\frac{51.92kN/m}{238.5mm} + 195.93\frac{kN}{m}\right) = 3.918 \times 10^{-4}$$

$$k_{dg} = \frac{32}{16 + d_g} = \frac{32}{16+16} = 1 \geq 0.75$$

$$k_v = \frac{0.4}{1+1500\varepsilon_x} \times \frac{1300}{1000+k_{dg}z} = \frac{0.4}{1+1500\times 3.918\times 10^{-4}} \times \frac{1300}{1000+239mm} = 0.264$$

$v_{Rd,c} = k_v \frac{\sqrt{f_{ck}}}{1.5} z = 0.264 \frac{\sqrt{21.71}MPa}{1.5} 239mm = 195.92 \frac{kN}{m}$ equal to the assumed value.

Shear resistance of the effective width:

$$V_{Rd,c} = v_{Rd,c} b_{eff} = 195.92 \frac{kN}{m} \times 1500mm = 293.87kN$$

After accounting for the self-weight, it is:

$$V_{Rd,c} = 293.87kN - 21.3kN = 272.57kN$$

One-way shear resistance: Eurocode 2

$$V_{Rd,c} = b_{eff}\, d\left[C_{Rd} k (100\rho_l f_{ck})^{1/3}\right] =$$

$$= 1500mm \times 265mm \left[0.12 \times 1.869 (100 \times 9.484\times 10^{-3} \times 21.71)^{1/3}\right] = 244.31kN$$

Where:

$$k = 1 + \sqrt{\frac{200}{d}} = 1 + \sqrt{\frac{200}{265}} = 1.869 \le 2$$

$$\rho_l = \frac{A_s}{d \times s} = \frac{314.15mm^2}{265mm \times 125mm} = 9.484 \times 10^{-3}$$

and the resistance is greater than:

$V_{Rd,c,\min} = v_{\min} \times b_{eff} \times d = 0.035 k^{\frac{3}{2}} f_{ck}^{\frac{1}{2}} \times b_{eff} \times d = 0.417MPa \times 1500mm \times 265mm = 165.6kN$ After accounting for the self-weight, it is:

$$V_{Rd,c} = 244.31kN - 21.3kN = 223.01kN$$

Punching strength: Regan's equation

In order to evaluate the punching strength P_R, a rectangular control perimeter u, outlined in red color in Figure 6-6 is determined.

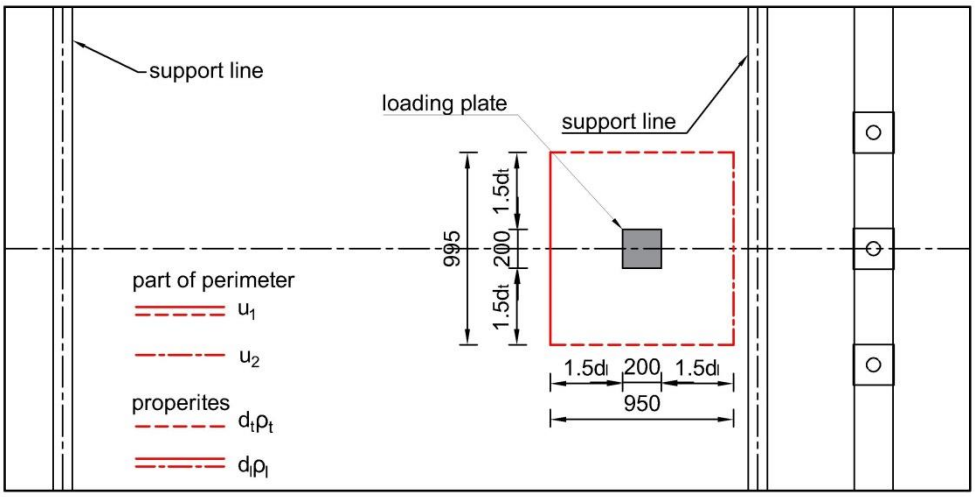

Figure 6-6: Case RS4. Control perimeter according to Regan's formulation

$$P_R = P_{R1} + P_{R2}$$

P_{R2} refers to the edge of the perimeter running parallel to the support; P_{R1} refers to the remaining part.

$$P_{R2} = \frac{2d_l}{a_v}\xi_{sl} v_{cl} u_2 d_l$$

$$\xi_{sl} = \sqrt[4]{\frac{500}{d_l}} = \sqrt[4]{\frac{500}{265}} = 1.172$$

$$\rho_l = \frac{\pi\phi_l^{\,2}}{4} \times \frac{1}{s_l \times d_l} = \frac{\pi \times (20mm)^2}{4} \times \frac{1}{125mm \times 265mm} = 9.484 \times 10^{-3}$$

$$v_{cl} = \frac{0.27}{\gamma_c}\sqrt[3]{100\rho_l f_{ck}} = \frac{0.27}{1.5}\sqrt[3]{100 \times 9.484 \times 10^{-3} \times 21.71}MPa = 0.493MPa$$

$a_v = 450mm$ is net distance between support 1 and a loading plate

$$u_2 = 1.5 \times d_t + 200 + 1.5 \times d_t = 1.5 \times 250 + 200 + 1.5 \times 250 = 950\,mm$$

And

$$d_t = h - c - \phi_1 - \phi_2/2 = 300mm - 25mm - 20mm - 5mm = 250\,mm$$

$$P_{R2} = \frac{2d_l}{a_v}\xi_{sl} v_{cl} u_2 d_l = \frac{2 \times 265mm}{450mm} \times 1.172 \times 0.493MPa \times 950mm \times 265mm = 171.44kN$$

$$P_{R1} = \xi_{sl} v_{cl} u_2 d_l + 2\xi_{st} v_{ct} u_1 d_t$$

$$\xi_{st} = \sqrt[4]{\frac{500}{d_t}} = \sqrt[4]{\frac{500}{250}} = 1.189$$

$$\rho_t = \frac{\pi\phi_t^{\,2}}{4} \times \frac{1}{s_t d_t} = \frac{\pi \times (10mm)^2}{4} \times \frac{1}{250mm \times 250mm} = 1.257 \times 10^{-3}$$

$$v_{ct} = \frac{0.27}{\gamma_m}\sqrt[3]{100\rho_t f_{ck}} = \frac{0.27}{1.5}\sqrt[3]{100 \times 0.001257 \times 21.71}MPa = 0.252MPa$$

$$u_1 = 1.5d_l + 200 + 1.5d_l = 1.5 \times 265 + 200 + 1.5 \times 265 = 995\,mm$$

$$P_{R1} = \xi_{sl} v_{cl} u_2 d_l + 2\xi_{st} v_{ct} u_1 d_t =$$
$$= 1.172 \times 0.493MPa \times 950mm \times 265mm + 2 \times 1.189 \times 0.252MPa \times 995mm \times 250mm =$$
$$= 294.37kN$$

Total punching shear resistance:

$$P_R = P_{R1} + P_{R2} = 294.37kN + 171.44kN = 465.81kN$$

At a continuous support, the total shear resistance is multiplied with a factor α.

$\alpha = \sqrt{\frac{M_1 + M_2}{M_1}} = \sqrt{\frac{209.61kNm + 55.9kNm}{209.61kNm}} = 1.125$ where M_1 is the larger moment at the end of the shear span and M_2 is the lower moment; both moments with absolute values.

$P_R = 1.125 \times 465.81kN = 524.3kN$. After taking into account the contribution of self-weight to the resistance assumed as the weight of a punching cone, the resistance is:

$P_R = 522.98kN$

Punching strength: Eurocode 2 formulation

The reduced control perimeter u, outlined in red color in Figure 6-7, is determined to calculate the punching strength. This solution is a conservative approximation due to the fact that the load is located close to the edge of the line support. For such a case, a portion of the applied load is transferred directly to the support increasing in this way the shear resistance. In the assumed solution, the control perimeter would suggest that shear stresses are of the same value along the punching cone contour, thus it is conflicting with the statement above. The increase of the shear resistance resulting from direct load transfer can be also motivated by the final conclusion of the source

document. The document claims that one-way slabs under concentrated load close to the support fail in a combination of one-way (thus where compressive strut action is permitted within a certain distance) and two-way shear.

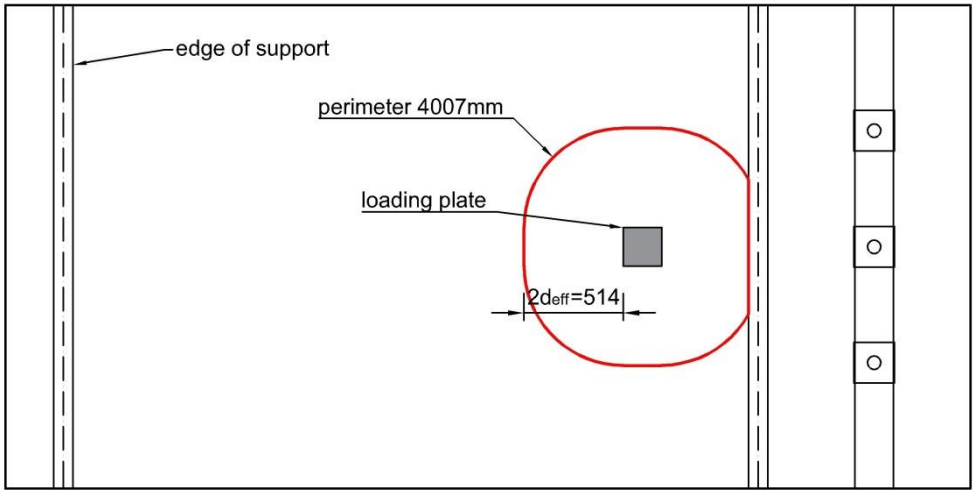

Figure 6-7: Case RS4. Control perimeter according to Eurocode 2 formulation

$$V_{Rdc} = v_{Rdc} \times u \times d_{eff}$$

$$d_{eff} = \frac{d_l + d_t}{2} = \frac{265mm + 250mm}{2} = 257.5mm$$

$$k = 1 + \sqrt{\frac{200}{d_{eff}}} = 1 + \sqrt{\frac{200}{257.5mm}} = 1.881$$

$$\rho = \sqrt{\rho_l \times \rho_t} = \sqrt{0.00948 \times 0.00126} = 0.00345$$

$$v_{Rdc} = C_{Rd,c} k (100 \times \rho \times f_{ck})^{1/3} = 0.12 \times 1.88 \times (100 \times 0.00345 \times 21.71)^{1/3} = 0.442MPa$$

$$V_{Rdc} = v_{Rdc} u d_{eff} = 0.442MPa \times 4007mm \times 257.5mm = 459.13MPa$$

After taking into account the contribution of self-weight to the resistance assumed as the weight of a punching cone, the resistance is:

$$P_R = 458.01kN$$

In Table 6-2 the design values of beam resistance associated to one-way shear failure and punching failure expressed in terms of applied load P_{Rd} reduced by effect of dead weight are summarized.

Table 6-2: Case RS4. Design values of beam resistance expressed in terms of applied load P_{Rd}

	One-way shear (MC 2010)			Punching	
	Level I (kN)	**Level II (kN)**	**EC2 (kN)**	**Regan (kN)**	**EC2 (kN)**
P_{Rd} **(kN)**	132.79	272.57	223.98	522.98	458.01

Slab RS4 fails due to one-way shear, indeed the design shear resistance associated to one-way shear failure is lower than the design punching resistance.

6.3 Finite element model

Units

Units are N, mm.

Material models and parameters

The concrete model is based on a total strain rotating crack model with:

- exponential softening in tension and parabolic behavior in compression,
- variable Poisson's ratio of concrete
- increase in compressive strength due to lateral confinement according to the model proposed by Selby and Vecchio (Selby and Vecchio 1993).

The mechanical properties are summarized in Table 6-3. The uniaxial stress-strain curve is shown in Figure 6-8. The model for the reinforcement bars is based on hardening plasticity. Geometrical and mechanical properties of reinforcement are summarized Table 6-1. The stress-strain curve of bars ϕ20 is plotted in Figure 6-9.

Table 6-3: Case RS4. Constitutive model parameters for concrete

	f_{cm} (N/mm^2)	f_{ctm} (N/mm^2)	E_c (N/mm^2)	ν	G_F (Nmm/mm^2)
Mean measured value	29.71	2.79**	30910*	var	0.134*

*Not specified in reference; estimated according to Model Code 2010 (fib, 2013)
**Estimated from the mean splitting tensile strength of concrete as $f_{ctm} = 0.9 f_{ctm,sp}$ according to Eurocode 2 formulation (CEN, 2005)

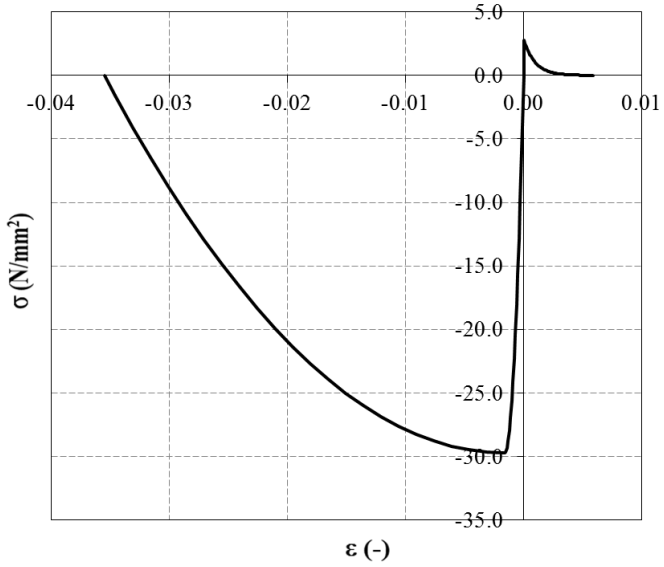

Figure 6-8: Case RS4. Stress-strain curve for concrete

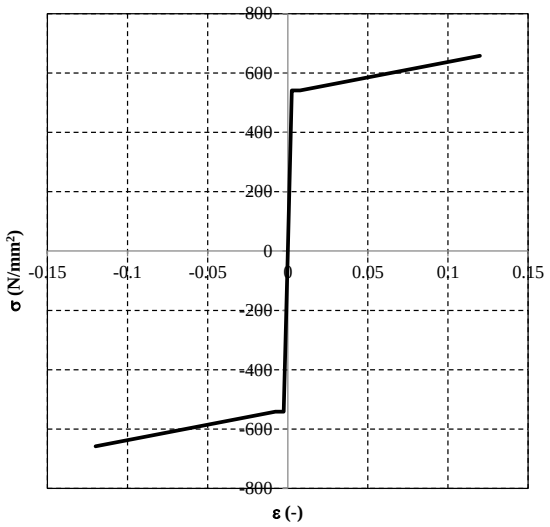

Figure 6-9: Case RS4. Stress-strain curve adopted for ϕ20

For the steel plates a linear elastic behavior is assumed, see Table 6-4.

Table 6-4: Case RS4. Steel plates properties

E **(N/mm^2)**	***ν***
210000	0.3

Interface: interface elements were placed between steel plates, steel profiles and concrete slab at the location of supports and loading positions.For construction of the support-concrete slab interface, 10 mm layer of P50 Nevima felt and 8 mm layer of plywood were used at the simple and continuous support. At the prestressed end, a layer of 5 mm thick P50 felt was used. The nonlinear mechanical behaviour of felt and plywood/felt in the normal direction is evaluated from experimental test, Figure 6-10. A linear elastic behaviour is assumed in the shear and tensile directions, with stiffness value almost equal to zero. In Figure 6-11 the non-linear mechanical behaviour of felt and plywood/felt used in the analysis is plotted. The displacement was calculated by multiplying strain by the thickness of the felt (5 mm) and plywood/felt (18 mm) respectively.

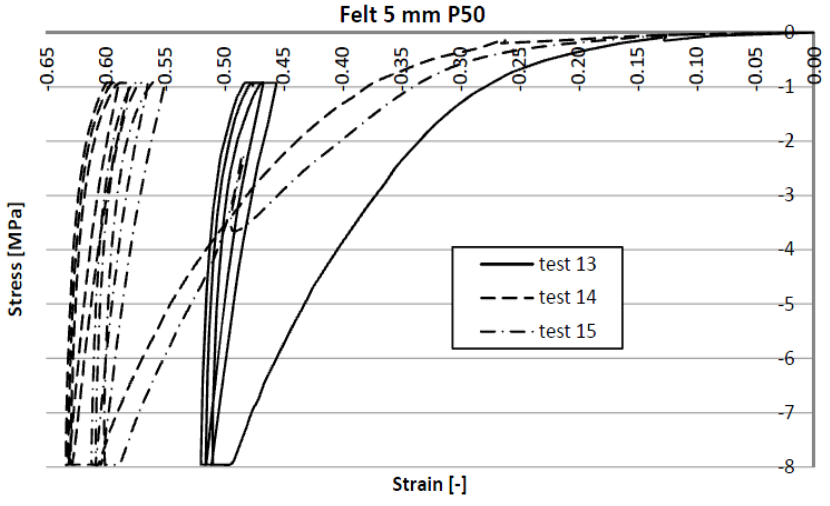

(a)

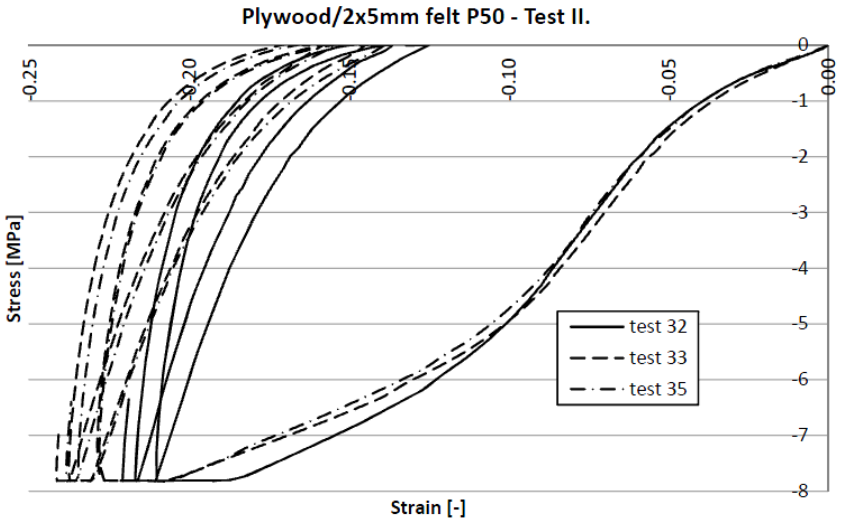

(b)

Figure 6-10: Case RS4. (a) Experimental stress-strain diagram of felt, (b) experimental stress-strain diagram of plywood/felt (Lantsoght 2012)

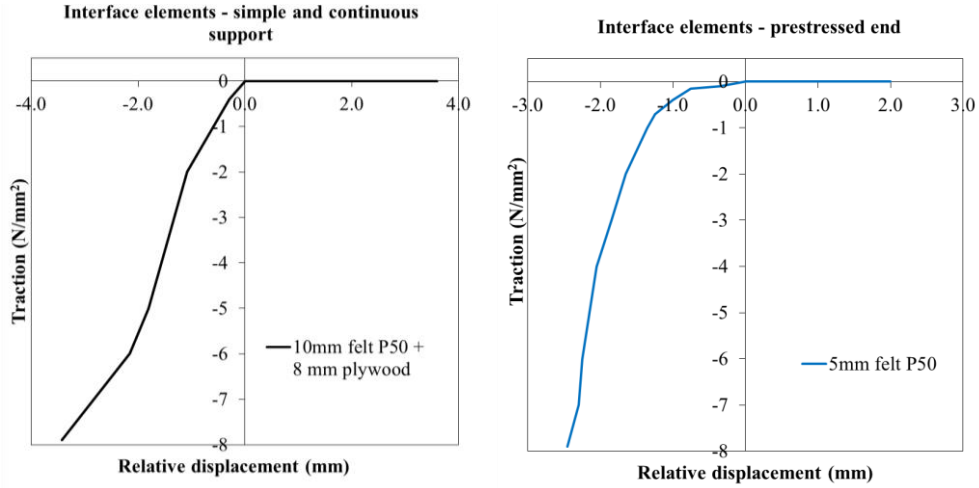

Figure 6-11: Case RS4. Traction-relative displacement diagram of plywood/felt and of felt used in NLFEA

Element types and finite element mesh

For meshing the concrete slab 20-node solid elements (CHX60) are used. The generated mesh has a regular pattern. The specified element size is 50×50×50 mm and is governed by the minimum number of elements over the slab thickness which for a 3D model of a slab is *h/6*. The reinforcement bars were modelled with embedded truss elements with two Gauss integration points along the axis of the element. Perfect bond was assumed. Dywidag bars were modelled with 2-node truss elements. The dywidag bars consist of only one element over the whole length. The elements in the steel plates of an increased thickness to avoid uplifting of the corners as the result of an applied load were generated with 20-node solid elements (CHX60). The properties of interface between loading plate, supporting steel profiles, the beam accommodating the prestressed bars and concrete slabs were assigned through 16-node (CQ48I) interfaces elements.

The mesh of the slab is shown in Figure 6-12(a) whereas the reinforcement layout is illustrated in Figure 6-12 (b). Different material properties for solid elements as well as

different element geometries i.e. a cross-sectional area of reinforcement are indicated with diverse colors.

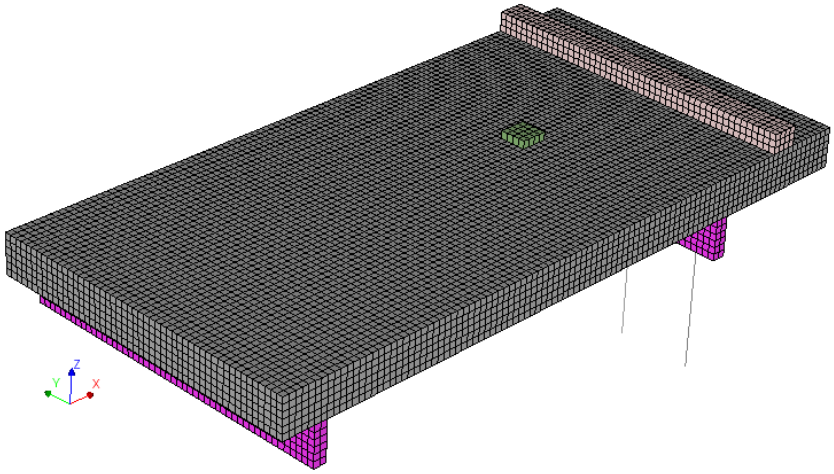

(a)

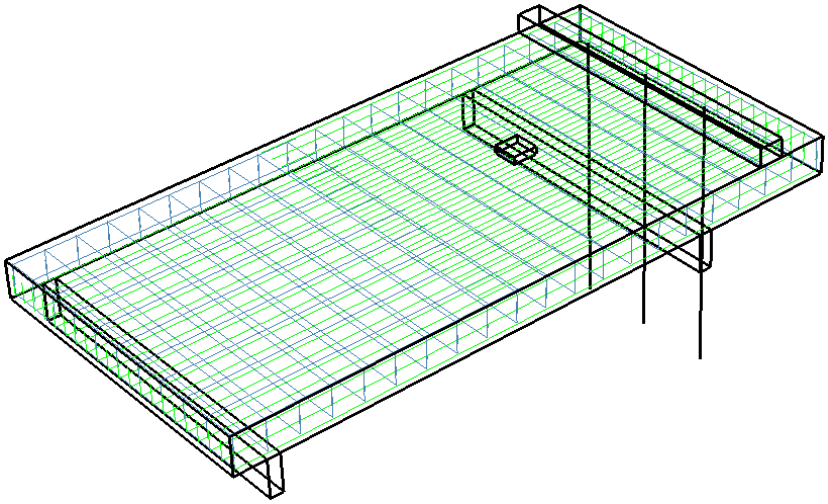

(b)

Figure 6-12: Case RS4. (a) Mesh, (b) reinforcement layout

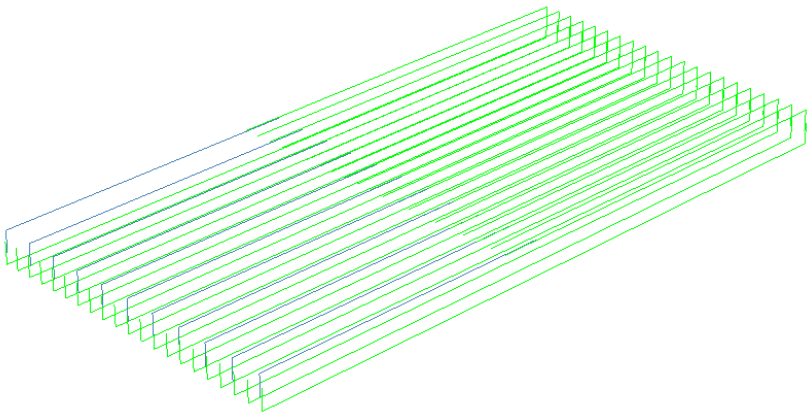

Figure 6-13: Case RS4. Groups of longitudinal reinforcement elements: "TOPF10L" (blue), "TOPF20L" (top rebars in green), "BOTF20L" (bottom rebars in green)

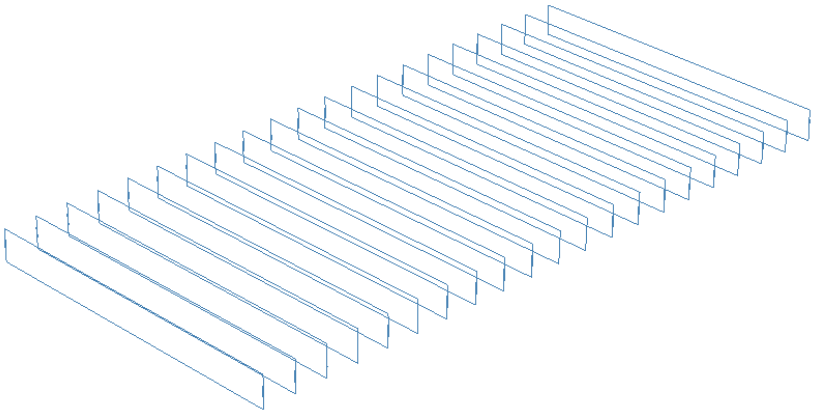

Figure 6-14: Case RS4. Groups of transverse reinforcement elements: "TOPF10T" and "BOTF10T"

Boundary conditions and loading

Boundary conditions are applied to nodes of steel profiles, steel plate and dywidag bars, Figure 6-15. The following sets of constraints were applied:

- translation in *x*, *y* and *z* direction was constrained through supports applied to the nodes at the bottom face of the supporting steel profiles (support 1 and 2)
- translation along *z* direction at the middle node of the loading plate was constrained
- the dywidag bars were constrained along *z* direction at the bottom and along *y* and *x* at the top end

The analysis was carried out in displacement control by applying a displacement along *z* axis at the middle node of the loading plate.

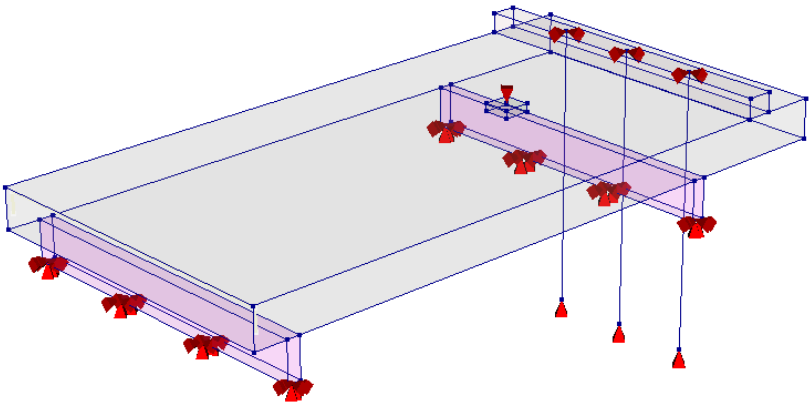

Figure 6-15: Case RS4. Boundary conditions

Phased analysis was executed which enabled application of prestressing to the dywidag bars. In the first phase, the dead load *q* and an axial force *F* equal to 15 kN were applied to the dywidag bars, load case 1 and 2 respectively in Figure 6-16(a). In the second phase shown in Figure 6-16(b), supports were added to the bottom ends of dywidag bars. Additionally, in the second phase, a prescribed displacement *d* was applied to the node situated at the center of the loading steel plate as load case 3, Figure 6-17.

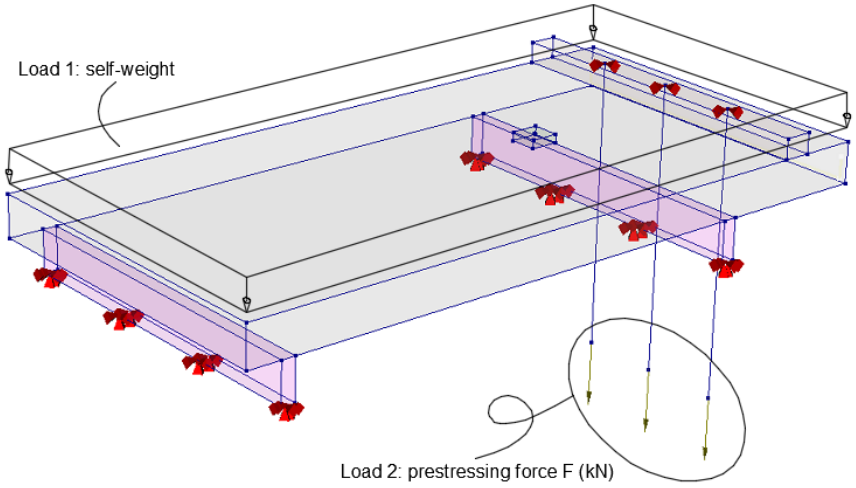

(a)

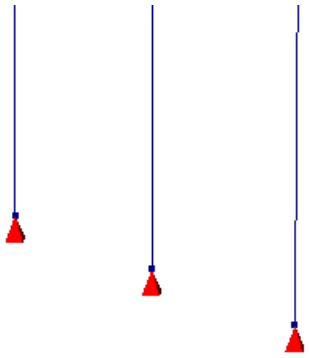

(b)

Figure 6-16: Case RS4. Loading components of phased analysis: (a) load cases 1 and 2 of analysis phase 1, (b) attached supports to dywidag bars in analysis phase 2

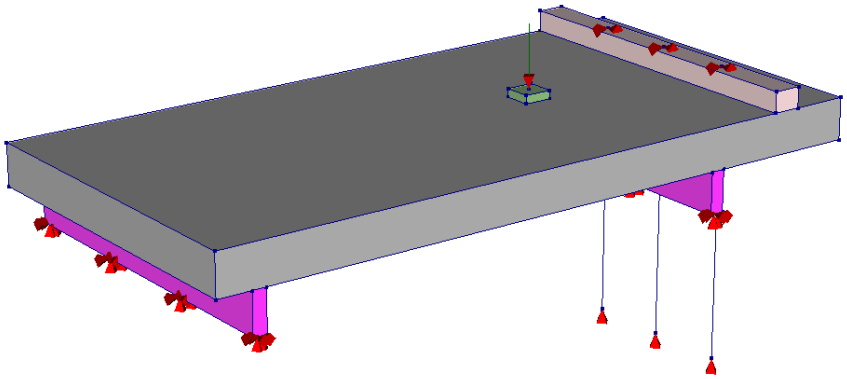

Figure 6-17: Case RS4. Load case 3 in phase analysis 2

Load increments and convergence criteria

Load case 1 and Load case 2: both loads were applied simultaneously using a single load increment. Regular Newton-Raphson method with a maximum of 25 iterations was adopted. As the convergence criteria, force and energy norms were selected. The analysis was set to continue even if the convergence criteria were not satisfied. Convergence tolerances equal to 1×10^{-3} and 1×10^{-2} were specified for energy and force norms, respectively.

Load case 3: the prescribed displacement in the *z* direction equal to -1mm was applied to the middle node of the steel plate. The user specified load step size of 0.2 of the whole prescribe deformation was applied in a total of 50 steps. To find the state of equilibrium, Regular Newton-Raphson iterative procedure was incorporated with a maximum of 140 iterations in each load increment. The equilibrium iterations were set to continue even if the convergence criteria were not satisfied. Convergence tolerances were equal to 1×10^{-3} and 1×10^{-2} for energy and forces, respectively.

6.4 Nonlinear finite element analysis

Force-displacement response

The force-displacement curve is presented in Figure 6-18(b). Besides the general response of the structure, the curve pinpoints the load steps attributed to: onset of yielding of bottom transverse bars and crushing of concrete. Crushing of concrete in the analysis was recognized when the value of minimum principal strain of -3.5‰ in the first integration point was reached

In order to preserve the consistency between the tests and the NLFEA the same procedure of determining the mean displacement was put into effect. The values of mean deflection were established based on the readings from lasers surrounding the loading plate at the distance of 265mm from the application of the load. The positions of the lasers are designated as points A, B, C, D in Figure 6-18(a). Following suit, the mean deflection from NLFEA was obtained considering the displacements of four corresponding nodes

The peak load is defined as the highest load step which satisfies the fixed energy norm tolerance of 1×10^{-3}. Prior to the peak load all load steps converged within the specified number of iteration except for step 20 at which local crushing of concrete near the loading plate took place. The convergence norm was satisfied in the consecutive load step after 117 iterations. After reaching the peak load in step 28 of 769kN, 7 consecutive steps converged (up to step 35) followed by a lack of convergence in the remaining steps until the end of the analysis.

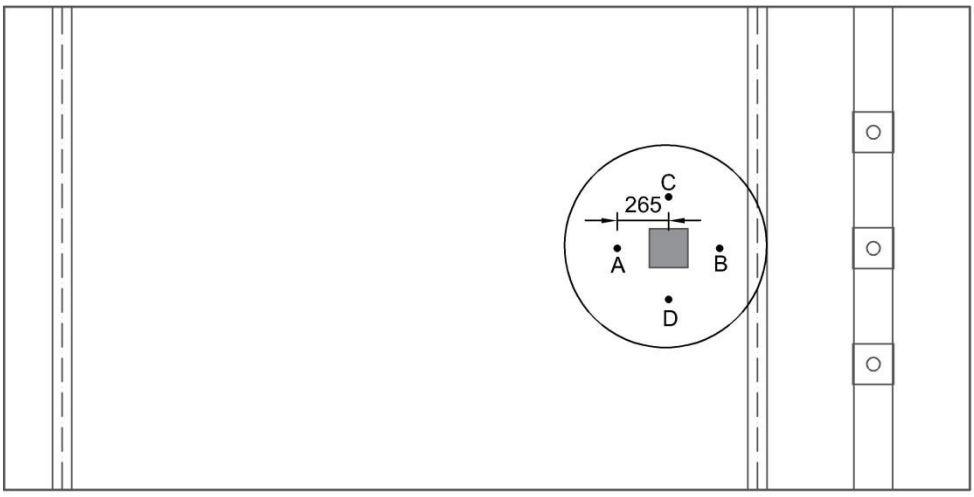

(a)

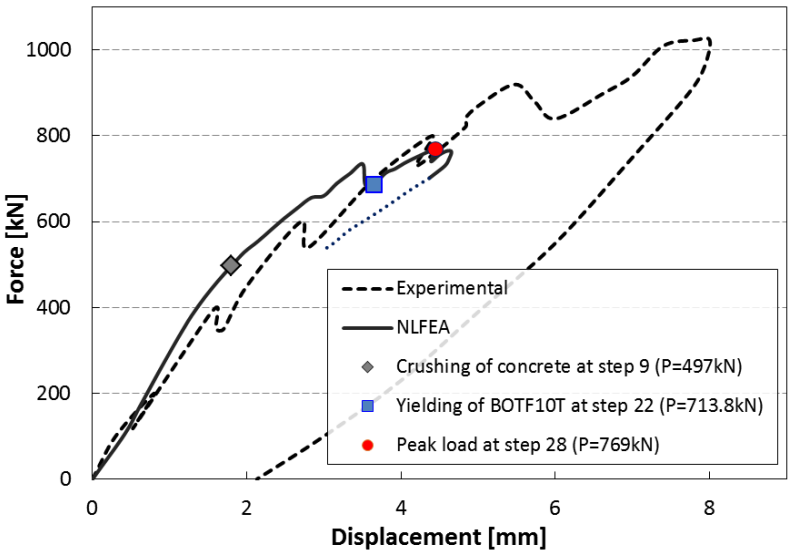

(b)

Figure 6-18: Case RS4. (a) Determination of mean deflection, (b) Force-displacement curve

Convergence behavior

For a vast majority of steps, convergence was reached only on the basis of an energy criterion, Figure 6-19 and Figure 6-20. Prior to the peak load, the energy norm ratio has not satisfied the fixed tolerance of 1×10^{-3} only in step 20. It is indicated in Figure 6-19 with a yellow marker. Contrary to that, very few of the load steps reached convergence based on the force norm. In Figure 6-19, a red circle indicates the peak load position on the graph.

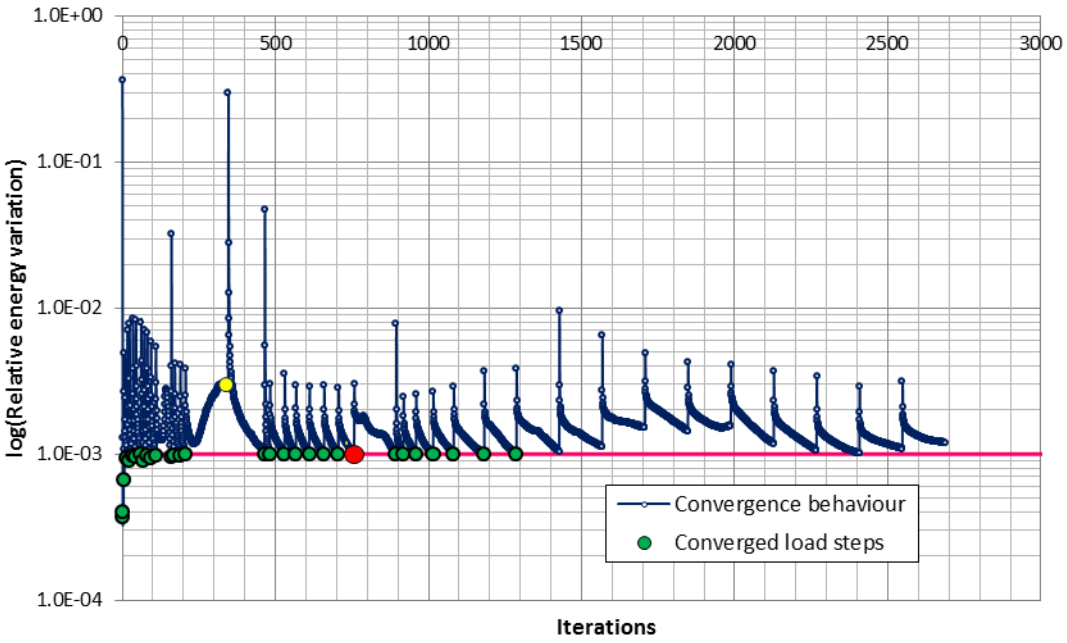

Figure 6-19: Case RS4. Evolution of the energy norm (markers indicate iterative results)

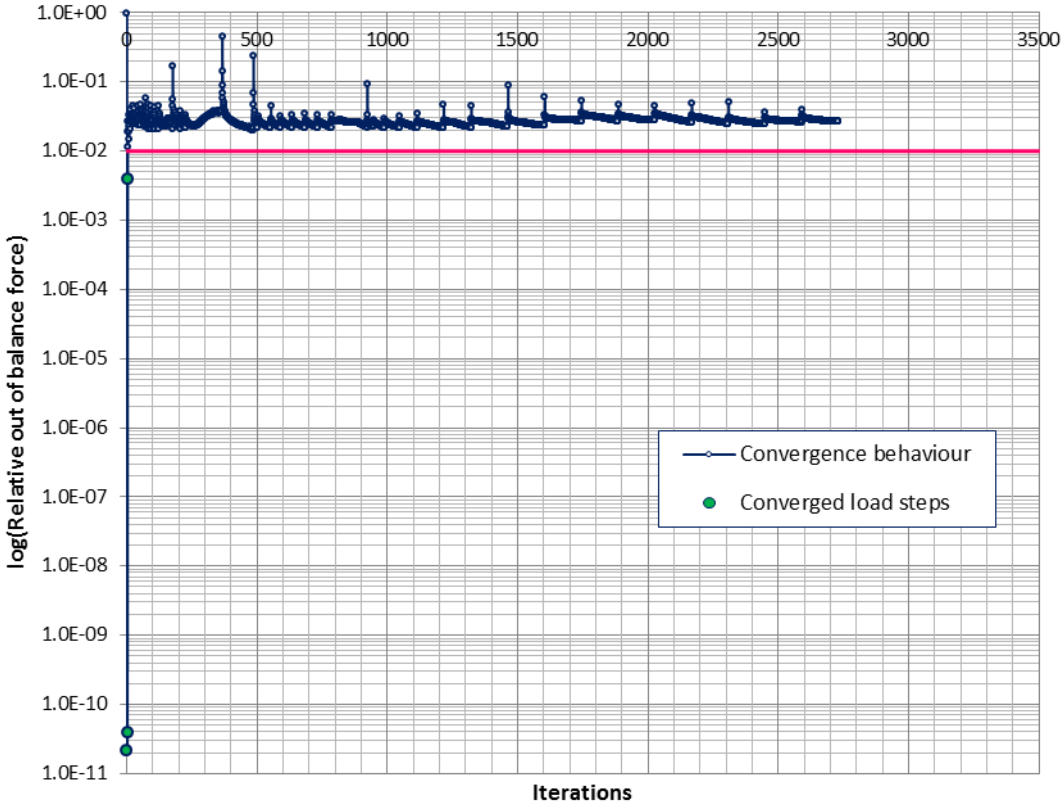

Figure 6-20: Case RS4. Evolution of the force norm

Strains in concrete

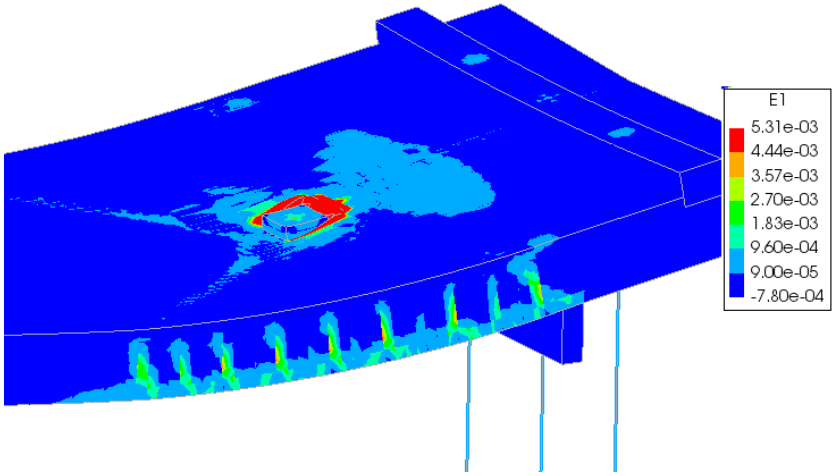

Figure 6-21: Case RS4. Minimum principal strain at step 28 - peak load

Figure 6-22 and Figure 6-22 show the positive principal strain values at the peak load (at step 28) and step 29, for the whole slab and at the section with normal in global *y* direction near the location of loading plate. The displayed colors in the contour plots correspond to the assigned values in the concrete softening curve in Figure 6-22(e). Special attention is drawn to three values of principal strain. The first principal strain value 9.06e-5 indicates occurrence of cracking. The second principal strain value equal to 0.000963, corresponds to the ultimate strain value calculated as $\varepsilon_{t,u} = \frac{G_F}{h \cdot f_{ctm}}$, while

the third principal strain value, equal to 0.0044, is the strain value corresponding to 1% of f_{ctm}. Intermediate principal strain values have been added in the contour plot for clarity.

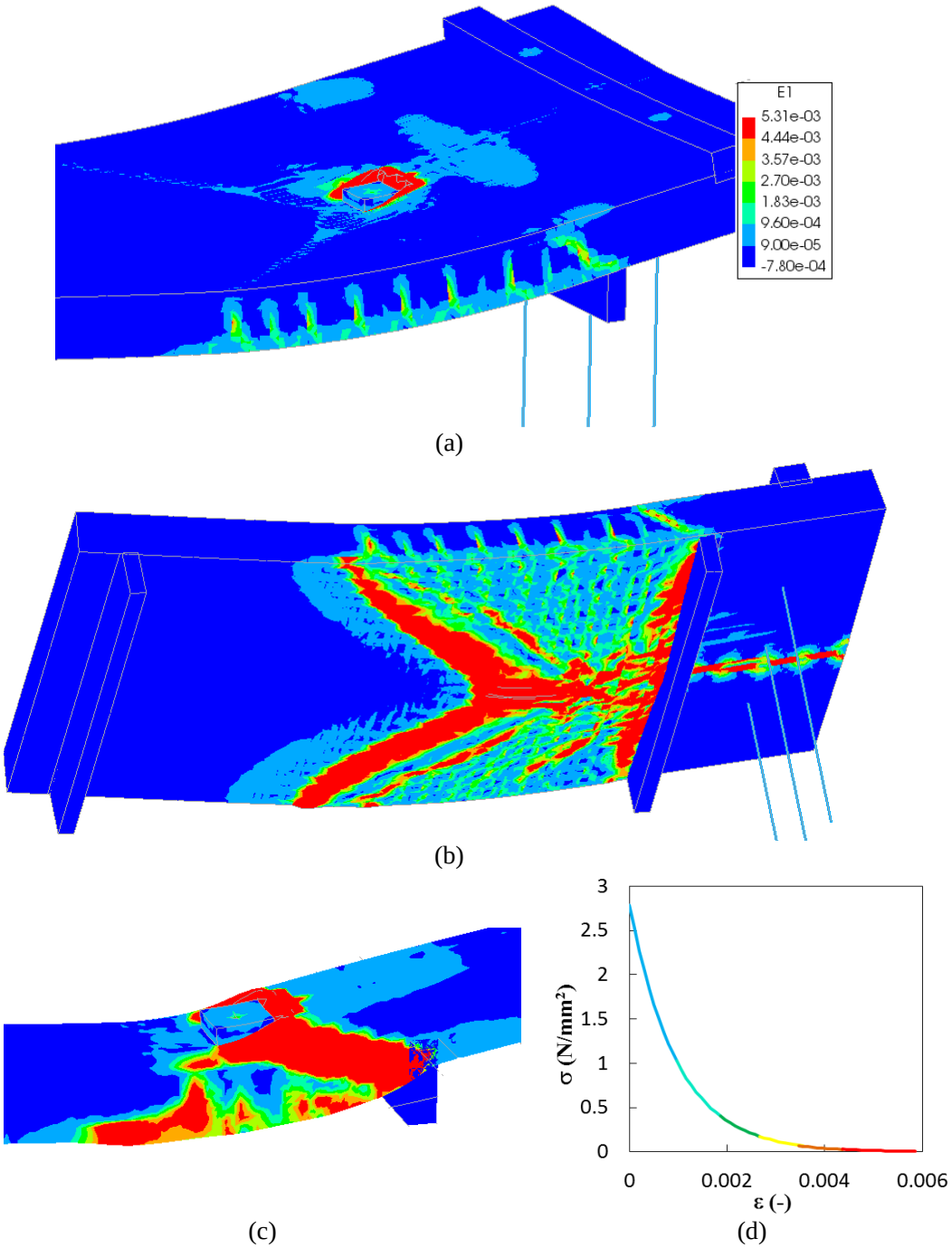

Figure 6-22: Case RS4. Positive principal strains at step 29: (a) top surface, (b) bottom side, (c) cross section near the loading plate, (d) exponential softening curve in tension

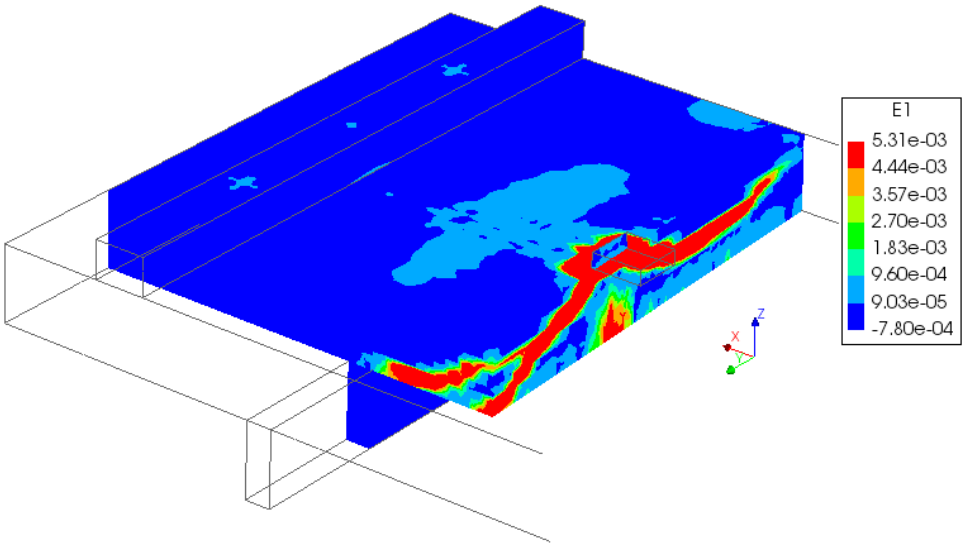

Figure 6-23: Case RS4: Section of slab limited by planes with normal in global *x* and *y* directions, step 29

Figure 6-24 shows the minimum principal strain values at the peak load and the subsequent step for the whole slab as well as a section along the *y* axis near the loading plate. A number of critical values has been highlighted. The first value of minimum principal strain, equal to -3.2e-4 corresponds to the limit principal strain value in the elastic range according to expression $\varepsilon_{c,el} = \frac{f_{cm}}{3 \cdot E_c}$. The second negative principal strain value -0.0016 is the peak strain value determined with the formula: $\varepsilon_{c,p} = -\frac{5}{3}\frac{f_{ctm}}{E}$. The last minimum principal strain value, equal to -0.0355 is the crushing strain value calculated as $\varepsilon_{c,u} = \varepsilon_{c,p} - \frac{3G_c}{2 \cdot h \cdot f_{cm}}$. The presented values in the legend in Figure 6-24 and contour plots can be related to the parabolic curve in Figure 6-25(d) where the exact compressive softening of concrete is portrayed.

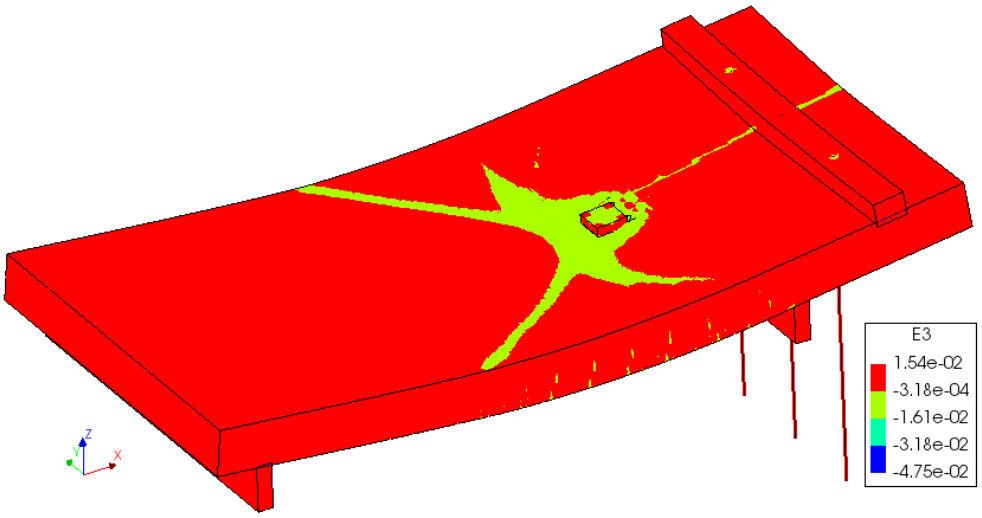

Figure 6-24: Case RS4. Minimum principal strain values at step 28-peak load

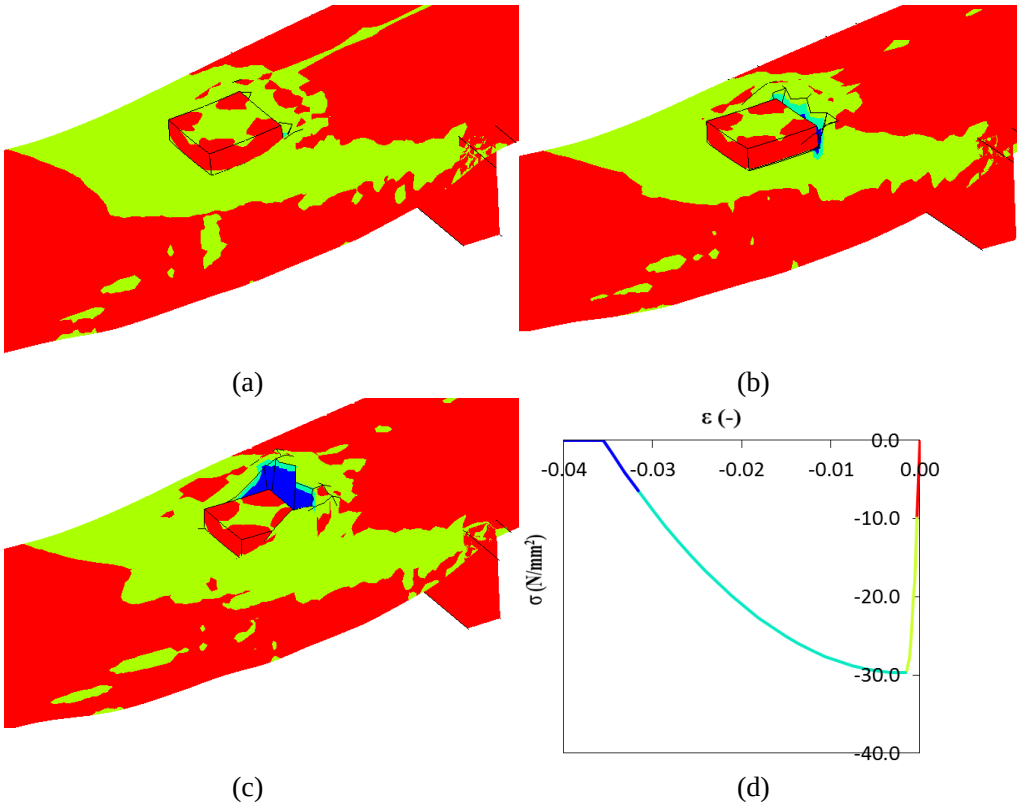

Figure 6-25: Case RS4. Normalized deformation of concrete near the loading plate at: (a) step 28 – peak load, (b) step 29, (c) step 35 – the last converged step, (d) compressive softening of concrete

Strains in steel

Yielding strain of bottom transversal bars ϕ10 BOTF10T is equal to 537MPa/210000MPa = 2.56 10^{-3}. BOTF10T bars began to yield at a load equal to 713.8 kN (step 22). Figure 6-26 shows yielding of bars a few steps after the yielding point (at step 29).

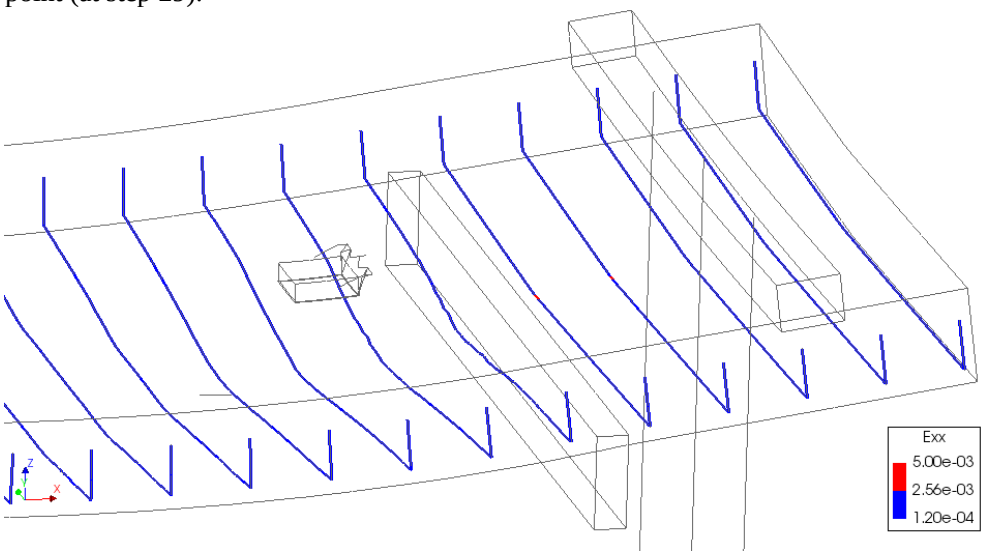

Figure 6-26: Case RS4. Yielding in tension of BOTF10T at step 29

Based on the results, it is possible to conclude on a number of distinctive characteristics. From the contour plots of positive principal strains in Figure 6-21, Figure 6-22 (a)-(c) and Figure 6-23, which can be regarded as representation of a crack pattern, one can see that the slab is extensively cracked both due to flexure and shear. The major traits however are the inclined critical shear cracks. What can be also seen in Figure 6-23, is that this cracks propagate in two directions – longitudinally and transversely from the point of load application, indicating mixed mode of failure thus a combination of one-way and two-way shear. Further, from values of principal strain it can be noticed that the critical cracks are fully open – stress free. Cracking in tension is accompanied by high compressive stress in concrete struts along the critical shear cracks and crushing of concrete near the point of load application resulting in sinking of the loading plate. From the foregoing observation and the fact the no yielding in flexural reinforcement took place, it is concluded that the slab failed in a combination of one-way and two-way shear. This outcome is contradictory with the results of the experimental test which was concluded with wide beam shear failure shown in Figure 5-6 in the previous case study RS3. In addition to that, cracking in the longitudinal direction is better described by cracking pattern assumed for beam shear failure shown in Figure 6-27 (a) whereas in transverse direction by punching shear failure in Figure 6-27 (b).

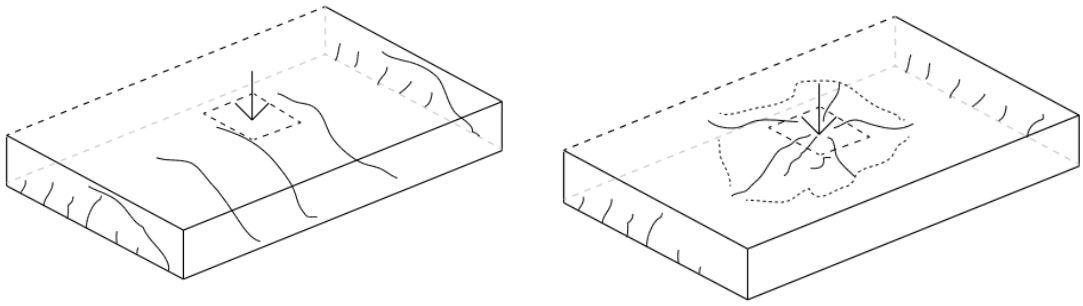

(a) (b)

Figure 6-27: Case RS4: Assumed crack pattern for: (a) beam shear failure, (b) punching shear failure (Lantsoght, 2013)

6.5 Application of safety format

A safety assessment of resistance calculated by non-linear analysis is carried out with application of safety formats. The methods included, as proposed in Model Code 2010, are: GRF (Global Resistance Factor method), PF (Partial Factor method) and ECOV (Method of Estimation of a Coefficient of Variation of resistance). The safety assessment with safety formats requires a total of four nonlinear analyses. The mechanical properties of steel and concrete used in the analyses are given in Table 6-5 to Table 6-7. The analyses were carried out adapting the same load increments and convergence criteria as described in the earlier part of the case study.

Table 6-5: Case RS4. Constitutive model parameters for concrete

	f_c (N/mm^2)	f_{ct} (N/mm^2)	E_c (N/mm^2)	ν	G_F (Nmm/mm^2)	G_C (Nmm/mm^2)
Mean measured	29.71	2.79	30910	var	0.134	33.60
Characteristic	21.71	1.95	27841	var	0.127	31.76
Mean GRF	18.46	2.09	26373	var	0.123	30.84
Design	14.48	1.30	24321	var	0.118	29.52

Table 6-6: Case RS4. Constitutive model parameters for reinforcing bars (ϕ10)

	ϕ (mm)	A_s (mm^2)	f_y (N/mm^2)	f_t (N/mm^2)	E_s (N/mm^2)	ε_{sy} (-)
Mean measured	10	79	537	628	210000	0.0026
Characteristic	10	79	486.38	568.81	210000	0.0023
Mean GRF	10	79	535.02	625.69	210000	0.0025
Design	10	79	422.94	494.61	210000	0.0020

Table 6-7: Case RS4. Constitutive model parameters for reinforcing bars (ϕ20)

	ϕ (mm)	A_s (mm^2)	f_y (N/mm^2)	f_t (N/mm^2)	E_s (N/mm^2)	ε_{sy} (-)
Mean measured	20	314	541	658	210000	0.0026
Characteristic	20	314	490.01	595.98	210000	0.0023
Mean GRF	20	314	539.01	655.58	210000	0.0026
Design	20	314	426.09	518.24	210000	0.0020

In Figure 6-28 the load-deflection curves obtained with mean measured, characteristic, mean GRF and design values of material strengths are shown. The peak load values are indicated in the graph with circular indicators. As far as a failure mode of the safety format analyses is concerned, all models failed in a similar manner thus due to shear accompanied by crushing of concrete near the loading plate and limited yielding of reinforcement. In contrast to the analysis with mean measured material properties, the NLFEA with safety format methods failed only in one way shear described as beam shear failure, Figure 6-27(a). The positive principal strains contour plots at step 26 – being one load step after the peak load, are presented in Figure 6-29.

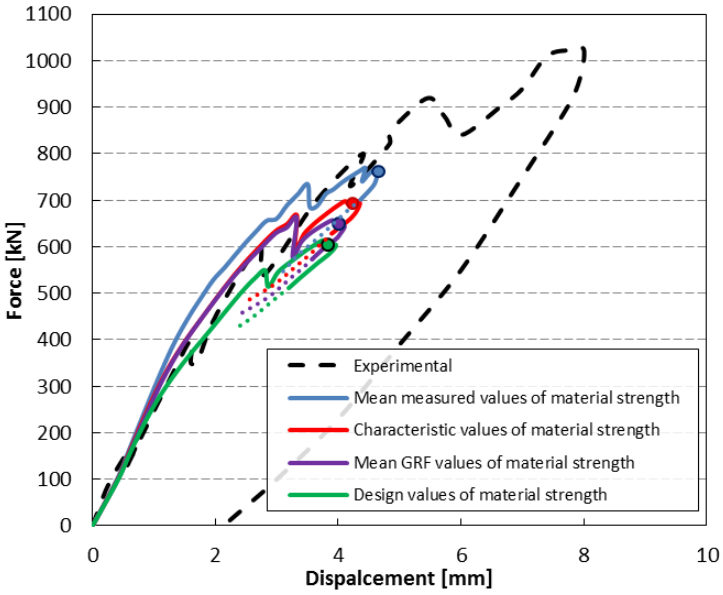

Figure 6-28: Case RS4. Force-displacement curves obtained with mean measured, characteristic, mean GRF and design mechanical properties

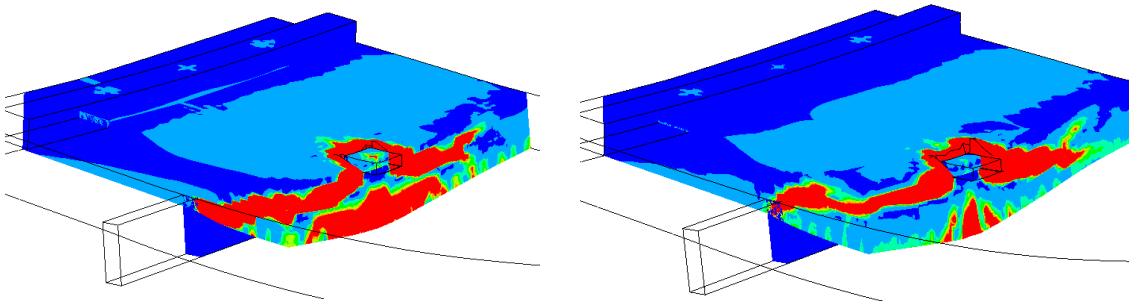

(a) (b)

Figure 6-29: Case RS4: Positive principal strain contours at step 26 for: (a) GRF method, (b) PF method

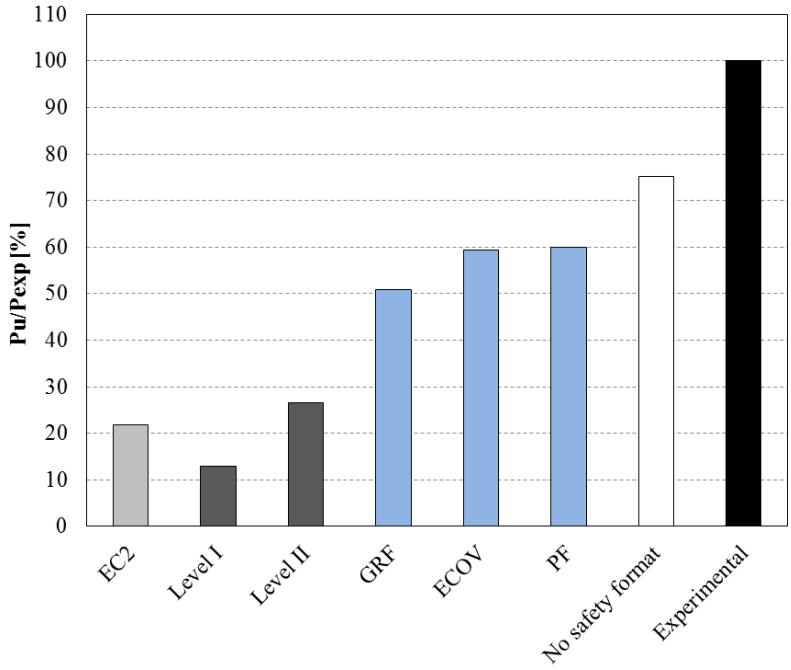

Figure 6-30: Case RS4. Analytical and numerical design values of slab resistance expressed in terms of a percentage of the experimental ultimate value of applied load

The design and real resistance of slab RS4 was searched for by means of analytical and numerical methods. Figure 6-30 shows the comparison of analytical and numerical design values of slab resistance P_{Rd} expressed in terms of a percentage of the experimental ultimate value of applied load. The analysis named "no safety format" refers to a NLFE analysis carried out using mean measured values of material strengths without applying any safety coefficient. The calculated design resistances of all numerical simulation and analytical calculations are summarized in Table 6-8.

Table 6-8: Case RS4. Values of slab resistance

P_{Exp}	EC2	Level I MC2010	Level II MC2010	GRF	PF	ECOV	No safety formats
(kN)	(kN)	(kN)	(kN)	(kN)	(kN)	(kN)	(kN)
1023	223.01	132.8	272.57	520.8	613.4	607.3	769.0

6.6 Concluding remarks

The benchmark slab used in the current case study is a simply support at one end and clamped at the other end continuous slab containing only flexural reinforcement. The clamping conditions were possible to create by means of prestressing bars attached at the overhanging end which restrained rotation of the slab. The geometry of the beam is 5m × 2.5m × 0.3m. The intention of the study was to investigate the shear resistance of the slab with concentrated load applied in vicinity of the continuous support. For such loading scheme the beams exhibited a one-way shear failure mechanism at the load equal to P=1023kN.

To simulate the experiments a numerical model of the slab was created and its behaviour analysed. The slab has been modelled with 20-node brick elements for the concrete and embedded truss elements for the reinforcement. Perfect bond is assumed. The concrete model was based on a total strain rotating crack model with exponential tension softening in tension and parabolic behavior in compression, variable Poisson's ratio of concrete and no reduction of compressive strength of concrete due to lateral cracking. The model for the reinforcement bars was based on hardening plasticity.

The obtained failure mechanism from NLFEA is concluded to be a combination of beam shear failure and punching shear failure. The shear failure was accompanied by crushing of concrete near the loading plate and local yielding of transversal bars. The peak value of applied load obtained from NLFEA is equal to 736.2 kN.

In the case study, safety assessment was performed with application of safety formats for NLFEA as proposed by the Model Code 2010.The design value of slab resistance obtained from safety formats methods resulted to be higher than the design value of slab resistance obtained with different analytical methods for one and two way shear.

Based on the results it can be concluded that consistent and reliable results can be obtained with a rotating crack model with variable Poisson's ratio decreasing from its actual value in the elastic phase up to 0.0 as the finite element undergoes cracking. Reliable results were obtained by neglecting the reduction of the compressive strength of concrete due to lateral cracking. This assumption is also tied to the more simplified 3D material modeling with respect to the 2D modeling.

7 Case RS5 (S4T1): Lantsoght et al. (2012)

The present chapter treats a one-way slab in the test configuration S1T2(Lantsoght, 2012; Lantsoght 2013; Lantsoght et al. 2013) tested in an experimental program at Stevin Laboratory executed at Delft University of Technology. The focus of the program was to derive design recommendations for evaluation of shear resistance of slabs with loads near line support applicable for the assessment of both new and old structures. The considered variable of the test program were: load position, transverse reinforcement ration, concrete strength, size of a loading plate and type of support (simple or continuous). The selected specimen S1T2 is denoted here as case RS5.

7.1 Experimental setup and results

Geometry

The main dimensions of slab RS5 are: length of 5 m, width of 2.5 m and thickness 0.3 m. In Figure 7-1 the geometrical dimensions of the slab and the reinforcement layout are given. Longitudinal reinforcement at the bottom consists of 21ϕ20/125. Longitudinal reinforcement at the top is 21 ϕ 20/125 in the zone subjected to negative moments (over the distance of 3 m from the prestressed end) and 11ϕ10/250 in the zone subjected to positive moments (over the distance of 2.3 m from the simply supported end). The transversal reinforcement for the current benchmark slab is the same as in the previously considered slabs, thus ϕ10/250 across the whole beam and additionally doubled in the vicinity of the supports at the top and bottom sides as shown in Figure 7-1. The concrete cover is 25 mm.

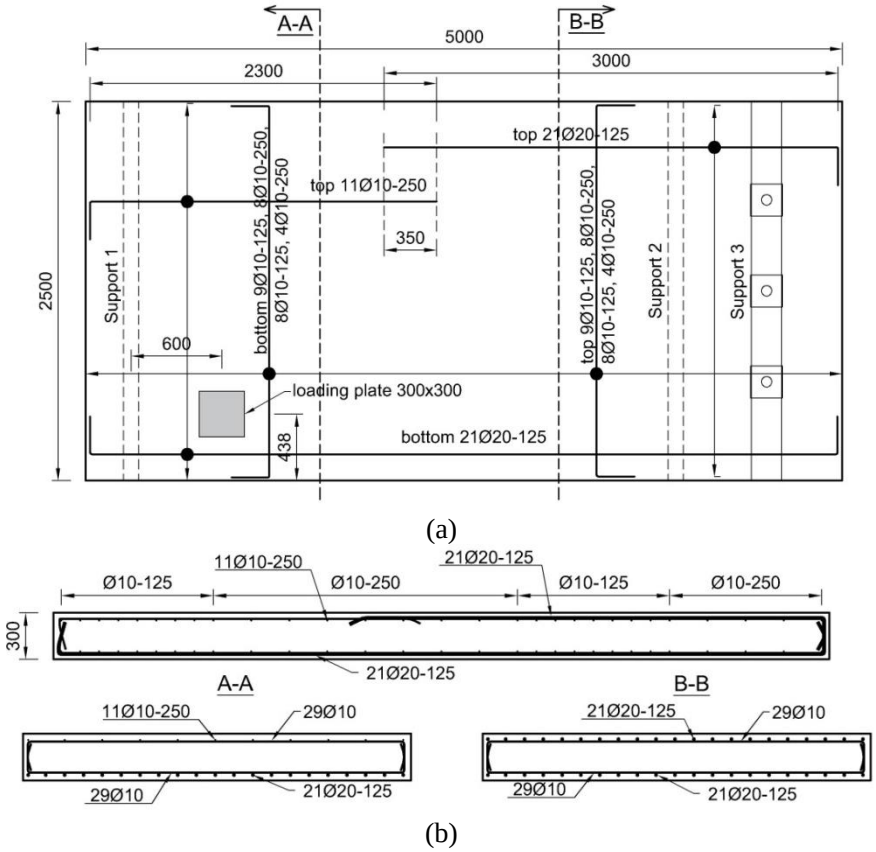

Figure 7-1: Case RS5. (a) Geometrical and (b) reinforcement details (in mm)

Material Properties

Concrete and reinforcement properties given in reference are reported in Table 7-1.

Table 7-1: Case RS5. Concrete and reinforcement properties

Concrete properties					
f_{cm} (N/mm^2)		$f_{ctm,sp}$ (N/mm^2)		d_{max} (mm)	
42.91*		4.2		16	
Reinforcement properties					
Bar	Φ (mm)	A_s (mm^2)	E_s (N/mm^2)	f_{ym} (N/mm^2)	f_{tm} (N/mm^2)
Φ 10	10	79	210000	537	628
Φ 20	20	314	210000	541	658
Φ 36 Dywidag	36	1018	210000	1000	-

*f_{cm} is a converted value using a conversion factor of 0.83
$f_{cm,cyl} = 0.83 \times f_{cm,cub} = 0.83 \times 51.7MPa = 42.91MPa$ where 51.7MPa is given in the reference

Loading and Boundary Conditions

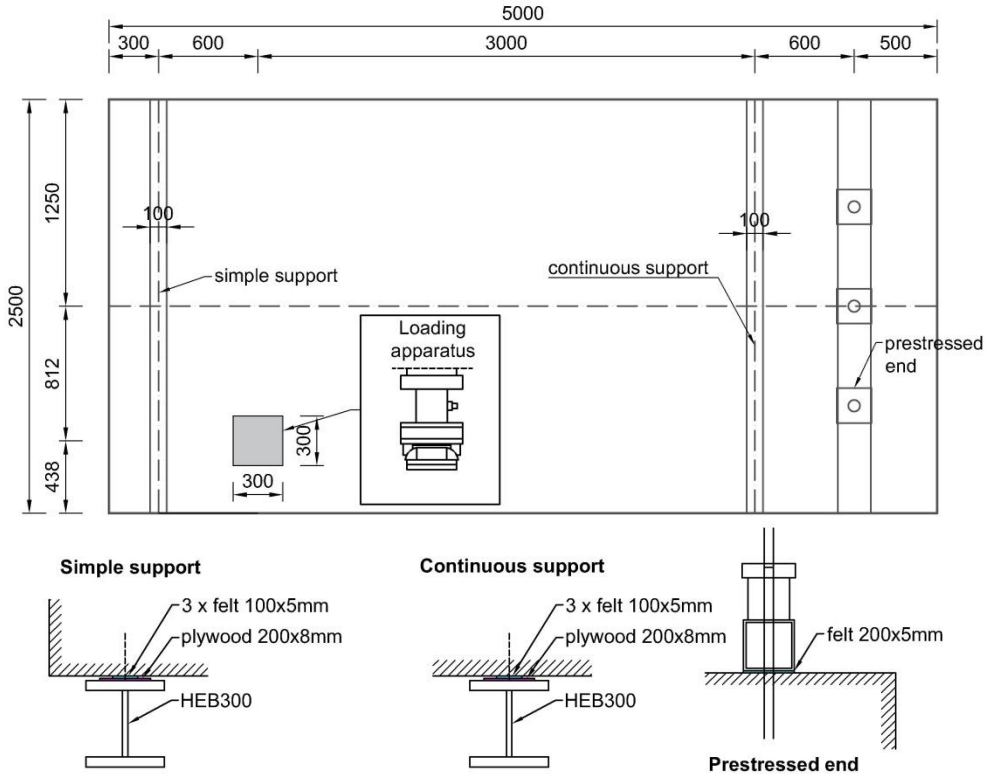

Figure 7-2: Case RS5. Boundary conditions with details of support and of loading apparatus (dimensions in mm)

The test setup for slab S4T1 is the same as presented in the previous cases except for the location of application of the load. For the complete visualization of the experimental setup reference to the description in the preceding case study is made.
In the current case, the load applied in a displacement-controlled way through a hydraulic jack is located unsymmetrically with respect to both transversal and longitudinal axes of the slab. It is positioned at the distance 600 mm from the line

support of the simply supported end and near to the long edge of the element. The slab is supported by two line support placed along the short edges. The support consist of a steel beam 300mm wide, a layer of plywood and a layer of felt 100 mm wide restraining the longitudinal translation at supports and mitigating stress concentration. The overview of boundary conditions and loading position are presented in Figure 7-2. The support 1 represents a simple support. The other end of the beam is fixed to the laboratory floor through the vertical 3Φ36 Dywidag prestressing bars. This measure restrains the rotation at Support 2 causing hogging moment over the support and therefore simulating the conditions of a continuous support. The applied prestress equal to 15kN/bar was applied before the test, initially compensating for the self-weight.

Experimental Results

At 400 kN a crack of 0.15 mm was observed along the side face. Flexural cracks were observed at side and bottom faces. At 800 kN the crack along the lateral face was 0.4 mm wide and the first shear crack became visible. At 990 kN a second shear crack appeared. Failure occurred at 1153.85 kN. The maximum crack width at the top face was 0.45 mm. The width of the shear crack along the west side face was 4 mm. The failure mode of Slab S4T1 was clearly due to shear. In Figure 7-3 the crack patterns of Slab S4T1 along bottom and on the front side face are presented

(a)

(b)

Figure 7-3: Case RS5. Experimental crack pattern (a) at bottom side, (b) on the front face

7.2 Analytical analysis

The analytical analysis scrutinizes the predictions of design shear resistance attributed to different possible shear mechanism. The cases under investigation are: one way shear calculated according to the Model Code 2010 formulation and Eurocode 2 as well as punching shear strength evaluated with the Regan's formulation and according to Eurocode 2. The simplified static scheme is shown in Figure 7-4. The consideration of the clamping support at the continuous does not fall far from the reality as due to the action of prestressing bars, only very limited rotation at the support can be facilitated.

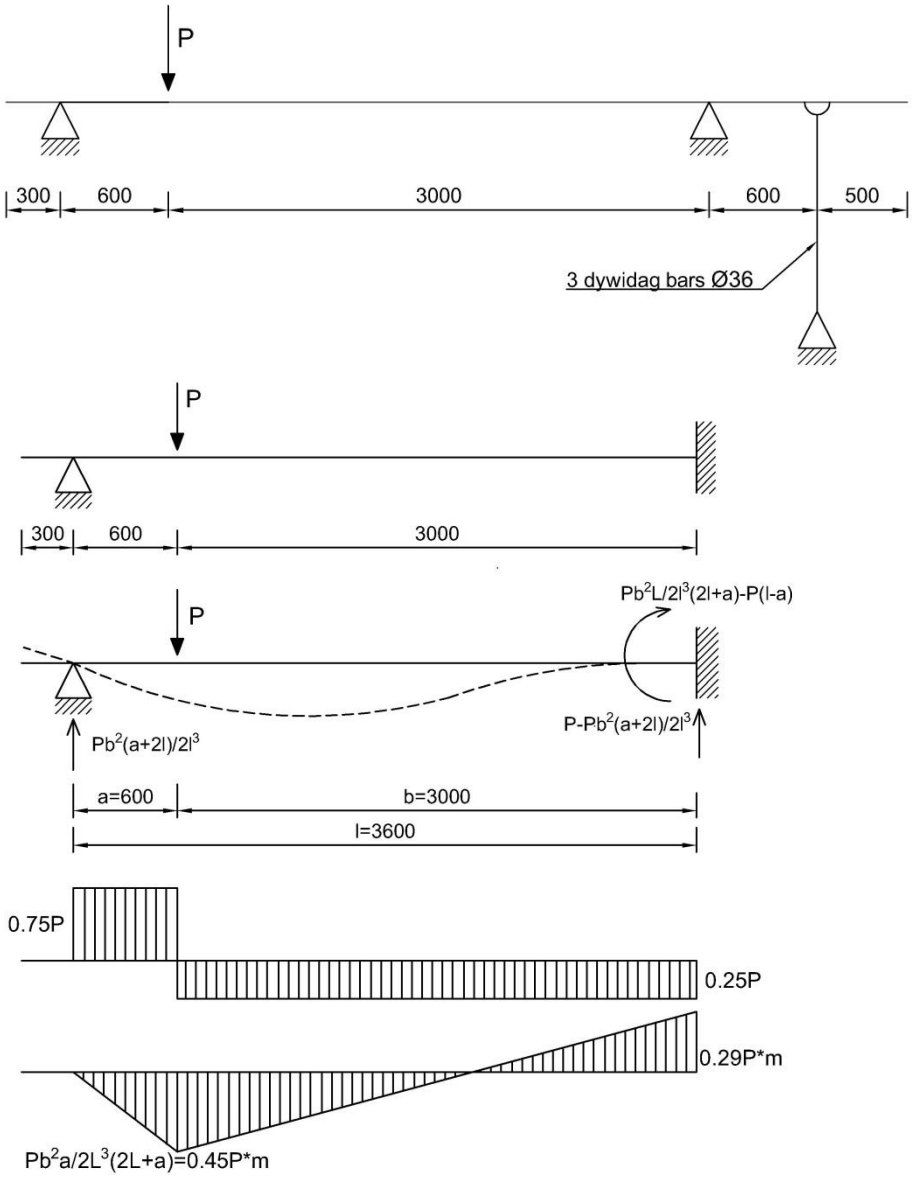

Figure 7-4: Case RS5. Internal forces (in mm)

One-way shear resistance: Model Code 2010

The design shear resistance of a slab is analyzed as a member without shear reinforcement and therefore there are two levels of approximation I and II available at hand. The general expression for the resistance of concrete against the shear is:

$$V_{Rd,c} = k_v \frac{\sqrt{f_{ck}}}{\gamma_c} z b_w$$

$d_l = 300mm - 25mm - 10mm = 265mm$

$z = 0.9d_l = 0.9 \times 265mm = 238.5mm$

Value of the concrete compressive strength in the above expression is calculated as: $f_{ck} = 42.91MPa - 8MPa = 34.91MPa$

Depending on the considered level of approximation, the expression for parameter k_v varies.

In the expression for the concrete shear resistance,the width b_w is replaced by the effective width b_{eff}, calculated by assuming a 45-degree horizontal load distribution from the far corners of the load (the so-called French method) as suggested in (Lantsoght et al. 2013), Figure 7-5. In (Lantsoght et al. 2013) it is shown that for such a determined effective width predictions of shear resistance can be improved.

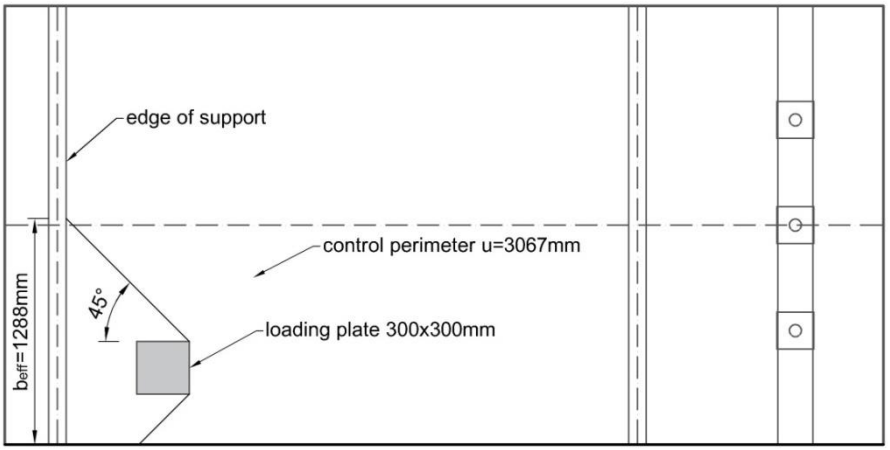

Figure 7-5: Case RS5. Assumed effective width b_{eff} (dimension in [mm])

$b_{eff} = 1288mm$

Level I Approximation

$$k_v = \frac{180}{1000 + 1.25z} = \frac{180}{1000 + 1.25 \times 238.5mm} = 0.139$$

$$V_{Rd,c} = k_v \frac{\sqrt{f_{ck}}}{\gamma_c} z b_{eff} = 0.139 \times \frac{\sqrt{34.91}MPa}{1.5} 238.5mm \times 1288mm = 167.78kN$$

After accounting for the self-weight which at location d from the support is equal to 7.8kN/m, shear resistance is:

$V_{Rd,c} = 167.78kN - 7.8kN/m \times 1.288m = 157.7kN$

Level II Approximation

Assumed resistance $v_{Ed} = 232.41\frac{kN}{m}$ and bending moment calculated at a distance d from the support $m_{Ed} = d \times v_{Ed} = 265mm \times 232.41kN/m = 61.59kNm/m$

$a_s = \frac{\phi^2 \pi}{4} \Big/ 125mm = 2513mm^2/m$

Strain parameter:

$$\varepsilon_x = \frac{1}{2E_s a_s}\left(\frac{m_{Ed}}{z} + v_{Ed}\right) = \frac{1}{2\times 200GPa\times 2513mm^2/m}\left(\frac{61.59kN/m}{238.5mm} + 232.41\frac{kN}{m}\right) = 4.648\times 10^{-4}$$

$$k_{dg} = \frac{32}{16+d_g} = \frac{32}{16+16} = 1 \geq 0.75$$

$$k_v = \frac{0.4}{1+1500\varepsilon_x}\times\frac{1300}{1000+k_{dg}z} = \frac{0.4}{1+1500\times 4.648\times 10^{-4}}\times\frac{1300}{1000+239mm} = 0.247$$

$v_{Rd,c} = k_v\frac{\sqrt{f_{ck}}}{1.5}z = 0.247\frac{\sqrt{34.91}MPa}{1.5}239mm = 232.41\frac{kN}{m}$ thus equal approximately to the assumed value.

Shear resistance of the effective width:

$$V_{Rd,c} = v_{Rd,c}b_{eff} = 232.41\frac{kN}{m}\times 1288mm = 299.34kN$$

Further reduction due to self-weight results in shear resistance:

$$V_{Rd,c} = 299.34kN - 7.8kN/m\times 1.288m = 289.29kN$$

One-way shear resistance: Eurocode 2

$$V_{Rd,c} = b_{eff}d\left[C_{Rd}k(100\rho_l f_{ck})^{1/3}\right] =$$

$$= 1288mm\times 265mm\left[0.12\times 1.869\left(100\times 9.484\times 10^{-3}\times 34.91\right)^{1/3}\right] = 245.78kN$$

Where:

$$k = 1+\sqrt{\frac{200}{d}} = 1+\sqrt{\frac{200}{265}} = 1.869 \leq 2$$

$$\rho_l = \frac{A_s}{d\times s} = \frac{314.15mm^2}{265mm\times 125mm} = 9.484\times 10^{-3}$$

and the resistance is greater than:

$$V_{Rd,c,\min} = v_{\min}\times b_{eff}\times d = 0.035k^{\frac{3}{2}}f_{ck}^{\frac{1}{2}}\times b_{eff}\times d = 0.528MPa\times 1288mm\times 265mm = 180.317kN$$

Shear resistance after extraction of the effect of self-weight:

$$V_{Rd,c} = 245.78kN - 7.8kN/m\times 1.288m = 235.73kN$$

Punching strength: Regan's equation

In order to evaluate the punching strength P_R, a rectangular control perimeter u, outlined in red color in Figure 7-6, is determined.

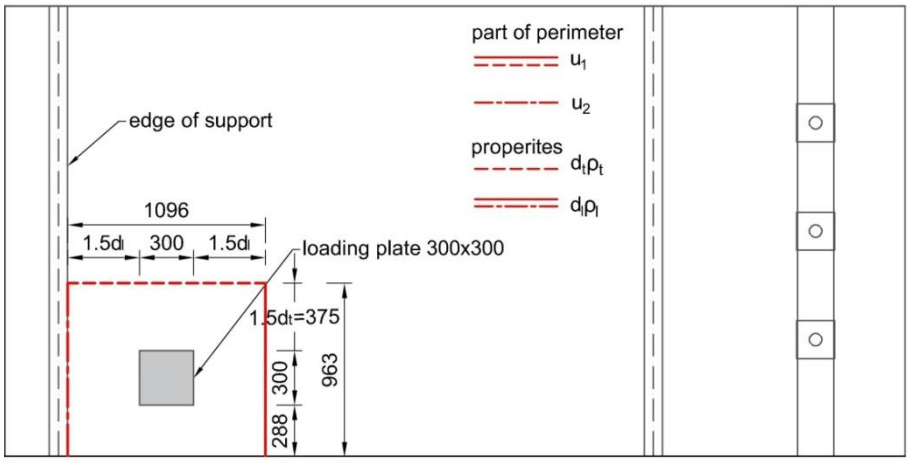

Figure 7-6: Case RS5. Control perimeter according to Regan's formulation

$P_R = P_{R1} + P_{R2}$

P_{R2} refers to the edge of the perimeter running parallel to the support; P_{R1} refers to the remaining part.

$$P_{R2} = \frac{2d_l}{a_v}\xi_{sl} v_{cl} u_2 d_l$$

$$\xi_{sl} = \sqrt[4]{\frac{500}{d_l}} = \sqrt[4]{\frac{500}{265}} = 1.172$$

$$\rho_l = \frac{\pi\phi_l^{\,2}}{4} \times \frac{1}{s_l \times d_l} = \frac{\pi \times (20mm)^2}{4} \times \frac{1}{125mm \times 265mm} = 9.484 \times 10^{-3}$$

$$v_{cl} = \frac{0.27}{\gamma_c}\sqrt[3]{100\rho_l f_{ck}} = \frac{0.27}{1.5}\sqrt[3]{100 \times 9.484 \times 10^{-3} \times 34.91}MPa = 0.578MPa$$

$a_v = 600mm - 300mm/2 - 50mm = 400mm$ is net distance between support 1 and a loading plate

$u_2 = 438mm + 300mm/2 + 1.5d_t = 438mm + 300mm/2 + 375mm = 963mm$

And

$d_t = h - c - \phi_1 - \phi_2/2 = 300mm - 25mm - 20mm - 5mm = 250mm$

$$P_{R2} = \frac{2d_l}{a_v}\xi_{sl} v_{cl} u_2 d_l = \frac{2 \times 265mm}{400mm} \times 1.172 \times 0.578MPa \times 963mm \times 265mm = 229.06kN$$

Because the major part of horizontal control perimeter lies in the region where spacing is smaller, the control perimeter is divided into parts: first with spacing of 125mm and second with 250mm. For each part the ultimate shear stresses v_c are calculated separately.

$$\rho_{t1} = \frac{\pi\phi_t^{\,2}}{4} \times \frac{1}{s_l \times d_l} = \frac{\pi \times (10mm)^2}{4} \times \frac{1}{125mm \times 265mm} = 2.513 \times 10^{-3}$$

and $\rho_{t2} = 1.257 \times 10^{-3}$ resulting from halving the first reinforcement ratio.

The corresponding ultimate shear stresses:

$$v_{ct1} = \frac{0.27}{\gamma_c}\sqrt[3]{100\rho_{t1} 1 f_{ck}} = \frac{0.27}{1.5}\sqrt[3]{100 \times 2.513 \times 10^{-3} \times 34.91}MPa = 0.371MPa$$

$$v_{ct2} = \frac{0.27}{\gamma_c}\sqrt[3]{100\rho_{t2} f_{ck}} = \frac{0.27}{1.5}\sqrt[3]{100 \times 1.257 \times 10^{-3} \times 34.91}MPa = 0.295MPa$$

With:

$$\xi_{st} = \sqrt[4]{\frac{500}{d_t}} = \sqrt[4]{\frac{500}{250}} = 1.189$$

The lengths of the individual parts are: 0.7m and 0.395m for denser and wider spacing respectively.

The resistance therefore is:

$$P_{R1} = (\xi_{st} v_{ct1} 700mm\, d_t + \xi_{st} v_{ct2} 395mm\ d_t) + \xi_{sl} v_{cl} 963mm\ d_l = 111.87kN + 172.87kN = 284.7kN$$

Total shear resistance:

$$P_R = P_{R1} + P_{R2} = 284.7kN + 229.06kN = 513.8kN$$

After taking into account the contribution of self-weight assumed as the weight of a punching cone, the resistance is:

$P_R = 512.5kN$

Punching strength: Eurocode 2 formulation

The control perimeter *u*, outlined in red color in Figure 7-7 is determined to calculate the punching strength.

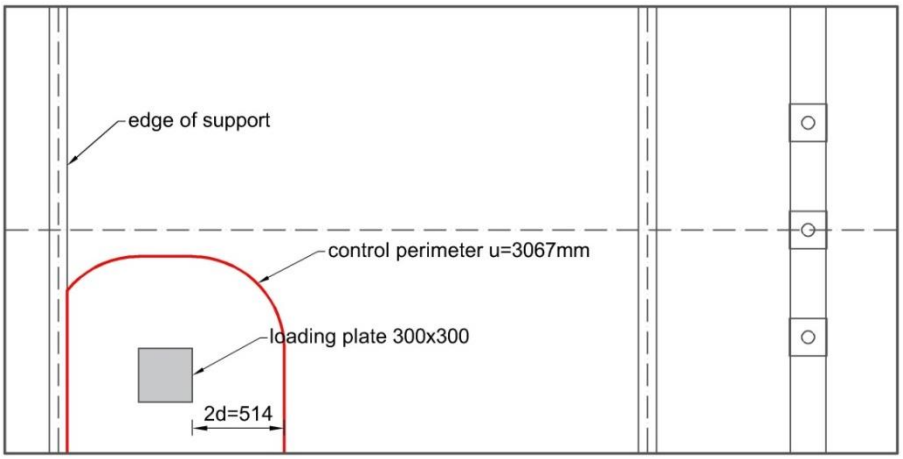

Figure 7-7: Case RS5. Control perimeter according to Eurocode 2 formulation

$$V_{Rdc} = v_{Rdc} \times u \times d_{eff}$$

$$d_{eff} = \frac{d_l + d_t}{2} = \frac{265mm + 250mm}{2} = 257.5mm$$

$$k = 1 + \sqrt{\frac{200}{d_{eff}}} = 1 + \sqrt{\frac{200}{257.5mm}} = 1.881$$

$$\rho = \sqrt{\rho_l \times \frac{\rho_{t1} + \rho_{t2}}{2}} = \sqrt{0.00948 + \frac{0.002513 \times 0.00126}{2}} = 0.00423$$

$$v_{Rdc} = C_{Rd,c} k (100 \times \rho \times f_{ck})^{1/3} = 0.12 \times 1.88 \times (100 \times 0.00423 \times 34.91)^{1/3} = 0.554MPa$$

$$V_{Rdc} = v_{Rdc} u\, d_{eff} = 0.554MPa \times 3067mm \times 257.5mm = 437.36MPa$$

After taking into account the contribution of self-weight assumed as the weight of a punching cone, the resistance is:

$$P_R = 436.23kN$$

In Table 7-2 the design values of beam resistance expressed in terms of applied load P_{Rd} associated to one-way shear failure and punching failure are summarized. The design values reported in Table 7-2 are reduced by the effect of dead load. From the results of the analytical analysis, the governing failure mechanism is one-way shear. It is substantiated by the fact that the design shear resistance associated to one-way shear failure is lower than the design punching shear resistance.

Table 7-2: Case RS5. Design values of beam resistance expressed in terms of applied load P_{Rd}

	One-way shear (MC 2010)			**Punching**	
	Level I (kN)	**Level II (kN)**	**EC2 (kN)**	**Regan (kN)**	**EC2 (kN)**
$\boldsymbol{P_{Rd}}$ **(kN)**	157.7	289.29	235.73	512.5	436.23

7.3 Finite element model

Units

Units are N, m.

Material models and parameters

The concrete model is based on a total strain rotating crack model with:

- exponential softening in tension and parabolic behavior in compression,
- variable Poisson's ratio of concrete
- increase in compressive strength due to lateral confinement according to the model proposed by Selby and Vecchio (Selby and Vecchio 1993).

The mechanical properties are summarized in Table 7-3. The uniaxial stress-strain curve is shown in Figure 7-8.
The model for the reinforcement grid is based on hardening plasticity. Geometrical and mechanical properties of reinforcement are summarized Table 7-1. The stress-strain curve of ϕ20 bars is plotted in Figure 7-9.

Table 7-3: Case RS5. Constitutive model parameters for concrete

	f_{cm} (N/mm^2)	f_{ctm} (N/mm^2)	E_c (N/mm^2)	ν	G_F (Nmm/mm^2)
Mean measured value	42.91	3.78**	34938*	var	0.143*

*Not specified in reference; estimated according to Model Code 2010 (fib, 2013)
**Estimated from the mean splitting tensile strength of concrete as $f_{ctm} = 0.9 f_{ctm,sp}$ according to Eurocode 2 formulation (CEN, 2005)

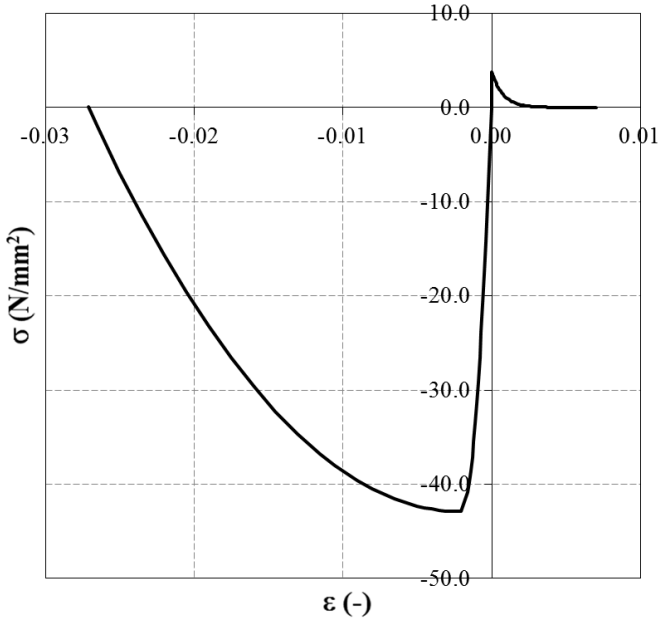

Figure 7-8: Case RS5. Stress-strain curve for concrete

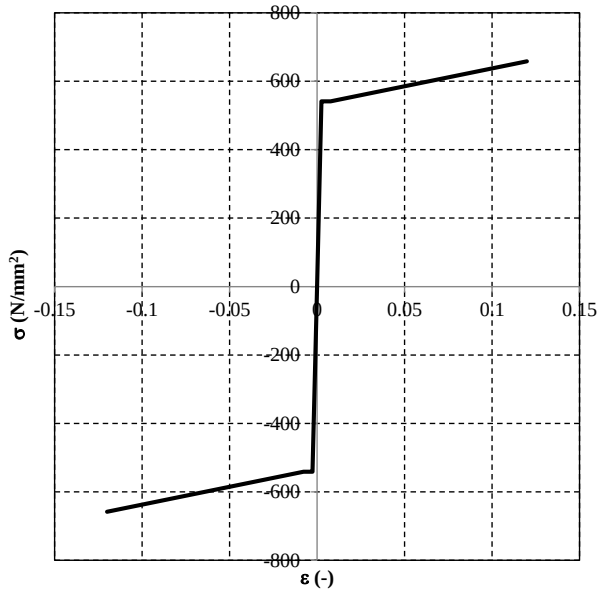

Figure 7-9: Case RS5. Stress-strain curve adopted for Φ20

For the steel plates a linear elastic behavior is assumed, see Table 7-4.

Table 7-4: Case RS5. Steel plates properties

E (N/mm^2)	ν
210000	0.3

Interface: interface elements were placed between steel plates, steel profiles and concrete slab at the locations of supports and loading positions.
For construction of the support-concrete slab interface, 15 mm layer of P100 Nevima felt and 8 mm layer of plywood were used at the simple and continuous support. At the prestressed end, a layer of 5 mm thick P50 felt was used. The non linear mechanical behaviour of felt and plywood/felt in the normal direction is evaluated from experimental test, Figure 7-10. A linear elastic behaviour is assumed in the shear and tensile directions, with stiffness value almost equal to zero. In Figure 7-11 the non-linear mechanical behaviour of felt and plywood/felt used in the analysis is plotted.

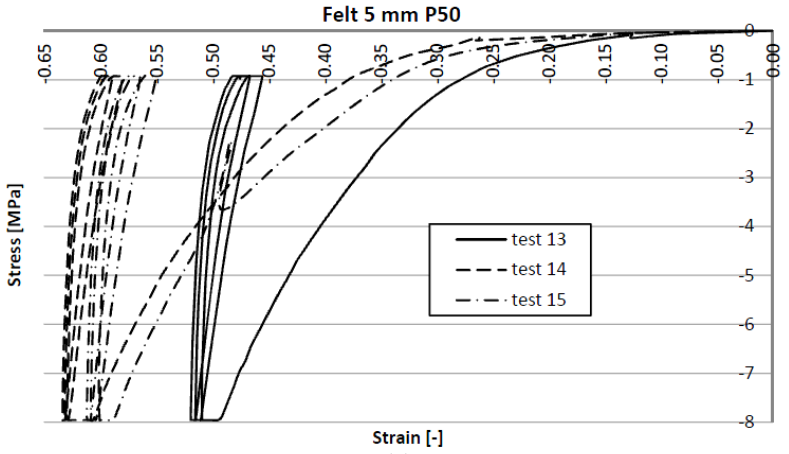

(a)

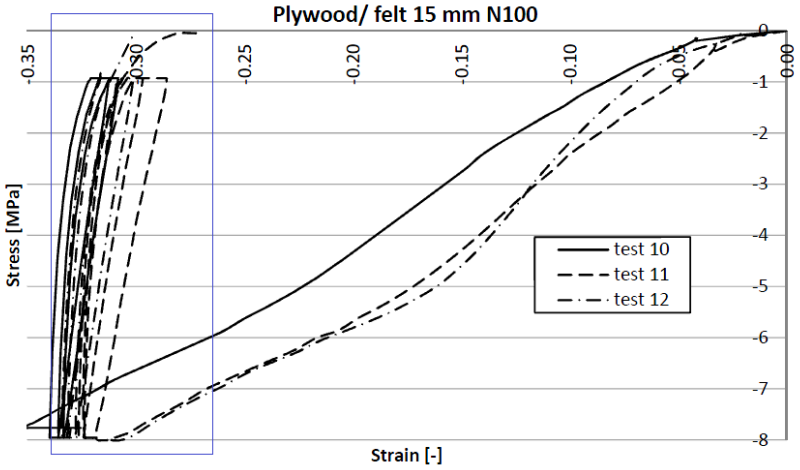

(b)

Figure 7-10: Case RS5. (a) Experimental stress-strain diagram of felt, (b) experimental stress-strain diagram of plywood/felt (Lantsoght 2012)

To comply with experiments, the chosen stress-strain relation for the simple supports is described in Figure 7-10(a) with an initial value of strain. It is equivalent to properties of a re-used plywood/felt interface. The relative displacement in Figure 7-11 was calculated by multiplying strains by the thickness of the felt (5 mm) and of plywood/felt (23 mm) for prestressed end and the simple supports respectively.

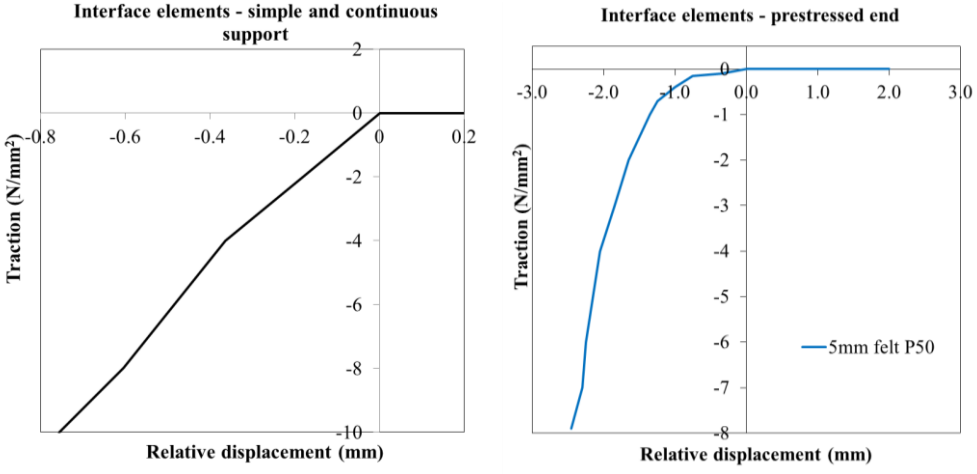

Figure 7-11: Case RS5. Traction-relative displacement diagram of plywood/felt and of felt used in NLFEA

Element types and finite element mesh

For meshing the concrete slab 20-node solid elements (CHX60) are used. The generated mesh has a regular pattern. The specified element size is 50×50×50 mm and is governed by the minimum number of elements over the slab thickness which for a 3D model of a slab is *h/6*. The reinforcement bars were modelled with embedded truss elements with two Gauss integration points along the axis of the element. Perfect bond was assumed. Dywidag bars were modelled with 2-node truss elements. The dywidag bars consist of only one element over the whole length. The elements in the steel plate of an increased thickness to avoid uplifting of the corners as the result of applied load were generated with 20-node solid elements (CHX60). The properties of interfaces between the loading plate, supporting steel profiles, the beam accommodating the

prestressed bars and concrete slabs were assigned through 16-node (CQ48I) interface elements.

The mesh of the slab is shown in Figure 7-12 (a) whereas the reinforcement layout is illustrated in Figure 7-12 (b). Different material properties for solid elements as well as different element geometries i.e. a cross-sectional area of reinforcement are indicated with diverse colors.

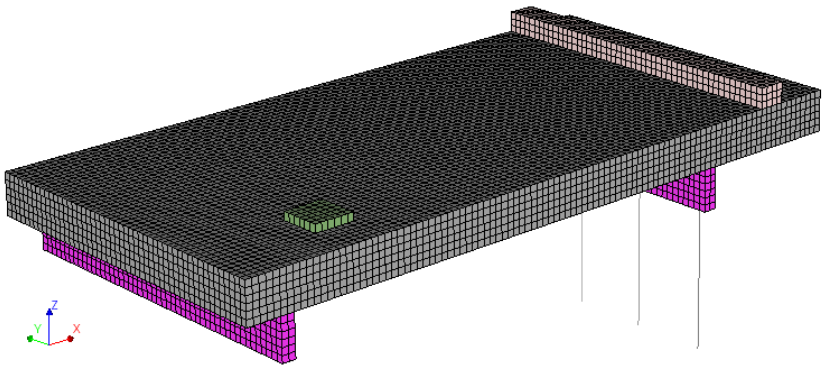

(a)

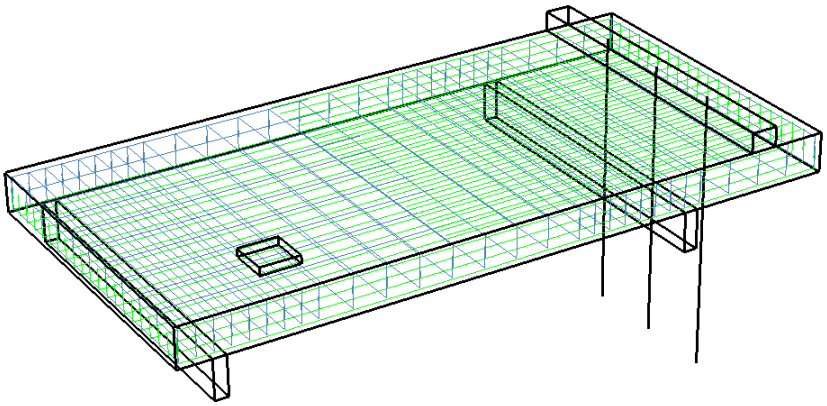

(b)

Figure 7-12: Case RS5. (a) Mesh, (b) material sets

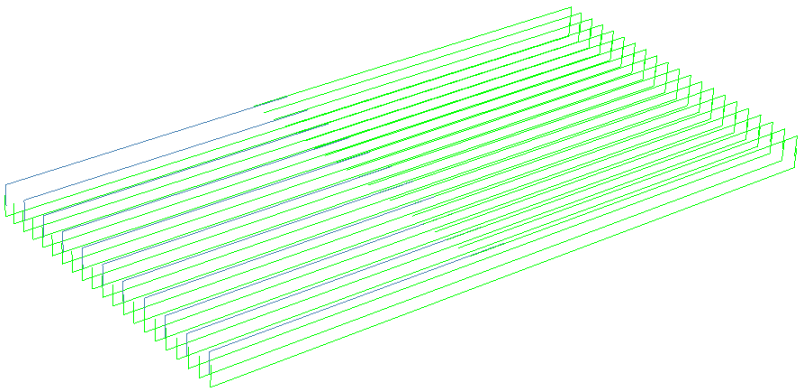

Figure 7-13: Case RS5. Groups of longitudinal reinforcement elements: “TOPF10L” (blue), “TOPF20L” (top rebars in green), “BOTF20L” (bottom rebars in green)

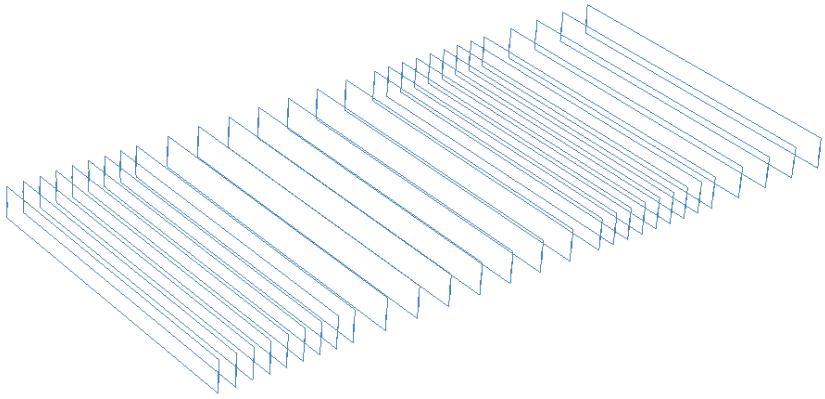

Figure 7-14: Case RS5. Groups of transverse reinforcement elements: "TOPF10T" and "BOTF10T"

Boundary conditions and loading

Boundary conditions are applied to nodes of steel profiles, steel plate and dywidag bars, Figure 7-15. The following sets of constraints were applied:

- translation in *x*, *y* and *z* direction was constrained through supports applied to the nodes at the bottom face of the supporting steel profiles (support 1 and 2)
- translation along *z* direction at the middle node of the loading plate was constrained
- the dywidag bars were constrained along *z* direction at the bottom and along *y* and *x* at the top end

The analysis was carried out in displacement control by applying a displacement along *z* direction at the middle node of the loading plate.

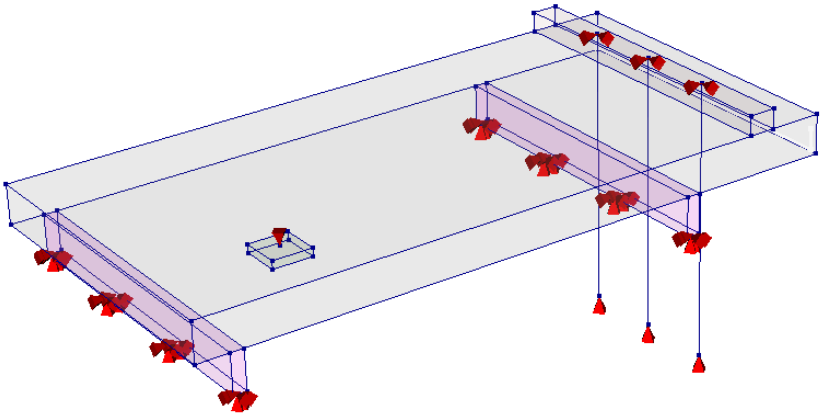

Figure 7-15: Case RS5. Boundary conditions

Phased analysis was executed which enabled application of prestressing to the dywidag bars. In the first phase, the dead load *q* and an axial force *F* equal to 15 kN were applied to the dywidag bars, load case 1 and 2 respectively in Figure 7-16(a). In the second phase shown in Figure 7-16(b), supports were added to the bottom ends of the dywidag bars. Additionally, in the second phase, a prescribed displacement *d* was applied to the node situated at the center of the loading steel plate as load case 3, Figure 7-17.

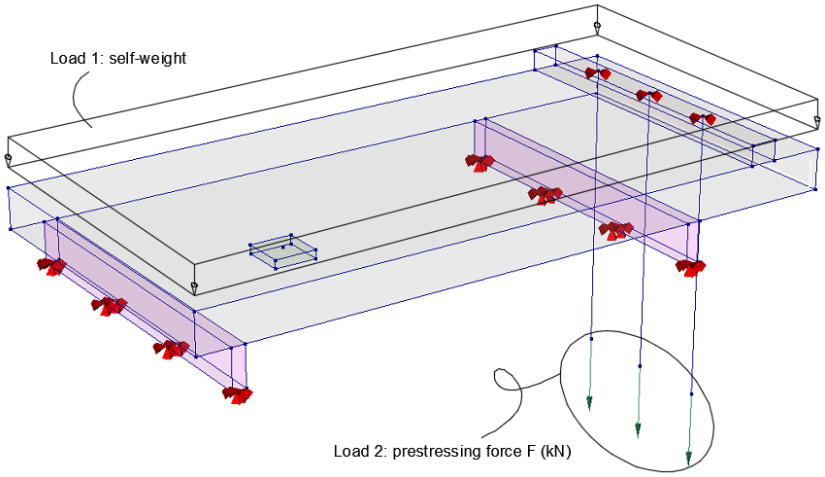

(a)

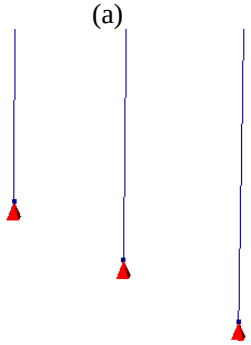

(b)

Figure 7-16: Case RS5. Loading components of phased analysis: (a) load cases 1 and 2 of analysis phase 1, (b) attached supports to dywidag bars in analysis phase 2

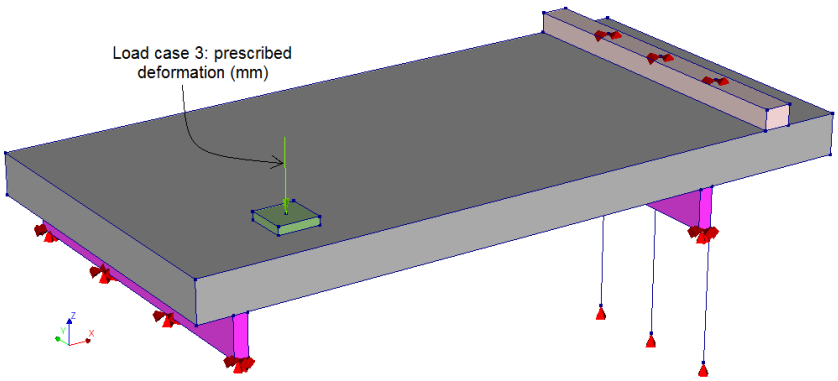

Figure 7-17: Case RS5. Load case 3 in phase analysis 2

Load increments and convergence criteria

Load case 1 and Load case 2: both loads were applied simultaneously using a single load increment. Regular Newton-Raphson method with a maximum of 25 iterations was adopted. As a convergence criteria, force and energy norms were selected. The analysis was set to continue even if the convergence criteria were not satisfied. Convergence tolerances equal to 1×10^{-3} and 1×10^{-2} were specified for energy and force norms, respectively.

Load case 3: the prescribed displacement in the z direction equal to -1mm was applied to the middle node of the steel plate. The user specified load step size of 0.2 of the

whole prescribe deformation was applied in a total of 50 steps. To find the state of equilibrium, Regular Newton-Raphson iterative procedure was incorporated with a maximum of 140 iterations in each load increment. The equilibrium iterations were set to continue even if the convergence criteria were not satisfied. Convergence tolerances were equal to 1×10^{-3} and 1×10^{-2} for energy and forces, respectively.

7.4 Nonlinear finite element analysis

Load deflection

The load-deflection curve is presented in Figure 7-18(b). In order to preserve the consistency between the tests and the NLFEA the same procedure of determining the mean displacement was put into effect. The values of mean deflection were established based on the readings from lasers surrounding the loading plate at the distance of 265mm from the application of the load. The positions of the lasers are designated as points A, B, C, D in Figure 7-18(a). Following suit, the mean deflection from NLFEA was obtained considering the displacements of four corresponding nodes.

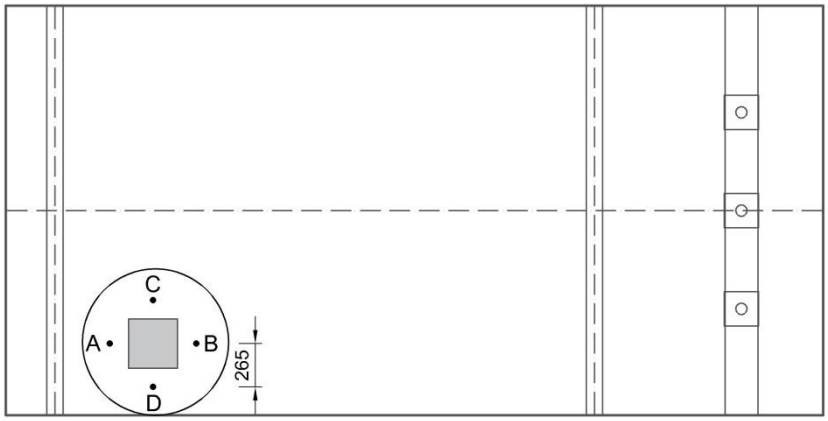

(a)

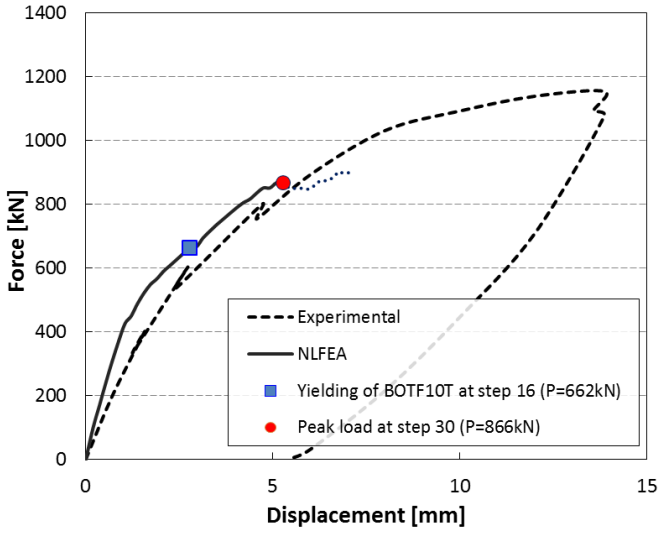

(b)

Figure 7-18: Case RS5. (a) Determination of the deflection points plotted, (b) Load-deflection curve

Beside general response of the slab load-deflection curve highlights at the load steps corresponding to yielding of reinforcement and the peak load. The peak load is defined

as the highest load step where the energy norm ratio satisfies the fixed tolerance of 1×10^{-3}. Prior to the peak load all load steps converged within the specified maximum number of steps. The convergence behavior becomes poor after reaching the peak load at step 30. After that, the analysis continued even if the energy convergence criteria were not satisfied which is presented with a dotted line in the force-displacement diagram.

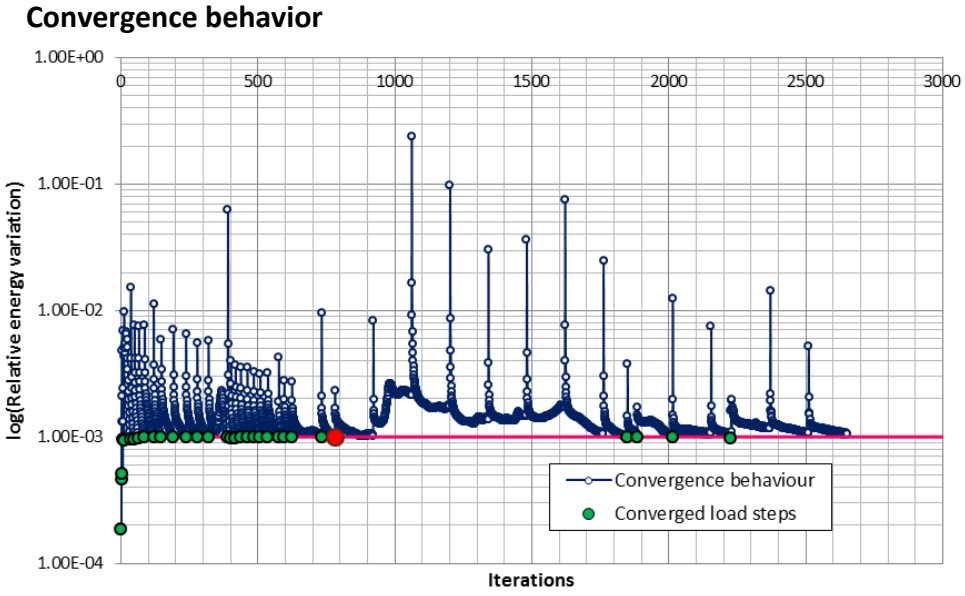

Figure 7-19: Case RS5. Evolution of the energy norm (markers indicate iterative processes)

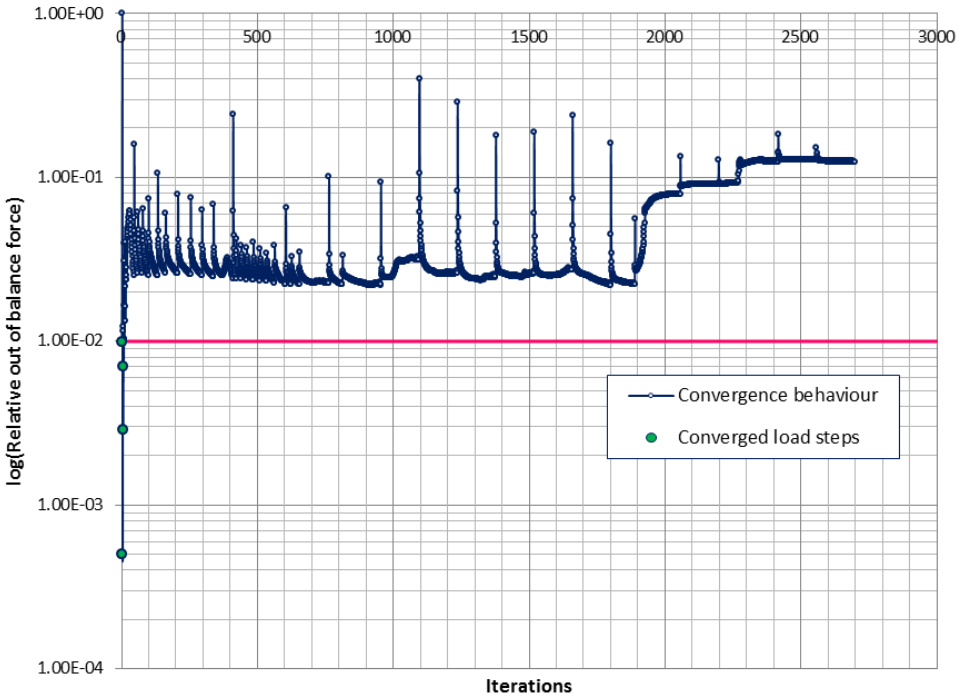

Figure 7-20: Case RS5. Evolution of the force norm

The state of equilibrium within the specified number of iteration and convergence tolerances was achieved almost only based on the energy criterion, Figure 7-19.

Converged criterion for the force norm was satisfied at few steps at the beginning of the analysis, Figure 7-20. For load case 3, the energy norm ratio satisfied the fixed tolerance of 1×10^{-3} for most of the steps of the analysis prior to the peak load. In Figure 7-19 and Figure 7-20 a red circle indicates the peak load.

Strains

Figure 7-21 to Figure 7-23 show contour plots of positive principal strain values at the peak load at step 30 and the successive load step 31 for the whole slab as well as sections with normal in *y* and *z* directions. The displayed colors in the contour plots correspond to the assigned values in the concrete softening curve in Figure 7-24. Special attention is drawn to the following values of principal strains. The first principal strain value equal 1.08e-4 indicates initiation of cracking. The second principal strain value equal to 7.6e-4, corresponds to the ultimate strain value calculated as $\varepsilon_{t,u} = \frac{G_f}{h \cdot f_{ctm}}$, while the third crack strain value, equal to 3.5e-3, is the strain value corresponding to 1% of f_{ctm}. Intermediate strain values have been added in the contour plot.

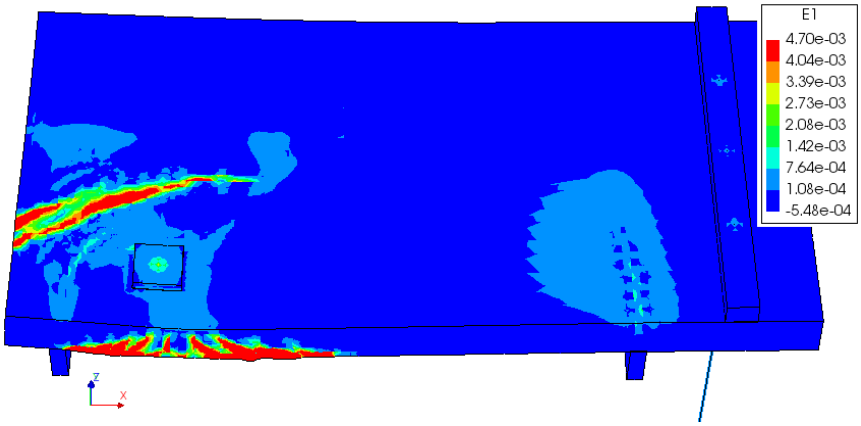

Figure 7-21: Case RS5. Positive principal strain values at step 30 (peak load)

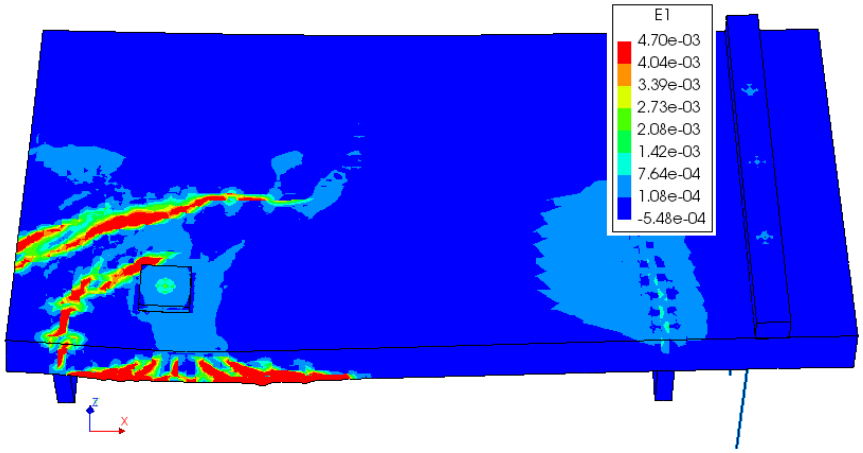

Figure 7-22: Case RS5. Positive principal strain values at step 31

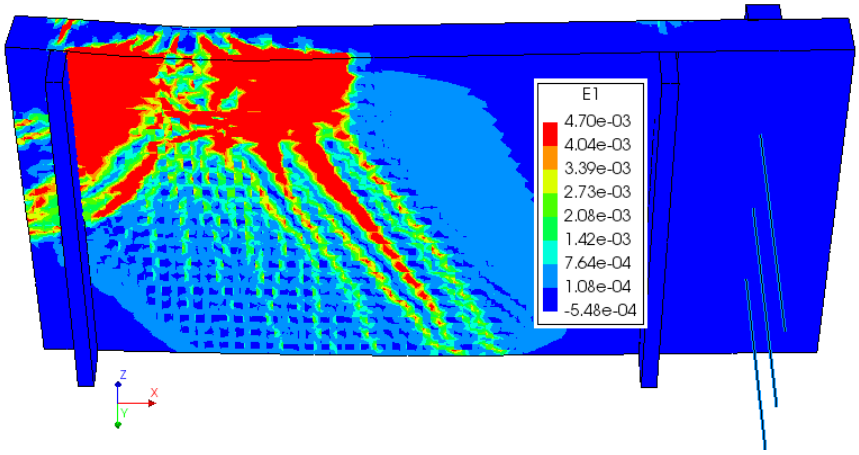

Figure 7-23: Case RS5. Positive principal strain values at step 31

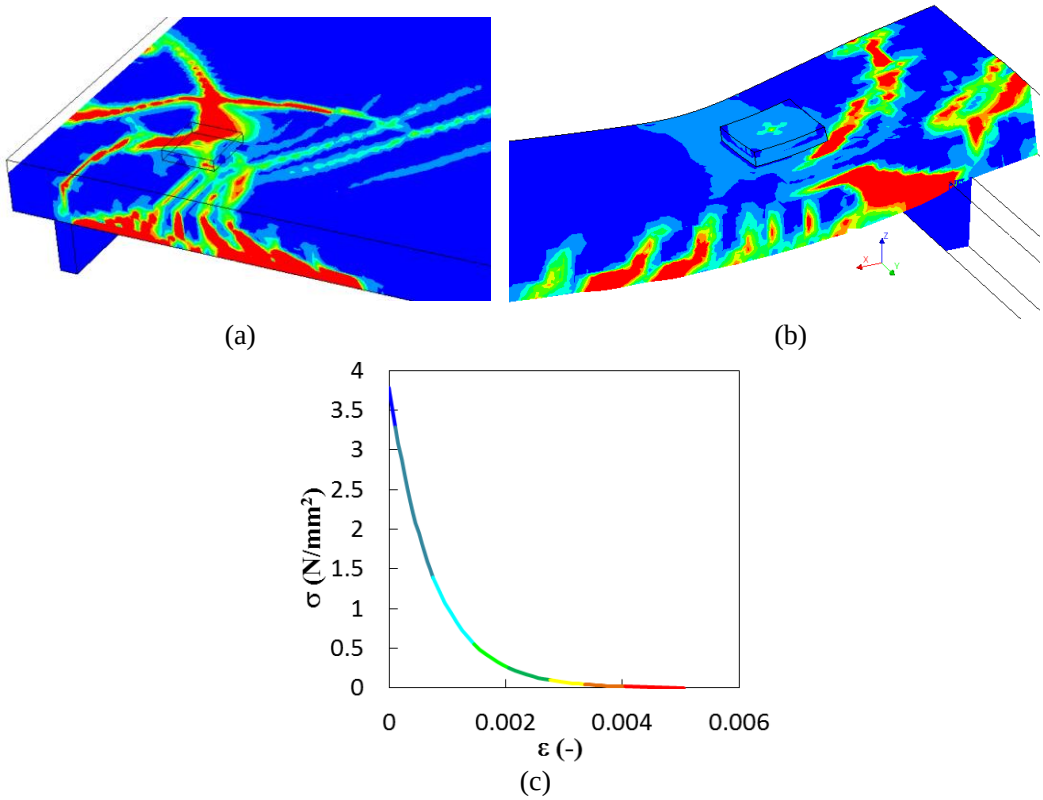

Figure 7-24: Case RS5. Positive principal strains for step 31: (a) at section z=230mm, at plane with normal in *y* direction, (c) tension softening curve

Figure 7-25 shows the minimum principal strain values at the peak load for the whole slab. A number of critical values has been highlighted. The first value of minimum principal strain, equal to -4.09e-4 corresponds to the limit principal strain value in the elastic range according to expression $\varepsilon_{c,el} = \frac{f_{cm}}{3 \cdot E_c}$. The second negative principal strain value -2.05e-3 is the peak strain value determined with the formula: $\varepsilon_{c,p} = -\frac{5}{3}\frac{f_{ctm}}{E}$. The last minimum principal strain value, equal to -0.0271 is the crushing strain value

calculated as $\varepsilon_{c,u} = \varepsilon_{c,p} - \frac{3G_c}{2 \cdot h \cdot f_{cm}}$. The presented values in the legend in Figure 7-25 and contour plots can be related to the parabolic compression diagram where the exact compressive softening of concrete is portrayed.

From the presented contour plots, it can be noticed that almost for the entire slab values of compressive strains are lower than the peak value. This holds even for the region directly loaded and in close proximity. Crushing of concrete is found only very locally near the side face of the slab.

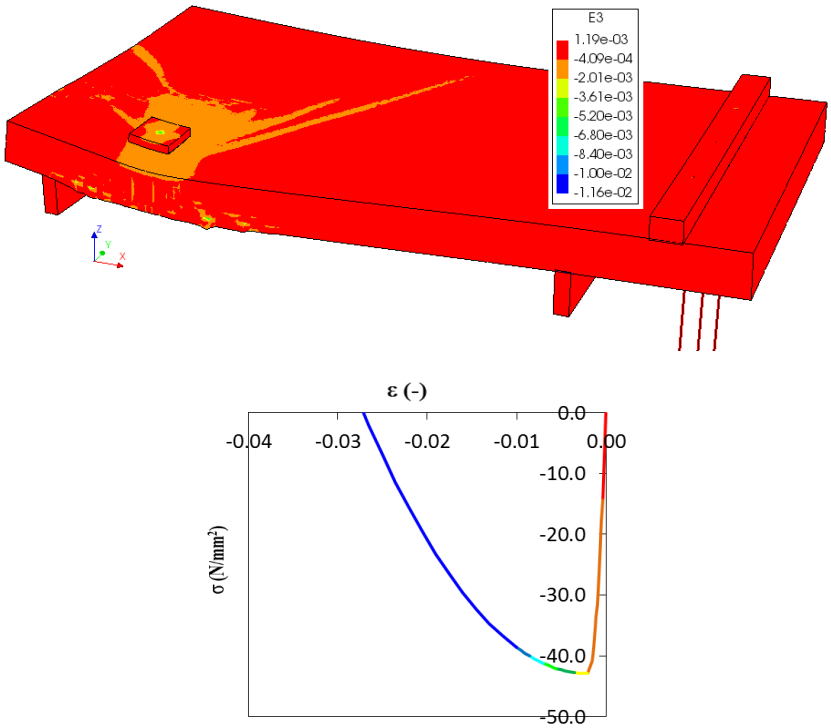

Figure 7-25: Case RS5. Minimum principal strain values at step 30 – peak load

Yielding strain of bottom transversal bars ϕ10 BOTF10T is equal to 537MPa/210000MPa = 2.56 10^{-3}. From Figure 7-26 it can be observed that the only regions undergoing yielding are the rebars bends. The onset of yielding occurred at step 16.

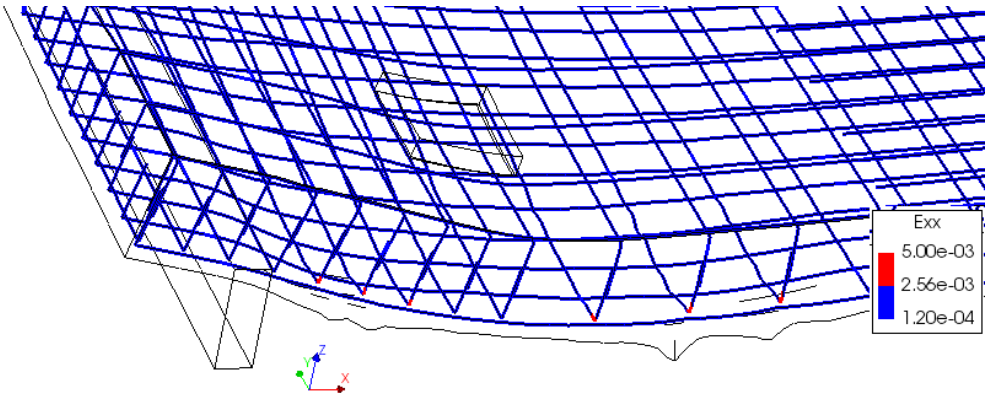

Figure 7-26: Case RS5. Yielding in tension of BOTF10T at step 30 - peak load

To conclude on the governing failure mechanism, contour plots of positive principal strains, which can be interpreted as a crack pattern, are analysed. From Figure 7-21and Figure 7-22, it can be seen that the analysis results in a complex crack pattern. From the comparison of two figures, upon the last converged load step, occurrence of a new crack can be noticed. The crack is fully open and because it leads to failure, it crack can be considered as critical. Moreover, from Figure 7-24(a) one can see that the newly created crack propagates almost over the whole depth of the slab and is accompanied by an already existing inclined crack visible in Figure 7-24(b).

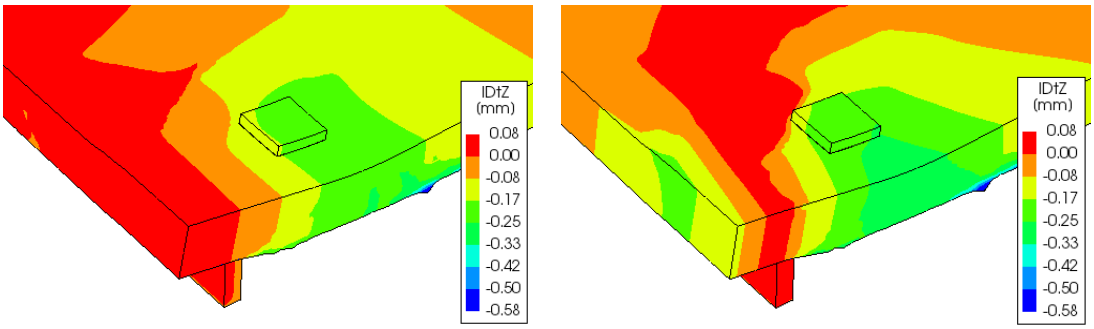

(a) (b)

Figure 7-27: Case RS5. Incremental displacement at load step (a) 30 and (b) 31

In Figure 7-27 contour plots with incremental displacements are presented. One can see that at step 30, thus before occurrence of the crack, the whole region around the loading plate follows the prescribed deformation of the loading plate having negative deformations. After the onset of cracking at step 31, the region is separated by the crack with a sudden displacement drop of roughly 0.10mm near the loading plate. The part of the slab near the edge deforms in the negative z direction whereas the cut off region has 0 or positive displacement.
The obtained crack pattern implies that a number of influencing factors contributed to the failure. The fact that reinforcement yields only locally at the rebars bends as well as the crack pattern and the observed behavior upon the last converged step suggest that the governing failure is due to punching shear. The result appears to be different than the experimental observation which was concluded as one-way shear.

7.5 Application of safety format

Safety assessment of resistance calculated by non-linear analysis is investigated with application of safety formats. The methods included, as proposed in Model Code 2010, are: GRF (Global Resistance Factor method), PF (Partial Factor method) and ECOV (Method of Estimation of a Coefficient of Variation of resistance). The safety assessment with safety formats requires a total of four nonlinear analyses. The mechanical properties of steel and concrete implemented in the analyses are given in Table 7-5 to Table 7-7.

Table 7-5: Case RS5. Constitutive model parameters for concrete

	f_c (N/mm^2)	f_{ct} (N/mm^2)	E_c (N/mm^2)	ν	G_F (Nmm/mm^2)	G_C (Nmm/mm^2)
Mean measured	42.91	3.78	34938	var	0.144	35.90
Characteristic	34.91	2.65	31284	var	0.138	34.59
Mean GRF	29.67	2.87	28755	var	0.134	30.84
Design	23.27	1.76	27701	var	0.128	31.16

Table 7-6: Case RS5. Constitutive model parameters for reinforcing bars (Φ10)

	Φ (mm)	A_s (mm^2)	f_y (N/mm^2)	f_t (N/mm^2)	E_s (N/mm^2)	ε_{sy} (-)
Mean measured	10	79	537	628	210000	0.0026
Characteristic	10	79	486.38	568.81	210000	0.0023
Mean GRF	10	79	535.02	625.69	210000	0.0025
Design	10	79	422.94	494.61	210000	0.0020

Table 7-7: Case RS5. Constitutive model parameters for reinforcing bars (Φ20)

	Φ (mm)	A_s (mm^2)	f_y (N/mm^2)	f_t (N/mm^2)	E_s (N/mm^2)	ε_{sy} (-)
Mean measured	20	314	541	658	210000	0.0026
Characteristic	20	314	490.01	595.98	210000	0.0023
Mean GRF	20	314	539.01	655.58	210000	0.0026
Design	20	314	426.09	518.24	210000	0.0020

In Figure 7-28 the load-deflection curves obtained with mean measured, characteristic, mean GRF and design values of material strengths are shown. The peak load values are indicated in the graph with circular markers. As far as a failure mode of the safety format analyses is concerned, all models failed in a similar way as described for the analysis with mean measured material properties. The difference between analyses lies in the extent to which the critical crack can develop before a lack of convergence. For the analyses with mean GRF and characteristic values of material properties convergence performance was poor after occurrence of the crack. A different situation applies to the analysis with design values of material properties. For this analysis, the development of the crack at step 25 does not imply a lack of convergence and the equilibrium criterion of the energy norm is satisfied in three subsequent load steps. This allows for further increase of loading until step 29 for which the load is considered to be the ultimate resistance of the slab. Such a behavior can be notice in Figure 7-28 following the reduction of the applied force.

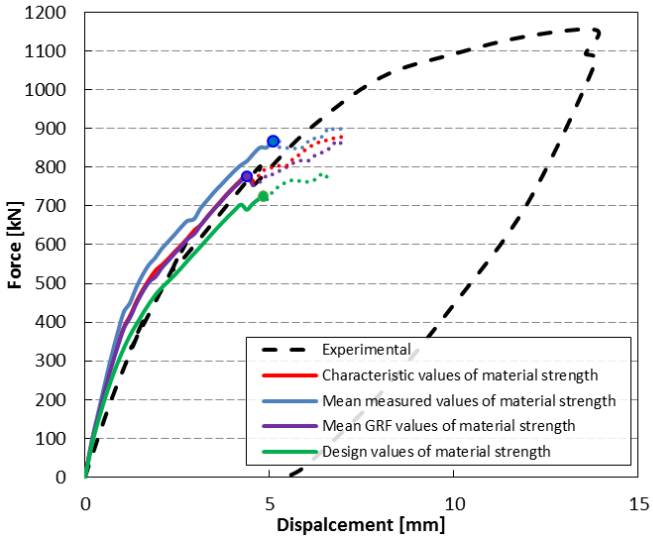

Figure 7-28: Case RS5. Load-deflection curves obtained with mean measured, characteristic, mean GRF and design mechanical properties

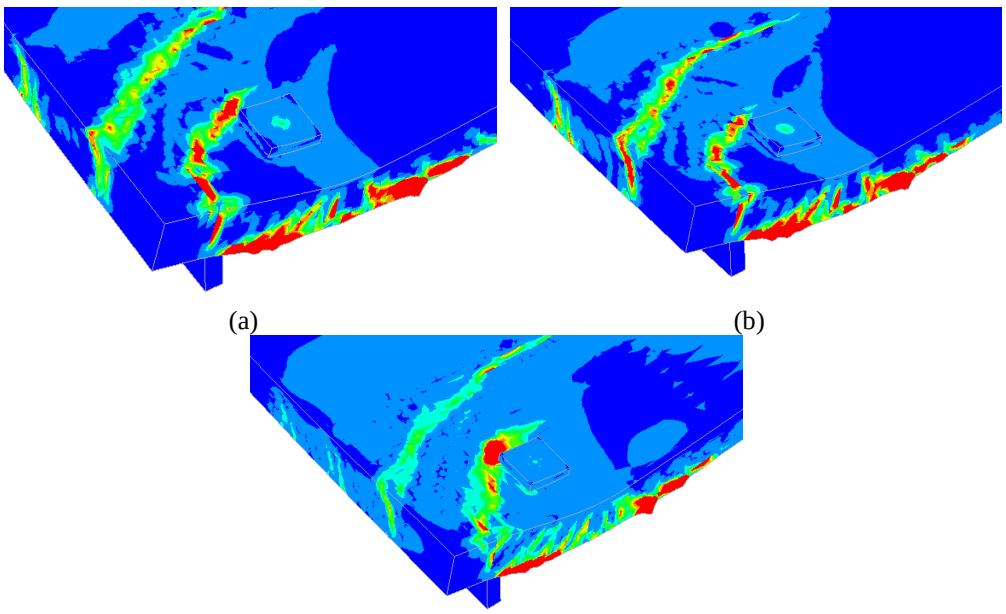

Figure 7-29: Case RS5. Positive principal strains for safety format methods: (a) GRF at step 26, (b) characteristic at step 26, (c) design at step 29

The design and mean resistance of the slab RS5 was searched for by means of analytical and numerical methods. Figure 7-30 shows the comparison of analytical and numerical design values of slab resistance P_{Rd} expressed in terms of a percentage of the experimental ultimate value of applied load. The collated results of the analyses indicate that for the considered case study, the predictions of design as well as mean shear resistance can be significantly improved when numerical methods are employed. The analysis named "no safety format" refers to a NLFE analysis carried out using mean measured values of material strengths without applying any safety coefficient.

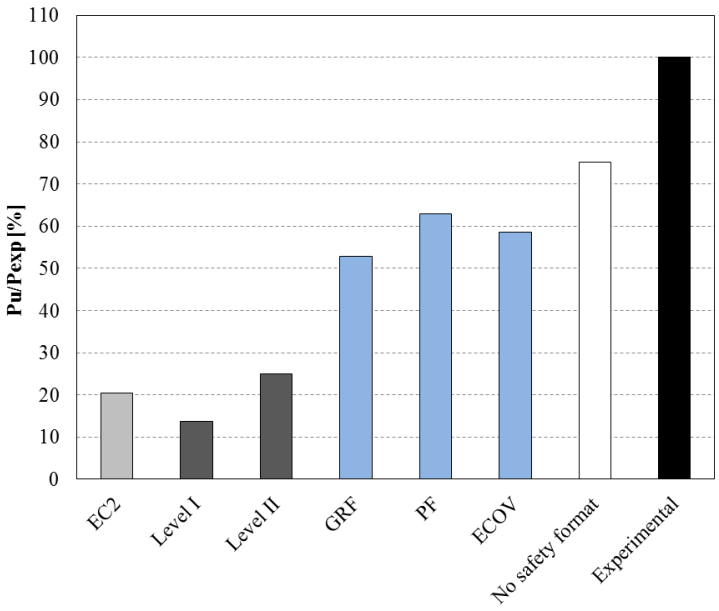

Figure 7-30: Case RS5. Analytical and numerical design values of slab resistance expressed in terms of a percentage of the experimental ultimate value of applied load, P_{Exp}=1153.85 kN

In Table 7-8 the design values of slab resistance, expressed in terms of applied load P_{Rd}, obtained from numerical and analytical procedures are highlighted.

Table 7-8: Case RS5. Values of slab resistance

P_{Exp}	EC2	Level I MC2010	Level II MC2010	GRF	PF	ECOV	No safety formats
(kN)	(kN)	(kN)	(kN)	(kN)	(kN)	(kN)	(kN)
1153.85	235.73	157.7	289.29	610.6	725.6	676.5	867

7.6 Concluding remarks

The benchmark for the case study RS5 is a simply supported at one end and clamped at the other slab subjected to an asymmetrical concentrated point load. The load is applied in the vicinity of the side edge and the simple support. The slab is 5 m long, has width of 2.5 m and thickness of 0.3 m. In the research program, at the ultimate applied load of 1153.85 kN the slab failed due to one-way shear described as a combination of wide beam shear failure and beam shear failure.

The numerical analyses of the slab considered a three dimensional model. The slab was modelled with 20-node brick elements for the concrete and embedded truss elements for the reinforcement. Perfect bond was assumed. The concrete model was based on a total strain rotating crack model with exponential tension softening in tension and parabolic behavior in compression, variable Poisson's ratio of concrete and no reduction of compressive strength of concrete due to lateral cracking. The model for the reinforcement bars was based on hardening plasticity.

From the analyses carried out on the model with mean measured material properties, the two-way shear failure mechanism was obtained. The failure mechanism was characterized by development of the vertical critical crack across almost the whole slab thickness which caused a sudden slide of concrete of a region near the loading plate. Such a behaviour suggests that the governing mechanism was punching shear. The resulting crack pattern, here identified as shear in two directions, appears to be different than the prediction of the analytical calculations which were concluded by one-way shear being the governing failure mechanism. The failure occurred that the ultimate value of 867kN.

The design resistance assessment was investigated by means of safety formats for non-linear finite element analyses. The design value of slab resistance obtained in this way resulted to be significantly higher than the design value of slab resistance calculated with analytical methods.

Based on the results it can be concluded that consistent and reliable results can be obtained with a variable Poisson's ratio that decreases from its actual value in the elastic phase up to 0.0 as cracking progresses. Reliable results were obtained by neglecting the reduction of the compressive strength of concrete due to lateral cracking. This assumption is also tied to the more simplified 3D material modeling with respect to the 2D modeling.

References

CEB-FIP Model Code 1990. (1993), *Bullettin d'Information n° 213/214*. Thomas Telford.

CEN (2005), Eurocode 2 - Design of concrete structures - Part 1-1: General rules and rules for buildings, EN 1992-1-1, Brussels: CEN.

Cope, R.J. & Rao P.V. (1983), "Moment redistribution in skewed slab bridges", *Proc. Instn Civ. Engrs*, 75(2), 419-451.

R.J. Cope, L.A. Clark (1984), Concrete Slabs: Analysis and Design, Elsevier Applied Science Publishers, London and New York.

fib (2013), fib Model Code for Concrete Structures 2010, Ernst & Sohn.

Lantsoght E, van der Veen C, Walraven JC (2013). Shear in One-Way Slabs under Concentrated Load Close to Support, *ACI Struct J*;110:275-84.

Lantsoght E. (2012). "Shear tests of Reinforced Concrete Slabs Experimental data of Undamaged Slabs". Technical Report 06-01-2012, Stevin laboratory, Delft University of Technology.

Lantsoght E. (2013). "Shear in Reinforced Concrete Slabs under a Concentrated Load Close to the Support", PhD thesis Delft University of Technology.

Muttoni A. (2003) Shear Strength and Punching of Concrete Slabs without Transverse Reinforcement (in German: Schubfestigkeit und Durchstanzen von Platten ohne Querkarftbewehrung). Beton- und Stahlbetonbau, 98:74-84.

Muttoni A. (2008) Punching Shear Strength of Reinforced Concrete Slabs without Transverse Reinforcement, ACI Struct J 105:440-450.

Muttoni, A. & Ruiz, M.F. (2012), "Levels-of-Approximation Approach in Codes of Practice", *Structural Engineering International*, 22, 190-194.

Nakamura, H. & Higai T. (2001), "Compressive Fracture Energy and Fracture Zone Length of Concrete" in "Modeling of Inelastic Behavior of RC Structures under Seismic Loads", Benson P. Shing (editor), *ASCE J. Str. Eng.*, 471-487, Benson P. Shing.

Oliver, J. (1989), "A consistent characteristic length for smeared cracking models", *International Journal for numerical Methods in Engineering*, 28, 461- 474

Prochazkova, Z. & Lantsoght, E.O.L. (2011), "Material properties – Felt and Reinforcement for Shear test of Reinforced Concrete Slab", Stevin Report No. 25.5-11-11, Delft University of Technology, The Netherlands, 28.

Regan PE, Rezai-Jorabi H. (1988). Shear Resistance of One-Way Slabs under Concentrated Loads. ACI Struct J 85:150-157.

Rodrigues, R.V. (2007), "Shear strength of reinforced concrete bridge deck slabs", Ecole Polytechnique Fédérale de Lausanne. Ph.D. thesis.

Selby R.G., Vecchio F.J. (1993). "Three-dimensional Constitutive Relations for Reinforced Concrete", Tech. Rep. 93-02, Univ. Toronto, dept. Civil Eng., Toronto, Canada.

Vervuurt, A.H.J.M. & Leegwater, G.A. (2008), "Workshop on the assessment of the shear strength of concrete structures", TNO report 2008-D-R0010.